11-10-2015

Silica Generated Reactive Oxygen Species, Phagolysosomal Leakage and Cell Death in Alveolar Macrophages

Gaurav Joshi
University of Connecticut - Storrs, gauravnjoshi@gmail.com

Silica Generated Reactive Oxygen Species, Phagolysosomal Leakage and Cell Death in Alveolar Macrophages

Gaurav N. Joshi, Ph.D.
University of Connecticut, 2015

Silicosis is a lung disease characterized by pulmonary fibrosis that arises from chronic inhalation of silica dust in various occupational settings. Inhaled silica particles get deposited in the alveoli where macrophages engulf them leading to inflammation and macrophage cell death. The presence of apoptotic macrophages in the lungs is sufficient to cause inflammation and fibrosis whereas; inhibition of macrophage cell death prevents fibrosis. The goal of this study is therefore to identify the processes within an alveolar macrophage leading to cell death after uptake of silica particles. In order to accomplish this goal, we have utilized various fluorescent probes and microscopy based methods to visualize and quantify the processes of particle phagocytosis, phagosome maturation, phagolysosome damage, reactive oxygen species (ROS) generation and a role of various apoptotic proteins in cell death.

We show that following silica particle phagocytosis by a macrophage, a phagolysosome containing a silica particle leaks after an average of 25 minutes. A leaky phagolysosome is then resealed 10 minutes later and stops leaking. Toxic silica particles were able to generate phagosomal ROS independent of NADPH oxidase whereas non-toxic latex particles could not. Latex particles also did not cause phagolysosomal leakage or cell death. Release of cathepsins during phagolysosomal leakage is hypothesized to activate proapoptotic proteins to cause cell death. We did not observe activation of pro-apoptotic proteins such as Bid and Bax immediately after phagolysosomal leakage but only hours later close to the time of apoptosis. A unique

increase in mitochondrial membrane potential was observed during apoptosis where as cells undergoing necrosis showed a decrease in mitochondrial membrane potential. In apoptotic cells mitochondrial hyperpolarization, caspase -9 and -3 activation and cell blebbing were observed together in a 5-minute temporal window. The order of events leading to cell death was same in all cells but there was a temporal heterogeneity between these events in cells.

Silica Generated Reactive Oxygen Species, Phagolysosomal Leakage and Cell Death in Alveolar Macrophages

Gaurav N. Joshi

M.S., University of Connecticut, 2006

A Dissertation

Submitted in Partial Fulfillment of the

Requirements for the Degree of

Doctor of Philosophy

at the

University of Connecticut

2015

2015

APPROVAL PAGE
Doctor of Philosophy Dissertation

Silica Generated Reactive Oxygen Species, Phagolysosomal Leakage and Cell Death in Alveolar Macrophages

Presented by

Gaurav N. Joshi, M.S.

Major Advisor

David A. Knecht

Associate Advisor

Adam Zweifach

Associate Advisor

Andrea Hubbard

University of Connecticut
2015

ACKNOWLEDGEMENTS

My graduate career at UCONN has truly been a journey. I have spent two-thirds of my life back home in Ahmedabad and the rest in Storrs. Without the support and mentorship of Dr. David Knecht, I would not be reaching this milestone in my journey. You have helped me grow both as a scientist and as a person. A simple "thank you" would not suffice to express my gratitude for everything that you have done for me. Thank you for letting me loose to explore the endless possibilities that science has to offer. Thank you for providing me with resources and facilities to play with cells, watch them do beautiful things and most importantly understand the processes of oxidative stress and cell death. Thank you for making me a part of your family on Thanksgiving.

I also want to thank my committee members for their immense patience with me throughout this process. Dr. Adam Zweifach, you have been tough but for my own good. I hope to find a new fierce critic of my work. Without an initial collaboration between Dr. Andrea Hubbard and Dr. Knecht, I would not have an opportunity to understand the effect of silica on macrophages. Thank you to Drs. Nathan Alder and Philip Yeagle for their insight with questions pertaining to everything lipid biology. Dr. Urs Boelsterli, thank you for helping me believe in my data of oxidative stress, a field I was new to. A number of scientists around the world have contributed with probes and reagents for my work. Without their help, I would not be able to achieve all the cool data. Thank you for your support.

Two hands are never enough to do science. I am fortunate to be helped by two very talented undergraduates Allie and Chris (now in medical school). With their help, I was able to explore new areas and both have contributed extensively to various aspects of my project. A special thanks to Dr. Renee Gilberti for developing some of the assays during her graduate work in Knecht lab that was immensely helpful to me. Roman Shrestha worked for two summers in our lab. His help provided me with a head start on the project related to the investigation of intrinsic cell death.

Watching fluorescent structures in a cell is similar to star gazing in a clear night. This immersive experience would not be complete without the help from Dr. Carol Norris who not only maintains the microscopy facility but also has helped with experiments and given critical feedback. A very special thanks to many, many, many of my friends and colleagues who have helped me in the journey. Without you this would be difficult. Karen Lombard, Mary Manning and Mary Pat have filled the void of talking to a mother like figure. Their kindness, love and comfort helped me get through some of the tough days at UCONN. Penny Dobbins, thank you for helping me earn my first real paycheck. Anne St. Onge, Lois Limberger, Bob Chudy and Laurie Tompkins, thank you for your help and support over these years.

Thank you to my aunt and uncle in NJ for all their help and support during my initial years in USA. My parents, Naishadh and Jayshree and my sister, Nidhi, you have been a pillar of strength to me. Without your encouragement, I may not have persisted to achieve this milestone in my career. Nidhi, thank you for the best surprise I have gotten in my life. It will always remain special to me. I love you all.

Abbreviations

Bax: Bcl-2 associated x protein
Bcl-2: B-cell lymphoma-2
BH: Bcl-2 homology region
BSA: Bovine serum albumin
CM-H_2DCFDA: Carboxy methyl-dihydro dichlorofluorescein diacetate
CMFDA: Chloromethyl fluorescein diacetate
EPR: Electron paramagnetic resonance
FITC: Fluorescein Isothiocyanate
GPx: Glutathione peroxidase
GSH: reduced glutathione
GSSH: oxidized glutathione
H_2HFF: Dihydro hexafluorofluorescein
H_2O_2: Hydrogen peroxide
IAP: Inhibitor of apoptosis protein
LLOMe: Leucyl-Leucyl-O-Methyl Ester
LPS: Lipopolysaccharide
NOS: Nitric oxide synthase
NOX: NADPH oxidase
$O_2^{\bullet -}$: Superoxide anion
$^{\bullet}OH$: Hydroxyl radical
PI: Phosphoinositides
Prx: Peroxiredoxin
PS: Phosphotidylserine
SiO_2: Silicon dioxide ROS: Reactive oxygen species
Smac: Second mitochondria derived activator of caspase
SR: Scavenger Receptor
TLR: Toll like receptor
TMRE: Tetramethyl Rhodamine ester
TRITC: Tetramethyl rhodamine isothiocyanate
XRF: X-ray fluorescence

Table of Contents

List of Figures

Chapter 1: Introduction

1.1: Overview

Occupational exposure to silica has been shown to result in the development of pulmonary fibrosis. Over the years, work by different groups has increased our understanding of the processes leading up to inflammation and pulmonary fibrosis after inhalation of silica particles. In rodents, a period of latency is observed after which the animal develops inflammation characterized by an increase in various cytokines and chemokines. The presence of these molecules is associated with the processes of tissue remodeling and pulmonary fibrosis (Porter *et al.*, 2004). The understanding of the events during the period of latency that result in inflammation is therefore of great interest. In humans, a similar period of latency could lead to the chronic nature of the disease in which fibrosis develops after many years. Various cells present in the lung alveoli contribute to the release of the inflammatory cytokines. Alveolar macrophages are the first responders to counteract the presence of inorganic silica particles that have made their way into the alveolar space (Huaux, 2007; Hamilton *et al.*, 2008). These cells are the professional phagocytes of the lung and proceed to take up the silica particles. A consequence of this is an increase in cellular reactive oxygen species and macrophage cell death. Chronic inhalation of silica and the resulting cell death perpetuates the cycle of death and inflammation (Kawasaki, 2015). The objective of this work is therefore to understand the events leading to macrophage cell death following particle uptake.

Lungs can tolerate apoptotic cells to a certain threshold following which an increase in accumulation of apoptotic cells could initiate the inflammatory process leading to fibrosis (Wang *et al.*, 2003). Pre-treatment of mice with inhibitor of apoptosis was shown to significantly reduce various pro-inflammatory mediators and could prevent fibrosis (Borges *et al.*, 2002).

Investigation into alveolar macrophage cell death following exposure to silica has revealed phagolysosomal leakage and activation of caspase -9 and -3, confirming this process is a form of apoptosis (Thibodeau *et al.*, 2003; 2004). The work in the thesis: 1) Advances on the results of Thibodeau et. al, and establishes a precise temporal order to various events leading up to cell death, 2) Investigates the process of phagolysosomal leakage and 3) Compares the mechanism of intrinsic cell death by different inducers of lysosomal leakage to understand the role of various pro-apoptotic proteins during apoptosis.

1.2: Silicosis - historical and current perspective

Silicosis was prevalent but ill-defined in the 19th century. Depending on the occupation of a person it was referred to as miners consumption or stonecutters phthisis as these individuals would suffer from symptoms of coughing, wheezing, dyspnea, spitting blood, weight loss and ultimately wasting, making them unable to earn their livelihood. Life expectancy for these individuals was short and many did not live past 50 years. In the late 19th century, with the understanding of bacterial diseases, silicosis was thought to be a form of tuberculosis due to bacterial transmission from stone cutting and poor living conditions of these workers (Rosner *et al.*, 1994). In the town of Barre, Vermont, workers not only from United States but also European countries came to work for what was once a world-renowned granite industry. In 1920 roughly 93% of these workers were believed to have suffered from silicosis. Learning from their experience, the workers and their union took pro-active measures to limit dust in the working environment resulting in an improvement in workers health (D Rosner, 1991) (https://vermonthistory.org/journal/misc/CurseofOurTrade.pdf). The single largest exposure to silica occurred during mining of Hawks Nest tunnel in West Virginia in 1927 during which close

to 3000 people were employed. Dust exposure during tunnel construction led to the death from acute silicosis of 476 workers in a two-year period (Cherniack, 1986) and a total of 700 people within 5 years of exposure while the rest suffered from irreparable lung damage (Thomas and Kelley, 2010). Public service announcement campaigns were carried out by the US Department of Labor (OSHA did not exist then) in 1938 to educate people about silicosis, which by then was an accepted term.

Currently 2.2 million workers in the United States are exposed to crystalline silica in various occupational environments (OSHA factsheet). Repeated exposure to silica takes place in industrial activities related to mining, tunneling, sandblasting, milling, construction, ceramic manufacturing, amongst others (Madl *et al.*, 2008). Over the years, with strong OSHA regulations and federal laws, the incidence of silicosis has been reduced in the United States. There were 8.91 deaths per million in 1968. This rate has steadily decreased with 2.5 deaths per million in 1981, 0.74 deaths per million in 2001 to 0.39 deaths per million in 2010 (Madl *et al.*, 2008; http://www.cdc.gov/mmwr/preview/mmwrhtml/mm6405a1.htm). In contrast, a developing country like India has 11.5 million workers exposed to silica (Jindal, 2013) with a high mortality rate due to lack of strict compliance to industry standards. The World Health Organization (WHO) and International Labor Organization (ILO) have initiated a campaign to eliminate silicosis around the world by the year 2030. Exposure to silica not only results in silicosis but also puts a person at risk for lung cancer (National Toxicology Program, 2002), autoimmune and kidney diseases (Steenland, 2005).

Silicosis is, after all, completely preventable in industrial situations by wearing an appropriate particle mask and adhering to particle exposure standards set out by OSHA (http://www.cdc.gov/niosh/docs/2004-108/). A lack of total safety compliance either by industry

(to reduce costs) or by workers (for sake of convenience) has prevented the total control of silicosis. The current permissible exposure limit (PEL) to crystalline silica is 100 $\mu g/m^3$ in inhaled air as an 8-hour time weighted average which according to a new proposed regulation from OSHA would come down to 50 $\mu g/m^3$ in inhaled air. The industry lobby is opposed to this regulation, as it will increase their costs (http://www.cdc.gov/niosh/docs/96-112/default.html). Expansion of procedures like fracking to extract shale oil has resulted in an increased exposure to silica. A survey by NIOSH at well sites found levels of silica ten times higher than the permissible limit (Esswein *et al.*, 2013).

1.3: Silica chemistry

Silica (silicon dioxide) is the second most common material in earth's crust and exists either in crystalline or amorphous form. Various polymorphs of crystalline silica exist as a result of different geochemical parameters, such as temperature and pressure. Quartz is the most common form of crystalline silica to which people are exposed during mechanical breakdown of various stones and rocks in mining, tunneling, quarrying and other activities in which silica becomes suspended in the air (http://www.cdc.gov/niosh/docs/96-112/default.html). Cristobalite and tridymite forms of crystalline silica are formed at high temperatures and occur naturally in lava. Various industrial applications like brick and ceramic manufacturing where silica is heated to high temperatures result in generation of cristobalite and tridymite forms. The PEL for cristobalite and tridymite is 50 $\mu g/m^3$ (https://www.osha.gov/dts/chemicalsampling/data/CH_266720.html) as they are more toxic than the quartz form (Castranova *et al.*, 1995). Other forms of crystalline silica, namely coesite and stishovite, are found from meteorite impact and are not relevant to toxicological outcomes.

Naturally occurring forms of amorphous silica, the diatomite and vitreous are nontoxic. However, synthesized forms of amorphous silica have varied industrial applications and are routinely used. The heating of amorphous silica has been proposed to impart it with crystalline form resulting in its toxicity.

The molecular packing of Si and O groups in silica vary depending on the change in temperature and pressure during mineral formation. Thus the crystal lattice structure of SiO_2 has either a tetrahedral or an octahedral symmetry. An inverse correlation is observed between packing of atoms in the crystal structure and toxicity. Quartz has tighter packing and exhibits lower toxicity compared to cristobalite and tridymite that have loose packing and exhibits higher toxicity. A free space or molecular pockets formed due to the oxygen - oxygen distance has also been shown to have a direct correlation to membranolytic (cell membrane lysis) (Pavan *et al.*, 2014) ability of silica polymorphs. The following order of membranolytic activity was observed across the polymorphs, stishovite, coesite < quartz, cristobalite < tridymite. Due to the toxicity associated with cristobalite and tridymite, the PEL is half of that of crystalline silica.

The surface of silicon dioxide (SiO_2) is altered upon interaction with water. Hydration results in formation of silanol group (-SiOH). The hydroxyl groups on the surface can form hydrogen bonds with electronegative oxygen or nitrogen on biological membranes. This affects the hydrophilicity, binding and absorption of silica particles to the cell surface and clearance (Fubini, 1998; Fubini and Hubbard, 2003). The silanol groups also contribute to free radical generation. The importance of the silica surface chemistry in causing toxicity has been demonstrated by treating silica with the polymer polyvinyl-pyridine-N-oxide (PVPNO) (Nash *et al.*, 1966; Knaapen, 2002; Schins *et al.*, 2002; Peeters *et al.*, 2014) or aluminum lactate (Schins *et al.*, 2002; Thibodeau *et al.*, 2004) which masks the surface reactive sites.

Freshly fractured silica has been reported to be more toxic than aged silica in *in vitro* and *in vivo* studies. In many occupational scenarios, inhalation of freshly fractured particles is likely to occur. During fracturing, hemolytic and heterolytic cleavage of Si-O bond takes place resulting in formation of ≡Si and Si-O on the fracture planes of quartz. The freshly fractured particles showed stronger peaks of •OH radicals compared to unground silica or aged silica during electron paramagnetic resonance (EPR) analysis. This shows that grinding of silica particles generate more •OH radicals than the unground silica. (Castranova *et al.*, 1995; 1997; Fubini and Hubbard, 2003). The presence of iron as a contaminant on the surface of silica can further result in the generation of more damaging reactive oxygen species (Ghio *et al.*, 1992). Once the particles are inhaled, the toxicity of the particles will depend on many factors, such as their penetration into the alveolar space and antioxidant balance in the lungs (Fenoglio *et al.*, 2003).

1.4: Pathophysiology of Silicosis

Silicosis can be divided into acute or chronic types depending on the duration and extent of exposure to silica. Acute silicosis develops within a short period of time due to repetitive high exposures. This results in flooding of alveoli with proteinaceous material and is referred to as alveolar silicoproteinosis. In chronic silicosis, which occurs due to inhalation of low amounts of silica over a long period of time (10-20 years), interstitial pulmonary fibrosis (IPF) develops which obstructs airflow. Chest radiographs can help diagnose silicosis but they fail to detect the disease at early stages. High resolution computed tomography provides an advantage over traditional x-ray as it can detect any opacities arising from formation of fibrotic nodules at early stages of silicosis (Castranova *et al.*, 1995).

Inhaled air passes through the nasal airway, pharynx, larynx, trachea and branched bronchi to reach the alveoli. Alveoli are the terminal region of the lung where gas exchange takes place. Bronchi are largely made up of ciliated epithelial cells and interspersed among them are the mucous secreting goblet cells. The mucous traps any foreign material and with a continuous ciliary action results in formation of a muco-ciliary escalator that pushes mucous into the oropharynx. Alveoli are composed of three cell types; type I and II pneumocytes that are epithelial in nature and macrophages. Type I pneumocytes are flat and contribute to 95% of the alveolar surface area due to their thin morphology that allows for gas exchange. Type II pneumocytes are ciliated and secrete surfactant that prevents collapse of alveoli during exhalation (Oberdörster *et al.*, 2005; Donaldson and Borm, 2006).

Particulate matter from 10 nm -10 μm in size can reach alveoli. However, these particles can also get deposited in the naso-pharyngeal, larynx and tracheo-bronchial space (Oberdörster *et al.*, 2005; Donaldson and Borm, 2006). In other studies, particles with mass median aerodynamic diameter (MMAD) of 1-5 μm were mainly found to be deposited in the alveoli where as particles from 5-10 μm were found be deposited in the tracheobronchial and oropharyngeal area (Labiris and Dolovich, 2003). Any silica particle that gets trapped in the mucous in the bronchial space will be either spit out or directed to gastrointestinal tract. In the alveoli, the main function of macrophages that are professional phagocytes is to clear any foreign material that enters the alveolar space. An important modification to the surface chemistry of silica takes place in the lung. The silica particle gets coated with lung surfactant consisting of various proteins before entering the alveoli. The coating of silica particles with proteins is likely to alter particle-cell interaction and any toxic outcome when compared to naked silica particles.

Chronic exposure to silica particles leads to lung inflammation that is followed by tissue repair. Inflammation starts when particulate matter reaches the alveolar space where uptake of silica particles by alveolar macrophage takes place by the process called phagocytosis. Silica particles reside in a structure called the phagolysosome, formed by fusion of a phagosome and lysosome. Silica has been specifically shown to cause damage to the phagolysosome and this has been shown to contribute towards inflammation as well as cell death. A detailed description of phagocytosis is part of the next section. Silica particle uptake results in macrophage activation and an upregulation of various pro-inflammatory chemokines and cytokines. This pro-inflammatory response initiates a complex cross-talk between various immune and non-immune cells (macrophages and epithelial cells). An end result is accumulation of fibroblast cells that secrete extracellular matrix contributing to formation of fibrotic nodules. These events following inflammation are similar to what would be found during wound healing. Thus a *de novo* response to resolve inflammation upon chronic particulate exposure results in fibrosis.

It is agreed that the generation of various cytokines and chemokines results in inflammation followed by fibrosis (Mossman and Churg, 1998; Fubini and Hubbard, 2003; Castranova, 2004; Rimal *et al.*, 2005; Huaux, 2007). However, the exact sequence of events that cause an increase in these cytokines and chemokines in various cell types and the delay in the manifestation of the disease is not well understood. Silica particles cause generation of cellular reactive oxygen species (ROS) (Lim *et al.*, 1997; Cho *et al.*, 1999; Shen *et al.*, 2001; Deshpande *et al.*, 2002; Fubini and Hubbard, 2003; Fazzi *et al.*, 2014) resulting in activation of the master transcription factor NF-κB (Rojanasakul *et al.*, 1999; Kang *et al.*, 2000; Fubini and Hubbard, 2003). This causes upregulation of TNF-α (Barrett *et al.*, 1998; Roursgaard *et al.*, 2010), IL-1β

(Srivastava *et al.*, 2002), IL-8 and macrophage inflammatory protein-2 (MIP-2) (Driscoll *et al.*, 1993; 1996; Driscoll, 2000).

Release of TNF-α from macrophages can activate other cell types such as endothelial cells and fibroblasts. It can also activate epithelial cells to release TGF-β that is important in tissue remodeling during fibrosis. An inhibition of NF-κB or supplementation of antioxidants to prevent any ROS generation blocked TNF-α release from macrophages (Rojanasakul *et al.*, 1999; Di Giuseppe *et al.*, 2009). TNF-α also induces the upregulation of chemokines such as the monocyte chemotactic protein-1 (MCP-1) and macrophage inflammatory protein-2 (MIP-2) from the epithelial cells (Barrett *et al.*, 1998). Consistent with this, after silica instillation in rats an increase in neutrophils was observed that returned to its normal values followed by an increase in macrophages in the broncho-alveolar lavage fluid (Porter *et al.*, 2004). Treatment of mice with human recombinant soluble TNF-α receptor prevented collagen deposition (a marker of fibrosis) with a reduction in the volume of fibrotic nodules (Piguet and Vesin, 1994) demonstrating a role for TNF-α in the fibrosis process.

Various studies have shown a role of IL-1β in contributing towards pathogenesis of silicosis. Alveolar macrophages treated with crystalline silica were shown to generate IL-1β at a 24-hour time point (Iyer *et al.*, 1996). The complexity involved in IL-1β activation and the role of inflammasome activation following silica induced phagolysosomal leakage has been uncovered in the past few years (Cassel *et al.*, 2008; Hornung *et al.*, 2008; Davis and Swanson, 2010; Hornung and Latz, 2010). The activation of IL-1β by the inflammasome has been detailed in the section titled “inflammasome”. IL-1β neutralizing antibodies reduced cell death in macrophages following silica exposure whereas silica induced inflammation was reduced and fibrotic plaques were not observed in an IL-1β knockout mouse (Srivastava *et al.*, 2002).

Consistent with the above observation, a similar study not only found a decrease in fibrosis with neutralization of IL-1β but a decrease in neutrophils, lymphocytes, TNF-α and MCP-1 (Guo *et al.*, 2013).

TGF-β is not under the transcriptional regulation of NF-κB. TNF-α has been shown to activate the transcription factor activator protein-1 (AP-1) that results in upregulation of TGF-β along with other pro-inflammatory cytokines. TGF-β can induce epithelial to mesenchymal transition (EMT) causing epithelial cells to lose their polarity and proliferate to a fibroblast like cell type. It also acts a chemotactic agent for fibroblasts (Postlethwaite and Seyer, 1990) and results in their proliferation (Battegay *et al.*, 1995). Collagen secretion from fibroblasts contributes towards formation of fibrotic nodules. Along with collagen, the fibrotic nodule has been found to contain macrophages, neutrophils and epithelial cells. Recently IL-17A, a glycoprotein secreted from IL-17 producing cells was shown to mediate TGF-β activation resulting in collagen synthesis and suppressing IL-17A prevented fibrosis (Mi *et al.*, 2011). Pulmonary fibrosis was also observed in rats where silica exposure was terminated prior to development of initial fibrosis indicating that even after cessation of exposure to silica an individual could be at a risk of developing silicosis (Porter *et al.*, 2004). In fact there is evidence that long after occupational workers ceased working in the environment exposing them to silica, they developed silicosis.

1.5: Phagocytosis

Uptake of silica particles by macrophages takes place by a highly coordinated process known as phagocytosis. Phagocytosis of a silica particle is a necessary step in silica induced cell death. Inhibition of silica particle uptake by inhibitors of actin polymerization are sufficient to prevent cell death (Cassel *et al.*, 2008; Gilberti and Knecht, 2015). It is also important to

understand the fate of the phagosome containing a silica particle. Similar to any other phagosome, a phagosome containing silica undergoes maturation by various molecular mediators resulting in fusion with endosomes and lysosomes. However, unlike most of the phagosomes, silica results in phagolysosomal leakage and triggers cell death.

Alveolar macrophages are professional phagocytes that play an important role in innate immune system by sequestering and eliminating foreign particulate matter that is larger than about 0.5 μm in size. The presence of various ligands on the surface of a pathogen aids in its recognition and uptake by a macrophage, however, silica particles lack these ligands. In spite of this, i*n vitro* studies have shown phagocytosis of inorganic particulate matter such as silica and polystyrene beads by macrophages. Thus macrophages are able to scavenge a variety of materials, irrespective of the presence of any biological recognition ligands. For silica that is deposited in the alveolar space, it could be coated with proteins or immunoglobulins (Huang *et al.*, 2001). Since immunoglobulins are not expected to be present at an early stage in development of silicosis, recognition of particles coated with proteins might be the prominent mode of silica particle-macrophage interaction at an early stage of the disease.

The silica particle if opsonized (antibody labeled) will be recognized by Fc receptor that will initiate a cascade of events resulting in Fc mediated silica particle phagocytosis. The non-specific recognition of proteins on the surface of a particle and the mechanism of phagocytosis is an active area of investigation. Recently it was shown that microtubules are required for the uptake of protein coated particles (Gilberti and Knecht, 2015). However, following phagocytosis of protein-coated particles, events similar to that of Fc receptor mediated phagocytosis are observed (Gilberti and Knecht, 2015). Specific to silica, the scavenger receptor has been proposed to play a major role in recognition of these particles due to the receptor's affinity for

negatively charged molecules (Iyer *et al.*, 1996; Hamilton *et al.*, 2000). Since the proteins that coat the silica particles also have a net negative charge, it is possible that scavenger receptors may facilitate recognition of protein-coated particles as well. In a study from our laboratory, no difference in uptake or toxicity was observed between silica particles that were coated with either histone protein that has net positive charge or casein protein that has a net negative charge (Gilberti *et al.*, 2008). In addition, latex particles of negative or positive surface charge are taken up equally well. Thus it is unclear that negative surface charge is a requirement for silica particle uptake.

During Fc receptor mediated phagocytosis, presentation of a particle with an Fc region on an antibody to a cell expressing FcR results in clustering of Fc receptors at the site of contact (Swanson and Hoppe, 2004). This triggers activation of various Rho families of GTPases like Cdc42 and Rac1 that cause actin polymerization and extension of the cell membrane around the particle to form a phagocytic cup. The cell membrane then seals resulting in formation of a phagosome. This newly formed phagosome undergoes maturation by a precisely regulated process during which it fuses with endosomes and lysosomes. The engagement of the Fc receptor by a particle labeled with Fc ligand results in phosphorylation of the tyrosine domains of immune receptor tyrosine based activation motif (ITAM) on the cytoplasmic side of the Fc receptor by Src family kinases (Daëron, 2003). This results in recruitment of Syk kinase required for activation of PI-3 Kinase (PI3K), crucial for phagosome maturation. Syk kinase also results in activation of protein kinase C (PKC) via the phospholipase C pathway (PLC) (Vieira *et al.*, 2002). The GTPase Rac1, PI3K and PKC that are required for phagocytosis are also important in activation of NADPH oxidase (NOX). NOX is recruited onto the phagosome during the

maturation process and generates phagosomal ROS (DeLeo *et al.*, 1999). A detailed role of NOX is described in the next section.

During phagosome maturation, the phosphoinositides (PI) signaling cascade helps with recruitment of various proteins with PI binding domains onto the phagosome. $PI(4,5)P_2$ is expressed on the inner leaflet of the plasma membrane but during phagosome formation it is converted by PI3K to $PI(3,4,5)P_3$ which binds to PH domains of various proteins. $PI(3,4,5)P_3$ is dephosphorylated by SHIP-1 to $PI(3,4)P_2$ that binds to proteins with PX domains. This undergoes another step of dephosphorylation to form PI(3)P which binds to proteins with FYVE domains. All forms of the above mentioned PI's are present on the phagosome even before it has completely closed. Typically the lipid modifications happen within a minute of appearance of actin on the phagosome and get over by 5 minutes demonstrating the dynamic nature of the phagosome membrane (Swanson and Hoppe, 2004; Steinberg and Grinstein, 2008).

During maturation, phagosomes fuse with early and late endosomal vesicles. Rab5 are the early endosomal vesicles characterized by the presence of early endosomal antigen-1 (EEA-1) having FYVE domain that binds to PI(3)P allowing the fusion of endosome to the phagosome. As the phagosome matures, it binds to late endosomes that can be confirmed by the presence of Rab7 protein. It has been observed that inhibition of PI3K stalls the process of uptake and phagosome maturation. Early and late endosomes are found to have a pH of 5.5 and 5.0 respectively (Vieira *et al.*, 2002; Flannagan *et al.*, 2012). Lysosomes are acidic vesicles where pH is maintained between 4.5-5.5 with the help of vacuolar ATPases (vATPases) that pump the protons in to the lumen. Lysosomes are characterized by the presence of lysosomal associated membrane proteins (LAMP)-1 and 2 and contains various proteases and enzymes. Most of the proteins in lysosomes require acidic pH for their activity, for example: cathepsins.

Any silica particle including the freshly fractured silica that has been shown to be membranolytic will be coated with proteins in the lung before their interaction with any cell. Even if the silica particles are coated with proteins, following particle phagocytosis, within a phagolysosome there will be proteolytic cleavage of the proteins due to the presence of various proteases. This will result in direct contact between the silica surface and phagolysosome membrane. While the damage to a phagolysosome containing silica is now widely recognized, this was first reported in 1970 (Nadler and Goldfischer, 1970). The mechanism by which phagolysosomal leakage occurs is investigated in the thesis. During phagolysosomal leakage cathepsins are released into the cytoplasm (Hornung *et al.*, 2008). Cathepsin-B can trigger inflammasome activation causing release of the pro-inflammatory cytokine IL-1β whereas cathepsin-D can initiate the intrinsic cell death pathway. The work from our laboratory has already shown the phosphoinositide signaling and early endosomal fusion upon phagocytosis of silica particle (Gilberti and Knecht, 2015). The work presented in the thesis will further investigate the pH dynamics and the fate of this phagosome.

1.6: NADPH oxidases

There are two aspects of NADPH oxidase that are relevant to silicosis and that makes investigation of its role important. One is the role of NOX2 in generating ROS in the phagosome. It is not known if this ROS plays any role in silica induced phagolysosomal leakage or whether it results in an increase in cytoplasmic ROS as reported by some studies (Deshpande *et al.*, 2002; Persson, 2005). The second is, the role of NADPH oxidase in *in vivo* models that show reduced inflammation and greater survival with NOX inhibition (Becher *et al.*, 2007; Sato *et al.*, 2008;

van Berlo *et al.*, 2010). The work presented in the thesis will focus on understanding the role of NOX in silica induced phagolysosomal leakage and generation of cytoplasmic ROS.

There are five different types of NADPH oxidases (NOX 1-5) and two types of dual oxidases (Duox 1-2). NOX functions to reduce oxygen to superoxide where as DUOX converts oxygen to hydrogen peroxide. They are categorized separately due to structural differences as well as their selective presence in particular tissues. Cells of the myeloid lineage such as macrophages and dendritic cells express only NOX2, whose function is critical for degradation of phagocytic material and antigen processing (Lambeth, 2007).

NOX2 is a multi subunit complex that is activated when the cytoplasmic $p47^{phox}$, $p67^{phox}$ and $p40^{phox}$ and Rac1 associate with membrane bound $gp91^{phox}$ and $p22^{phox}$, on the cytoplasmic side of the phagosomal membrane. $gp91^{phox}$ is the catalytic subunit with two hemes that allow passage of electrons to reduce oxygen to superoxide. $gp91^{phox}$ undergoes a conformational change upon binding of Rac1 and $p67^{phox}$. $p67^{phox}$ is sandwiched between $p47^{phox}$ that binds to $PI(3,4)P_2$ and $p40^{phox}$ that binds to PI(3)P via the PX domain (Kanai *et al.*, 2001; Ellson *et al.*, 2006; Suh *et al.*, 2006). The tetra tri-copeptide repeat (TPR) region of $p67^{phox}$ interacts with Rac1 (Babior, 2004; Matute *et al.*, 2005; Kao *et al.*, 2008). The proline rich region (PRR) domain on $p22^{phox}$ provides a tether for cytoplasmic subunits by interacting with SH3 domains of $p47^{phox}$. Various NOX2 subunits and their interaction on a phagosome are summarized in Figures 1.1 and 1.2. A critical role of NOX2 was first identified in patients suffering from chronic granulomatous disease (CGD) who are susceptible to bacterial and fungal infections due to mutation in NOX2 subunits. Recent data from 287 patients has led to identification of mutations in various subunits of NOX2 that could reduce ROS generation (Kuhns *et al.*, 2010). Depending on the site of

recruitment of NOX, either on the cell membrane or on a phagosome, the reduction of oxygen to superoxide takes place in the extracellular area or inside a phagosome.

NOX normally gets recruited to a phagosome leading to ROS generation within the phagosomal lumen. In order to understand NOX activation *in vitro,* cells are sometimes primed with PMA or LPS. This results in assembly of NOX on the cell membrane and as a consequence extracellular ROS would be generated (Tian *et al.*, 2008). This also results in activation of NF-κB that upregulates various pro-inflammatory cytokines (Hubbard *et al.*, 2002; Brass *et al.*, 2012). We do not know whether pre-activation of NOX in cells with LPS or PMA will in anyway affect phagosomal ROS generation. Therefore, throughout the work in this thesis, non-stimulated macrophages are used as a model to understand effects of silica on phagosomal NOX activation, its effect on a phagolysosome and cell death. This model reflects the exposure of naïve macrophages in the alveoli to silica. The situation might be different for macrophages in a chronically exposed individual who lung is already undergoing an inflammatory response.

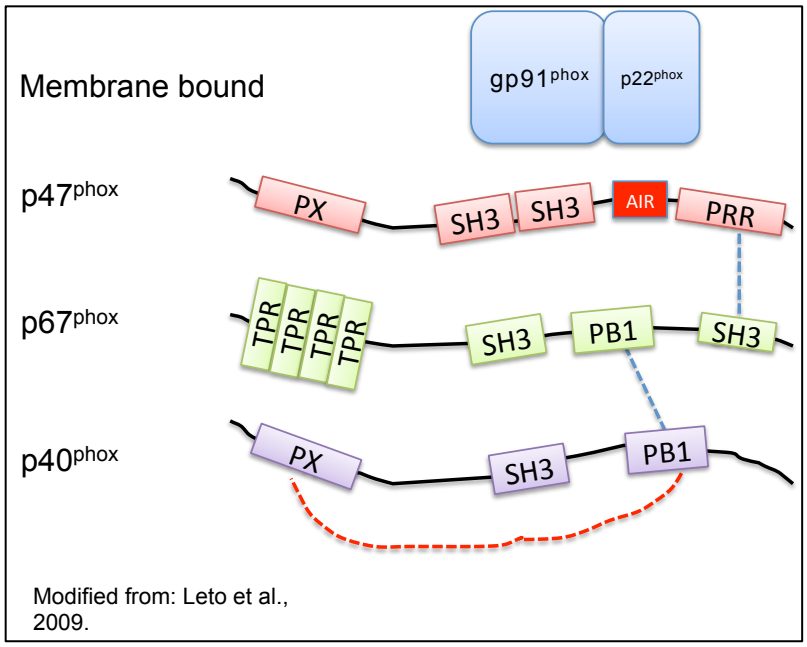

Figure 1.1: Various subunits of NADPH oxidase 2

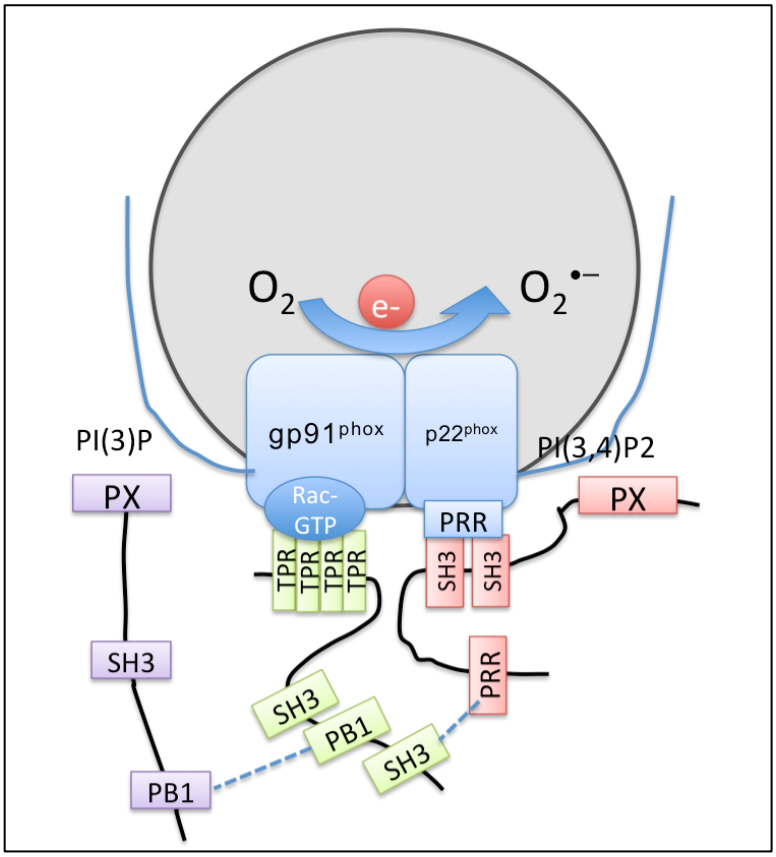

Figure 1.2: Phagosomal NADPH oxidase 2 activation

1.7: Reactive oxygen species

An increase in cellular ROS following silica exposure has been observed and proposed to be the reason for inflammation and cell death following silica exposure. Treatment of cells with antioxidants reduced the amount of ROS generated upon silica exposure. This directly correlated with a decrease in the generation of pro-inflammatory cytokines as well as cell death (Shen *et al.*, 2001; Deshpande *et al.*, 2002; Hu *et al.*, 2006; 2007). These studies looked at ROS generation within the cytoplasm of cells whereas silica particles are isolated within a phagolysosome and are not freely present in the cytoplasm. A basic understanding of ROS generation in phagosomes is focused on neutrophil phagosomes rather than macrophage phagosomes. A notable difference between these cells is that the oxidative burst (phagosomal ROS due to NOX) is more robust in a neutrophil than a macrophage. Also, neutrophil phagosomes contain myeloperoxidase (MPO), which catalyzes the generation of hypochlorous acid from hydrogen peroxide. It is not known if the reaction between hypochlorous acid and silica in a neutrophil will have any consequences, as there is an increase in neutrophil numbers during inflammation. MPO is absent from macrophage phagosomes (Hampton *et al.*, 1998; Halliwell, 2006; Winterbourn, 2008).

Various ROS are generated within a cell by a four-step single electron reduction of oxygen that eventually converts oxygen to water (Figure 1.3). Oxygen (O_2) has two unpaired electrons in its outer shell. A single step reduction of oxygen by an electron results in the generation of superoxide anion radicals ($O_2^{\bullet -}$), referred to as superoxide. In a cell, this reaction is carried out by NOX2 in the phagosomal membrane causing superoxide generation in the phagosomal lumen. Intracellular generation of superoxide also occurs in the process of electron transport during ATP generation in the mitochondria. Approximately 0.2-2% of oxygen consumed by cells gets converted to ROS in mitochondria. Superoxide dismutates spontaneously

or with the help of the enzyme superoxide dismutase (SOD) generating hydrogen peroxide (H_2O_2). Dismutation by SOD is 10,000 times faster than self-dismutation (Kalyanaraman, 2013). In an acidic environment, like that of a phagosome, the spontaneous dismutation will be quicker compared to cytoplasm (Roos, 1979). The H_2O_2 is converted to water with the help of the enzymes catalase and glutathione peroxidase (GPx) and its substrate glutathione. Therefore, under normal circumstances, ROS are kept in check by the antioxidant defenses of the cell. For ROS to cause damage to the cellular system either there has to be a significant reduction in the antioxidant levels or there has to be a significant increase in ROS that overwhelms the antioxidant machinery. In support of these redox conversions in a phagosome, various proteomic studies done on phagosomes isolated from macrophages and dendritic cells have shown the presence of NOX subunits, SOD, catalase, and peroxiredoxin-1 (Shui *et al.*, 2008; Buschow *et al.*, 2012; Goyette *et al.*, 2012).

Superoxide generated during the oxidative burst is not a strong oxidant and reacts very slowly with thiols in various proteins and is likely detoxified by SOD's so that it is unlikely to produce any physiologically relevant effect. H_2O_2 generated from reduction of superoxide reacts poorly with most biological molecules including low molecular weight antioxidants such as glutathione. It is only in the presence of catalase or seleno- or thiol peroxidases like the glutathione peroxidase (GPx) or peroxiredoxin (Prx) respectively that hydrogen peroxide is efficiently converted to water. While there is no evidence for the presence of GPx in phagosomes from proteomic analysis, Prx was detected. The cytosolic concentration of gluathione is reported to be ~8 mM and the GSH:GSSG ratio ranges between 1:1 and 3:1, however a decrease in this ratio has been reported during silica induced cell death (Hu *et al.*, 2006).

Superoxide in the presence of nitric oxide generated by the nitric oxide synthase (iNOS) forms peroxynitrite, a type of reactive nitrogen species (RNS) that is a highly potent and a short-lived oxidant. *In vitro*, iNOS is not present unless cells are stimulated by endotoxins such as LPS (Weisz *et al.*, 1996) or by pro-inflammatory cytokines such as IL-1β (Tsujino *et al.*, 1994) or TNF-α. The resulting peroxynitrite can also be damaging to membranes by generation of hydroxyl radicals. iNOS deficient mice show resistance towards silica induced inflammation as well as cell death (Srivastava *et al.*, 2002; Becher *et al.*, 2007).

Inside a cell, H_2O_2 is normally converted to water with the help of the peroxidases and catalase. However, a single step reduction of H_2O_2 by either Fenton chemistry or Haber-Weiss reaction will result in the generation of hydroxyl radicals ($^{\bullet}OH$). The latter reaction is unlikely to occur in biological systems except in the presence of ferrous iron. $^{\bullet}OH$ radicals are a highly reactive ROS that have been proposed to cause lipid peroxidation. The half-life of $^{\bullet}OH$ radicals is 10^{-9}s, and they will react with compounds at a nearly diffusion controlled rate of 10^{9} - 10^{10} $M^{-1}s^{-1}$ (Winterbourn, 2008; Kalyanaraman, 2013). The Fenton chemistry requires the transition metal ion ferrous iron (Fe^{2+}). The ferric iron (Fe^{3+}) can be reduced to ferrous (Fe^{2+}) by superoxide generated upon reduction of oxygen

$$Fe^{3+} + O_2^{\bullet -} \rightarrow Fe^{2+} + O_2$$

The ferrous iron can now react with hydrogen peroxide resulting in the formation of a hydroxyl radical and a hydroxyl anion.

$$Fe^{2+} + H_2O_2 \rightarrow Fe^{3+} + OH^- + {}^{\bullet}OH$$

An alternate way of producing $^{\bullet}OH$ radical is via Haber-Weiss mechanism

$$O_2^{\bullet -} + H_2O_2 \rightarrow OH^- + {}^{\bullet}OH + O_2$$

The generation of $^{\bullet}OH$ radicals has been reported from freshly fractured silica contaminated with iron in the presence of H_2O_2. In cells, the hydroxyl radical has been proposed to damage membranes and cause phagolysosomal leakage (Ghio *et al.*, 1992; Persson, 2005). The authors showed a decrease in phagolysosomal leakage in cells that were allowed to endocytose an iron chelator followed by exposure to silica (Persson, 2005). $^{\bullet}OH$ radicals will rapidly react with the phospholipid bilayer resulting in membrane lipid peroxidation through intermediates of various lipid radicals. Yet there is no direct evidence of $^{\bullet}OH$ radical generation in phagolysosomes or the lipid peroxidation of the phagolysosomal membrane upon exposure to silica particles as proposed by many studies. Molecular simulation studies of the phospholipid bilayer have shown that a conformational change in the bilayer due to presence of oxidized lipids can result in membrane damage (Wong-Ekkabut *et al.*, 2007).

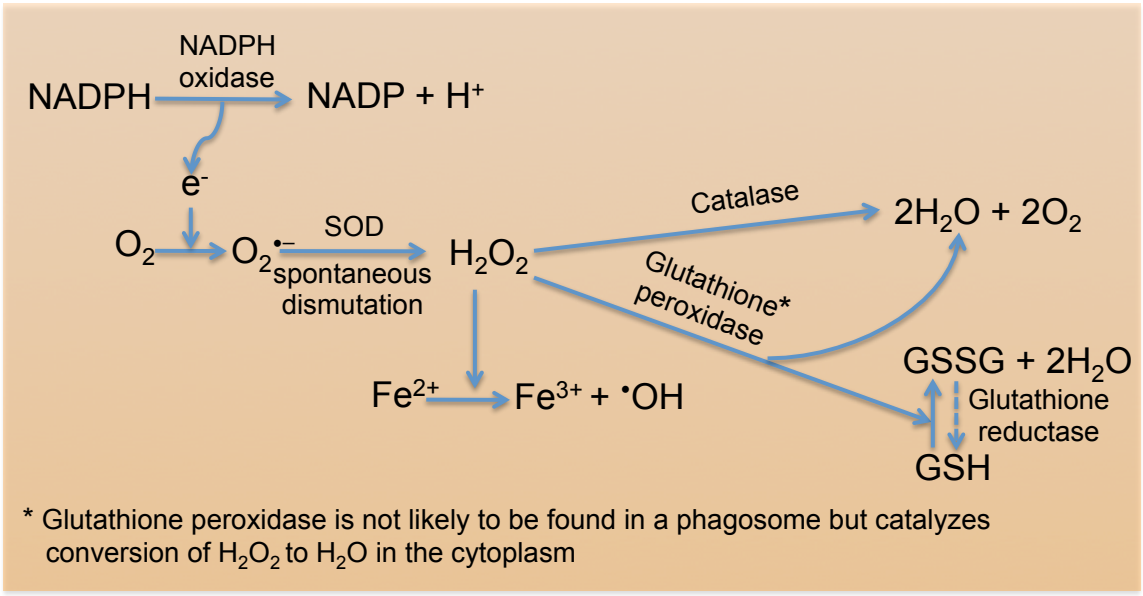

Figure 1.3: Generation of various Reactive Oxygen Species

1.8: Inflammasome

Upon phagolysosomal leakage, the release of the serine protease cathepsin-B has been shown to activate the inflammasome resulting in IL-1B activation and subsequent release ref. Inhibiting cathepsin-B prevented inflammasome activation and the production of pro-inflammatory IL-1B (Hornung *et al.*, 2008). The inflammasome is a multi-protein complex that includes Nod Like Receptor Protein (NLRP). Various families of NLRP have been shown to be involved in the formation of the inflammasome but NLRP-3 is best studied. It is activated by various pathogen associated molecular pattern (PAMP) signals associated with various bacteria, fungal agents and viral RNA, danger associated molecular pattern (DAMP) signals such as extracellular ATP, monosodium urate and amyloid β aggregates. Environmental particles such as silica, asbestos and alum have been shown to activate the inflammasome by induction of lysosomal leakage (Bauernfeind *et al.*, 2009).

The structure of the inflammasome consists of a receptor and an adaptor region. NLRP-3 (a receptor) acts as a sensor that under normal condition is auto-repressed by the interactions of its NACHT domain with a leucine rich region (LRR). Upon activation by various PAMP's, the auto-repression is relieved, resulting in oligomerization of NLRP-3 mediated by its NACHT domain. The pyrin domain (PYD) associated with NACHT interacts with the apoptosis associated speck like protein (ASC) that is linked to caspase recruitment domain (CARD) on the adaptor region of the inflammasome complex. CARD recruits the effector pro-caspase 1, which upon clustering becomes auto-activated (Lamkanfi and Dixit, 2014).

The function of the inflammasome complex is to activate caspase-1 which in turn activates IL-1β and IL-18 (Bauernfeind *et al.*, 2009). A relationship between pro-inflammatory IL-1β and development of silicosis has been well established. Whether IL-18 plays any role in

the development of silicosis is not known. IL-1β knock out mice exposed to silica show a reduction in the development of fibrotic nodules. Further the role of the inflammasome complex in mediating IL-1β induced fibrosis upon silica exposure is also established by studies in which mice lacking NLRP-3 show decreased inflammation and collagen deposition following intratracheal silica instillation (Cassel *et al.*, 2008; Dostert *et al.*, 2008). Alternatively, extracellular ATP can also activate NLRP-3. Cell injury and necrosis releases ATP that activates to P2X7 receptor that provides for an alternate way of activating NLRP3. Consistent with this, a recent study has shown reduction in inflammation and fibrosis upon exposure to silica in mice lacking the P2X7 receptor (Monção-Ribeiro *et al.*, 2014; Luna-Gomes *et al.*, 2015). Considering NLRP3 activation converges at IL-1β induced inflammation, targeting IL-1β provides for an effective management and treatment of silicosis patients.

1.9: Cell Death

It has been known for some time that macrophage cells exposed to silica particles die within hours. The presence of apoptotic cells has been hypothesized to result in a persistent state of inflammation in various organs and tissues (Wang *et al.*, 2003). Mice that were pre-treated with a caspase inhibitor required for apoptosis and exposed to silica particles show a reduction in pulmonary inflammation, collagen fiber deposition and development of fibrotic nodule (Maeda *et al.*, 2010; Gao *et al.*, 2011). Further, intratracheal instillation of apoptotic macrophages was found to increase the expression of TNF-α and TGF-β that correlated with lung inflammation and fibrosis (Wang *et al.*, 2003; Gao *et al.*, 2011). Thus apoptotic cell death contributes towards silicosis. There have been rapid developments in the field of cell death from the time this project was initiated. This brief introduction will focus on two main types of cell death processes, apoptosis and necrosis and highlight the current state of the field of cell death.

Apoptosis is a regulated and controlled cell death mechanism characterized by cell shrinkage, cell membrane blebbing, caspase activation, nuclear fragmentation and condensation. This prevents the release of cellular contents from the dying cell and an ensuing inflammation as an apoptotic cell is engulfed by phagocytic cells. The instillation of apoptotic cells causing inflammation and fibrosis is indicative of This process was first reported by J.F Kerr in hepatocytes and based on cell blebbing observed using an electron microscope the process was named apoptosis (falling off petals) (J F R Kerr, 1972). Early studies characterizing genes involved in the process of apoptosis came from Robert Horvitz work in *C. elegans*. During the development of *C. elegans* exactly 131 cells were found to undergo programmed cell death and

several Bcl-2 family of proteins involved in this process were identified (Hengartner *et al.*, 1992; Lettre and Hengartner, 2006)**.**

Necrosis, in contrast to apoptosis, was defined as an unregulated process that results in massive cell swelling with release of cellular contents into the extra cellular space resulting in inflammation and tissue damage. Necrosis is a form of caspase independent cell death characterized by swelling of cells. The past few years have seen a change in this definition where swelling of cells can occur by regulated necrosis. Various proteins involved in regulating the process of necrosis have been characterized. Necroptosis can be triggered by activation of Toll like receptors (TLR) 3 or 4, Fas or Fad receptor activation or by Interferon-γ leading to RIPK3 activation and plasma membrane rupture (Galluzzi *et al.*, 2014a). An inhibition of caspase-8 during apoptosis was shown to route Fas mediated cell death to RIPK3 mediated necroptosis. An increase in calcium can result in mitochondrial permeability transition mediated regulated necrosis (MPT-RN) that can cause exit of apoptosis inducing factor (AIF), a pro-apoptotic protein into the cytoplasm. Parthanatos is characterized by hyperactivation of poly (ADP-ribose) polymerase-1 (PARP-1) resulting in MOMP (Linkermann *et al.*, 2014). Ferroptosis is defined by glutathione deprivation due to inhibition of cystine/glutamate antiporter resulting in a deficiency of cysteine, a substrate for glutathione synthesis. This results in inhibition of glutathione peroxidase and subsequent lipid peroxidation of the cell membrane in an iron dependent manner (Dixon *et al.*, 2012). It is not known if any of these well-defined necrotic processes occur upon silica exposure.

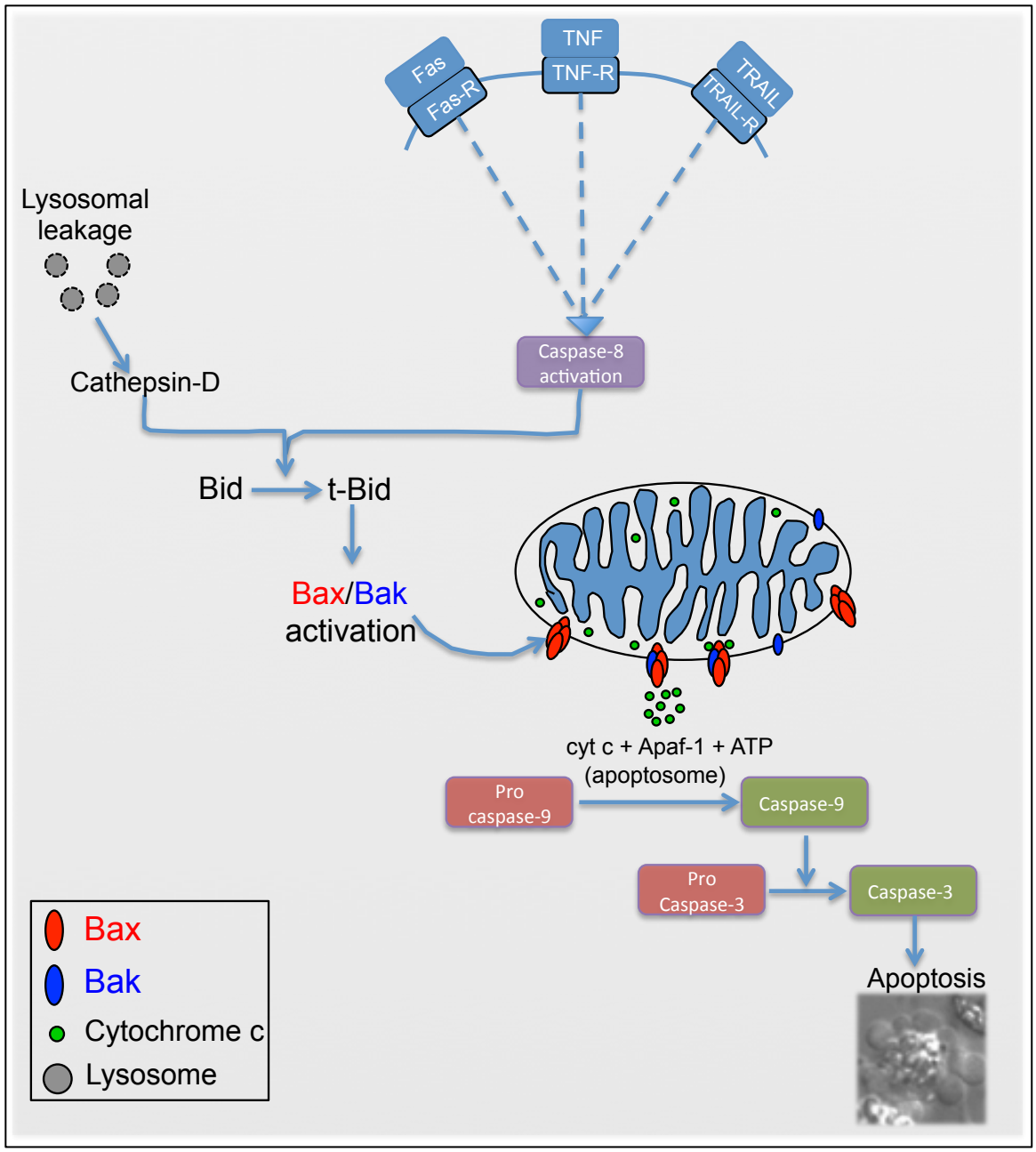

Figure 1.4: Intrinsic and extrinsic apoptosis cell death pathway

Chapter 2: Materials and Methods

2.1: Materials

All chemicals were obtained from Sigma Aldrich (St. Louis, MO) unless specified otherwise.

2.2: Cell Culture

MH-S alveolar macrophages (ATCC CRL-2019) were maintained at 37°C in RPMI-1640 media supplemented with 10% heat inactivated FBS, 10 mM HEPES, 2 mM L-Glutamine and 100 μg/ml Ampicillin/Streptomycin (complete media) at 37 °C in a 5% CO_2 incubator.

Cos7 African green monkey kidney fibroblasts (ATCC CRL-1651) were maintained in Dulbecco's Modified Eagle medium (DMEM) supplemented with 10% heat inactivated FBS, 2 mM L-Glutamine, 19.4 mM D-glucose, 100 μg/ml of Ampicillin/Streptomycin at 37°C in a 5% CO_2 incubator.

For imaging experiments cells were maintained in CO_2 independent medium (ThermoFisher Scientific, Waltham, MA).

2.3: Plating of cells

For live cell imaging experiments, cells were plated at varying densities depending on the glass bottom dish. In an 8 well chamber slide (Labtek Inc.) cells were plated at $3x10^4$ cells/well in 500 μl of complete media for 18 hours before the start of an experiment. In a 35 mm bioptechs dish (Bioptechs Inc, Butler, PA) or a WillCo dish (WillCo Wells, Amsterdam, Netherlands or MatTek corporation, Ashland, MA) cells were plated at 1.2×10^5 cells/ml in complete medium for 18 hours before the start of an experiment.

2.4: Cell transfection

Cells were transfected with DNA obtained by plasmid midi prep kit (Promega Inc, WI) using either Lipofectamine 2000 (ThermoFisher Scientific, Waltham, MA) or Fugene HD (Promega Inc, WI) lipid transfection reagents. For both methods, 12 x 10^4 MH-S murine alveolar macrophages or Cos7 cells were plated in 35 mm Willco glass bottom dishes (Willco Wells BV, Amsterdam, Netherlands) in 1 ml complete media.

For transfection with Lipofectamine, media in the plate was replaced with serum and antibiotic free cell culture media. In one of the eppendorf tube 2 µg DNA was mixed in 100 µl of serum and antibiotic free media where as in another 5 µl Lipofectamine was added to 95 µl serum and antibiotic free medium. These were incubated for 30 minutes at room temperature following which the two solutions were mixed in a single tube and allowed to incubate for another 10 minutes at room temperature. The media in the plate containing cells was replaced with 800 µl serum and antibiotic free medium. To this the DNA and Lipofectamine mix as added drop wise, the plate was swirled and incubated at 37ºC for 10 hours following which the media was replaced by complete medium. Cells transiently expressing the fluorescent protein were used for further experimentation or split into 8 well-chambered slides for further experimentation.

For transfection using Fugene HD, media in the plate was replaced to 875 µl fresh complete medium. 2 µg of DNA was mixed with 100 µl serum and antibiotic free cell culture medium and 6 µl of FuGene HD transfection reagent was added. DNA complexes were incubated for 15 minutes at room temperature then added to cells. Transient expression of the cells was checked after 10 hours and the media replaced with fresh complete media. These cells were either used for the experiment or split into 8 well-chambered slides for experiments the next day.

In order to obtain cells that stably expressed the desired probe, cells were selected by addition of G418 (1mg/ml) 48 hours after the transient transfection. 48 hours after the addition of antibiotic, media was removed to clear off the dead cells and replaced with complete cell culture media. Cells were allowed to grow and fluorescent colonies were directly picked from the culture dish manually with a pipette while viewing cells on the microscope stage.

List of various probes used for transfection

CFP-IETD-YFP: FRET based sensor to detect initiator caspase-9 activation (He *et al.*, 2006)

CFP-DEVD-YFP: FRET based sensor to detect initiator caspase-9 activation (Tyas *et al.*, 2000).

roGFP2-Orp1: Ratiometric redox sensor to detect cytoplasmic H_2O_2 (Morgan *et al.*, 2011)

mito-roGFP2-Orp1: Ratiometric redox sensor to detect mitochondrial H_2O_2 (Morgan *et al.*, 2011).

GFP-Bax: GFP fused to N-terminus of Bax to detect Bax translocation in to mitochondria (Tait *et al.*, 2010).

Bid-FRET: FRET based sensor to detect Bid activation (Onuki *et al.*, 2002)

Smac-mcherry: A mitochondrial intermembrane space protein to detect MOMP (Bhola *et al.*, 2009).

PX-GFP: GFP fused to PX domain of $p40^{phox}$ (Ellson *et al.*, 2006)

FcγRIIA-GFP: For expression of Fc-receptor in Cos7 cells.

mCherry-actin: To detect actin dynamics during particle phagocytosis.

2.5: Particles and particle preparation

Particles used for various experiments include Minusil-5 crystalline silica referred as crystalline silica (US Silica, MD), 3 μm amorphous silica (Alltech/Grace-Davison, MD), 3 μm

polystyrene latex particles (Polysciences, PA), 200 nm and 50 nm red fluorescent silica particles (Kisker Biotech, Steinfurt, Germany) and 200 nm green fluorescent latex particles (Polysciences Inc, Warrington, PA). Both crystalline silica and 3 μm amorphous silica particles were baked at 83°C for 18 hours to remove any endotoxins.

Stock solution containing 2 mg/ml of either crystalline or amorphous silica particles was prepared in the CO_2 independent medium and used at different concentrations described throughout the studies. For other particle types that came suspended in solution from the supplier, particles were washed 3 times by centrifugation using PBS and resuspended in CO_2 independent medium and used at varying concentrations as described throughout the studies.

To prepare protein coated (non-opsonized) particles, 2 mg of silica particles or 100 μl of latex particles were added to 1 ml of 10 mg/ml Bovine Serum Albumin (BSA, Research Organics) in particle coating buffer (PCB - 0.15 mM NaCl, 1.8 mM Na_2CO_3, 3.2 mM $NaHCO_3$, pH 9.5) and rotated for 90 minutes at 37 °C. Particles were spun down at 5000 rpm for 2 minutes, washed 3 times and resuspended in 1 ml PBS. 500 μl of these non-opsonized particles were aliquoted and stored at 4 °C. To opsonize particles, 5 μl of Rabbit Anti-BSA antibody (ICL labs, Portland, OR) was added to the remaining 500 μl of non-opsonized particles for 90 min at 37 °C. Particles were spun down at 5000 rpm for 2 minutes and washed 3 times with PBS. Opsonized particles were resuspended in 500 μl of PBS and stored at 4 °C. To determine that particles were coated with antibody, a 1/150 dilution of goat anti-rabbit Texas Red secondary antibody was added to 10 μl of opsonized particles and incubated for 30 minutes at room temperature. The particles were pelleted, resuspended in 100 μl distilled water and examined by fluorescence microscopy.

To prepare FITC labeled silica particles, silica particles were opsonized as described earlier. A 500 µl aliquot of opsonized particles was pelleted and resuspended in 400 µl of 0.1M $NaHCO_3$, pH 8.5. Fifty microliters of 50 mg/ml FITC (dissolved in dH_2O) was added to the particles and the tube was rotated at room temperature for 2 hours protected from room light. Particles were pelleted at 5000 rpm for 2 minutes and resuspended in 500 µl of 0.1M glycine. The particles were then pelleted and washed once in 500 µl of 0.1M glycine and once in 500 µl PBS, then stored at 4 °C.

2.6: Particle uptake assays

2.6.1: Fixed cell internalization assay

$5x10^4$ cells (MH-S, Cos7 or Fc-Cos7) plated on a sterilized 22 mm square glass coverslip in a 35 mm petri dish were incubated overnight in complete medium. The next day, the media was aspirated, replaced with 500 µL CO_2-independent media and incubated at 37°C in an ambient air incubator for 30 min. Plates were chilled on ice for 15 min following which they were exposed to 20 $\mu g/cm^2$ of either opsonized or non-opsonized silica particles suspended in 500 µl of 4°C CO_2 independent media. Plates were centrifuged at 500xg for 5 min at 4°C and either fixed immediately or incubated at 37°C for different times prior to fixation. Media was aspirated and cells fixed by adding 500 µl 4% formaldehyde (Polysciences, Warrington, PA) in PBS for 6 min at 25°C. The fixative was aspirated and the reaction quenched with 500 µl of 50 mM NH_4Cl for at least 6 minutes at 25°C. For non-opsonized particles, the PBS was aspirated, 200 µL of 1:800 rabbit anti-BSA primary antibody was added and the cells were incubated for 15-20 minutes at 25°C followed by aspiration, one wash with PBS and addition of 200 µL 1:150 goat anti-rabbit Texas Red secondary antibody. The cells were incubated for 15-20 min at 25°C. For opsonized particles, only the Texas Red secondary antibody was added and the cells were

incubated for 15-20 min at 25°C. Following the antibody incubations, cells were washed in PBS twice and once with 1 mL distilled water and inverted onto a slide with mounting media (10% MOWIOL/ 2.5% DABCO). Particles on the outside of cell are expected to be fluorescent whereas internalized particles are not. The proportion of particles internalized was quantified by comparing the total number of particles in the transmitted light image to the number of fluorescent particles. A schematic for the same is presented in Figure 2.1 for non-opsonized particles and in Figure 2.2 for the opsonized particles. The particles that are internalized are not labeled with a secondary antibody conjugated to a red fluorophore and hence do not get labeled red. These are depicted in blue color in the cartoon.

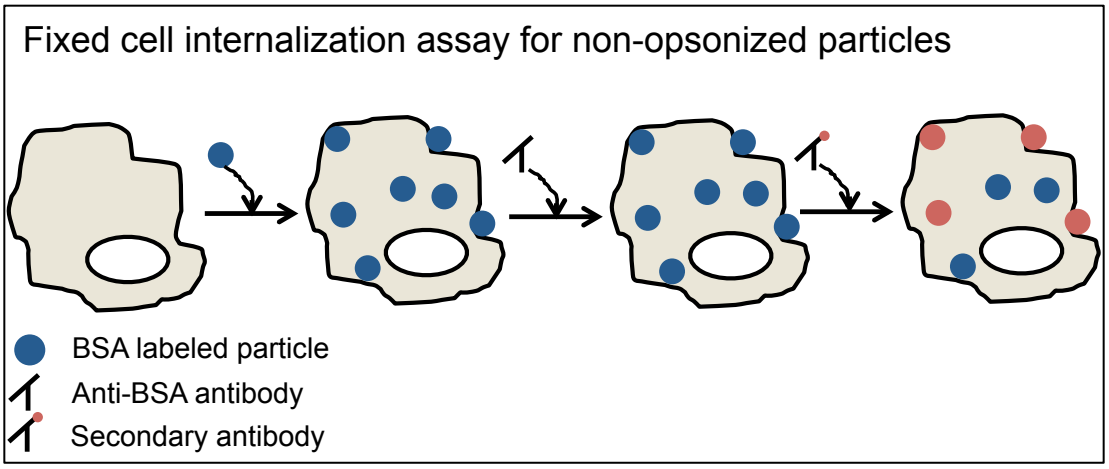

Figure 2.1: Fixed cell internalization assay for non-opsonized particles

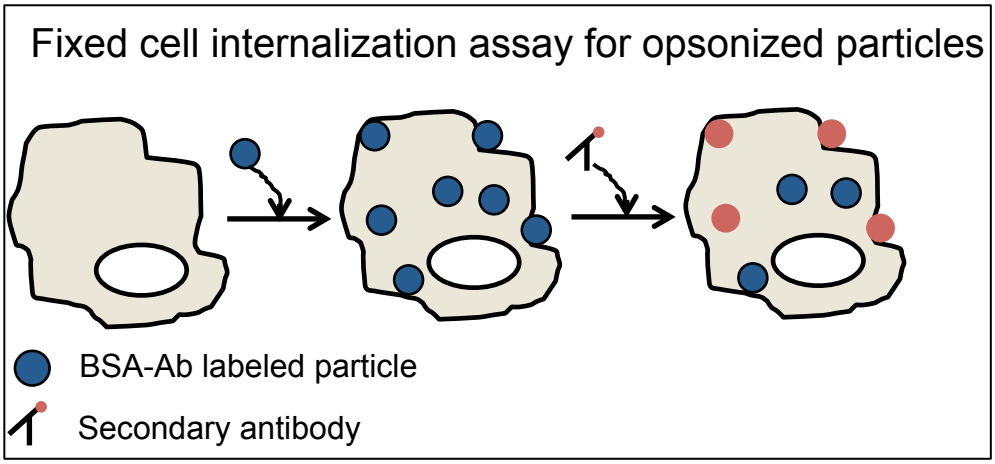

Figure 2.2: Fixed cell internalization assay for opsonized particles

2.6.2: Live-cell imaging assay

15 x 10^4 macrophages expressing mCherry-actin were plated in a WillCo well overnight. These were exposed to 20 μg/cm^2 all-sphere silica particles in a microscope chamber set to perform live cell imaging at 37 ºC. Images were acquired every 30 seconds or minute apart. Particles that are internalized are expected to show a transient mCherry-actin fluorescence during phagocytosis.

2.7: Phagolysosomal leakage assay

Cells were plated as described earlier and incubated with 1 mg/ml of 4 kD FITC-dextran or 4 kD TRITC-dextran in complete medium for 2.5 hours at 37 °C. For dual dextran experiments, cells were co-incubated with 0.5 mg/ml each of 4 kD FITC-dextran and 4 kD TRITC-dextran. Cells were then washed twice with complete media and then the media was replaced with CO_2 independent medium (ThermoFisher Scientific, MA) for imaging. Leakage was measured by drawing an ROI over the nuclear area and measuring mean pixel intensity for every time point (Joshi and Knecht, 2013a).

2.8: Detection of Reactive oxygen species (ROS)

2.8.1: Phagosomal ROS detection

To detect ROS in a phagosome upon particle phagocytosis, silica and latex particles were labeled with H_2HFF-BSA (Life Technologies, OR). Particle coating buffer was deoxygenated by bubbling nitrogen gas for 30 minutes. 1 ml of deoxygenated PCB was added to a vial containing 1mg of H_2HFF-BSA. Silica particles (2 mg/ml) or latex particles (100 μl) were added and then incubated for 90 minutes at 37 °C while rotating the tube. Meanwhile, PBS was deoxygenated by

bubbling nitrogen gas for 30 minutes. This was achieved by filling up a 50 ml tube with 20-25 ml of PBS. Two layers of parafilm were kept on the mouth of tube and a glass Pasteur pipette was inserted. Holes were made on the periphery of the mouth area of 50 ml tube in the parafilm to allow air to pass through during bubbling process. Nitrogen gas was passed into a pump to regulate the pressure of gas. A small tubing from this pump was then inserted into the pasteur pipette and the gas was passed continuously for 30 minutes. After 30 minutes, the pasteur pipette was quickly removed and the cap was placed immediately on the mouth of the 50 ml tube without removing the parafilm. The particles were spun down at 5000 rpm for 2 minutes, washed 3 times and resuspended in 1 ml deoxygenated PBS. These steps were performed quickly to minimize equilibration of deoxygenated PBS with atmospheric oxygen. 500 µl of these non-opsonized particles were aliquoted and stored at 4 °C. To opsonize particles, 5 µl of Rabbit Anti-BSA antibody (ICL labs, Portland, OR) was added to remaining 500 µl of non-opsonized particles and allowed to rotate for 90 minutes at 37 °C. Particles were spun down at 5000 rpm for 2 minutes and washed 3 times with deoxygenated PBS. Opsonized particles were resuspended in 500 µl of deoxygenated PBS and stored at 4 °C. Labeling efficiency was tested in a similar manner as described above. Due to the sensitivity of H_2HFF to auto-oxidation, its ability to oxidize upon H_2O_2 addition was tested for each batch of particles. 10 µg of labeled particles were suspended in 500 µl PBS and imaged at 488nm/510 nm on a Nikon Ti Eclipse epifluorescence microscope. 0.5 M H_2O_2 was added to fully oxidize the H_2HFF to check for oxidative capacity of H_2HFF and set imaging parameters. H_2HFF labeled particles were used within 48 hours of preparation due to auto-oxidation during storage at 4 °C.

To detect ROS in a phagosome using dihydrorhodamine-123 (DHR), latex particles were labeled with DHR. 50 µl of a 2.59% aqueous suspension of 3 µm amino latex particles was

suspended in 500 µl of PBS and centrifuged at 5000 rpm for 2 minutes. The pellet was dissolved in 450 µl of 0.1 M $NaHCO_3$, pH 8.5. To this 50 µl of DHR (20 mg/ml) was added and the tube was wrapped in aluminum foil and set on a rotator for 2 hours at room temperature. The tube was centrifuged, supernatant aspirated and pellet dissolved 1000 µl of 0.1 M glycine in PBS and again centrifuged. The last step was repeated twice following which the pellet was resuspended in 40 µl of sterile PBS. The particles were stored at 4 °C and used on the same day due to auto-oxidation of DHR

2.8.2: Phagosomal H_2O_2 detection

To detect H_2O_2 in a phagosome cells were incubated with 10 µM Peroxy-Fluor 6 AM (PF6-AM) for 30 minutes. With dye in the media, cells were exposed to 20 µg/cm^2 3 µm opsonized amorphous silica particles and imaged at 488nm/510 nm on a Nikon Ti Eclipse epifluorescence.

2.8.3: Cytoplasmic-ROS detection

Cytoplasmic-ROS was detected by loading cells with 10 µM CM-H_2DCFDA (Life Technologies, OR) in complete medium for 30 minutes at 37 °C following which cells were washed twice and incubated in CO_2 independent medium. Cells were exposed to either opsonized or non-opsonized latex or 3µm amorphous silica particles and imaged using 488nm/510nm A1R confocal microscope.

2.8.4: Cytoplasmic and mitochondrial H_2O_2 detection

Cells transiently expressing either roGFP2-Orp1 or mito-roGFP2-Orp1 were exposed to either opsonized or non-opsonized latex or 3µm amorphous silica particles. Dual excitation and

single emission ratiometric imaging of roGFP2 was done by exciting cells at 405 nm and 488 nm while collecting emission using 525/50 nm bandpass filter on Nikon A1R confocal microscope.

2.9: Cell Death Assays

2.9.1: Bid activation

To detect activation of Bid, MH-S cells stably expressing Bid-FRET probe were exposed to 50 μg/cm^2 crystalline silica and imaged over time. FRET imaging was done using a CFP-YFP FRET filter set with excitation at 436 nm and emission at 480 nm and 535 nm for CFP and YFP-FRET respectively on a Zeiss Axiovert epifluorescence microscope.

2.9.2: Bax activation

To detect Bax activation and mitochondrial localization MH-S cells transiently expressing GFP-Bax were exposed to either 30 μg/cm^2 3 μm amorphous silica particles or 1 μM Staurosporine and imaged at 488nm/510 nm on a Nikon Ti Eclipse epifluorescence microscope. To simultaneously detect any alteration in mitochondrial membrane potential cells were pre-loaded with TMRE.

2.9.3: Smac release

To detect release of mitochondrial intermembrane space protein in to the cytoplasm MH-S cells were transfected with Smac-mcherry and exposed to 1 μM staurosporine. Cells were at 562nm/624nm on a Nikon Ti Eclipse epifluorescence microscope.

2.9.4: Mitochondrial membrane potential

Mitochondrial transmembrane potential (ΔΨm), was measured using the potentiometric dye TMRE. In order to correlate the dynamics of caspase activation with changes in

mitochondrial transmembrane potential ($\Delta\Psi m$), MH-S cells were plated in a Bioptechs dish and then incubated with 45 nM Tetramethyl rhodamine ester (TMRE, Invitrogen, Carlsbad, CA) for 20 minutes in complete media. After 20 minutes, the cells were washed two times with complete media and then 1 ml of CO_2 independent media without serum. To relate the timing of hyperpolarization to caspase activation, cells expressing either the initiator or the effector caspase FRET probe were labeled with TMRE as indicated above. Cells were at 562nm/624nm on a Nikon Ti Eclipse epifluorescence or on a Zeiss Axiovert microscope.

2.9.5: Caspase-FRET

MH-S macrophages stably expressing either the initiator or effector caspase FRET probes were exposed to 50 $\mu g/cm^2$ crystalline silica. FRET imaging was done using a CFP-YFP FRET filter set with excitation at 436 nm and emission at 480 nm and 535 nm for CFP and YFP-FRET respectively on a Zeiss Axiovert epifluorescence microscope.

2.9.6: Phosphatidylserine exposure

To determine when surface exposure of phosphatidyl serine (PS) occurs, 30 ng/500 µl Annexin V-FITC (BD Biosciences, San Jose, CA) was added to cells cultured in CO_2 independent media. The probe was left in the medium throughout the experiment. This generated weak background fluorescence, but the concentration of the probe at the membrane of apoptotic cells was easily visualized above this background. Cells were then exposed to 50 $\mu g/cm^2$ crystalline silica and DIC and fluorescence images captured at different time intervals.

2.9.7: Nuclear condensation

Changes in nuclear morphology and nuclear condensation were analyzed using the vital nuclear dye Hoechst 33342. Cells plated in complete RPMI medium were incubated with 5 μg/ml Hoechst 33342 for 30 minutes, washed two times with complete medium and then cultured in CO_2 independent medium. DIC and fluorescence images were taken every 30 minutes. This stained the nuclei that remained fluorescent throughout the experiment.

2.10: Pharmacological alterations

To measure drug induced mitochondrial hyperpolarization or depolarization, MH-S cells incubated with TMRE were treated with either 5 μg/ml Oligomycin or 10 μM FCCP respectively and imaged every minute. In order to inhibit the vATPase, cells loaded with FITC-dextran were exposed to different concentrations of Bafilomcyin A1 (25, 75 and 150 nM) for 30 minutes. For data presented here, 150 nM Bafilomycin A1 was used. Following this pre-treatment, cells were exposed to 3 μm opsonized silica particles and imaged every minute. NADPH oxidase was inhibited by exposing cells loaded with FITC-dextran to dipheneylene iodonium (DPI) at concentrations of either 5 or 10 μM. Cells were then exposed to 3 μm opsonized silica particles and imaged every minute.

2.11: Microscopy

Live cell microscopy was performed on a Nikon A1R confocal, Nikon Ti Eclipse epifluorescence microscope or Zeiss Axiovert 200 M epifluorescence microscope. Both Nikon microscopes were fitted with OKO lab temperature control microscope enclosures (OKO labs, Italy) and stage top dish incubators for temperature and humidity control (Pathology devices, MD). Both microscopes had motorized stages allowing imaging of multiple fields of view in a

well and multiple wells over time. Focus drift over time due to any temperature fluctuations was controlled by use of Nikon perfect focus system. The Nikon A1R confocal system was controlled by Nikon Elements software (Nikon instruments, Melville, NY) where as the Nikon Ti Eclipse epifluorescence microscope was controlled using Micromanger (Edelstein *et al.*, 2010). This software also facilitated with complex image acquisition routines as well as controlling the instrumentation. Image acquisition on Nikon Ti Eclipse epifluorescence microscope was done using an Andor iXon 897 EMCCD camera or an Andor Clara megapixel camera (Andor, South Windsor, CT).

Zeiss microscope was fitted with a Bioptechs stage top incubator (Bioptechs Inc, Butler, PA) to maintain a constant temperature. For this the cells were plated in a specialized bioptechs dish designed to fit in to the delta T stage holder of the system. Due to periodic focus drift due to any changes in temperature during time-lapse imaging focus was periodically checked and readjusted if necessary. Image acquisition on Zeiss fitted with a Hamamatsu Orca camera was done using Openlab software (Improvision, Lexington, MA). Images on all microscopes were acquired using a 1.4 NA Plan Apochromatic 60 X oil immersion lens.

2.12: Image quantification

All acquired data sets were opened in Fiji for quantification (Schneider *et al.*, 2012). For phagolysosomal dextran fluorescence measurements, a region of interest (ROI) was drawn around a particle and the mean pixel intensity (MPI) was measured for the TRITC and FITC channels for every time point. For nuclear fluorescence, an ROI was drawn on the nuclear region and the mean pixel intensity of FITC was measured. ROS generation in a phagolysosome with H_2HFF labeled silica or latex particles was quantified in a similar manner. CM-H_2DCFDA

fluorescence was measured by drawing an ROI over the entire cell and measuring MPI over time. TMRE fluorescence was measured by drawing a ROI around a cell and measuring mean fluorescence. Background fluorescence value of media was subtracted from mean fluorescence. For 2ex/1em imaging data, ratiometric image analysis was accomplished using an ROI over an individual cell to measure MPI of the 510 nm emission with 405 nm and 488 nm excitation. For FRET imaging data, ratiometric image analysis was accomplished using an ROI over an individual cell from the data of CFP and FRET emission channels. For ratiometric imaging the MPI of the background fluorescence was subtracted from the MPI values of the cells. The CFP/YFP ratio was obtained by exporting these values to Excel (Microscoft Corporation, Redmond, WA) and graphs were made using Prism (Graphpad Inc, La Jolla, CA). To generate pseudo-colored ratiometric images, the Ratio plus plugin for ImageJ was used to divide the CFP image set by the FRET image set or the 405 nm data by the 488 nm data. The spectrum look up table was assigned to the resulting ratiometric data set.

2.13: Electron microscopy

15×10^4 MH-S macrophage cells were plated on aclar in bioptech dishes overnight. RPMI cell culture medium was replaced with CO_2 independent medium and cells were either treated with 50 $\mu g/cm^2$ of silica for 4.5 hrs or left untreated. Cells were fixed in 2.5 % gultaraldehyde, 0.1 M sodium cacodylate, pH 7.3 for 30 minutes at room temperature. Primary fixed cells were washed with same buffer and fixed in 1% Osmium tetroxide, 0.1 M sodium cacodylate for 30 mins at 4ºC and washed. Cells were *en bloc* stained with 1% Uranyl Acetate in 70% ethanol for 1 hr at 4ºC and subjected to dehydration in ethanol gradient with propylene oxide used as a clearing agent. This was later embedded in Araldite 506. Ultrathin sections of

10nm were cut using diamond knife and stained with 1:1 Uranyl acetate: alcohol and Lead citrate. Elemental composition of particles was determined using X-rays at 100 keV on Zeiss EM910 120 keV scanning/transmission/analytical electron microscope.

Chapter 3: Silica phagocytosis causes apoptosis and necrosis by different temporal and molecular pathways in alveolar macrophages

3.1: Introduction

The intense cross-talk and signaling between various cells following silica exposure makes it difficult to pin-point a role or an importance of an event in initiating silicosis. The two prevalent theories behind development of fibrosis during silicosis is inflammation and cell death. There is substantial evidence that apoptosis of macrophages that take up silica particles plays a role in etiology of silicosis (Borges *et al.*, 2002; Wang *et al.*, 2003). Mice pre-treated with a pan-caspase inhibitor z-VAD-fmk to inhibit apoptosis show a reduction in both macrophage cell death and the collagenous deposits that indicate fibrosis following exposure to silica. We were therefore interested in understanding the process behind cell death in alveolar macrophages following silica particle uptake. Apart from macrophages, silica induced cell death has been shown in epithelial and endothelial cells (Thibodeau *et al.*, 2003; Santarelli *et al.*, 2004; Thibodeau *et al.*, 2004; Hu *et al.*, 2006; Costantini *et al.*, 2011; Sellamuthu *et al.*, 2011). Compared to epithelial and endothelial cells, macrophages are critical in establishing the inflammatory milieu within the lung. Thus macrophages were used to understand the mechanism underlying cell death following particle uptake. Throughout the study, we have used MH-S, an immortalized alveolar macrophage cell line derived from mice (Mbawuike and Herscowitz, 1989).

Apoptosis is a well-characterized process that can be initiated by various stimuli that activate either the extrinsic or the intrinsic pathway (Bossy-Wetzel *et al.*, 1998; Slee *et al.*, 1999; Goldstein *et al.*, 2005; Albeck *et al.*, 2008a). When alveolar macrophages are exposed to crystalline silica *in vitro*, the cells show a loss in mitochondrial membrane potential and

activation of caspases-9 and -3 (Shen *et al.*, 2001; Thibodeau *et al.*, 2003). Another mode of cell death is necrosis, which is characterized by the swelling of a cell and release of its contents into the external milieu, thereby causing tissue inflammation (Galluzzi *et al.*, 2007; Berghe *et al.*, 2010). Necrosis has been measured in cells exposed to crystalline silica by an LDH release assay in which an increase in LDH release was measured with increase in particle concentration (Vallyathan *et al.*, 1988; Englen *et al.*, 1990; Thibodeau *et al.*, 2004). Upon exposure to silica, whether apoptosis or necrosis contributes more towards silica induced cell death is not clear.

The best understanding of the events following exposure of macrophages to silica comes from studies by Thibodeau et al., that show cells to follow intrinsic cell death pathway. The earliest event to take place upon exposure of cells to crystalline silica is phagolysosomal leakage with caspase activation at a later time (Ross and Murray, 2004; Thibodeau *et al.*, 2004; Pelucchi *et al.*, 2006). However, the methods used in these studies measure the population average at different times following treatment with silica. The response is synchronized by the time of addition of silica to cells, but it was unknown if the cells respond in a synchronous manner. Thus the population approach does not provide a precise temporal relationship between various events at a single cell level. In this study we have utilized time lapse imaging in conjunction with fluorescent reporter probes to map the temporal sequence of molecular events that occur in individual cells exposed to crystalline silica particles. Information from single cell imaging can be helpful to create a hierarchy between various processes involved in cell death.

We find that apoptosis and necrosis occur with distinct temporal sequences, but the time when events associated with either process occurs varies significantly from cell to cell. Most cells exposed to silica undergo apoptosis. Single cell analysis has revealed a novel transient increase of mitochondrial membrane potential ($\Delta\Psi m$) at the initiation of apoptotic cell death.

Furthermore, caspase activation, cell blebbing and hyperpolarization of mitochondria during apoptosis occur essentially simultaneously, but many hours after leakage of phagolysosomes. A smaller proportion of cells underwent necrosis, characterized by swelling and a rapid mitochondrial depolarization without any caspase activation.

3.2: Investigation of silica particle uptake

A review of literature at the beginning of the work revealed that silica was proposed to result in cytotoxicity by either binding to the cell surface or upon getting internalized. The latter was interpreted from the evidence that silica caused phagolysosomal leakage (Nadler and Goldfischer, 1970; Kane *et al.*, 1980). The evidence that inhibition of silica particle uptake prevented cell death (Haberzettl *et al.*, 2008) and uptake could induce phagolysosomal leakage (Thibodeau *et al.*, 2004) was sufficient to further investigate silica particle uptake and its downstream effects. Thus, there was evidence that some particles got into cells, but the extent of particle uptake, the mechanism of recognition and uptake, nor the trafficking of phagosomes if particles were taken up by the normal phagocytic pathway was not well understood when this project was initiated. Since the particles used this study were not opsonized (not antibody labeled) but naked, the mechanism of cell-particle interaction was unknown. One possibility was the scavenger receptor (SR) that bind to negatively charged particles (SiOH groups are negatively charged in an aqueous environment) (Iyer *et al.*, 1996). Whether SR could bind silica particles and whether the engagement of SR would lead to particle uptake (Hamilton *et al.*, 2008) in a manner similar to Fc receptor recruitment with opsonized particles was not known. Many of the early studies relied on leukostat staining (Iyer *et al.*, 1996; Hamilton *et al.*, 2000), light

microscopy (Schins *et al.*, 2002) or flow cytometry based methods (Chao S K et al, 2001) to investigate particle-cell interaction, These methods could not distinguish binding from uptake.

To understand if silica particles were present inside the cell, MH-S alveolar macrophages were exposed to crystalline silica particles. Cells were fixed 1.5 hours after particle exposure, embedded in a resin, sliced and imaged using the electron microscope. Transmission electron microscope (TEM) images of cells show the presence of silica particles as dark particulate matter (Figure 3.1 A) that was not present in control. Due to the toughness of the particle it was difficult to get clean sections resulting in visible holes in the specimen. To confirm that small size particulate matter was silica, it was subjected to X-ray microanalysis, which can reveal elemental composition of the area in question (Figure 3.1 B). Both particles 1 and 2 (data for particle 2 not shown) show a characteristic peak at 1.741 keV indicating presence of silica. Large silica particles were displaced during the course of sectioning due to their toughness, leading to appearance of knife marks (Particle 2). Elemental analysis on a control area (Figure 3.1 C) did not give higher counts for silica at 1.741 keV confirming these peaks do not arise from embedding medium. Particle 1 gives a high count at 1.741 keV indicative of silica particles.

Published studies from members of our laboratory further confirmed particle uptake. In these experiments, naked crystalline silica particles were labeled with TRITC (red dye) and the cytoplasm of cells labeled with CMFDA (green dye). Cells were optically sectioned using confocal microscopy to visualize particles in the center of the cell (Gilberti *et al.*, 2008). Uptake of opsonized (antibody labeled) silica particles was confirmed in macrophages by exposing cells to these particles, fixing after various time points and exposing them to a secondary antibody conjugated to a fluorophore. The particles on the outside of the cells are accessible to the secondary antibody whereas the one on the inside of the cell are not. Hence the external particles

appear fluorescent; the internalized particles are not fluorescent whereas all the particles can be visualized by light microscopy. Using this assay, the maximum uptake of opsonized particles was observed within the first 10 minutes, which is consistent with literature on Fc receptor mediated uptake. After one hour 90% of antibody labeled particles were found to be internalized (Gilberti *et al.*, 2008). Since visualizing uptake of naked crystalline silica particles in real time was challenging, these were substituted by 3 μm spherical amorphous silica particles and actin localization around the particle confirmed particle phagocytosis (Costantini *et al.*, 2011).

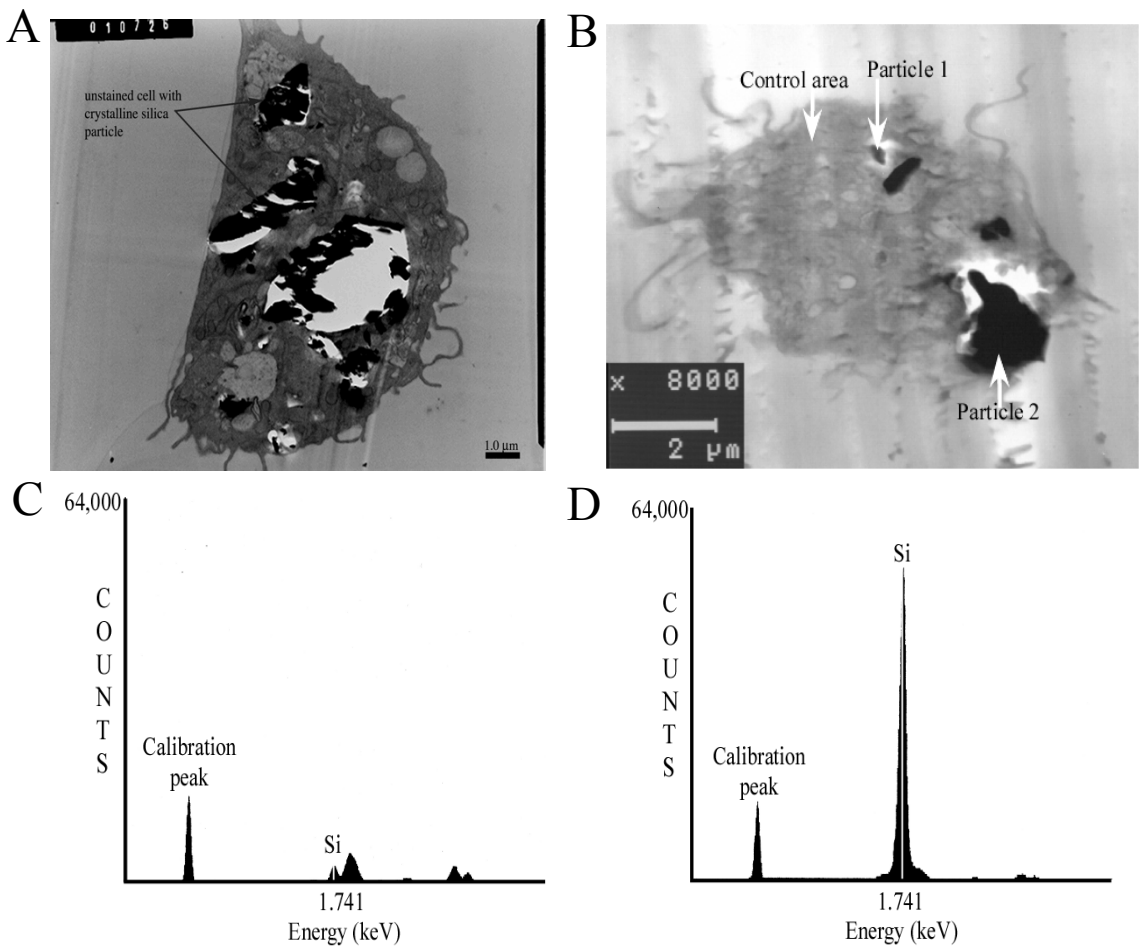

Figure 3.1: Internalization of crystalline silica particle as investigated by electron microscopy

(A) Following exposure of silica particles for 1.5 hours, fixing, embedding and sectioning, TEM analysis show particulate matter in the cytoplasm. Sectioning with glass knife resulted in breaking of crystalline silica particles. (B) EM elemental microanalysis confirmed that the particles observed are silica and not an EM artifact. (C and D) Both particles 1 and 2 in B) show a peak at 1.741 keV characteristic of silica.

3.3: Investigation of phagolysosomal leakage in macrophages exposed to silica

Thibodeau et al., have shown leakage of FITC-dextran pre-loaded into endosomes into the cytoplasm at one hour of crystalline silica treatment (Dauber *et al.*, 1980; Gardner, 1984; Thibodeau *et al.*, 2003). To determine more precisely the time when leakage occurs and the size of the pores through which molecules can pass into the cytoplasm, cells were pre-loaded with either 4 or 70 kD FITC-dextran and then imaged over time after addition of crystalline silica particles. Individual cells were tracked for phagolysosomal leakage following particle-cell interaction. FITC-dextran is endocytosed by cells following which it gets redistributed into endolysosomal vesicles where due to low pH the FITC fluorescence is quenched. It should be made clear that quenching does not mean a complete loss of fluorescence but rather a relative decrease in fluorescence in endolysosomal vesicles due to a low pH (4-5.5) when compared to neutral pH in cytoplasm. When a silica particle is phagocytosed by a macrophage, the phagosome containing a silica particle will fuse with endolysosomes to form a terminal vesicle called the phagolysosome. Upon phagolysosomal leakage, FITC-dextran will redistribute into the cytoplasm resulting in unquenching of FITC fluorescence due to the neutral pH of the cytoplasm. A 4 kD dextran can passively diffuse into the nucleus via the nuclear pore complex whereas 70 kD dextran cannot. Therefore, it was expected that upon leakage of 4 kD FITC-dextran, an increase in fluorescence in both the cytoplasm and nucleus is expected whereas with 70 kD FITC-dextran an increase in FITC-dextran fluorescence is only expected in the cytoplasm.

Following exposure of macrophages to crystalline silica and widefield imaging at 5 minute intervals, leakage of both 4 kD (Figure 3.2 A) and 70 kD FITC-dextran could be seen within 30 minutes (Figure 3.2 B). With 4 kD FITC-dextran there was an increase in both cytoplasmic and nuclear fluorescence, consistent with the cut-off limit for passive diffusion

through nuclear pores. In cells loaded with 70 kD FITC-dextran, there was labeling of the cytoplasm, but not the nucleus. Since not all vesicles leak, quantification of the cytoplasmic fluorescence increase will be affected by the presence of intact vesicles. This problem was minimized by the increased emission from fluorescein as it moved from acidic vesicles to the more pH neutral cytoplasm. A measurable increase in cytoplasmic fluorescence could be detected as early as 30 minutes after crystalline silica addition (Figure 3.2 C and D).

In cells loaded with 70 kD FITC-dextran, a detectable increase in the FITC fluorescence around the crystalline silica particles was also observed at 45 minutes (Figure 3.2 E and F). This is likely to be due to an increase in the pH of phagolysosomal compartments arising from equilibration of the contents with the cytoplasm as the vesicles become permeabilized. The time of initiation of FITC-dextran leakage varied from cell to cell. Cells were seen leaking as early as 30 minutes after addition of crystalline silica particles but some cells took as long as 135 minutes to begin leaking (Figure 3.2 G and H). The data show a gradual increase in cytoplasmic FITC-dextran fluorescence over time in all cells and eventual plateauing of the signal. At this point, no more punctate vesicles were observed in the cells indicating that either the entire endolysosomal compartment has become permeabilized or the cytoplasmic fluorescence is too high to visualize them. Averaging over many cells shows that leakage mostly occurred over a 2 hour period, starting about 30 minutes after crystalline silica addition (Figure 3.2 I). From the same set of data, individual cells were quantified based on the time that leakage was initiated (Figure 3.2 J). This clearly demonstrates the variability in the timing of leakage with 60% of the cells leaking between 60 and 105 minutes after particle addition.

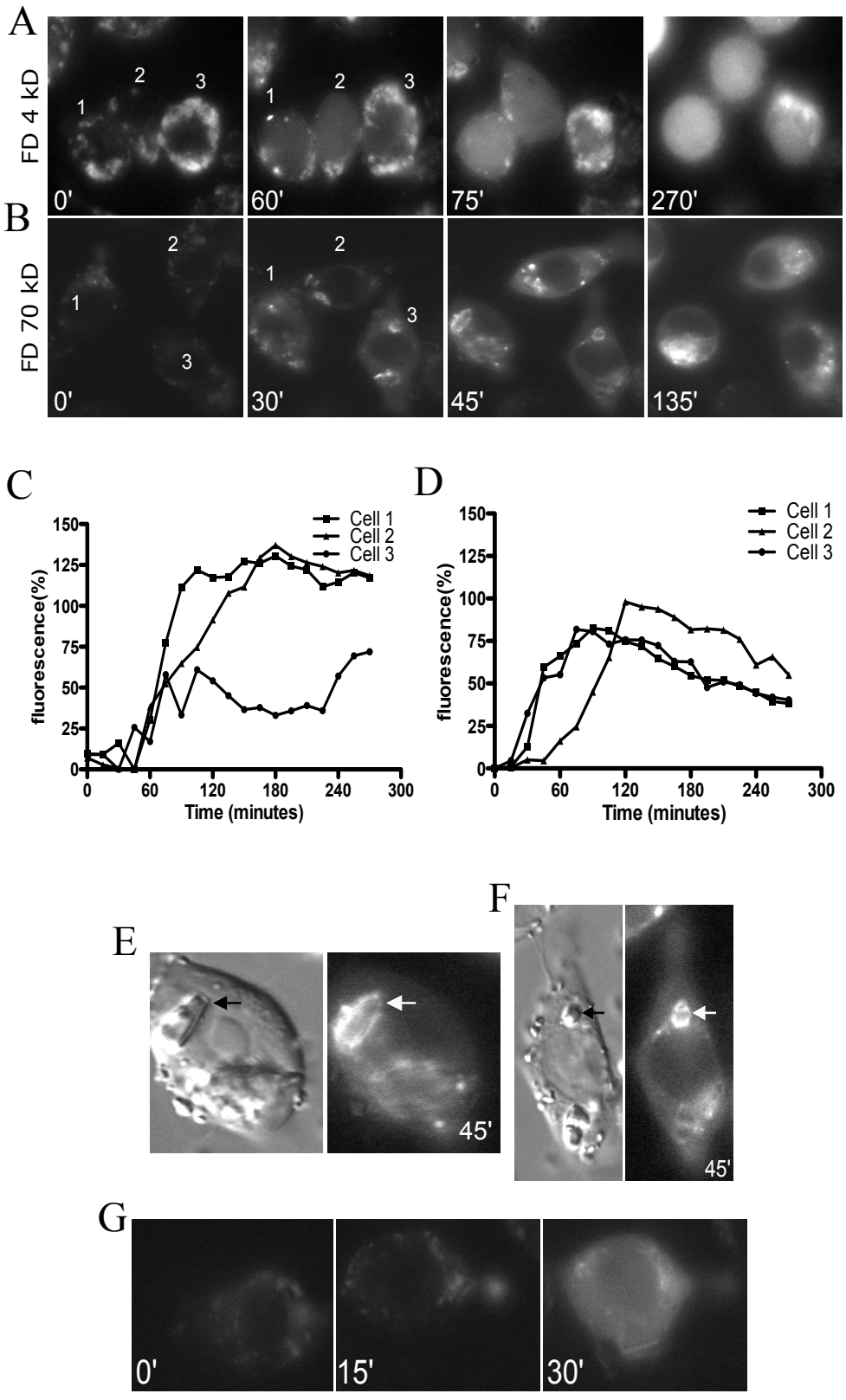
A
FD 4 kD
1
2
3
0'
60'
75'
270'
B
FD 70 kD
1
2
3
0'
30'
45'
135'
C
fluorescence(%)
Time (minutes)
Cell 1
Cell 2
Cell 3
D
fluorescence(%)
Time (minutes)
Cell 1
Cell 2
Cell 3
E
45'
F
45'
G
0'
15'
30'

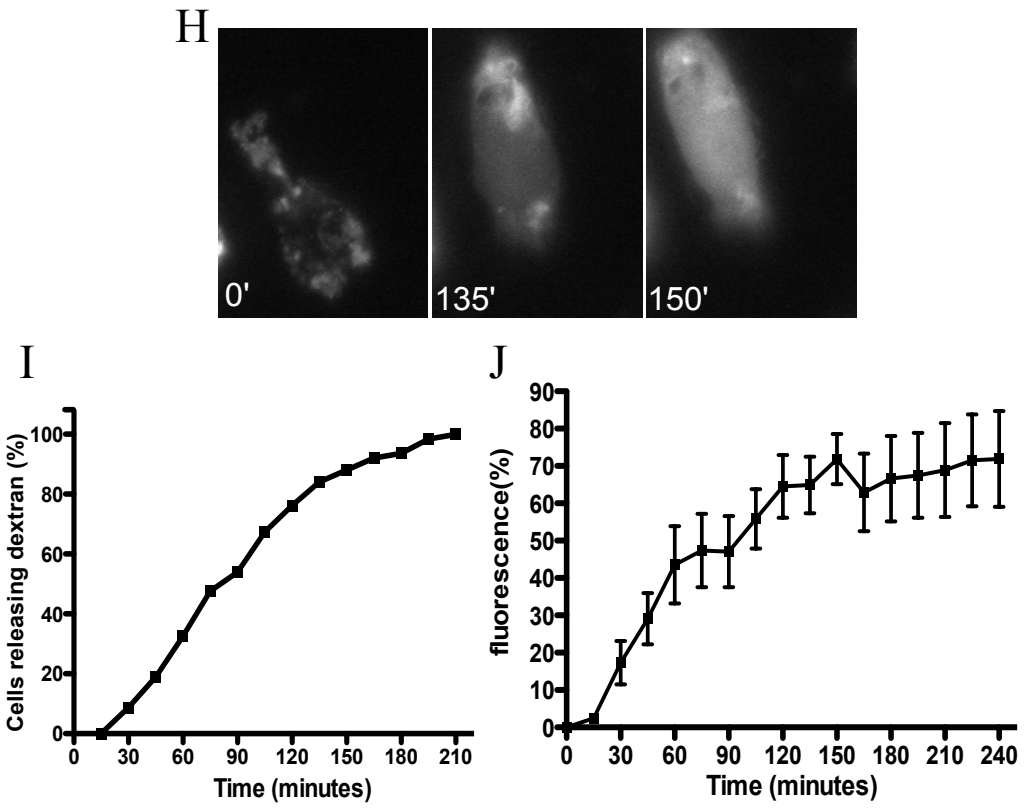

Figure 3.2: Phagolysosomal leakage is the earliest event to occur after exposure to silica

(A and B) MH-S cells were loaded for 2.5 hours with either 4 kD (A) or 70 kD FITC-dextran (B) to label endolysosomal compartments. Upon addition of crystalline silica cells were imaged 5 minutes apart using an epifluorescence microscope. After crystalline silica addition, 4 kD FITC-dextran moves to both the cytoplasmic and nuclear compartments (A), whereas 70 kD FITC-dextran is only found in the cytoplasm (B). The fluorescence increase was quantified as percent increase over the time with respect to 0 hour in the nuclear region for 4 kD FITC-dextran (C) and the whole cell for 70 kD FITC-dextran (D). (E and F) In cells loaded with 70 kD FITC-dextran an increase in fluorescence was observed around silica particles as shown by arrows indicative of an increase in the pH of the permeabilized phagolysosome. Because 70 kD FITC-dextran cannot enter nucleus the increase in fluorescence is only observed in the cytoplasm. (G and H) Release of dextran into the cytoplasm can occur at different times as shown by a cell which shows

cytoplasmic 4 kD FITC-dextran fluorescence early (G, 30 minutes) or late (H, 150 minutes). (I) Phago-lysosomal leakage occurred began to increase between 15 and 30 minutes and continued until plateauing about 120 minutes later. Data is represented as a mean of percent increase in the fluorescence intensity $\pm$ S.E.M from 10 separate experiments. (J) From these 10 experiments, individual cells were analyzed for the time at which they first show an increase in fluorescence over background indicating the start of leakage. Although leakage began within 30 minutes in some cells, 60% of cells show leakage between 60 – 105 minutes.

3.4: Apoptotic cells undergo transient mitochondrial hyperpolarization

Mitochondria are key players in events leading to cell death by apoptosis. Some changes in mitochondrial function have been found following crystalline silica treatment using approaches which provide an average value for an asynchronous population of cells (Shen *et al.*, 2001; Borges *et al.*, 2002; Thibodeau *et al.*, 2003). For our single cell time-lapse approach, cells were loaded with the cell permeable cationic potentiometric dye tetramethylrhodamine ester (TMRE) that partitions across the mitochondrial membrane based on the charge across the inner mitochondrial membrane. The greater the mitochondrial membrane potential ($\Delta\Psi m$), the greater the fluorescence observed (Loew *et al.*, 1993). During apoptosis, mitochondrial membrane potential collapses (mitochondrial depolarization) resulting in a decrease in TMRE fluorescence (Ly *et al.*, 2003). Alternately, there have been instances where a transient increase in TMRE fluorescence has been observed resulting from an increase in mitochondrial membrane potential (mitochondrial hyperpolarization) (Banki *et al.*, 1999; Perl *et al.*, 2004). We report it for the first time with silica.

TMRE labeled cells were exposed to 50 $\mu g/cm^2$ crystalline silica and imaged over time. There was little change in fluorescence for about 5 hours and then the fluorescence signal from individual cells would rapidly increase (hyperpolarization) and then slowly decrease until reaching a background level characteristic of depolarized mitochondria (Figure 3.3 A). The cells that showed hyperpolarization were simultaneously observed to be undergoing membrane blebbing in the differential interference contrast (DIC) image. Most cells went through a phase of hyperpolarization, but the time at which cells began to show hyperpolarization was quite variable ranging from 330 minutes to 1100 minutes after silica addition (Figure 3.3 B).

Hyperpolarization is not a commonly observed feature of the apoptotic cell death pathway and TMRE is known to have possible artifacts. A high concentration of TMRE within the inner mitochondrial membrane can result in fluorescence quenching. If this was the case then during an actual mitochondrial membrane depolarization, there would be a decrease in the concentration of TMRE causing unquenching and an increase in TMRE fluorescence without an increase in membrane potential. This would give a false readout of mitochondrial hyperpolarization while mitochondria are actually getting depolarized. The concentration of TMRE used in this study (50 nM) is consistent with what is used in literature (Tait and Green, 2010) and below the concentration at which self-quenching is observed (400 nM and above) (Ehrenberg *et al.*, 1988). In order to verify that the hyperpolarization was due to an increase above normal $\Delta\Psi m$ and not an artifact of unquenching of TMRE, cells were treated with oligomycin, an F_1-F_0 ATP'ase (complex V) inhibitor of oxidative phosphorylation. This compound prevents protons from getting pumped back into the matrix space, resulting in hyperpolarization of mitochondria (vander Heiden *et al.*, 1997). When TMRE labeled MH-S cells were treated with oligomycin, there was an increase in TMRE fluorescence within 1 minute (Figure 3.3 C and E). To test the sensitivity of TMRE towards loss of $\Delta\Psi m$, FCCP, a nonspecific protonophore and uncoupler of oxidative phosphorylation, was added to cells loaded with TMRE (vander Heiden *et al.*, 1997). Upon addition of FCCP, TMRE fluorescence decreased immediately indicating mitochondrial depolarization (Figure 3.3 D and F). To confirm that the increase in TMRE fluorescence observed with widefield imaging was not due to aggregation of mitochondria during cellular contraction, multi-plane confocal imaging was performed. An increase in TMRE fluorescence was also observed in these images prior to cellular contraction (Figure 3.3 G-H). Thus cells go

through a period in which mitochondrial function is altered to generate excessive trans-membrane potential before they become depolarized.

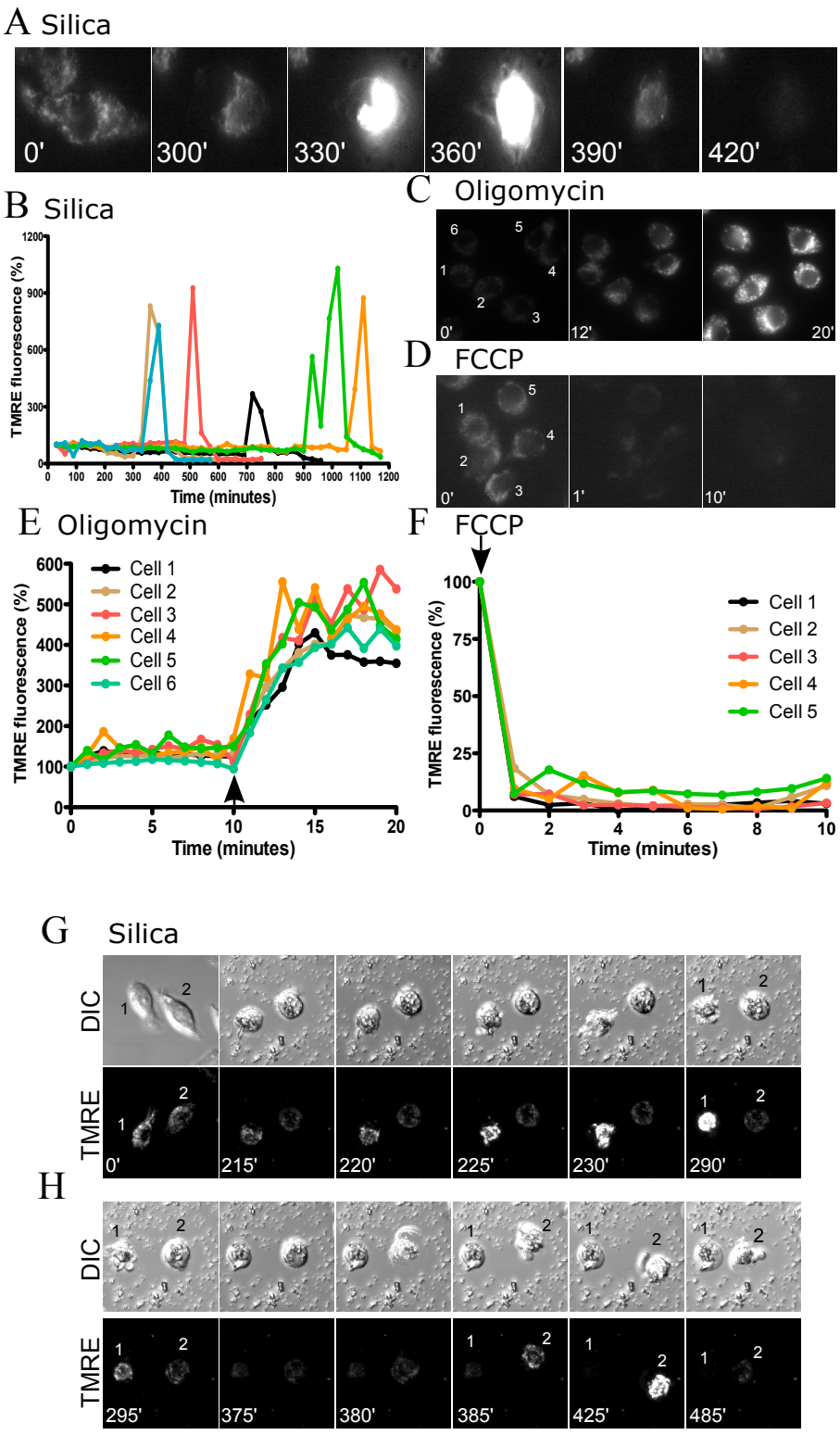

Figure 3.3: Mitochondria become transiently hyperpolarized in cells exposed to crystalline silica particles

Cells treated with TMRE were exposed to crystalline silica particles and imaged every 30 minutes to detect changes in mitochondria membrane potential (ΔΨm). Panel A shows a single cell that undergoes an increase in TMRE fluorescence at 330 minutes (hyperpolarization). Panel B is the quantification of TMRE fluorescence from 6 different cells over time after crystalline silica treatment. (C) Confirmation that mitochondrial hyperpolarization was not due to TMRE unquenching was obtained by treating cells with F_1F_0 ATPase inhibitor oligomycin, which caused a gradual increase in TMRE fluorescence. (E) Quantitative data for these six cells represents this trend. (D) Mitochondrial depolarization was confirmed by adding FCCP, a protonophore and uncoupler of mitochondrial oxidative phosphorylation. Cells immediately lose their fluorescence upon addition of FCCP. (F) Quantitative data for these five cells represents this trend. All images were captured at 1-minute interval. Arrows in Charts E and F indicates addition of Oligomycin and FCCP respectively. Cells were labeled with TMRE, exposed to silica particles and imaged every 5 minutes to detect changes in mitochondria membrane potential (ΔΨm). Seven slices were captured at each time point and shown as a maximum Z projection. (G) Mitochondria become hyperpolarized in cell 1 at 223 minutes remain hyperpolarized until 290 minutes and then depolarize. (H) Cell 2 shows a similar pattern with hyperpolarization from at 385-485 minutes.

3.5: Initiator and effector caspase activation occurs at the same time as mitochondrial hyperpolarization and cell blebbing

Crystalline silica exposure has been shown to cause activation of both caspase-9 and 3 in alveolar macrophages (Iyer *et al.*, 1996; Shen *et al.*, 2001; Thibodeau *et al.*, 2003; Rimal *et al.*, 2005). The temporal relationship between changes in mitochondrial membrane potential ($\Delta\Psi m$) and caspase activation or changes in cellular morphology during apoptosis has not been examined. To relate the timing of mitochondrial changes to other apoptotic events, MH-S cells were transfected with either initiator (caspase 9) or effector (caspase 3) FRET (Förster Resonance Energy Transfer) reporter probes and cells expressing these probes were isolated clonally (Tyas *et al.*, 2000; Kawai *et al.*, 2004). Förster Resonance Energy Transfer (FRET) based caspase sensors contain a substrate sequence IETD or DEVD specific for either caspase-9 or -3 respectively flanked by two different fluorescent proteins. When expressed in cells, the probe is fluorescent in the channels associated with the two fluorescent proteins. In addition, FRET occurs between them such that excitation of the shorter wavelength probe results in non-radiative energy transfer to the longer wavelength probe due to its close proximity resulting in fluorescent emission in both channels. For example, Figure 3.4 A shows a construction of an initiator caspase sensor where Cyan fluorescent protein (CFP) and Yellow fluorescent protein (YFP) are linked by the amino acid sequence IETD, a substrate for caspase-9. Because CFP and YFP are separated by a distance of only 10 nm, when CFP is excited by 433 nm light, there is both 475 nm emission from CFP and non-radiative excitation of YFP resulting in an emission at 535 nm. Upon activation of caspase-9, the linker sequence is cleaved so that CFP and YFP are now able to diffuse apart. This will prevent FRET from occurring and thus a decrease in the 535 nm emission of YFP and an increase in the 475 nm emission from CFP. While we have used a FRET sensor with the substrate sequence IETD, other studies have used sequence LEHD in their

FRET sensor to study caspase-9 activation (Kawai *et al.*, 2004; He *et al.*, 2006; McStay *et al.*, 2008). The FRET signal produced by the linked molecules is relatively weak and cannot be interpreted directly. Thus one needs to measure the ratio of the CFP and YFP signals to adjust for small inherent variations in signal strength from the two probes. It should be noted that the IETD sequence is also sensitive to caspase-8 and is used to detect caspase-8 activation following exposure of cells to TNF-α, which activates the extrinsic cell death pathway. In an earlier study caspase-8 activity was not reported upon addition to silica nor expected (Thibodeau *et al.*, 2003). Although this probe actually measures caspase 8 or 9 activity, but since silica does not activate caspase-8 this probe can be used to specifically measure caspase-9 activity.

Preliminary experiments were done in cells expressing either the initiator or effector caspase probes. Cells were exposed to crystalline silica following which they were imaged at 15 minute intervals. In these preliminary experiments, cells were not labeled with TMRE. Data from these experiments revealed a FRET change either during or after cell blebbing. A temporal heterogeneity was also observed between cells and most cells showed caspase activation after a period of 6 hours. It was therefore decided to image cells every 15 minutes for first 6 hours following which they were imaged 5 minutes apart for up to 15 hours. To limit variability between experiments as well as stress on cells after a transient transfection, cells stably expressing the FRET probe were clonally isolated and these were used for further experimentation.

Cells expressing the initiator caspase FRET probe were loaded with TMRE and then the cells were exposed to crystalline silica particles and imaged over time. An example of the progression of events for activation of caspase-9 is shown for a single cell in Figure 3.4B. No alterations in the probes were observed for about 300 minutes after crystalline silica particle

addition. At 335 minutes, the cell retracted and by 340 minutes started to bleb (Figure 3.4 B DIC). At 340 minutes, the TMRE fluorescence signal increased dramatically and the caspase-9 FRET reporter CFP/YFP ratio increased, indicative of caspase-9 activation. Mitochondrial hyperpolarization persisted for 15 minutes and then the $\Delta\Psi m$ decreased. Quantitative analysis of TMRE and FRET signals shows the extremely narrow window of time in which these two events are initiated (Figure 3.4 C). The first image where there was an increase in FRET ratio was also the first time point where there was a detectable increase in mitochondrial membrane potential. Since images were taken 5 minutes apart, this implies that the two events happen within 5 minutes of each other (Figure 3.4 D). Both events were also closely correlated with the start of cell membrane blebbing. In order to determine the consistency of this sequence of events, this analysis was extended to include multiple cells from multiple experiments. In each case (n=20), there was an overlap in the timing for initiator caspase activation (Figure 3.4 E) with an increase in $\Delta\Psi m$ (Figure 3.4 F) and blebbing.

A similar analysis was carried out to analyze the timing of effector caspase-3 activation relative to changes in the TMRE fluorescence and cell blebbing. For the cell shown in Figure 3.5 A, at 690 minutes the cell retracted and at 750 minutes began to bleb. Both the TMRE signal and the caspase-3 probe FRET ratio also began to increase at 750 minutes. Quantitative analysis of images confirms that the increase in hyperpolarization and effector caspase activation occurred in the same 5 minute time window (Figure 3.5 B and C). Similar events were observed in other cells where there was an overlap in the timing for effector caspase activation (Figure 3.5 D) with an increase in $\Delta\Psi m$ (Figure 3.5 E) and blebbing.

Examining the events in many cells, while initiator and effector caspase probe activation, cell morphology, and $\Delta\Psi m$ increase all occurred at the same time in each cell, the timing relative

to when crystalline silica was added varied dramatically between cells, ranging from 300–775 minutes. It could not be ascertained as to when silica was taken up, but presumably this was in the first 10 minutes as suggested by particle phagocytosis data (Costantini *et al.*, 2011) and our leakage data. Thus there is a difference in the time that each cell takes to initiate the changes associated with apoptosis, but every cell shows a similar critical time at which blebbing, mitochondrial hyperpolarization and caspase activation occurs. The data also suggests that following activation of the initiator caspase, the activation of effector caspase occurs quickly. This is the first study to our knowledge showing a temporal proximity of activation of these caspases during intrinsic apoptosis. This result is consistent with published work on extrinsic apoptosis initiated by TNF and TRAIL where activation of caspase 9, and caspase 3 overlap with each other (Albeck *et al.*, 2008a).

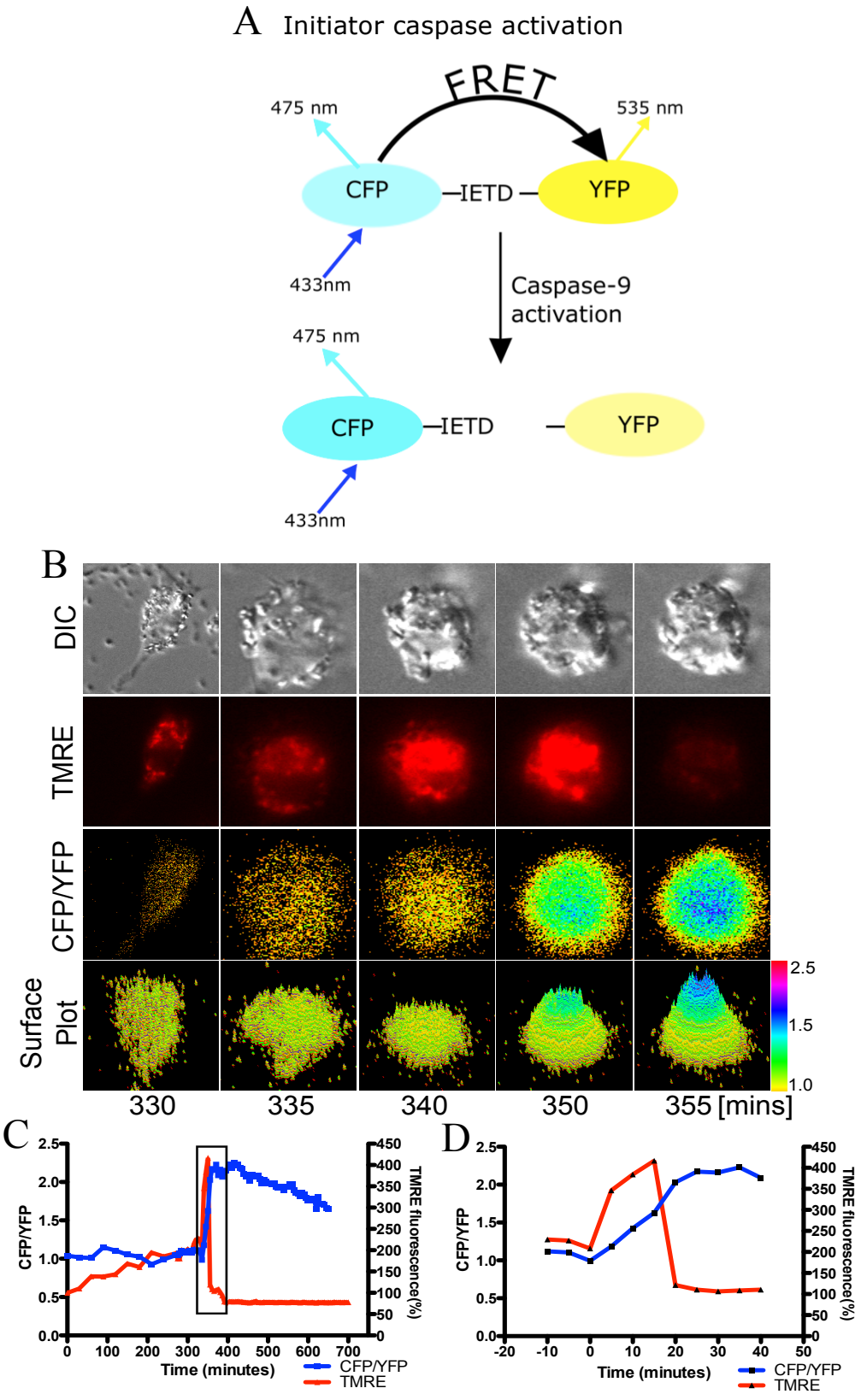
A
Initiator caspase activation
FRET
475 nm
535 nm
CFP
IETD
YFP
433nm
Caspase-9
activation
475 nm
CFP
IETD
YFP
433nm
B
DIC
TMRE
CFP/YFP
Surface Plot
2.5
1.5
1.0
330
335
340
350
355 [mins]
C
CFP/YFP
TMRE fluorescence(%)
Time (minutes)
CFP/YFP
TMRE
D
CFP/YFP
TMRE fluorescence(%)
Time (minutes)
CFP/YFP
TMRE

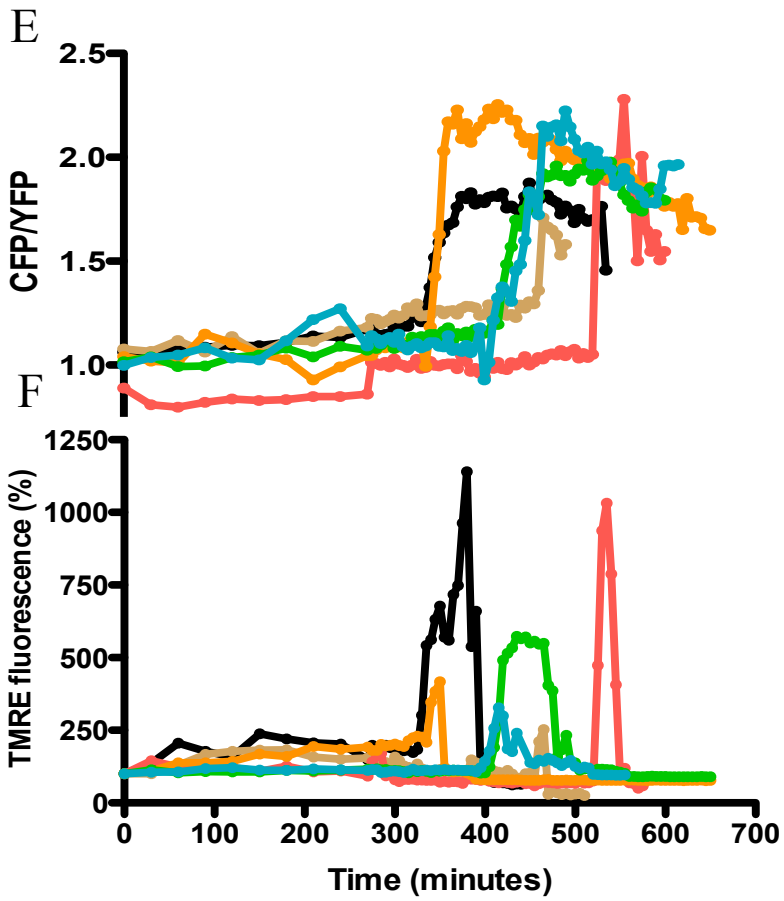

Figure 3.4: The timing of initiator caspase activation relative to mitochondrial membrane potential and cell morphology

(A) To understand caspase activation in real time, cells were transfected with a FRET caspase sensor for either caspase-9 or caspase-3. For caspase-9, the FRET pair is fused with IETD and for caspase-3, the FRET pair is fused with DEVD. Represented here is a FRET pair to detect caspase-9 activation. (B) MH-S cells expressing caspase 9-FRET probe were labeled with TMRE, exposed to 50µg/cm^2 of crystalline silica and then imaged every 30 minutes for 270 minutes and then every 5 minutes until the end of the experiment. At 330 minutes the cell was flattened and elongated with punctate mitochondrial fluorescence. It then rounded up at 335 minutes and began to bleb at 340 minutes. At the same time there was an increase in the TMRE fluorescence indicative of mitochondrial hyperpolarization and caspase activation that can be

seen in the series of pseudo colored CFP/YFP and a surface plot of the data. (C) Quantitative analysis of mitochondrial membrane potential and caspase activation shows that the events occur at the same time within the temporal resolution of the experiment (5 minutes). The caspase probe continues to increase for 150 minutes and then plateaus. Blebbing begins at the same time point where the other probes first show an increase. (D) Rectangular box in panel C) is expanded in panel D) with time 0 as a time point that precedes cell blebbing.

(E-F) Quantitative analysis of six representative cells expressing initiator caspase probe show similar changes as observed in B-D. In each cell represented by a similar colored line the increase in TMRE fluorescence and FRET ratio occur at the same time. Same trends were observed in a total of 15 cells that were quantified.

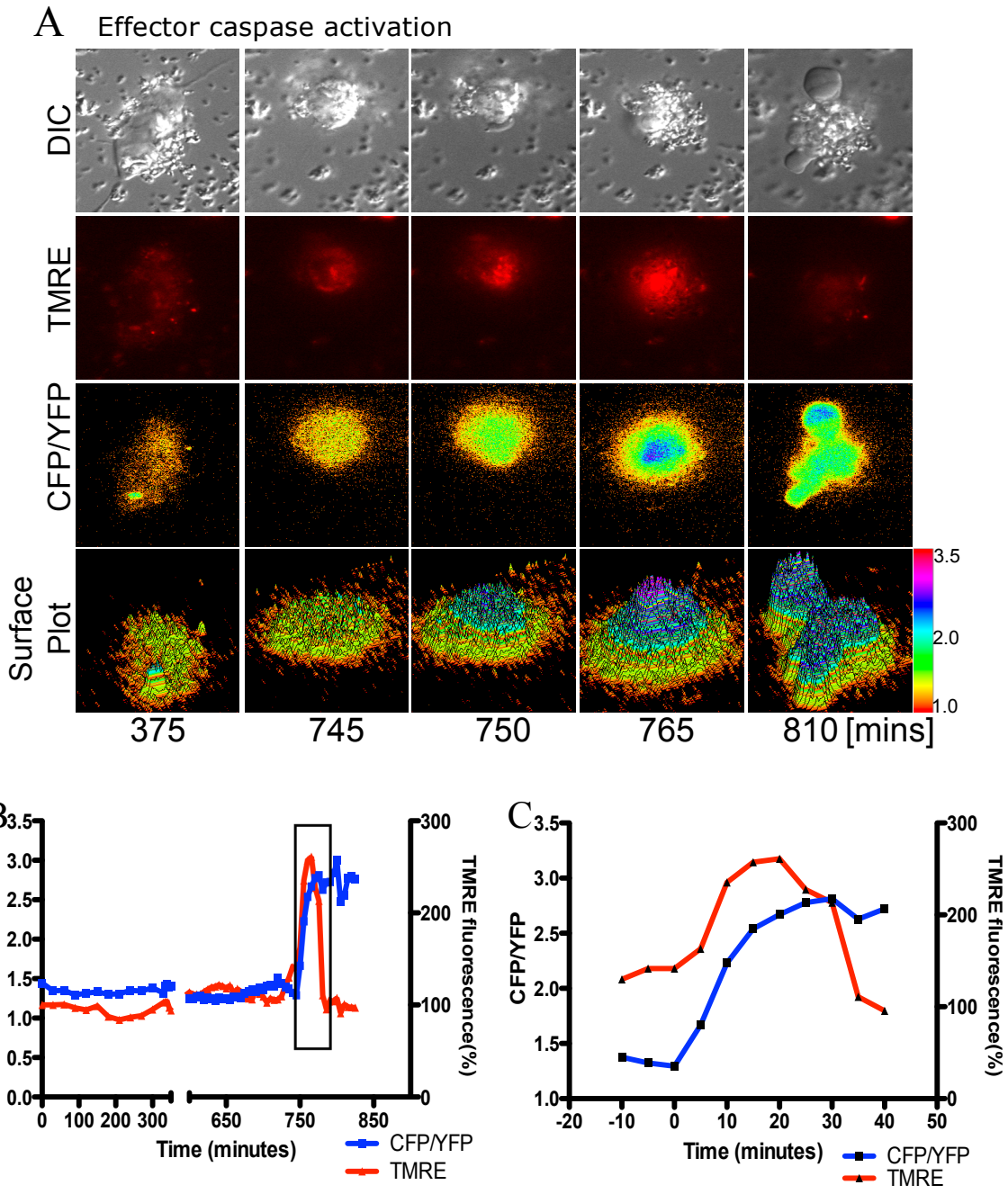
A
Effector caspase activation
DIC
TMRE
CFP/YFP
Surface Plot
3.5
2.0
1.0
375
745
750
765
810 [mins]
B
CFP/YFP
TMRE fluorescence(%)
Time (minutes)
CFP/YFP
TMRE
C
CFP/YFP
TMRE fluorescence(%)
Time (minutes)
CFP/YFP
TMRE

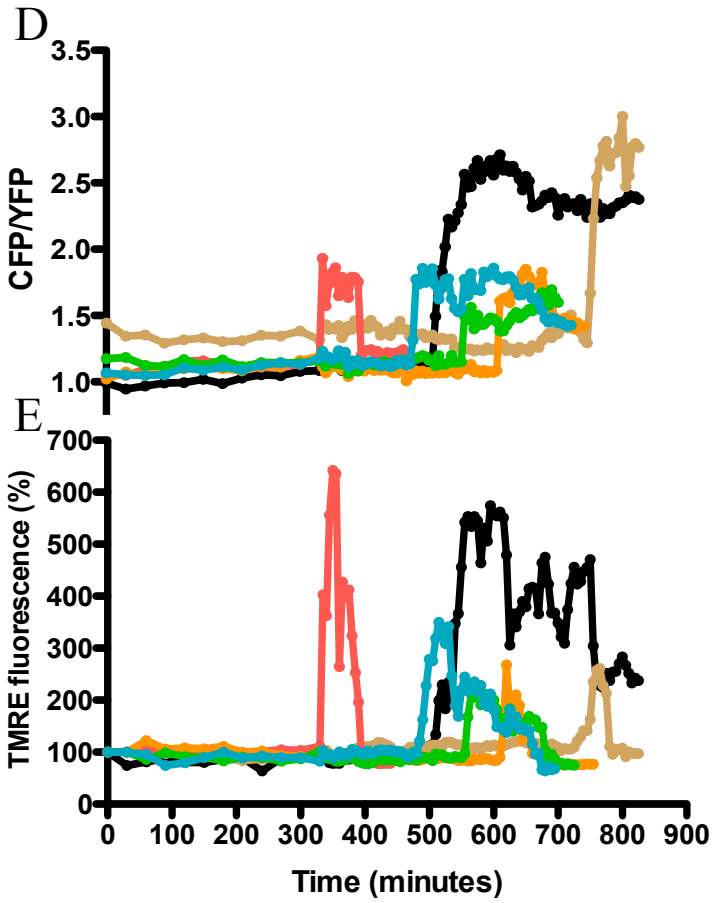

Figure 3.5: The timing of effector caspase activation relative to mitochondrial membrane potential and cell morphology

MH-S cells expressing Caspase-3- FRET probe were incubated with TMRE, exposed to 50μg/cm^2 of crystalline silica and imaged every 30 minutes for 330 minutes and then every 5 minutes till end of the experiment. (A) DIC, TMRE and CFP/YFP images represent any changes in cell morphology, mitochondrial physiology and FRET changes respectively. At 375 minutes a cell that was flat and elongated. The cell began to round up at 690 min and at 750 minutes cell began to bleb. At the same time, mitochondrial hyperpolarization and an increase in FRET ratio was detected. The mitochondrial hyperpolarization was sustained for 35 minutes and at 780 minutes the cell began to show a decrease in TMRE fluorescence indicative of mitochondrial depolarization. The data is also represented as surface plot that generates 3D view of the FRET

ratio increase in a cell. (B) Quantitative analysis of the images shows both mitochondrial hyperpolarization and caspase activation occur in close temporal proximity. (C) Rectangular box in panel B is the region magnified in this graph with time 0 as a time point that precedes cell blebbing. (D-E) Quantitative analysis of six representative cells expressing initiator caspase probe show similar changes as observed in A-C. In each cell represented by a similar colored line the increase in TMRE fluorescence and FRET ratio occur at the same time. Same trends were observed in a total of 23 cells that were quantified.

3.6: Cells that take up silica become Annexin V positive and undergo chromatin condensation

The phospholipid phosphatidylserine (PS) is restricted to the inner leaflet of the plasma membrane under normal circumstances. During apoptosis, phosphatidylserine is externalized to the outer leaflet of the plasma membrane. This change in membrane asymmetry is a gold standard in the field of apoptosis detection. The PS on the outer leaflet of the plasma membrane also is a signal for healthy macrophages to phagocytose an apoptotic cell (Daleke, 2007). Annexin V has a high affinity for PS and hence Annexin V conjugated to a fluorophore (example, Annexin V-FITC) is commonly used to detect PS externalization (Pfau *et al.*, 2004). Normal cells do not bind Annexin probes, while cells undergoing apoptosis show membrane staining.

Recently, it has been shown that the flipping of PS to the outer leaflet is mediated by caspase based inactivation of the flippase adenosine triphosphate type 11C (ATP11C) (Segawa *et al.*, 2014). The asymmetric distribution of the phospholipids on the outer and inner cell membrane is maintained by flippases (Daleke, 2007). We used Annexin V-FITC as a marker of PS flipping to determine when this event occurred relative to blebbing and caspase activation in silica treated cells. Cells were incubated in a low concentration of Annexin V-FITC following crystalline silica addition and imaged over time. At this low concentration, the concentrating effect of binding the probe to the membrane upon PS flipping produces a cell-associated signal much greater than the background from the media. Cells undergoing apoptosis show bright fluorescence around the cell membrane after they have started to bleb (Figure 3.6 A). Analysis of individual cells shows a temporal variation in PS flipping relative to membrane blebbing (Figure 3.6 B), however the sequence of events for every cell was still the same; a cell retracts, blebs and later becomes Annexin V positive while continuing to bleb. On average, it took 70 minutes after the start of blebbing for cells to become Annexin V positive. This temporal understanding of

Annexin V binding to cell membrane is of significance as studies have reported Annexin V to be an early marker of apoptosis. Our data shows that Annexin V is a late marker of apoptosis, which is consistent with the recently proposed mechanism of PS flipping that occurs following caspase activation (Segawa *et al.*, 2014).

Chromatin condensation has also been reported for cells undergoing apoptosis. Cells were loaded with vital nuclear dye Hoechst 33342 to visualize nuclei. Hoechst 33342 was found to be toxic to cells if they were frequently exposed to ultra violet light so the imaging interval was increased to 30 minutes. Upon crystalline silica treatment, no change in the nuclear morphology was observed until cells started to bleb. Chromatin condensation was observed approximately 60 minutes after blebbing (Figure 3.6 C). This is at approximately the same time, as cells become Annexin V positive.

The Annexin V assay is normally combined with propidium iodide, which is a non-membrane permeant nucleic acid binding dye. Following membrane leakage, propidium iodide crosses through the cell membrane and nuclear membrane to intercalate with the nucleic acids (both DNA and RNA). Since the DNA constitutes to be the major nucleic acid in the nucleus, the propidium iodide fluoresce the nuclear area stronger than the cytoplasm. PI does not detect apoptotic cells, as cells undergoing apoptosis are propidium iodide negative and Annexin positive. However once apoptotic cells die, they undergo secondary necrosis and the membrane becomes permeable. Thus propidium iodide detects both secondary necrotic cells following apoptosis (Annexin V positive and propidium iodide positive) or cells that directly undergo necrosis (Annexin V negative and propidium iodide positive). In macrophages that were incubated with Annexin V and propidium iodide and exposed to silica particles, Annexin V fluorescence (360 minutes) followed cell blebbing (300 minutes) for both cells 1 and 2. Cells did

not become propidium iodide positive till 510 minutes (cell 2) and 630 minutes (cell 1). Propidium Iodide positive fluorescence was associated with the nuclei that appear to have undergone nuclear fragmentation as visible by individual propidium iodide positive punctae within a single cell. The Annexin V-FITC fluorescence increased for cell 2 but not for cell 1 which could be due to binding of Annexin V-FITC to the PS in the inner side of the plasma membrane after cell membrane permeabilization during secondary necrosis (Figure 3.7 A). While most cells show these events, there were a few cells that did not become propidium iodide positive many hours after cell blebbing (Figure 3.7 B). Many experiments utilize propidium iodide as an end point measure of cell death. This data shows that depending on the cellular transition from apoptosis to secondary necrosis there will be a delay in obtaining a propidium iodide signal. Thus an actual timing of cell death will not be obtained with propidium iodide. Further, if propidium iodide fails to fluoresce the nuceli/fragmented nuclei, a true effect of an inducer will be under estimated. In necrotic cells due to membrane permeability, it would be expected that cells become Annexin V and propidium iodide positive. However, cells were found to become propidium iodide positive and after many minutes an intense membrane staining of Annexin V-FITC was observed showing a gradual process.

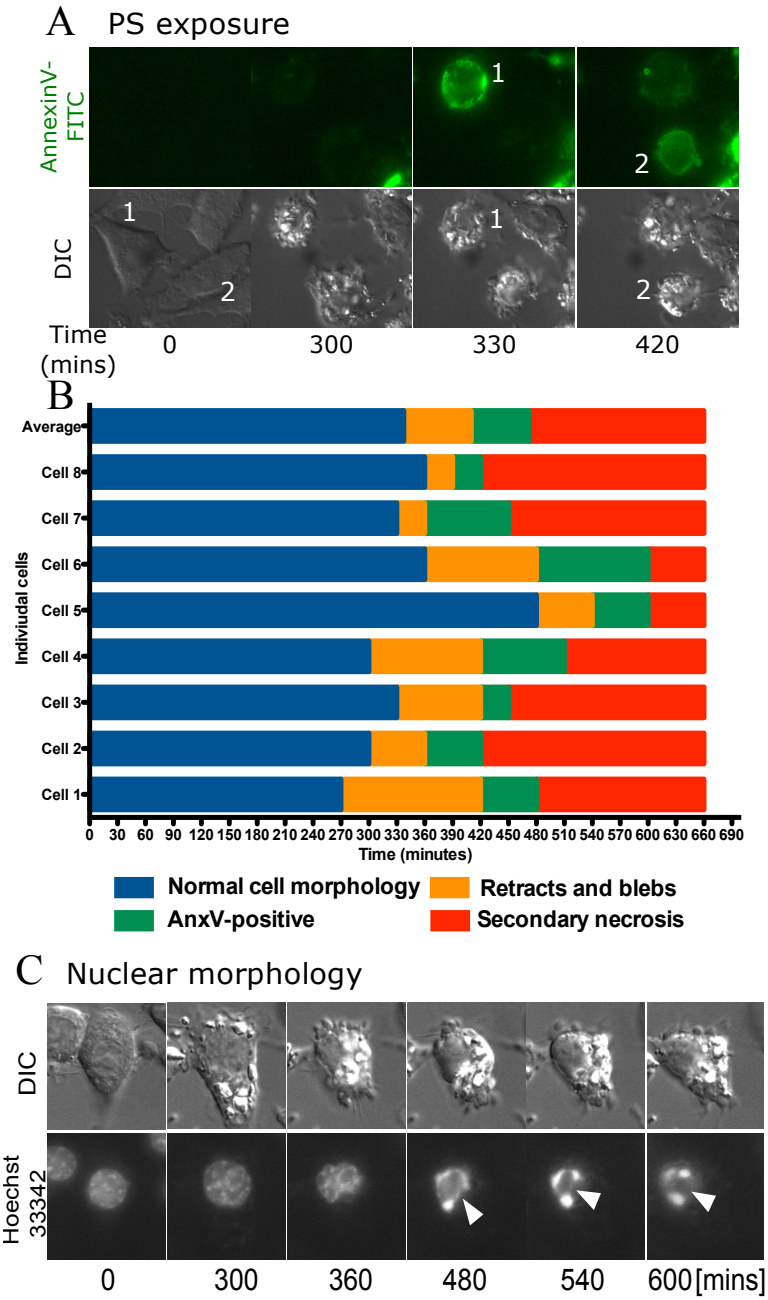

Figure 3.6: Cells undergoing apoptosis show phosphatidylserine exposure and nuclear condensation

(A) Cells were incubated with AnnexinV-FITC and then exposed to crystalline silica particles. AnnexinV-FITC fluorescence was seen only after the cells started to bleb. DIC images for cell 1 show rounding and blebbing at 300 minutes where as corresponding AnnexinV-FITC fluorescence is observed after cell starts to bleb at 330 minutes as marked by arrow. Similarly,

although, Cell 2 shows blebbing at 330 minutes (DIC), no visible AnnexinV-FITC fluorescence was seen till 390 minutes. (B) Comparison of the timing of AnnexinV-FITC binding versus morphological changes in the cell. There is variation in when blebbing and PS exposure occurs, but the order of events is the same in each cell. (C) Cells were incubated with Hoechst-33342 and imaged every 30 minutes to visualize any changes in the nucleus upon crystalline silica exposure. There was no change in the nuclear morphology until well after cell blebbing. Cells showed nuclear condensation 30-60 min after blebbing began.

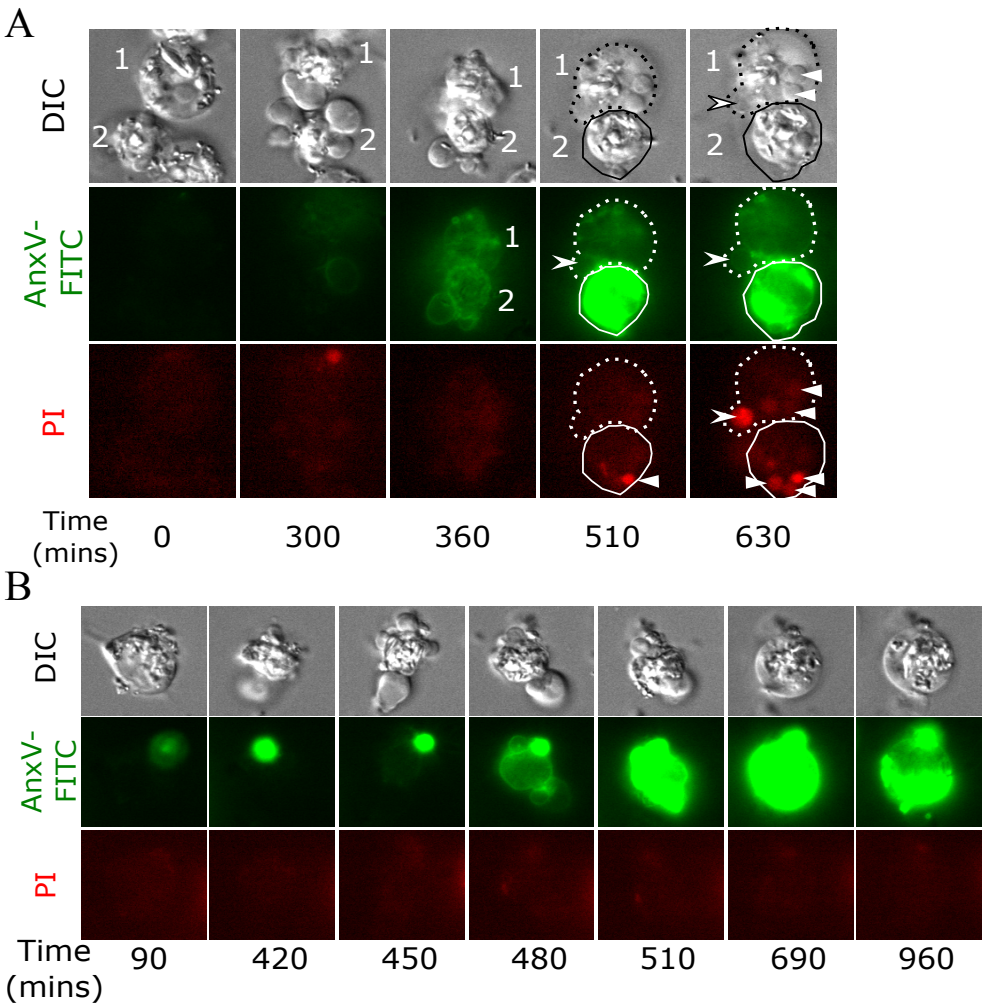

Figure 3.7: Annexin V- propidium iodide detects apoptosis after cell blebbing has initiated

(A and B) Cells were incubated with AnnexinV-FITC and propidium iodide and then exposed to crystalline silica particles. (A) AnnexinV-FITC fluorescence was seen only after the cells started to bleb at 300 minutes during which cells were not propidium iodide positive. Cell 1 does not acquire enough Annexin V-FITC signal compared to cell 2 at 360 minutes. Cells transition from apoptosis to secondary necrosis after 360 minutes. For cell 1, at 630 minutes the fragmented nuclei could be observed in the DIC images that are labeled with triangles. These fragmented nuclei are also fluorescent in the propidium iodide channel. The area labeled with an arrow does not show visible nuclei but still has a strong propidium iodide signal. Although fragmented

nuclei are not observed in DIC image for cell 2, it could be observed in the propidium iodide channel. (B) Although the cell represented here transitions from apoptosis as observed by cell blebbing at 420 minutes and Annexin V-FITC fluorescence from 480 minutes onwards, this cell did not get propidium iodide positive.

3.7: A small fraction of cells die by necrosis after silica exposure

Necrosis is a mode of cell death wherein a dying cell loses mitochondrial membrane potential, swells and then its contents begin to leak out. In the same population of crystalline silica treated cells that died by apoptosis, about 15% of cells died by necrosis (Figure 3.8 C). These cells do not bleb, do not show effector caspase activation or undergo mitochondrial hyperpolarization. Instead, they began to swell (Figure 3.8 A, DIC panel), lose mitochondrial $\Delta\Psi m$ (Figure 3.8 A, TMRE panel) and show no increase in the caspase reporter FRET ratio (Figure 3.8 A). The small decrease in the CFP/YFP ratio is likely due to leakage of the cytoplasmic contents and follows mitochondrial depolarization (Figure 3.8 B). Necrosis was more variable than apoptosis, occurring as early as 2 hours after crystalline silica addition and as late as 10 hours. Annexin V-FITC staining was not observed in cells undergoing necrotic cell death (Figure 3.8 D). Also, in cells undergoing necrosis, nuclear condensation as observed by Hoechst 33342 did not take place and there was no change in nuclear morphology (Figure 3.8 E). Following membrane swelling, propidium iodide labeled the nucleus in each cell and the nucleus was not fragmented (Figure 3.8 F). Thus some cells undergo necrosis after silica treatment, but the molecular pathway is clearly distinguishable from the apoptotic pathway.

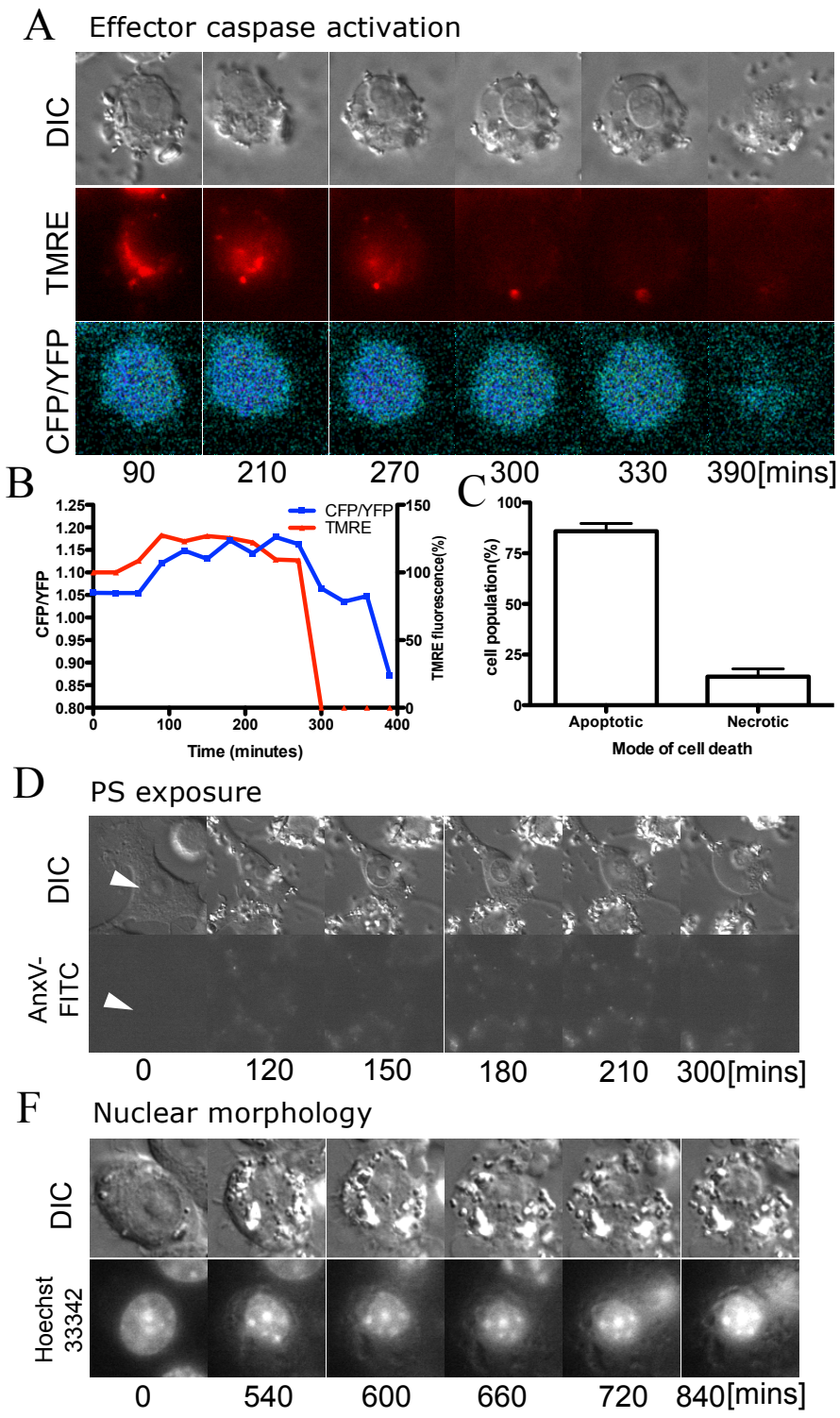
A
Effector caspase activation
DIC
TMRE
CFP/YFP
90
210
270
300
330
390[mins]
B
CFP/YFP
TMRE
CFP/YFP
TMRE fluorescence(%)
Time (minutes)
C
cell population(%)
Apoptotic
Necrotic
Mode of cell death
D
PS exposure
DIC
AnxV-FITC
0
120
150
180
210
300[mins]
F
Nuclear morphology
DIC
Hoechst 33342
0
540
600
660
720
840[mins]

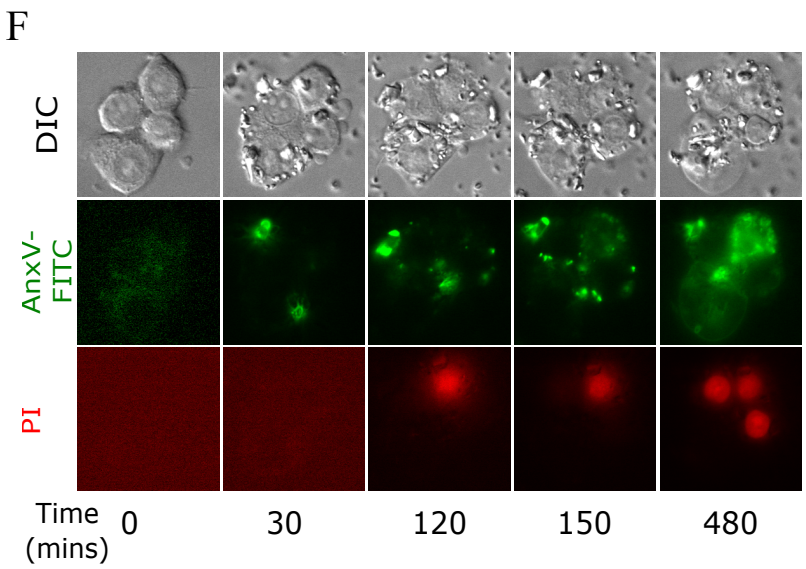

Figure 3.8: A small fraction of cells undergo necrosis upon exposure to silica

Some cells in the population undergo a distinct cell death process with hallmarks of necrosis rather than apoptosis. (A) Necrotic cells exhibit a swelling of cell membrane and nucleus with mitochondrial depolarization and no activation of the effector caspase as represented in the DIC, TMRE and the CFP/YFP images respectively. Similarly, for cells expressing the initiator caspase reporter probe there was no caspase activation observed (data not shown). (B) Quantitative analysis of these images show a decrease in TMRE fluorescence indicative of mitochondrial membrane depolarization during which there is no change in the FRET-ratio. (C) In cells expressing either of caspase reporter probes, approximately 15% of cells exposed to crystalline silica die by necrosis and 85% by apoptosis. Data of 444 cells from 12 separate experiments are shown as Mean $\pm$ S.E.M. Necrotic cells were identified by cell swelling (DIC) and then examined in the presence of either (D) Annexin V-FITC or (E) Hoechst 33342. (F) In cells incubated with a both Annexin V-FITC and propidium iodide and exposed to crystalline silica, Annexin V-FITC fluorescence does not appear on the cell membrane when the cell swells and

membrane permeabilization. Upon membrane permeabilization the propidium iodide labels the nuclei and the nuclei is not fragmented.

3.8: Temporal events during crystalline silica induced cell death

Integrating data from all the probes, we are able to establish a molecular pathway of events leading to cell death by either apoptosis or necrosis upon crystalline silica exposure to MH-S macrophages (Figure 3.9). The earliest apoptotic event that we can detect is the leakage of phagolysosomal compartments beginning around 30 minutes after exposure of cells to crystalline silica particles. Although this leakage begins as early as 30 minutes after crystalline silica addition, the downstream activation of initiator and effector caspases as well as the increase in mitochondrial membrane potential were not seen for at least another 3 hours. The timing of when these events start varies dramatically from cell to cell, but the pattern of events is very reproducible. Cell blebbing, an increase in mitochondria membrane potential and initiator and effector caspase activation all occurred within the same 5 minute time window. PS externalization and changes in nuclear morphology were observed to occur 30 minutes to two hours after the initiation of cell blebbing. Eventually the apoptotic cells underwent secondary necrosis in which they swelled and mitochondria depolarized. In cells undergoing necrosis, cells swell and mitochondria depolarize without any change in caspase activity, PS flipping and chromatin condensation.

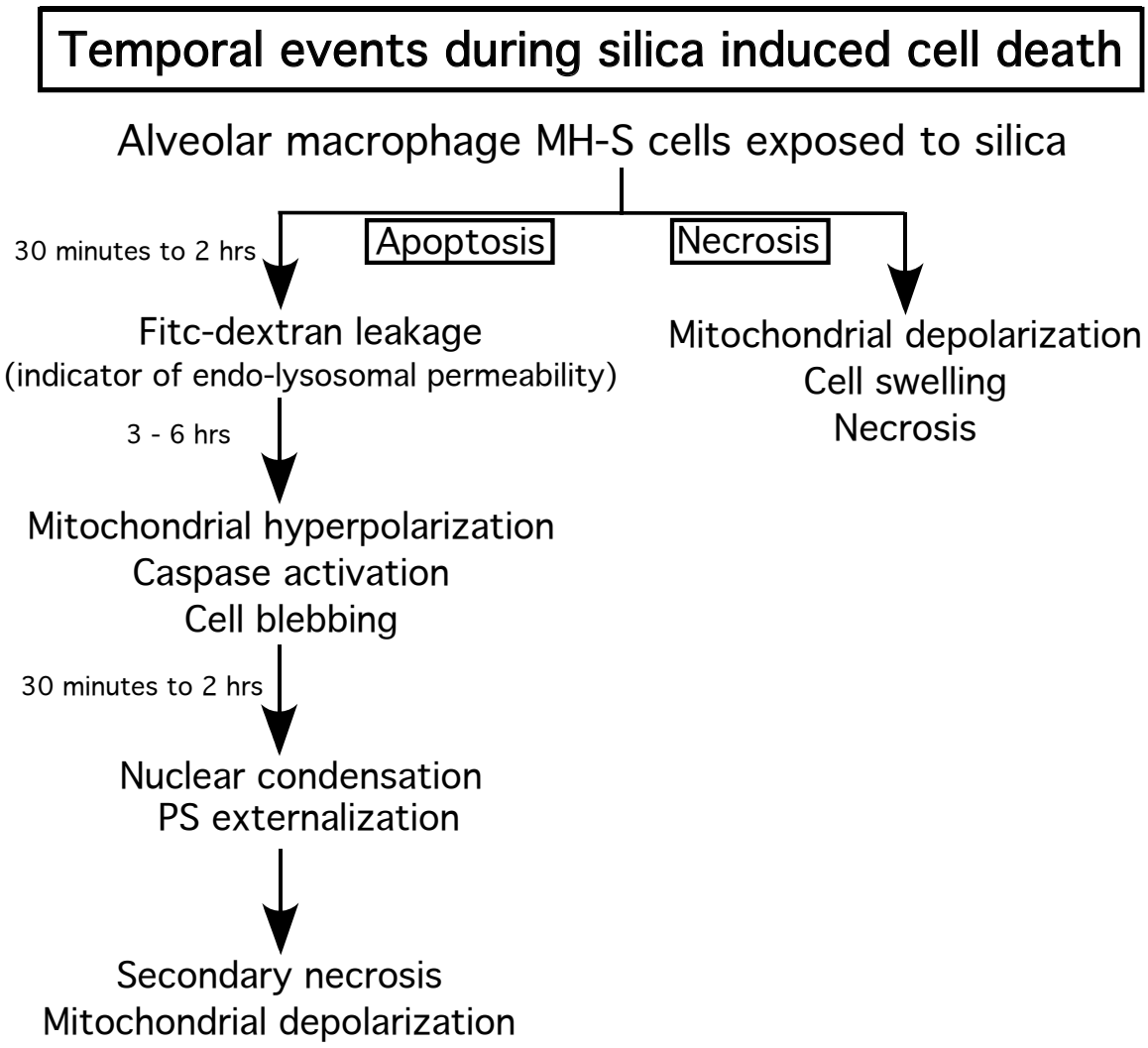

Figure 3.9: Pathway showing temporal difference between molecular events leading to cell death

A pathway of based on temporal variations in cell death summarizes the results from single cell analysis of different probes. Alveolar macrophages treated with crystalline silica die by either apoptosis or necrosis. 85% of cells undergo apoptosis and show FD leakage as early as 30 minutes and lasting until 2 hours after exposed to crystalline silica. After a long delay, cells begin apoptosis that is characterized by cell blebbing, mitochondrial hyperpolarization and caspase activation. These three events are tightly synchronized. Both PS externalization and nuclear shrinkage occur after 30 minutes to 2 hours after above-mentioned events followed by

secondary necrosis and mitochondrial depolarization. The 15% of cells undergoing necrosis show cell swelling characterized by mitochondrial depolarization. Caspase activation is not seen during this necrosis.

3.9: Discussion

Studies showing apoptosis or necrosis as a model of cell death leading to fibrosis have provided little information regarding the extent of coexistence of both types of cell death in cells exposed to crystalline silica. We have previously shown that MH-S macrophages phagocytose crystalline silica particles within 10 minutes of their exposure and that internalization of a single particle is sufficient to cause cell death (Gilberti *et al.*, 2008; Costantini *et al.*, 2011). Here, an examination of the molecular pathway leading to cell death shows phagolysosomal leakage to be the first event that we can detect suggestive of the sequence: phagocytic uptake, phagosomal maturation and damage to the phagolysosomal membrane. Since uptake of latex particles does not cause leakage or cell death, and since inorganic crystalline silica particles are not broken down by cells, there is something specific about the surface of crystalline silica particles entering the uptake pathway that must cause toxicity.

There are several models that have been proposed for the molecular triggers that lead to cell death. One possibility is that when NADPH oxidase becomes activated on the phagosomal membrane, the presence of iron contaminating the silicon dioxide causes hydrogen peroxide to be converted to hydroxyl radicals by a Fenton reaction (Ghio *et al.*, 1992; Castranova *et al.*, 1997; Persson, 2005). The release of phagolysosomal contents into the cytoplasm (particularly Cathepsin D), has been hypothesized to initiate intrinsic cell death. Consistent with this hypothesis, iron chelators like desferrioxamine (Persson, 2005) and surface modifying agents like Polyvinylpyridine-N-oxide (PVPNO) or aluminum lactate (Fubini and Hubbard, 2003; Thibodeau *et al.*, 2004) have been shown to reduce cell death in crystalline silica exposed cells. Hydroxyl radicals could damage lysosomal membranes leading to permeabilization and leakage of fluorescent dextran into the cytoplasm.

Our results show that phagolysosomal membrane damage is an early event following crystalline silica uptake, occurring as early as 20 minutes after crystalline silica uptake. Using different molecular weight FITC-dextrans we were able to show the release of molecules at least as large as 70 kD from phagolysosomes. Since molecules as large as 70 kD, and probably larger can pass through the membrane, the cytoplasmic milieu would be exposed to many enzymes and proteins normally restricted to the lysosome, including cathepsins. Lysosomes contain cysteine proteases like cathepsins that are less than 50 kD in size and therefore can leak into the cytoplasm following phagolysosomal membrane permeabilization (Droga-Mazovec *et al.*, 2008). Cathepsin-D inhibitors cause a reduction in apoptosis of crystalline silica treated macrophages (Thibodeau *et al.*, 2003). Cathepsin-D in the cytoplasm is able to activate the pro-apoptotic protein Bid (Droga-Mazovec *et al.*, 2008) that activates Bax (Bidère *et al.*, 2003) to cause mitochondrial outer membrane permeabilization (MOMP) and cytochrome c release from mitochondria (Droga-Mazovec *et al.*, 2008). Although a temporal sequence from lysosomal leakage to caspase activation has not been demonstrated our results show that the time lag from phagolysosomal leakage to caspase activation was usually more than 3 hours. It is possible that it takes long for cathepsin D to cleave enough Bid as it would work poorly in a neutral pH environment or not at all. The activity has of cathepsin D has been reported to be zero due to deprotonation of the active site aspartic acid residues (Turk and Turk, 2009). This is contradictory to studies that use cathepsin D inhibitor, pepstatin A to demonstrate its role in cell death (Bidère *et al.*, 2003; Thibodeau *et al.*, 2004). Our data also leaves a wide temporal gap between the proximal and late event during apoptosis.

Changes in mitochondrial membrane potential and caspase activation have been shown to be key indicators of apoptosis and a point of no return leading to cell death (Green and Reed,

1998; Schwartz, 1998). Exposure to crystalline silica has been shown to lead to activation of both caspase-9 and -3 and mitochondrial depolarization but previous studies have not been able to resolve how the events relate temporally to each other. This is the first study of crystalline silica exposure where this question is resolved. Cells expressing either initiator or effector caspase (FRET) reporter probes along with TMRE show dramatic mitochondrial hyperpolarization that occurs simultaneously with cleavage of caspase FRET probes and cell membrane blebbing in a 5-minute time interval. A decrease in mitochondrial membrane potential has been observed concurrently with cytochrome c release from IMS with various intrinsic and extrinsic inducers of apoptosis (Goldstein *et al.*, 2005). Also different mitochondrial IMS proteins are released simultaneously with cytochrome c (Muñoz-Pinedo, 2006). Release of IMS proteins occurs following mitochondrial outer membrane permeabilization (MOMP) and simultaneously initiator and effector caspase activation is observed (Albeck *et al.*, 2008a; Spencer and Sorger, 2011). Data similar to that of Albeck et al., was observed with regards to a gradual increase in the FRET signal of both intrinsic and extrinsic caspase probes (Albeck *et al.*, 2008a) in a extrinsic cell death pathway. Thus irrespective of the nature of the apoptosis pathway, the kinetics of caspase activation is same upon damage to the mitochondria. We add to the current knowledge that cell blebbing and caspase activation could not be separated from each other in the 5-minute time window.

The observation that mitochondria go through a stage of hyperpolarization en route to apoptosis is novel. Most studies of apoptosis, including silica have found only mitochondrial depolarization. Mitochondrial hyperpolarization has been observed previously during T cell activation (Perl *et al.*, 2004). It is not surprising that this phenomenon was missed in earlier studies of crystalline silica induced apoptosis. Population average measures of mitochondrial

potential (eg. from a fluorimeter) would not detect transient changes in a small population of cells. Even flow cytometry would likely miss these events because it is transient and occurs asynchronously in the population, so only a small proportion of the cells would be hyperpolarized at any time. One possibility that had to be eliminated is that the increase in fluorescence of TMRE during hyperpolarization was due to dye unquenching and so represented a decrease in membrane potential rather than an increase. TMRE has been shown to self-quench at high concentrations, so dilution of the dye can appear similar to hyperpolarization. The concentrations used in this study were 50 nM which is less than previous studies and well below the concentration at which self-quenching has been shown to occur (400 nM) (Ehrenberg *et al.*, 1988). In addition, the ability of TMRE to detect mitochondrial hyperpolarization at the concentration used in this study was tested by treating cells with a F1-F0 ATPase inhibitor, oligomycin (Rego *et al.*, 2001; Giovannini *et al.*, 2002). This compound causes an increase in $\Delta\Psi m$ by interfering with proton transport and causing a buildup of protons in the inter-membrane space. Cells treated with oligomycin show a rapid increase in TMRE fluorescence indicating the expected increase in $\Delta\Psi m$ and confirming that the TMRE probe is sensitive to increases in membrane potential.

Our data and other studies (Rehm *et al.*, 2002; Albeck *et al.*, 2008b; Spencer *et al.*, 2009) show cell to cell variation in the timing and extent of caspase activation and other molecular events leading to cell death. We also see this variation in the expression of markers like surface phosphatidylserine (PS) exposure and chromatin condensation. In spite of these intercellular temporal differences, every cell follows a similar order of events in the activation pathway leading to death (Fig. 8). In receptor mediated cell death this variability has been attributed to the differences in the state of protein expression required for cell death (Spencer *et al.*, 2009). Rehm

et al., saw sister cells from mitotic divisions die with less temporal variation than unrelated cells (Rehm *et al.*, 2009).

Annexin V binding to the outer leaflet of the plasma membrane has been proposed by some studies to be an early marker of apoptosis (Martin *et al.*, 1995; Zhang *et al.*, 1997; Santarelli *et al.*, 2004; Brumatti *et al.*, 2008) whereas others suggested it to be downstream of caspase activation (Goldstein *et al.*, 2000). In T-cells, PS exposure was downstream of mitochondrial hyperpolarization and caspase activation, however there was no correlation between hyperpolarization and caspase activation (Banki *et al.*, 1999; Perl *et al.*, 2004). Our time-lapse microscopy reveals crystalline silica treated macrophages become Annexin V positive about 70 minutes after they begin to bleb. Since caspase activation occurs at the same time as blebbing, it is clear that Annexin V staining is a late or terminal stage marker of apoptosis in crystalline silica induced apoptosis. Nuclear fragmentation has been demonstrated by the TUNEL assay in previous studies with crystalline silica (Shen *et al.*, 2001; Fubini and Hubbard, 2003; Wang *et al.*, 2003; 2005) but time-lapse microscopy using Hoechst as an indicator revealed nuclear shrinkage occurs only after blebbing had started. This result indicates that nuclear changes also occur at a late stage of apoptosis. Also, compared to caspase activation, the temporal information obtained from Annexin V activation for apoptosis does not reliably inform about the precise timing of cellular apoptosis.

PS externalization for cells *in vivo* would act as a signal for the neighboring cells to engulf apoptotic cells. However, in this *in vitro* assay, cells undergoing apoptosis do not have a nearby healthy population to phagocytose them and therefore they undergo secondary necrosis (Majno and Joris, 1995; Hu *et al.*, 2006). During secondary necrosis, cells that were apoptotic with high mitochondrial $\Delta\Psi m$, lost mitochondrial membrane potential and underwent plasma

membrane swelling. This is in contrast to cells that actually underwent necrosis directly as a result of crystalline silica exposure. About 15% of crystalline silica treated cells underwent rapid mitochondrial depolarization and membrane swelling, but showed none of the specific markers of apoptosis.

Phagolysosomal leakage from crystalline silica has been shown to result in inflammasome activation mediated by cathepsin-B. Cathepsin B has been proposed to be unstable at neutral pH but retains its activity for a short period of time (Turk and Turk, 2009). Therefore, it is likely that cathepsin B is able to result in inflammasome activation that further results in activation of caspase-1 and IL-1β (Dostert *et al.*, 2008; Davis and Swanson, 2010; Kuroda *et al.*, 2011). Thus it could be argued that caspase-1 could be involved in some of the necrotic effects observed in our cells and this could be pyroptosis in which cells also die by swelling. Pyroptosis is an anti-microbial response to various bacterial pathogens like *Legionella, Salmonella, Shigella*, *Yersinia* and requires caspase-1 activation (Bergsbaken *et al.*, 2009; Franchi *et al.*, 2009). Since NLRP-3 dependent caspase-1 activation is highly dependent on LPS (Schroder *et al.*, 2012) and MH-S macrophages were not treated with LPS, the observed swelling is likely to be necrosis rather than pyroptosis. There were no obvious differences in the morphology of the cells undergoing necrosis or apoptosis before exposure of cells to silica to indicate if these cells were stressed in any way.

Using cell blebbing as a reference point, temporal differences between different physiological activities within the cell can be compared. During apoptosis, phagolysosomal leakage started to occur within 30 minutes of exposure to crystalline silica particles, followed 3-6 hours later by mitochondrial hyperpolarization, caspase activation and cell blebbing. The latter three events occurred within a 5 minute time frame, and could not be more accurately temporally

resolved since imaging was done at 5 minutes intervals. Approximately 30 minutes to 2 hours after the initial apoptotic activation, nuclear condensation and PS exposure was observed. Post apoptosis, cells necrosed (secondary necrosis) during which they showed membrane swelling. Some cells also died by necrosis during which mitochondria rapidly depolarized followed by cell swelling. This establishes a timeline of events that clearly distinguishes the molecular events that take place in the two cell death pathways that occur in crystalline silica treated cells.

Chapter 4: Silica particles cause NADPH oxidase independent ROS generation and phagolysosomal leakage

4.1: Introduction

Data from chapter 3 shows silica induced phagolysosomal leakage to be the proximal event during silica induced cell death. It is important to understand the mechanism of phagolysosomal leakage as the release of lysosomal contents, for example cathepsin D, has been hypothesized as the trigger for the apoptotic cascade (Bidère *et al.*, 2003; Cirman *et al.*, 2004; Billen *et al.*, 2008b). Silica induced phagolysosomal leakage has been hypothesized to occur due to ROS generation within a phagosome (Hamilton *et al.*, 2008). One hypothesis as to why only silica containing phagosomes leak relates to Fenton chemistry. Iron contaminating the silica surface might react with phagosomal H_2O_2, forming $^{\bullet}OH$ that can cause lipid peroxidation leading to the loss of integrity of the phagosomal phospholipid bilayer (Persson, 2005). There is little data available on the role of ROS in causing membrane damage to phagolysosomes containing silica. ROS has also been suggested to have a direct role in inducing cell death (Shen *et al.*, 2001; Hu *et al.*, 2006). There is little information on how phagosomal ROS gets translated to cytoplasmic ROS or if there is any other source for this ROS. The goal of the work in this chapter was to develop methods to detect and understand the role of ROS to help determine the relationship between ROS and leakage as well as between ROS and apoptosis.

An alveolar macrophage in a lung does not encounter silica particles routinely and is not likely to have evolved to differentiate between a toxic and a non-toxic material. Moreover, a silica particle within the lung will be coated by a mixture of proteins and antibody present in the lung surfactant allowing it to be recognized by various receptors on the macrophage surface (Huang *et al.*, 2001). Phagosomal ROS generation is an ubiquitous phenomenon used by cells of innate immune system for microbial killing and antigen processing (Savina *et al.*, 2006; Russell

et al., 2009). ROS in a phagosome of immune cells is generated by an active NADPH oxidase 2 (NOX2) that throughout the chapter has been referred as NOX. Phagosomes containing bacteria or other particles have not been shown to become leaky under normal circumstances (Flannagan *et al.*, 2009). This further questions the harmful effect of NOX generated ROS in a phagosome.

This is the first study where an effect of NOX generated ROS in a phagosome containing silica (a toxic particle) and from a phagosome containing latex (a non-toxic particle) is compared. This has revealed new intracellular events to further our understanding of silica-induced toxicity as well as the effect of phagosomal ROS generated *de novo* following uptake of non-toxic particles. In order to accomplish this, robust and spectrally distinct assays were developed so that a temporal relationship between generation of phagosomal ROS, phagosome maturation and phagolysosomal leakage could be simultaneously measured. NOX inhibitors and a NOX deficient cell line, Cos7 was used to investigate if silica could induce phagolysosomal leakage independent of NOX. In macrophages, ROS was detected in both latex and silica containing phagosomes. However, only silica containing phagosomes transiently leak their contents into the cytoplasm. Interestingly, in Cos7 cells, we also detected ROS and leakage in phagolysosome containing silica in spite of the fact that these cells do not express NOX. Thus it appears that ROS generated directly by the silica particle surface is sufficient to cause membrane damage and leakage.

An increase in cytoplasmic and mitochondrial ROS has been shown by various studies upon silica exposure (Kang *et al.*, 2000; Fazzi *et al.*, 2014). This increase in ROS can result in NF-κβ activation (Kang *et al.*, 2000) and an up-regulation of various of pro-inflammatory cytokines that contribute to fibrosis (Rojanasakul *et al.*, 1999). Using various probes, a biphasic

increase in cytoplasmic ROS was observed; an initial increase that was parallel to phagosomal ROS and another increase that occur during apoptosis associated with mitochondrial ROS.

Due to the variation in size and crystalline nature of silica particles it is difficult to coat them with various probes as well as track them following exposure to cells. To accomplish the objectives of this study crystalline silica particles were replaced by 3 μm amorphous spherical silica particles. Previous data from our laboratory has shown that 3 μm amorphous spherical silica particles also cause phagolysosomal leakage and cell death (Costantini *et al.*, 2011). It is also predicted that porosity of the spherical silica particles should help in better visualization of the dynamic process of the phagosome fusing with endosomes and lysosomes. In place of using naked amorphous silica particles, we have used non-opsonized (protein-coated) and opsonized (antibody conjugated) silica particles for further study. This substitution was necessitated, as the ROS probe linked to silica particles was only available conjugated to the protein BSA. Coating of silica particles with proteins and/or antibodies would be a likely *in vivo* scenario, as discussed earlier.

4.2: 3 µm amorphous silica particles are internalized by MH-S macrophages

Uptake of amorphous silica particles was confirmed using transmission electron microscopy and epifluorescence microscopy. After exposure of MH-S macrophages to silica particles, cells were fixed, resin embedded and sectioned with either a glass or diamond knife. Silica particles were not sectioned properly with the glass knife and hence particle breakage is observed in EM micrographs (Figure 4.1 A). It still confirms the presence of particles within the cell. In a similar experiment where a diamond knife was used for sectioning, particles were not broken off in the sectioning process and hence can be seen intact inside the cells. A representative EM micrograph where particles are seen, presumably during pseudopod extension as well as in a phagosome is shown in Figure 4.1 B. Figure 4.1 C shows a zoomed in version of the particle that has presumably been phagocytosed following pseudopod extension.

Extension of cell membrane around the particle and subsequent particle phagocytosis and internalization is an actin driven process. To confirm that particle uptake in MH-S cells is an actin driven process, MH-S cells expressing mCherry-actin were exposed to opsonized latex particles and imaged every minute (Figure 4.2). The cell interacts with the particle at time 0 as highlighted by the arrow, following which it is internalized. The actin probe accumulates around the particle at 2 minutes that later dissociates at 4 minutes. Similar data is observed for the particle labeled with the solid triangle. This data is consistent with earlier published results of F-actin localization during uptake of latex and other particles (Swanson and Hoppe, 2004; Bohdanowicz *et al.*, 2010). Experiments using non-opsonized and opsonized amorphous silica particles have shown similar results for both, indicating that irrespective of a particle type and irrespective of surface coating, cells are able to recognize and phagocytose these different particles.

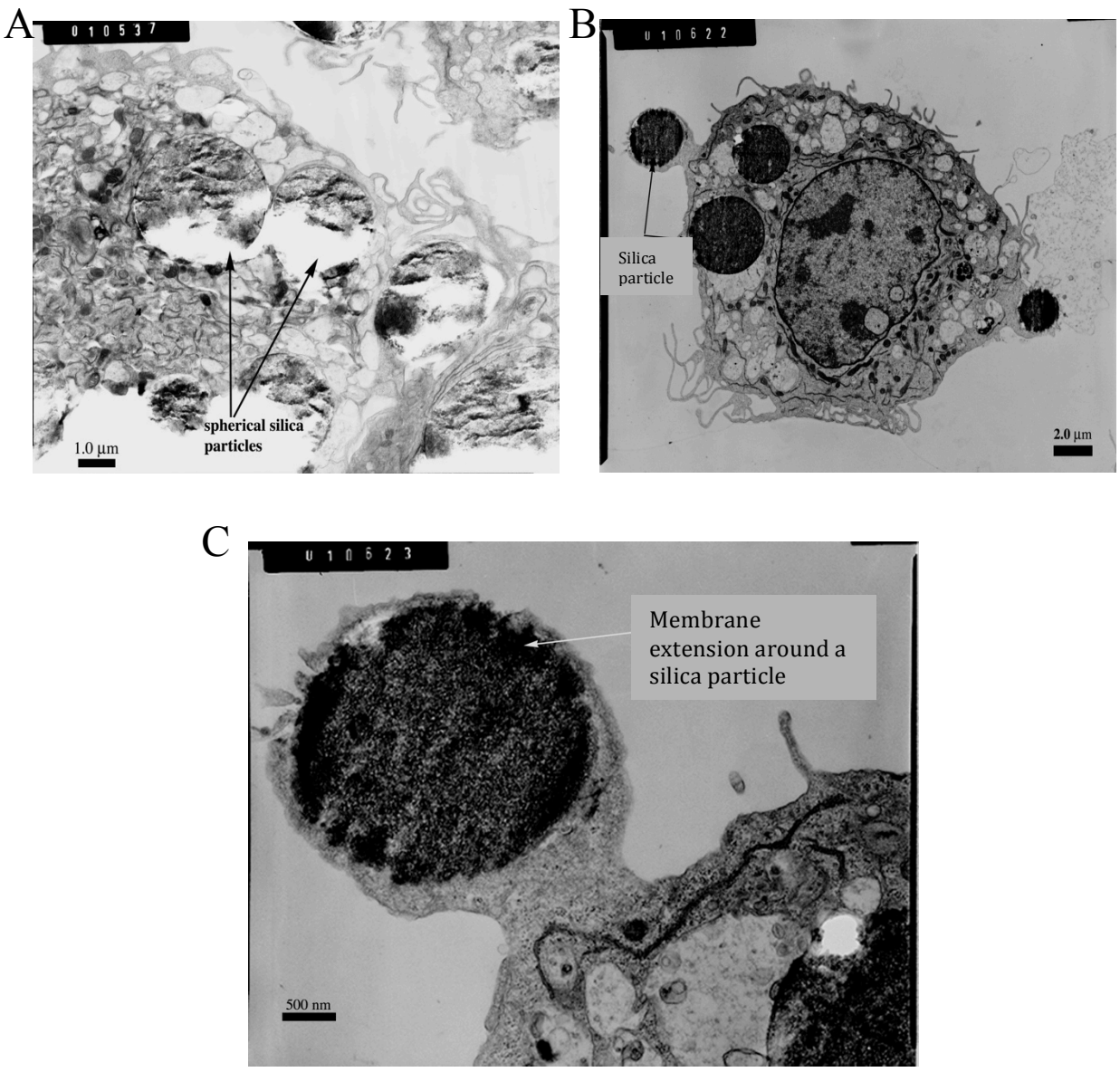

Figure 4.1: Internalization of amorphous silica particles in macrophages as demonstrated by electron microscopy

MH-S macrophages were exposed to opsonized 3 µm amorphous silica particles for 1 hour following which they were fixed and embedded in a resin. Sections were obtained using either A) the glass knife or B) the diamond knife. Following staining the sections were imaged using TEM. (A) Silica particles appear inside the cell indicative of particle uptake. The glass knife could not cut the porous silica particles efficiently resulting particle breakage. (B) Sections

obtained by diamond knife result in intact silica particles and show their presence within the cell. (C) A zoom in on an area from panel B) show membrane extension around the silica particle about to be internalized.

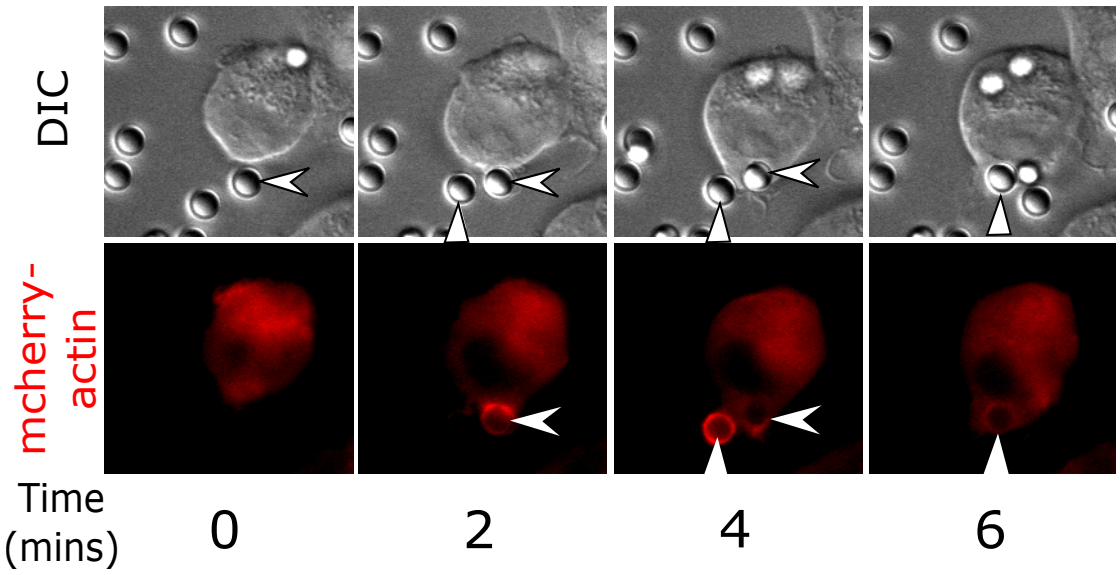

Figure 4.2: Actin remodeling upon phagocytosis of opsonized latex particles

To confirm phagocytosis of opsonized particles, macrophages expressing mCherry-actin were exposed to opsonized latex particles. For the two particles shown here as a representative example, actin polymerization driven particle uptake is visible. Upon particle internalization there is loss in mCherry-actin fluorescence in the phagosome indicative of actin depolymerization. Cell makes a contact with the particle represented by arrow-head between 0 and 2 minutes. This initiates the actin driven process of particle phagocytosis during which an increase in mcherry-actin fluorescence is visible around the particle at 2 minutes that disappear by 4 minutes. Similarly, for the particle indicated by a solid triangle, particle is outside the cell at 2 minutes, by 4 minutes the particle is phagocytosed indicated by the presence of mCherry-actin around the phagosome. By 6 minutes mCherry-actin fluorescence disappeared around the phagosome.

4.3: Dual-dextran assay reveals dynamics of phagosomal maturation and a transient phagolysosomal leakage in macrophages upon exposure to silica particles

Previous studies have shown that both crystalline- and amorphous-silica particles induce phagolysosomal leakage and apoptosis in alveolar macrophage cell lines (Costantini *et al.*, 2011; Joshi and Knecht, 2013b). This was measured by quantifying release of 4 kD FITC-dextran from phagolysosomes into the nucleus (Figure 3.2). The assay used earlier did not allow any visualization of phagosome maturation and any dynamic changes that occured during phagolysosomal leakage. These limitations were due to use of crystalline silica particles and FITC-dextran whose fluorescence is quenched at acidic pH. Hence, the assay was modified so that MH-S alveolar macrophages were allowed to simultaneously endocytose both 4 kD FITC-dextran and 4 kD TRITC-dextran to label endosomes and lysosomes (Humphries *et al.*, 2011). We refer to this as a dual-dextran assay. Having a pH insensitive probe like TRITC-dextran allows a continuous monitoring of phagosome dynamics even when FITC fluorescence is quenched as the phagolysosome gets acidified by the protons pumps delivered to the phagosome membrane upon fusion of endolysosomes. Thus the dual-dextran assay allows for visualization of pH dynamics and endolysosomal fusion in real time. These dextran-loaded cells were then exposed to either opsonized or non-opsonized spherical silica particles.

Opsonized silica particles are recognized by Fc-receptors and rapidly phagocytosed into fluorescent dextran loaded macrophages. A similar pattern of appearance of dextran fluorescence in phagosomes has been found for every phagosome that has been examined, although the precise timing varies from particle to particle (n=20, a representative example is shown in Figure 4.3). A frame in which the cell has made contact with a particle prior to uptake (as determined by the DIC image) was set as time 0. The cell membrane then extended around the particle and sealed resulting in the formation of a phagosome. Within a few minutes, both FITC-dextran and

TRITC-dextran fluorescence could be detected in the phagosome (Figure 4.3 A and B, 1-3 minutes). The porous nature of amorphous silica particles results in the appearance of fluorescent dextran throughout the volume of the phagosome. The FITC fluorescence then began to decrease from about 2 minutes after uptake consistent with acidification of the phagosome (Davis and Swanson, 2010). During this time, the TRITC-dextran fluorescence continued to increase, indicative of continuing delivery of dextran to the phagosome due to fusion of endolysosomes with the phagosome (Figure 4.3 B). Between 24 and 26 minutes (Figure 4.3 A and B), a rapid and dramatic increase in phagosomal FITC-dextran fluorescence was observed. Since the TRITC-dextran fluorescence did not change during this period of time, this is most likely indicative of a rise in phagosomal pH. This result reveals the first step of phagolysosomal leakage in which phagosomal membrane permeability increases allowing for the exchange of small molecules with the cytoplasm and thus neutralization of phagosomal pH. Within 1-2 minutes of the beginning of the increase in FITC-dextran fluorescence, a rapid decrease in both FITC-dextran and TRITC-dextran fluorescence was observed (Figure 4.3 A and B, 26-30 minutes). In parallel, an increase in FITC nuclear fluorescence was measured (Figure 4.3 A at 31 minutes and 4.3 B). This is indicative of phagolysosomal release of 4 kD FITC-dextran and passive diffusion in to the nucleus, similar to what was observed for crystalline silica. Surprisingly, within 10 minutes of the start of leakage, the increase in nuclear FITC-dextran fluorescence ceased and the phagosomal TRITC-dextran fluorescence began to increase again, indicating that the phagosomal membrane had resealed and endosomes were once again fusing with the phagosome. The increase in phagosomal TRITC-dextran fluorescence continued for nearly 30 minutes, and during this time, there was no increase in FITC-dextran fluorescence, indicating that the phagosome was also re-acidified. The average time over which leakage could

be measured was 9 minutes. A complete quantification of these phagosomal and cellular events can be seen in Figure 4.3 C. Thus phagolysosomal leakage caused by silica is a transient event allowing some exchange of material with the cytoplasm followed by the resealing of the phagosomal membrane and then continued fusion with endolysosomes.

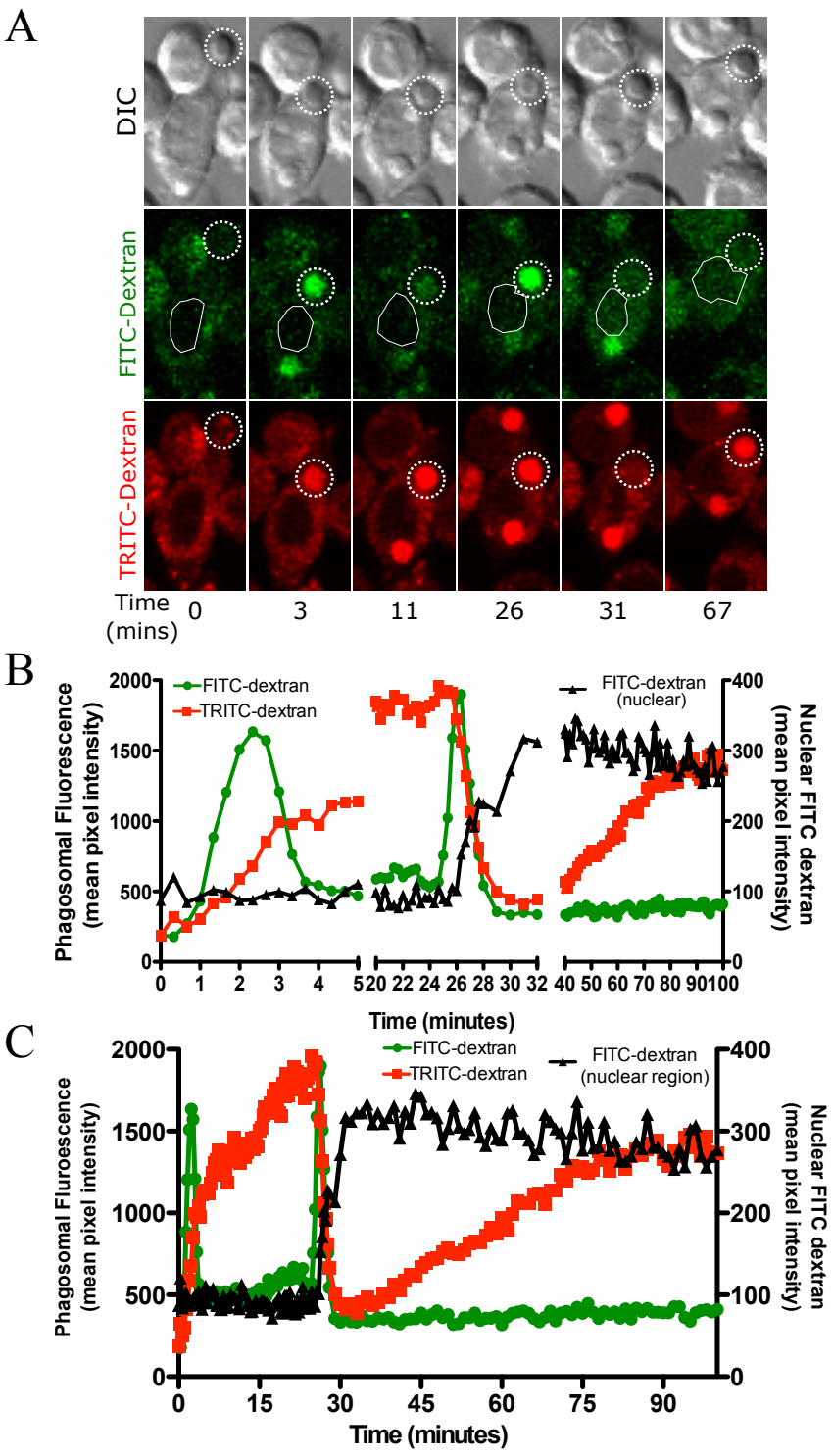

Figure 4.3: Investigation of phagosomal maturation using a dual dextran assay shows various steps in the maturation process and reveals a transient leakage of phagolysosome containing silica

(A and B) MH-S alveolar macrophages were loaded with 4 kD FITC dextran and 4 kD TRITC dextran (dual dextran) for 2.5 hours and then exposed to 20 μg/cm^2 amorphous opsonized 3 μm silica particles and images were captured through the volume of the cell at 2 μm intervals every 20 seconds. A plane in which a particle was in focus is shown. (A) In this sequence of images, the particle was phagocytosed and then the phagosome fused with endolysosomes resulting in an increase in phagosomal fluorescence for both FITC-dextran and TRITC-dextran is indicated by dotted circle throughout the dataset (3 minutes). FITC-dextran is pH sensitive and hence upon acidification the fluorescence decreased (11 minutes). Upon phagolysosome leakage, FITC-dextran fluorescence initially increased due to the influx of cytoplasm (26 minutes) followed by a decrease in fluorescence due to leakage into the cytoplasm (31 minutes). This leakage is detected as FITC-dextran signal appearing in the nuclear area of the cell indicated by a white outline. The TRITC-dextran fluorescence initially continuously increased since it is not affected by the pH change (3 – 26 minutes). At the same time that leakage of FITC-dextran occurred, the phagosomal TRITC-dextran fluorescence also rapidly decreased indicating leakage into the cytoplasm (31 minutes). This signal was harder to measure in the nuclear area due to signal from the rest of the cytoplasm contributing to nuclear background noise. The TRITC-dextran fluorescence then began to gradually increase beginning at 40 minutes presumably due to resealing of the phagosome and continued endolysosomal fusion. (B) Quantification of data for the cell in panel A showing the data from phagosomal TRITC-dextran and FITC-dextran as well as nuclear FITC-dextran. The trends seen are representative of 20 cells examined. Quantification for the entire duration of data in panel B is represented in (C).

4.4: Macrophages allowed to endocytose 4 kD TRITC-dextran and exposed to FITC-labeled silica particles support the outcome of dual-dextran experiment

To further validate this interpretation of the sequence of events observed above (Section 4.3), opsonized silica particles were pre-labeled by linking FITC to the protein coating the outside of the particles and exposed to macrophages pre-loaded with 4 kD TRITC-dextran. The fluorescence of FITC linked on to the surface of an opsonized silica particle that is porous does not appear throughout the volume of the particle. Instead it appears on the periphery indicating that FITC is linked on to the protein layer of the opsonized particle (0 min). Following exposure of MH-S cells to these particles and particle uptake a decrease in FITC fluorescence was observed starting from 3 minutes consistent with a decrease in phagosomal pH. At the same time the phagosomal TRITC-dextran fluorescence increased due to fusion of the phagosome with endolysosomal vesicles. It should be noted that the fluorescence observed in the TRITC-dextran channel around the particle at 0 minutes is due to background signal. It was not ascertained if this was coming from silica particle, protein coating or FITC or a combination of these (Figure 4.4 A and B). By 8 minutes the FITC fluorescence was completely quenched and stayed this way until 17 minutes. This shows that the pH in the phagolysosome stays low for this duration.

At 17 minutes an increase in FITC fluorescence was observed whereas the TRITC-dextran fluorescence did not change (Figure 4.4 C). This is suggestive of membrane permeability allowing molecules smaller than 4 kD to diffuse through the membrane leading to an unquenching of FITC fluorescence and hence an increase in pH. After one minute (at 18 minutes) a decrease in fluorescence of phagosomal TRITC-dextran took place indicative of an increase in permeability of the phagolysosomal membrane (Figure 4.4 B and magnified in 4.4 C). This is consistent with the data from dual-dextran assay in earlier section. During

unquenching of FITC fluorescence, the entire volume of the particle was fluorescent unlike the periphery of the particle at time 0 further confirming protein proteolysis to allow small molecule like FITC to diffuse through the particle volume. Phagolysosomal leakage was observed for 6 minutes based on a decrease in TRITC-dextran phagosomal fluorescence (Figure 4.4 C, 18-24 minutes), following which the TRITC-dextran fluorescence began to increase, indicating continued endolysosomal fusion with a phagosomal membrane was no longer permeable. Thus this assay where opsonized 3 μm spherical silica particles are linked to FITC is useful in characterizing multiple processes; (1) phagosome maturation, (2) pH change, (3) protease activity, (4) phagolysosomal leakage and (5) recovery of a damaged phagolysosome.

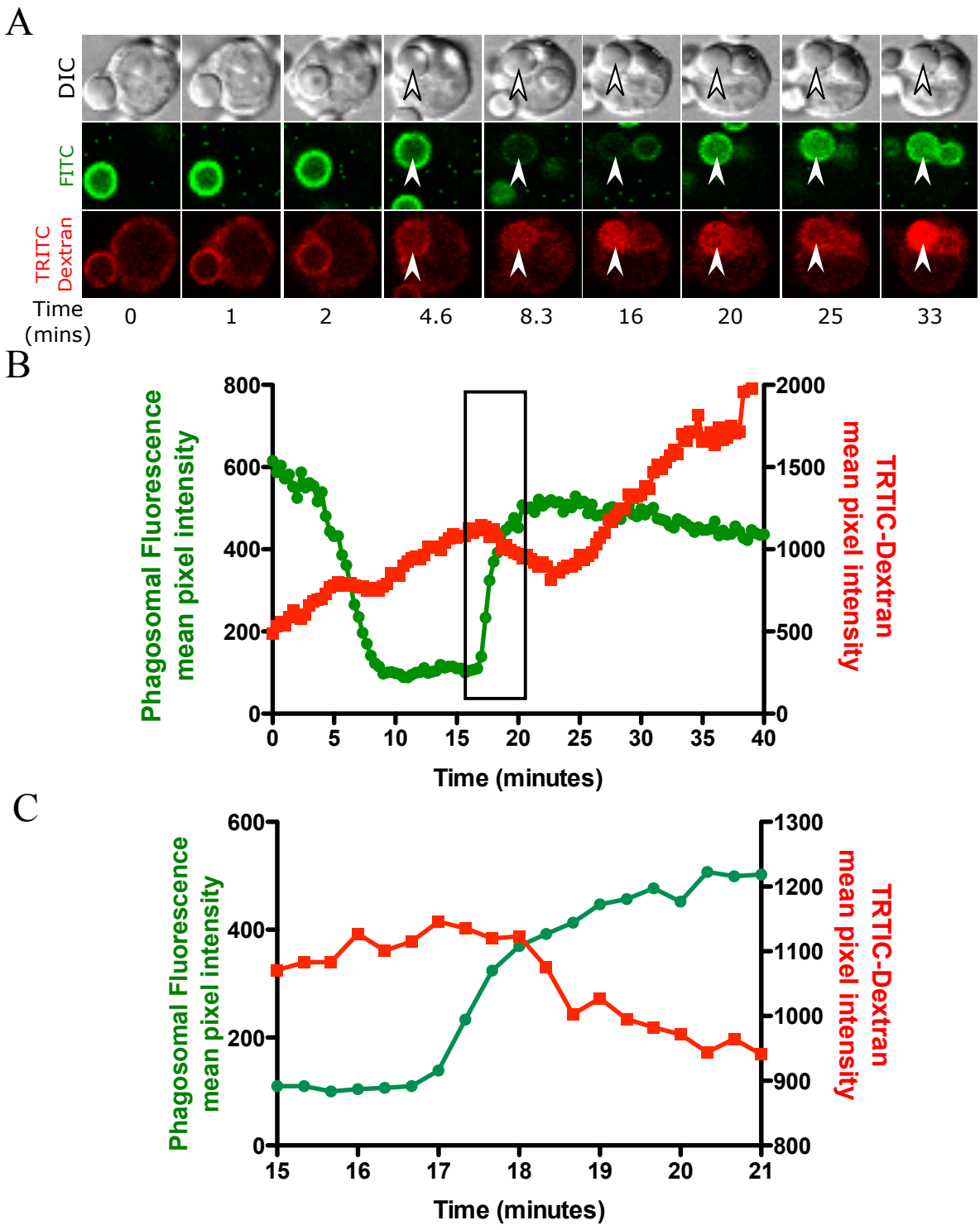

Figure 4.4: Analysis of phagosomal dynamics in macrophages loaded with 4kD TRITC-dextran and exposed to FITC-labeled silica particles confirms the outcome of dual dextran experiment

MH-S macrophages allowed to endocytose 4 kD TRITC-dextran were exposed to opsonized silica particles that were labeled with FITC. Cells were imaged 2 μm apart at every 20 seconds time interval. A representative particle is shown. (A) DIC images show a cell-particle interaction (0 minute) following which cell membrane extends around the particle to form a phagocytic cup (1 minute) resulting in particle phagocytosis (2 minutes). A gradual decrease in FITC fluorescence and an increase in TRITC-dextran fluorescence is seen from 2 minutes onwards. By 8 minutes FITC fluorescence is quenched and TRITC-dextran fluorescence is localized throughout the volume of the silica particle rather than the rim due to protein proteolysis. FITC fluorescence increases at 20 minutes and simultaneously a decrease in TRITC-dextran fluorescence is observed due to phagolysosomal leakage. During resealing of a leaky phagolysosome an increase in TRITC-dextran fluorescence is again observed at 33 minutes. (B) Quantification for the particle in panel A reveal temporal changes in FITC and TRITC-dextran fluorescence. An initial decrease in FITC fluorescence is due to phagosomal acidification where as upon leakage the fluorescence again increases. TRITC-dextran fluorescence increases initially during phagosome maturation, decreases during phagolysosomal leakage and again increases during resealing. (C) A zoom of the area highlighted in rectangular box in B shows a temporal gap of one minute between phagolysosomal leakage beginning at 17 minutes as indicated by an increase in FITC fluorescence and a release of TRITC-dextran beginning at 18 minutes.

4.5: FITC-dextran leakage occur only from a silica containing phagolysosome

Since cells contain multiple silica particles, it was of interest to determine if the event in one phagosome has an effect on other endolysosomal vesicles and cause them to leak. Because an increase in FITC fluorescence is easy to quantify following vesicle leakage due to its unquenching, cells were loaded with 4 kD FITC-dextran and exposed to opsonized silica particles such that every cell received no more than 3 particles. A sequence of events similar to Figure 4.3 was observed (Figure 4.5). Quantification of cells with a small number of phagosomes showed a stepwise increase in nuclear FITC fluorescence that correlated with distinct phagolysosomal leakage events. Upon leakage of phagosome 1, an increase in nuclear fluorescence was observed starting at 15 minutes. A further increase in nuclear fluorescence is not observed until leakage from phagosome 2 at 28 minutes, suggestive of a quantal transient release of FITC-dextran exclusively from phagolysosomes. This shows that FITC-dextran is exclusively released from silica containing phagolysosomes. Since the timing of phagolysosomal leakage and an increase in nuclear fluorescence parallel each other, the release of FITC-dextran from endolysosomal vesicles that have not fused and delivered their content to a phagolysosome is least likely.

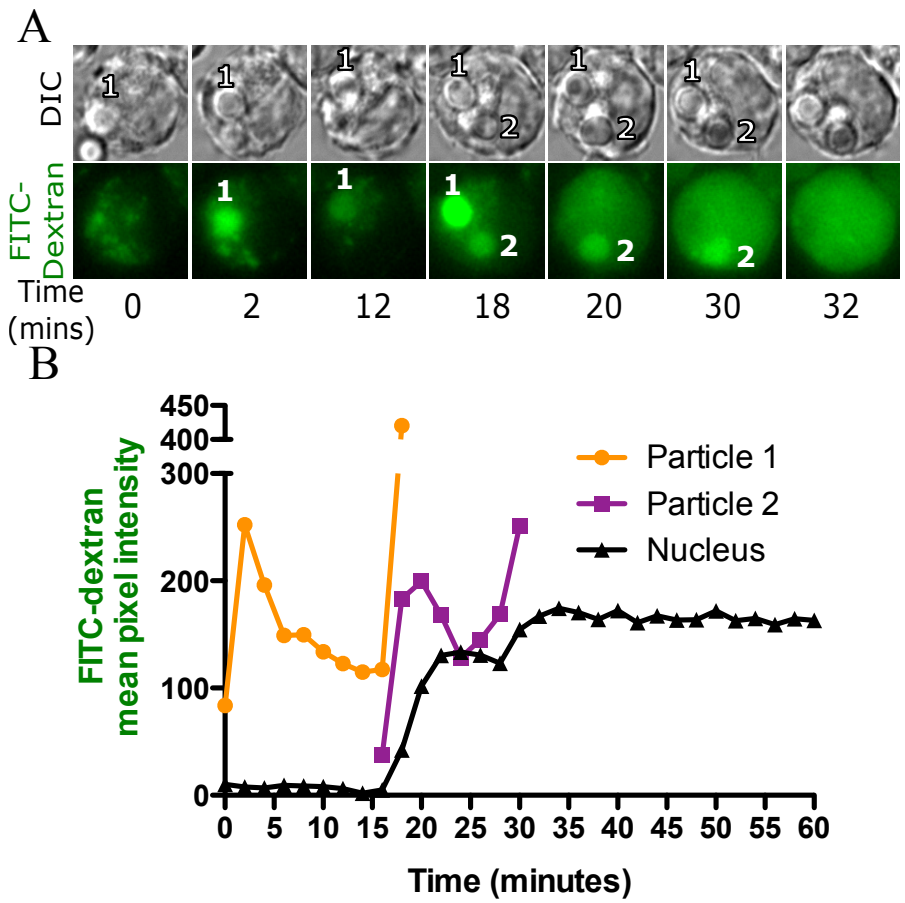

Figure 4.5: FITC-dextran leakage occurs only from a phagolysosome containing silica

(A) A representative series of images and quantification of the data (B) from a cell loaded with 4kD FITC-dextran for 2.5 hours and then exposed to a small number of silica particles so that each particle could be tracked. Images were captured 2 minutes apart on a widefield epifluorescence microscope. Each particle goes through the same sequence described in Figure 3. Particle 1 showed an initial increase in fluorescence then a decrease as the FITC-dextran was quenched. At the time of leakage, the phagosome became transiently bright and then dimmer while the nuclear fluorescence increased with a slight delay. Particle 2 showed the same pattern at a later time. Each particle seems to leak only once but each time a phagosome shows this pattern, there is a correlated increase in nuclear fluorescence. The same quantal changes in nuclear and phagosomal fluorescence were observed in 33 particles in 20 cells.

4.6: Macrophages exposed to latex particles do not result in phagolysosomal leakage

To understand whether non-toxic latex particles cause phagolysosomal leakage, MH-S cells pre-loaded with FITC-dextran and TRITC-dextran were exposed to 3 μm opsonized latex particles. Phagocytosed particles undergo phagolysosomal fusion as indicated by an increase in TRITC-dextran fluorescence surrounding the particle (Figure 4.6 A) similar to that observed with silica particles (Figure 4.3 A and B). An increase in FITC-dextran fluorescence is presumably not observed due to quenching of FITC fluorescence in an acidified phagosome. Since latex particles are not porous, an increase in fluorescence is observed only in a thin volume of fluid between the particle surface and the membrane making it difficult to detect a transient increase in FITC fluorescence. Phagolysosomes containing latex particles do not show any evidence of leakage either as a decrease in TRITC fluorescence or an increase in nuclear or vesicular FITC fluorescence. Following an increase in TRITC-dextran fluorescence for the first 20 minutes, the signal plateaued suggesting the fusion of endolysosomes with phagosomes had ceased. Similar data was obtained for multiple particles (n=20).

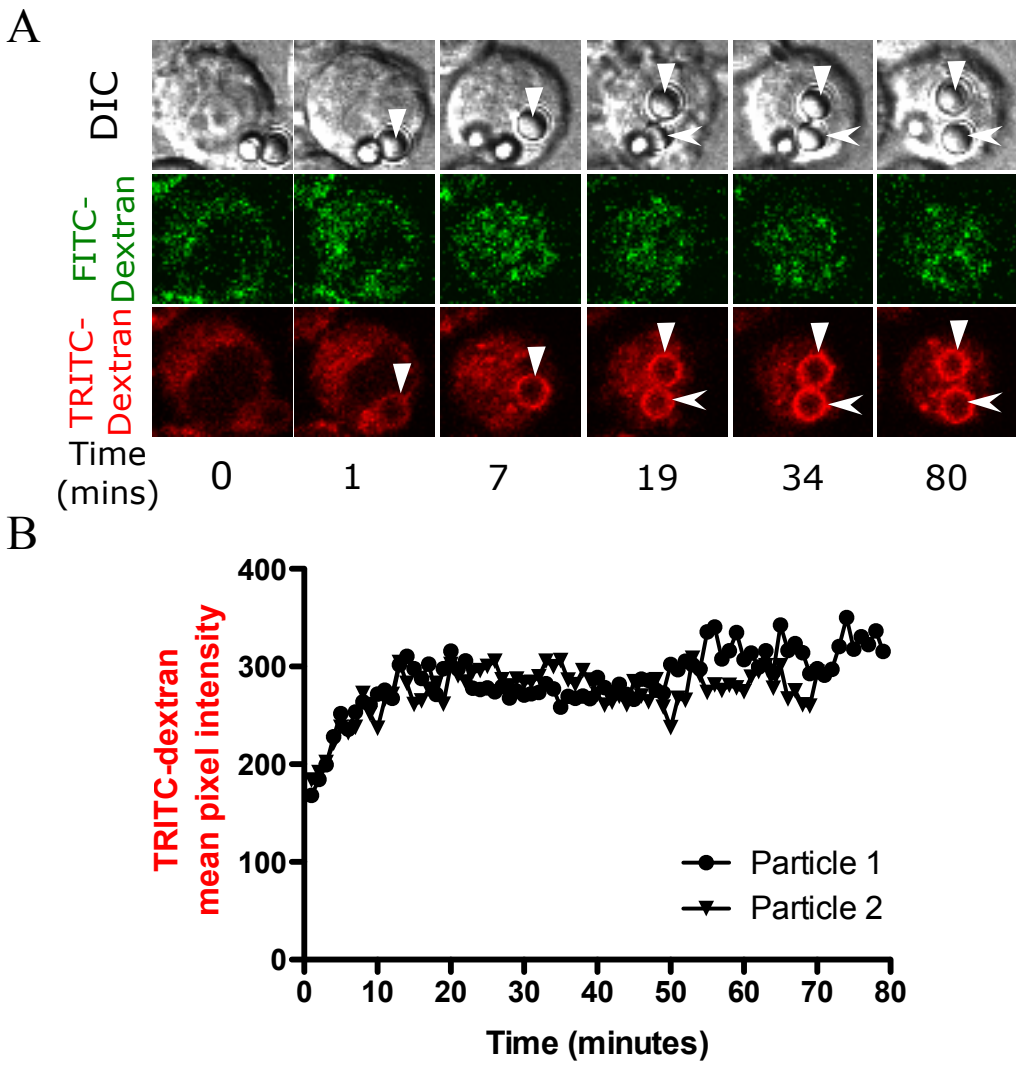

Figure 4.6: Exposure to latex particles does not result in phagolysosomal leakage

Alveolar macrophages were loaded with 4 kD FITC-dextran and TRITC-dextran (A and B) for 2.5 hours following which they were exposed to 20 μg/cm^2 opsonized 3 μm latex particles. Volumetric image stacks were captured 2 μm apart every minute. (A) A sequence of representative images and (B) quantification of the images. Latex particles are not porous, so the phagosomal fluorescence appears as a ring instead of an entire volume of circle filled with fluorescence. Phagosomes containing latex particles show the same pattern of fluorescence changes as silica phagosomes up to the point of leakage. A brief increase in FITC fluorescence is

observed around the particle at 7 minutes (marked by solid triangle) prior to phagosome acidification. (B) Particle 1 and particle 2 represent quantified data of particles in the TD channel from Panel A represented with solid triangle and an arrow respectively. These trends are representative of 20 cells examined.

4.7: PX-domain of NADPH oxidase subunit $p40^{phox}$ localizes to macrophage phagosomes

NOX activation following phagocytosis has been well documented for particles that are antibody opsonized. Following internalization, a phagosome undergoes maturation and this is mediated by a rapid conversion of one form of a phosphoinositide (PI) into another (Hoppe and Swanson, 2004). The PX domain of $p40^{phox}$ in the cytoplasm binds to newly formed PI(3)P on the phagosome membrane allowing for tethering of cytoplasmic trimeric phagocyte oxidase complex with the phagosome. The appearance of PX-GFP on a phagosome is indicative of an association of the trimeric complex with flavocytochrome b_{588} (Bedard and Krause, 2007). There is no evidence as to whether or not NOX activation and phagosomal ROS production occurs for particles that are non-opsonized (Huang *et al.*, 2009). This is an important consideration, as the inhaled particles in the lung might be coated with a variety of protein present in the lung fluid, but are not likely to be opsonized in the traditional sense due to specific antibody or complement binding.

To confirm NOX activation following the uptake of non-opsonized (protein coated) particles, the PX domain of $p40^{phox}$ fused to GFP (PX-GFP) was expressed in MH-S macrophages (Ellson *et al.*, 2006; Tian *et al.*, 2008). Upon phagocytosis of an opsonized silica particle, PX-GFP was recruited onto the phagosome and persisted for 4 minutes (Figure 4.7 A). After 4 minutes PX-GFP fluorescence disappeared from the phagosome. 47 phagosomes were counted and on average, PX-GFP persisted for 9 minutes. To confirm the affinity of PX-GFP to PI(3)P, ΔPX-GFP with a R58A mutation which prevents the binding of the PX domain to PI(3)P was expressed in macrophages. GFP localization was not observed on phagosomes upon particle uptake in these cells (Figure 4.7 C). PX-GFP was also recruited onto non-opsonized silica particle phagosomes and this fluorescence persisted for about 4 minutes (Figure 4.7 B). The

kinetics of PX-GFP appearance and disappearance is consistent with the kinetics of a 2xFYVE-GFP probe (Gilberti and Knecht, 2015) that also has an affinity for PI3P.

Upon exposure of macrophages to silica, it has been proposed that there is ROS generation in cells due to NOX activation. NOX activation and ROS generation is achieved by stimulating cells with PMA or LPS (Cassel *et al.*, 2008; Russell *et al.*, 2009; Sokolovska *et al.*, 2013). This results in recruitment of cytoplasmic subunits of NOX onto the plasma membrane. In our experiments, cells were not stimulated with PMA or LPS and NOX activation only happens on phagosomal membranes. Over the course of 60 minutes during the experiment, PX-GFP was restricted to phagosome and did not appear on the cell membrane. This suggests that in absence of stimulating agents like PMA or LPS, NOX is restricted to phagosome and should generate ROS in a phagosomal lumen. It has been shown that cells pre-stimulated with LPS and exposed to particles generate more phagosomal ROS compared to naïve cells (Russell *et al.*, 2009).

Before choosing to use PX-GFP, a probe consisting of $p67^{phox}$ fused with mCherry was expressed in cells in order to directly show the binding of the NOX subunit to the phagosomal membrane (Tlili *et al.*, 2010; 2012). There was no difficulty in transfecting cells or expressing this probe in MH-S macrophages, however, upon particle exposure the probe did not localize to the phagosome. Since initial imaging was done on a wide-field fluorescence microscope it was hypothesized that there was not enough localized signal relative to the cytoplasmic background of the probe to detect its localization to the phagosome. The experiments were repeated using a confocal microscope, however, the results were the same. Even when cells were pre-stimulated with PMA to activate NADPH oxidase. $p67^{phox}$-mCherry was only cytoplasmic. Even after exposure to various particles like zymosan as well as non-opsonized and opsonized silica particles following PMA pre-stimulation there was no localization detected and hence a decision

was made to use a PX-GFP probe that has been used by multiple studies, instead of $p67^{phox}$ probe that is not commonly used.

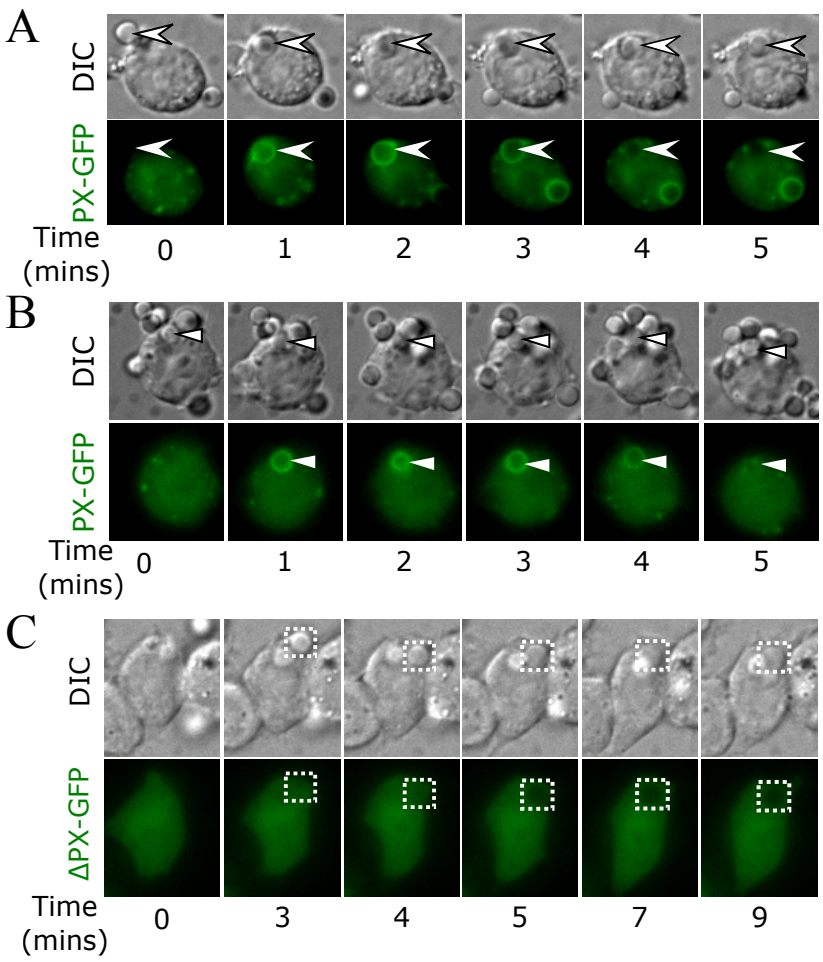

Figure 4.7: PX-domain of NADPH oxidase subunit p40phox localizes to a macrophage phagosome

MH-S cells were transiently transfected with a vector expressing the PX domain of $p40^{phox}$ fused to GFP (PX-GFP). These cells were then exposed to either opsonized or non-opsonized silica particles and imaged every minute. (A) Upon uptake of opsonized silica particles, PX-GFP localizes around the phagosomes and after 4 minute the fluorescence disappear (arrowhead). (B) Following uptake of non-opsonized silica particles, PX-GFP localizes around the phagosome and after 4 minutes the fluorescence disappear (solid triangle). (C) Cells were transiently transfected with a vector expressing the PX domain where arginine at position 42 is replaced by glutamine,

fused to GFP (ΔPX-GFP) and expressed in macrophages. As expected this probe does not show localization around the phagosomes.

4.8: Development of methods and detection of phagosomal ROS in MH-S macrophages

Having established the recruitment of NOX on the phagosome, the goal was to detect ROS in the phagosome of cells exposed to various particles. Following exposure of cells to silica, an increase in cytoplasmic ROS has been shown using a fluorescent dye H_2DCFDA that detects cytoplasmic ROS. The source of this cytoplasmic ROS has been proposed to be NOX generated ROS (Deshpande *et al.*, 2002) without infact detecting ROS in the phagosome and establishing a temporal relationship between phagosomal and cytoplasmic ROS.

4.8.1 - Dihydrorhodamine (DHR) conjugated to latex particles allows detection of phagosomal ROS but is poorly retained on the particle

Dihydrorhodamine-123 (DHR) has been used as a probe for detecting ROS since oxidation of the dye results in an increase in fluorescence. In an earlier study, DHR was adsorbed onto latex particles and these were used to detect ROS in phagosomes of dendritic cells (wild type or $gp91^{phox-/-}$) (Savina *et al.*, 2006). A similar approach was used to detect ROS in a macrophage phagosome following uptake of latex particles. Attempting to replicate that work, particles were labeled with DHR and found to be fluorescent (Savina *et al.*, 2010). Addition of H_2O_2 to further oxidize the particles did not result in an increase in DHR fluorescence indicating the conditions under which the particles were prepared resulted in oxidation of the dye. In a personal communication with Ariel Savina, a suggestion was made to deoxygenate media before particle labeling.

The effect of deoxygenated media on DHR oxidation was tested by adding DHR to native or deoxygenated CO_2 independent medium (CIM) prepared by bubbling nitrogen gas through the media for 30 minutes. To test for the oxidative capacity of DHR, H_2O_2 was added to the medium and fluorescence was measured every minute with a fluorometer. DHR in CIM without deoxygenation resulted in a gradual increase in fluorescence, whereas with deoxygenated CIM, the fluorescence stayed at initial levels indicative of auto-oxidation under non-deoxygenated conditions. Addition of H_2O_2 resulted in a gradual increase in DHR fluorescence in particles under non-deoxygenated condition (Figure 4.8 A). Exposure of DHR labeled particles to H_2O_2 in deoxygenated media resulted in a greater oxidation of DHR compared to auto-oxidation of DHR. Particles were therefore labeled with DHR under deoxygenated conditions.

Labeled particles were exposed to MH-S alveolar macrophages and oxidation of the dye was quantified. There was a gradual increase in particle fluorescence upon uptake (particles 1 and 2) (Fig 4.8 C, zoom in of DHR panel). This fluorescence did not seem to increase after 20 minutes indicating either saturation of DHR or a lack of ROS generation within a phagosome (Figure 4.8 C and D). In addition to an increase in fluorescence on latex particles (dotted box) an increase in mitochondrial fluorescence (solid triangles) was also observed that generated signal higher than the phagosomal signal (Figure 4.8 B and C). This is likely due to release of DHR from particle surfaces into the media or into the cells. Similar to TMRE, DHR has been used to measure mitochondrial membrane potential but toxicity concerns have limited its utility (vander Heiden *et al.*, 1997). Hence it was not a surprise to observe mitochondrial fluorescence as the cationic DHR partitioned in to the inner mitochondrial membrane. There was also a batch-to-batch variability in DHR labeling of particles. Therefore it was concluded that DHR had limited utility.

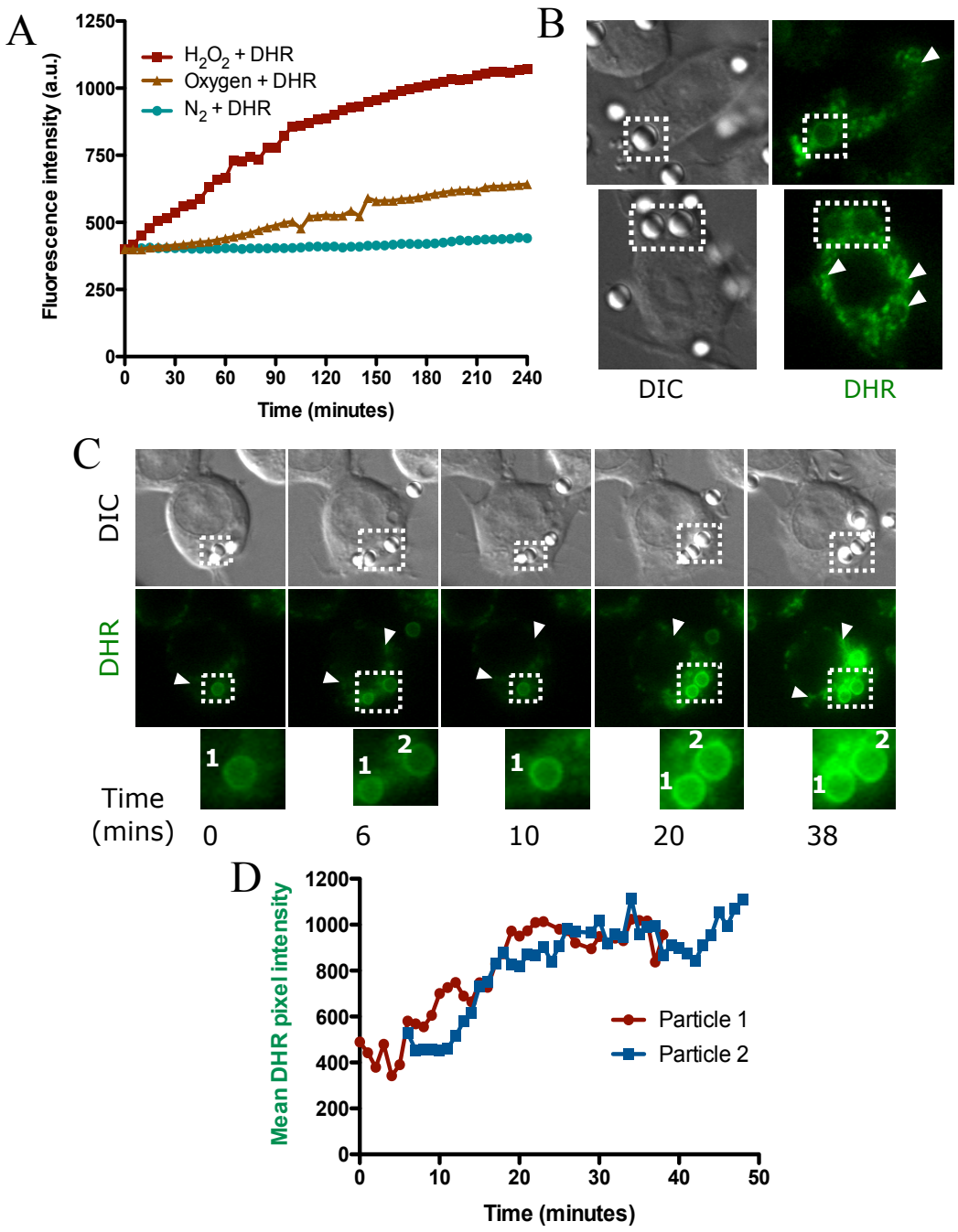

Figure 4.8: DHR labeled latex particles show ROS generation in a macrophage phagosome

(A) Using a fluorometer a change in dihydrorhodamine-123 (DHR) fluorescence was measured under different conditions. DHR suspended in medium that has been deoxygenated by bubbling

with nitrogen gas does not show oxidation of DHR (N_2 + DHR). An increase in DHR fluorescence is observed over time in the medium that has not been deoxygenated (Oxygen + DHR) and upon addition of H_2O_2 it results in maximum oxidation over time (H_2O_2 + DHR). (B) A representative of two cells where the dye is lost from the particle surface resulting in mitochondrial fluorescence is indicated by solid triangles. Opsonized latex particles were labeled with (DHR) and exposed to MH-S macrophages. Cells were imaged every minute. (C) The dotted box shows the particles that are phagocytosed by the cell (DIC). Upon uptake there is a gradual increase in the fluorescence of these particles (DHR) (dotted box and magnified view). A solid triangle is a representative area where a gradual increase in the mitochondrial fluorescence of cells over time is observed. (D) Quantification of the two particles in panel C shows a gradual increase in the fluorescence over time. Particle 2 is phagocytosed at 5 minute and hence the plot starts from 5 minute onwards.

4.8.2 - Dihydro hexafluorofluorescein (H_2HFF) conjugated to non-opsonized and opsonized latex and silica particles allows detection of phagosomal ROS

To achieve the goal of studying phagosomal ROS, the oxidation sensitive probe, H_2HFF-BSA was considered. H_2HFF, a chemical variant of H_2DCFDA is claimed by the manufacturer to be more sensitive than H_2DCFDA. Also, having H_2HFF conjugated with BSA makes it easy for the process of particle coating as well as with opsonization process. However, this also prevented use of naked silica particles, as the dye H_2HFF was not available in an unconjugated state.

Since H_2HFF-BSA is sensitive to oxidation, silica and latex particles were labeled under deoxygenated conditions using procedures previously worked out for protein coating of particles. Following preparation, particles were tested for their coating using a fluorescent secondary antibody. Oxidative capacity of H_2HFF was measured on a fluorescence microscope and on a microplate reader. Upon addition of H_2O_2, particles were found to exhibit up to a 4 fold increase in fluorescence intensity (Figure 4.9 A) whereas on a microplate reader this was up to 2 fold (Figure 4.9 B). For H_2HFF-BSA labeled silica particles the fluorescence was localized around the periphery of the particle, indicating that the BSA did not penetrate into the pores of the particles due to size restriction. This is similar to what was observed for opsonized particles that were coated with FITC (Figure 4.4 A) where the FITC becomes linked to surface bound protein.

Over the course of experimentation it was observed that H_2HFF labeled particles were prone to oxidation and yielded better signal to noise ratio when experiments were conducted on freshly prepared particles. Particles were therefore used within 48 hours of preparation. A variation in sensitivity to oxidation was observed between various batches of particles and hence H_2HFF fluorescence values in our data should not be used to compare levels of ROS generated in a phagosome between different experiments and particle types. An increase in H_2HFF

fluorescence in a phagosome is instead helpful to understand the temporal increase in ROS within the phagosome.

The goal of the experiments was to detect the appearance of phagosomal ROS in macrophages exposed to silica and latex particles to better understand a relationship between particle phagocytosis and ROS generation to phagolysosomal leakage. ROS was expected to be detected with either particle type due to recruitment of NOX2 and oxidative burst in a phagosome, however data in the silicosis literature have not compared opsonized and non-opsonized particles or different particle types. Upon phagocytosis of H_2HFF labeled opsonized silica particles, a gradual increase in H_2HFF fluorescence was observed that continued over time. The zero time-point is chosen based on when the particular particle is internalized as visualized in the DIC image. Before particle internalization, the H_2HFF fluorescence was restricted to the particle periphery, which cannot be seen in the images due to low signal. However, increasing the brightness of the image allows one to see and quantify the signal. Following particle uptake there is a gradual increase in the fluorescence and this fluorescence was localized to the entire volume of the phagosome. This is likely due to proteolysis of BSA by lysosomal proteases, allowing H_2HFF to access the entire volume of the porous particle. A particle representing this sequence of events is highlighted with a square (Figure 4.10 A) and quantification for the same particle is shown in Figure 4.10 B indicated by Particle 1. An increase in fluorescence is observed for 25 minutes following which there is a rapid decrease in fluorescence. This is presumably due to H_2HFF diffusing to the cytoplasm upon phagolysosomal leakage. This was confirmed by loading MH-S cells with TRITC-dextran and exposing them to H_2HFF labeled silica particles (Figure 4.10 C). Upon particle uptake an increase in H_2HFF fluorescence is observed due to ROS generation as well as an increase in TRITC-dextran fluorescence due to

vesicle fusion. At 24-minutes a decrease in H_2HFF fluorescence parallels the decrease in TRITC-dextran fluorescence linking a decrease in H_2HFF fluorescence to phagolysosomal leakage. After 25 minutes, as observed by an increase in TRITC-dextran fluorescence indicative of endolysosome fusion to the damage phagosome, the same particle is no longer able to show an increase in H_2HFF fluorescence.

A major concern with time-lapse imaging of oxidation sensitive dyes is that the fluorescence light source can cause photo-oxidation of the probe. As a control for this, the fluorescence of a particle that was in the field of view but not in contact with any cells (ie. not phagocytosed) was quantified (Fig 4.10 A, solid triangles). External particles did not show any increase in H_2HFF fluorescence indicating that a periodic exposure to fluorescence did not result in photo-oxidation of H_2HFF (Figure 4.10 B, non-phagocytosed trace). This shows that photo-oxidation does not contribute to the phagosomal ROS. Quantification of other phagocytosed silica particles (Particle 2-4) shows a consistent trend in which an increase in H_2HFF fluorescence is observed indicative of ROS generation, followed by a decrease at a later stage suggestive of phagolysosomal leakage (Figure 4.10 B).

To investigate if ROS generation also occurs in a phagosome containing latex particles, macrophages were exposed to H_2HFF-labeled opsonized-latex particles. A gradual increase in H_2HFF fluorescence was also observed in phagosomes containing latex particles (Figure 4.10 D) indicative of the presence of phagosomal ROS. This result is expected since activated NOX is associated with all types of phagosomes (Kamen *et al.*, 2008; Russell *et al.*, 2009; VanderVen *et al.*, 2009). However, unlike silica particles, there was no loss of fluorescence at later times of up to 50 minutes, consistent with the observation that phagosomes containing latex particles do not leak (Figure 4.6). Quantification of particle fluorescence shows an increase in H_2HFF

fluorescence reaching a plateau after about 20 minutes (Figure 4.10 D and E). A similar trend was observed for other particles (particles 2-5). An increase in fluorescence of these phagocytosed particles was not due to photo-oxidation as non-phagocytosed particles showed no increase (an example is marked by a triangle in Figure 4.10 D, E). Similar results were found for other particles outside of cells.

Above data where the H_2HFF fluorescence tapered off by 30 minutes is consistent with another study showing NOX activity tapering off after 25 minutes (VanderVen *et al.*, 2009) (VanderVen *et al.*, 2009). This could be due to saturation of H_2HFF or an inability to generate more ROS. We ruled out the possibility of H_2HFF saturation by inducing photo-oxidation of the particles or adding exogenous H_2O_2 after the fluorescence signal reached a plateau. In either case there was a further increase in the H_2HFF fluorescence suggesting that there was enough dye available for further oxidation. Our data detecting phagosomal ROS is consistent with other studies that have used H_2HFF and other sensors like H_2DCFDA and DHR in phagosomes (Savina *et al.*, 2006; Kamen *et al.*, 2008; Li *et al.*, 2009; VanderVen *et al.*, 2009; Tlili *et al.*, 2010). It further indicates that after 30 minutes, ROS is no longer produced. Data from Figure 4.7 shows dissociation of PX domains from phagosomes happens by 9 minutes after internalization, however, the catalytic subunit $gp91^{phox}$ responsible for electron transfer should persist on a phagosome suggestive of a continuous ROS generation. The fact that a further increase in phagosomal ROS was not detected after 30 minutes, assuming it is not due to limitations of the H_2HFF probe is suggestive of a mechanism that regulates phagosomal ROS generation. It should also be noted VanderVen et al., observed a 4-fold increase in phagosomal fluorescence of H_2HFF in macrophages that were pre-stimulated with LPS compared to resting

macrophages (VanderVen *et al.*, 2009). We have used resting macrophages throughout our study.

Because silica particles may also get coated with proteins in the lung fluid before being phagocytosed by macrophages, we were interested in comparing phagosomal ROS generation between non-opsonized and opsonized silica particles. Similar to opsonized particles, silica particles coated with H2HFF-BSA (non-opsonized) also shows an increase in particle fluorescence indicative of phagosomal ROS generation. As indicated for the particle marked by a square there is a loss of H_2HFF signal upon phagolysosomal leakage (Figure 4.11 A). Quantification of other particles shows a similar trend (Figure 4.11 B). The uptake of non-opsonized latex particles labeled with H_2HFF also leads to an increase in particle fluorescence indicative of phagosomal ROS generation. In this case, the fluorescence levels off after 30 minutes, similar to opsonized latex particles.

This data confirms that whether particles are silica or latex, opsonized or not, there is ROS generation in a macrophage phagosome. Because H_2HFF is a non-specific ROS sensor it cannot distinguish between various reactive oxygen species, or one that is membrane damaging versus a non-damaging one. These experiments have not detected the type of ROS that is generated or directly linked ROS with phagolysosomal leakage. It is a reasonable hypothesis given that ROS has been shown to chemically alter lipids in bilayers. An alternate possibility to explain leakage of silica phagosomes and not latex phagosomes is that silica can physically cause membrane damage unrelated to ROS. There is no literature to support this scenario and it seems unlikely as the negatively charged silica surface and negatively charged phospholipid head groups of the phagosomal membrane will not show favorable electrostatic interactions. There is substantial literature to support generation of a membrane damaging hydroxyl radical by silica

particles and therefore we favor a hypothesis where silica interacts with the phagosomal ROS to produce hydroxyl radicals.

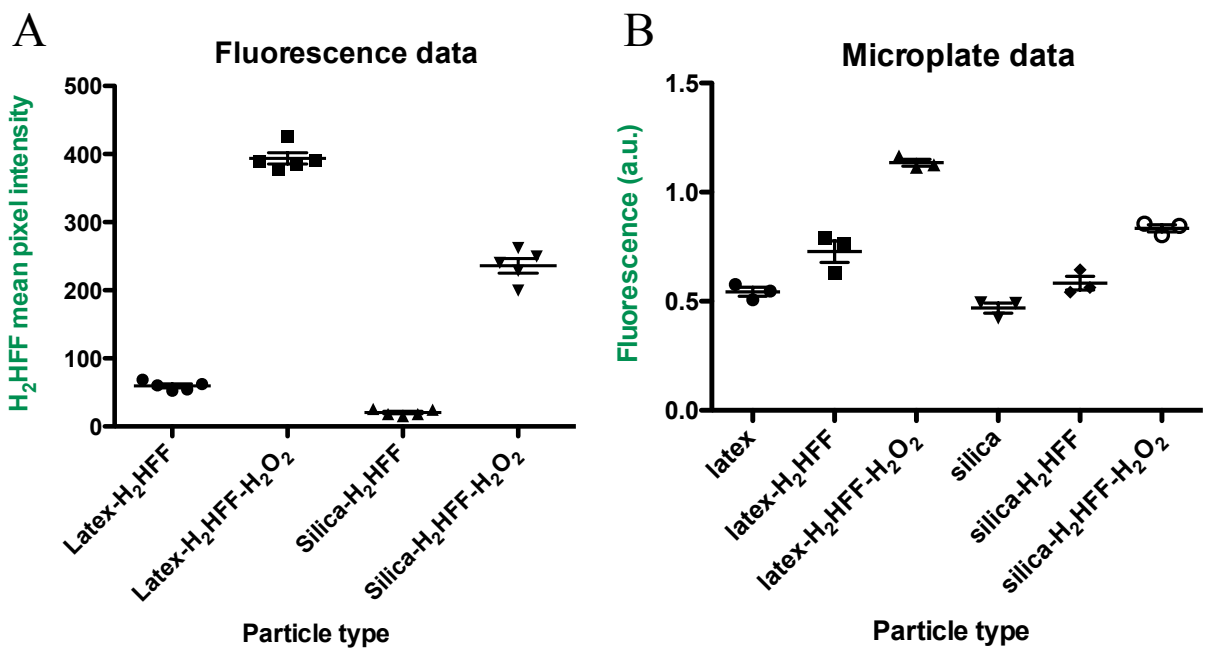

Figure 4.9: H_2HFF labeled silica and latex particle oxidize in presence of exogenous H_2O_2

Silica or latex particles labeled with H_2HFF-BSA were exposed to H_2O_2 in order to test sensitivity of H_2HFF towards oxidation. An increase in fluorescence on an individual particle was imaged using (A) fluorescence microscopy or a collective fluorescence from these particles was measured using (B) a microplate reader. (A) The dot plot represents quantification of fluorescence from an individual particle both pre and post-exposure to H_2O_2. (B) The dot plot of microplate data represents data set of an experiment done in triplicate. Data acquired on a microscope or on a microplate reader shows in increase in H_2HFF fluorescence following addition of H_2O_2.

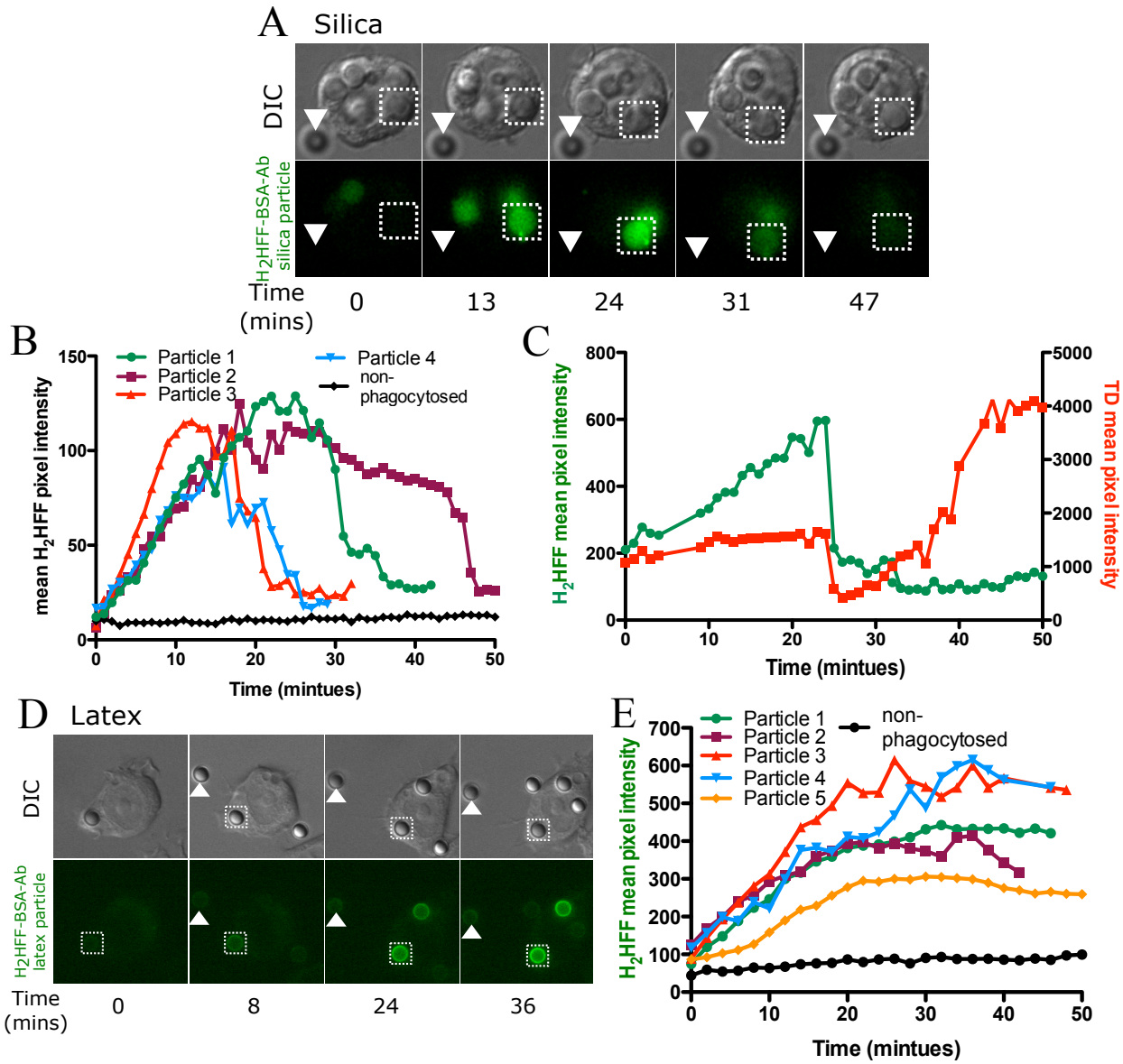

Figure 4.10: ROS is detected in a phagosome containing either opsonized silica or latex particle

H_2HFF-BSA was coupled to either silica or latex particles, following which they were opsonized. MH-S macrophage cells were exposed to either of these particles and imaged every minute for silica particles and imaged 2 minutes apart for latex particles using a widefield epifluorescence microscope. (A) Phagosomes containing opsonized silica particles labeled with H2HFF-BSA (square) show an increase in fluorescence indicative of ROS generation. The fluorescence of the phagosome later decreased indicative of leakage. Non-phagocytosed particles (triangle) did not

show any change in fluorescence. (B) Quantification of fluorescence of several particles from several cells. Particle 1 is the particle indicated by a square in Panel A. (C) To confirm that a decrease in H_2HFF fluorescence observed in Panel A is due to phagolysosomal leakage, macrophages loaded with TRTIC-dextran were exposed to H_2HFF-BSA labeled silica particles. A decrease in TRITC-dextran and H_2HFF fluorescence was observed simultaneously at 25 min confirming the decrease is due to phagolysosomal leakage. (D) Latex particles labeled with H_2HFF-BSA also showed an increase in fluorescence (square) indicative of ROS generation. Non-phagocytosed particles (triangle) do not show an increase in fluorescence (control). (E) Quantification of the fluorescence from Panel D and other cells. Particle 1 represents quantification of particle indicated by the square in Panel D.

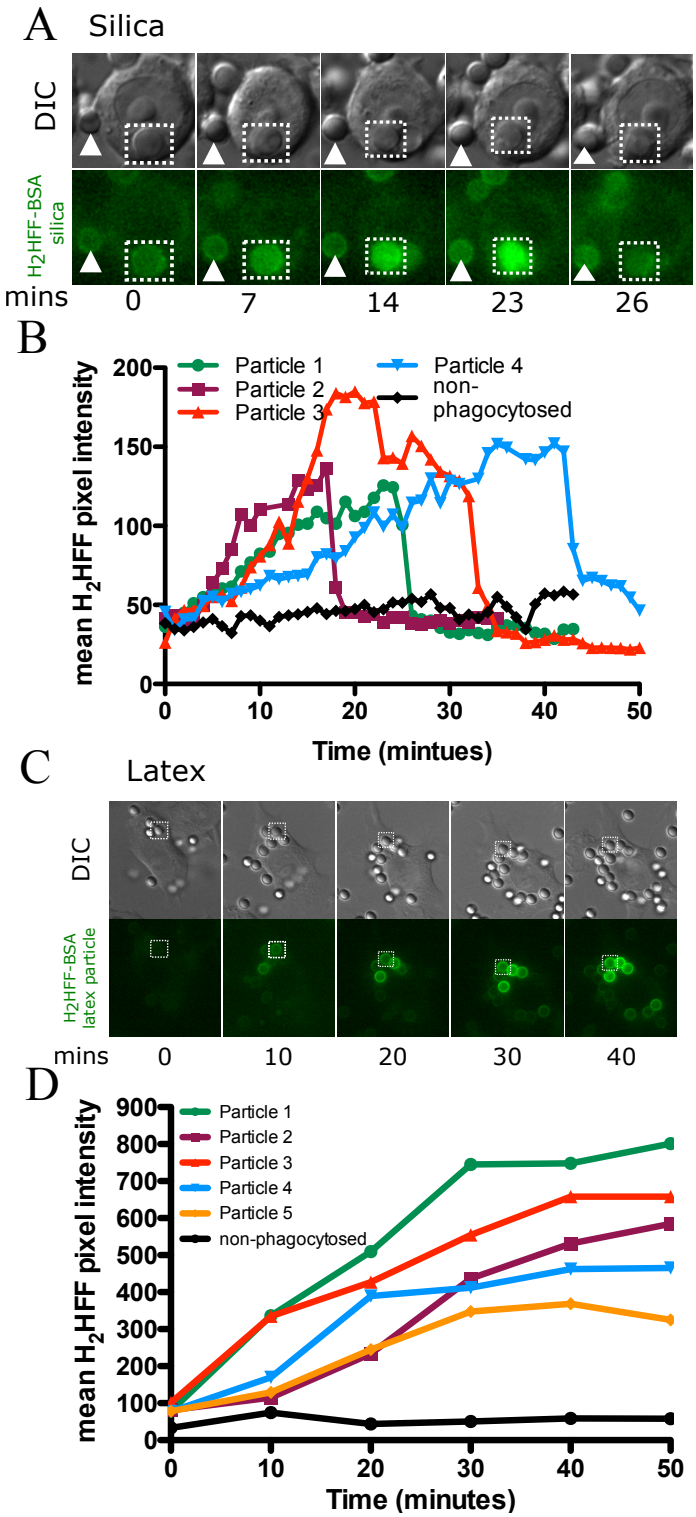

Figure 4.11: ROS is detected in a phagosome containing either non-opsonized silica or latex particle

H_2HFF-BSA was coupled to either silica or latex particles. MH-S macrophage cells were exposed to either of these particles and imaged every minute for silica particles and imaged 5 minutes apart for latex particles using an epifluorescence microscope. (A) Phagosomes containing opsonized silica particles labeled with H_2HFF-BSA (square) show an increase in fluorescence indicative of ROS generation. The fluorescence of the phagosome later decreased indicative of phagolysosomal leakage. Non-phagocytosed particles (triangle) did not show any change in fluorescence. (B) Quantification of fluorescence of 4 particles from 4 different cells. Particle 1 is the particle indicated by the square in Panel A. (C) Latex particles labeled with H_2HFF-BSA also shows an increase in fluorescence (square) indicative of ROS generation. Non-phagocytosed particles do not show an increase in fluorescence (control). (E) Quantification of the fluorescence from Panel D and other cells. Particle 1 represents quantification of particle indicated by the square in Panel D.

4.8.3: Investigation of phagosomal H_2O_2 using Peroxyfluor (PF)-6 AM

Hydrogen peroxide is a requirement for $^{\bullet}OH$ radical generation by Fenton chemistry and therefore detecting H_2O_2 will provide a clue to the ROS pathway where superoxide to hydrogen peroxide to hydroxyl radical formation takes place. Recently, fluorescence probes have been developed to specifically visualize H_2O_2 production. A palette of H_2O_2 specific probes (Dickinson *et al.*, 2010; Dickinson and Chang, 2011) were obtained from Dr. Christopher Chang at UC Berkeley to attempt to detect H_2O_2 within phagolysosomes. These new probes utilize a boronate group to mask the fluorescein moiety. Generation of H_2O_2 results in oxidation of boronate, which by subsequent chemical reactions results in unmasking of fluorescein and an increase in fluorescence (Lin *et al.*, 2013).

PF6-AM has relatively high specificity for detecting H_2O_2 relative to other ROS probes (Dickinson and Chang, 2011). To utilize PF6-AM for further studies, its sensitivity was compared to CM-H_2DCFDA, a non-specific ROS sensor. Macrophages were incubated with either of the probes and the cytoplasmic signal was compared following exposure of H_2O_2. A 12-fold average increase in fluorescence was observed in macrophages pre-loaded with PF6-AM when exposed to H_2O_2 (Figure 4.12 A). PF6-AM was fluorescent within 30 seconds of H_2O_2 addition (Figure 4.12 A and B). Single cell evaluation shows a variation in peak fluorescence between cells. This difference could be due to a variation in the loading of dye in each cell or retention of the dye in each cell or possibly a variation in ROS generation or anti-oxidant levels in every cell. In macrophages loaded with the pan-ROS sensor (CM-H_2DCFDA) and imaged at the same settings as PF6-AM, only a 2.5 fold increase in fluorescence was observed following H_2O_2 addition (Figure 4.12 C and D), showing PF6-AM to be better as it generated greater signal.

Before looking at generation of phagosomal H_2O_2 using PF6-AM, we wanted to confirm H_2O_2 generation in the cytoplasm using PF6-AM and compare it with CM-H_2DCFDA incubated macrophages exposed to crystalline silica. An increase in PF6-AM fluorescence was not observed within the first few hours of silica exposure or during cell death (Figure 4.13 A). This is contrary CM-H_2DCFDA data where such an increase has been shown upon silica exposure and a massive increase during cell death (Figure 4.21). To confirm that PF6-AM was retained throughout the time course, H_2O_2 was added after waiting for 30 minutes, 2 hours, 4 hours or 6 hours following loading of PF6-AM in the cells. After 30 minutes and 2 hours a progressive decrease in PF6-AM signal was observed but the signal was dectatable. After 4 hours, there was little PF6-AM signal to be detected (Figure 4.13 B-E and quantified in F). This result demonstrates that cells do not retain PF6-AM, which limits its application for detecting cytoplasmic H_2O_2. This is surprising as the intracellular esterase should cleave the acetoxymethyl (AM) group associated with the dye, trapping it within the cell. In a personal communication with Dr. Christopher Chang this shortcoming of the dye was confirmed.

To study phagosomal H_2O_2 generation upon silica particle phagocytosis, it was therefore decided to try leaving PF6-AM in the medium throughout the experiment instead of loading cells and then washing it out of the incubation medium. To facilitate visualization of phagosome maturation along with H_2O_2 detection, cells were pre-loaded with 4 kD TRITC-dextran. This was followed by incubation with PF6-AM and 3-μm opsonized silica particles. Cells were imaged one minute apart for the first 60 minutes and then at 5 minute intervals. Upon phagocytosis of silica particle and phagosome maturation, TRITC-dextran accumulated in the phagosome (Figure 4.14 A and B). A simultaneous increase in PF6-AM fluorescence in the phagosome was not observed over the first 30 minutes after uptake. The PF6-AM fluorescence increase preceded the

dextran leakage by a minute (Figure 4.14 C). Since PF6-AM is smaller than dextran it will diffuse into a leaking phagolysosome faster than dextran can diffuse out, resulting in an increase in phagosomal signal that is indicative of the presence of H_2O_2. As there was an increase in PF6-AM fluorescence in the phagosome, a decrease in cytoplasmic PF6-AM fluorescence was observed. It could be argued that this increase is due to PF6-AM diffusing into the phagolysosome from the cytoplasm and accumulating in the phagosomal lumen leading to an increase in PF6-AM fluorescence. But this is unlikely as TRITC-dextran fluorescence continues to decrease over time in the phagolysosome suggestive of membrane leakage while PF6-AM signal is increasing in spite of membrane permeability. An increase in PF6-AM fluorescence in the phagolysosome is likely to be due to oxidation of this dye by H_2O_2 in the phagolysosome and its diffusion back in to the cytoplasm during phagolysosomal leakage. Surprisingly, a continued decrease of cytoplasmic PF6-AM signal was observed throughout the 30 minutes prior to phagolysosomal leakage even though PF6-AM was in the media. Following leakage, cytoplasmic PF6-AM signal stabilizes and then starts to increase suggesting that oxidized dye was diffusing into the cytoplasm.

Another phagosome representing a similar trend is shown in Figure 4.14 D-F where vesicle refusion after phagolysosomal leakage is also observed. Since the events of phagolysosomal leakage occur during a 5 minutes time interval, this data lacks temporal resolution compared to Figures 4.14 A-C but shows a similar trend.

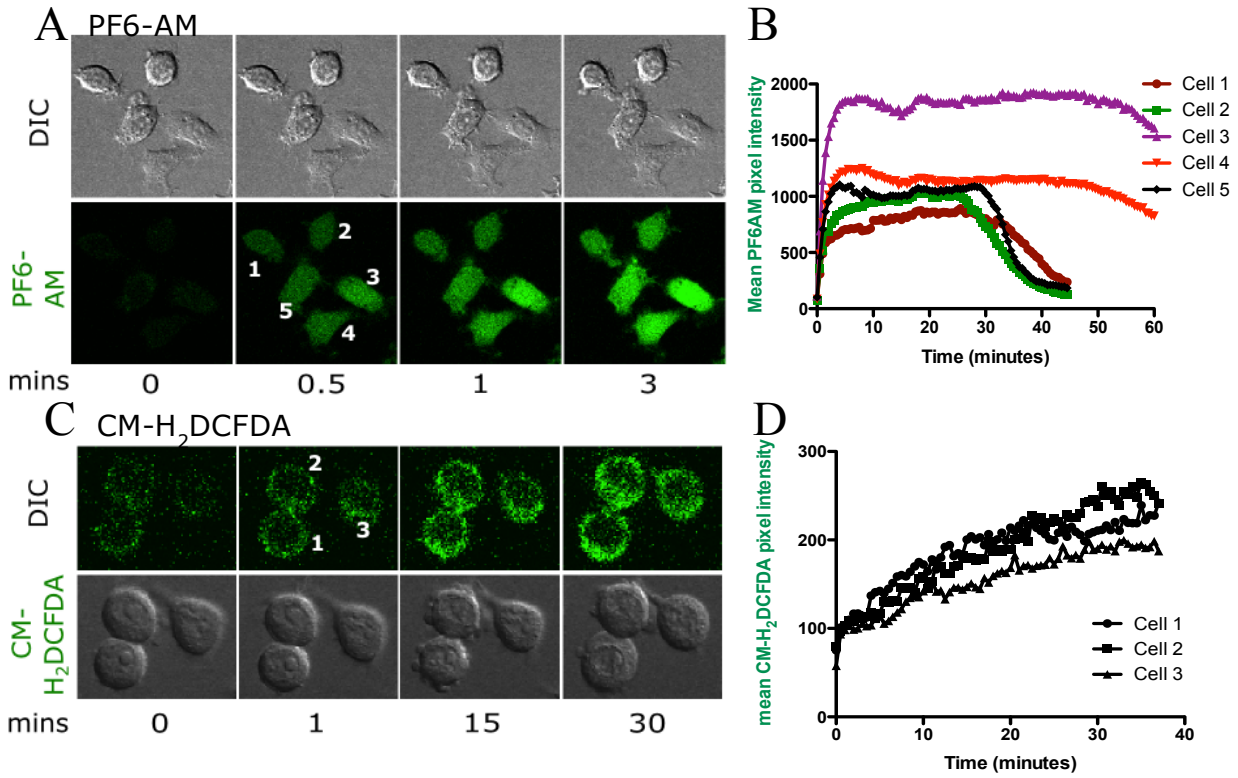

Figure 4.12: PF6-AM dye is more sensitive in detecting H_2O_2 compared to CM-H_2DFCDA

In order to detect ROS, specifically H_2O_2, macrophages were loaded with PF6-AM and CM-H_2DCFDA. Sensitivity of each probe towards H_2O_2 was tested by addition of exogenous H_2O_2. (A) Cells were loaded with 10 µM PF6-AM and following a washout of the dye 0.5 M H_2O_2 was added to the cells. Cells were imaged 30 seconds apart for 1 hour. (B) A quantification of cells in panel A show a rapid increase in fluorescence within first few minutes of the addition of H_2O_2 that reaches peak levels within 5 minutes. (C) Cells were loaded with 10 µM CM-H_2DCFDA and following a washout of the dye 0.5 M H_2O_2 was added to the cells. Cells were imaged 1 min apart for 1 hour. (D) A quantification of cells in panel C shows a gradual increase in fluorescence that continues over a period of 30 minutes.

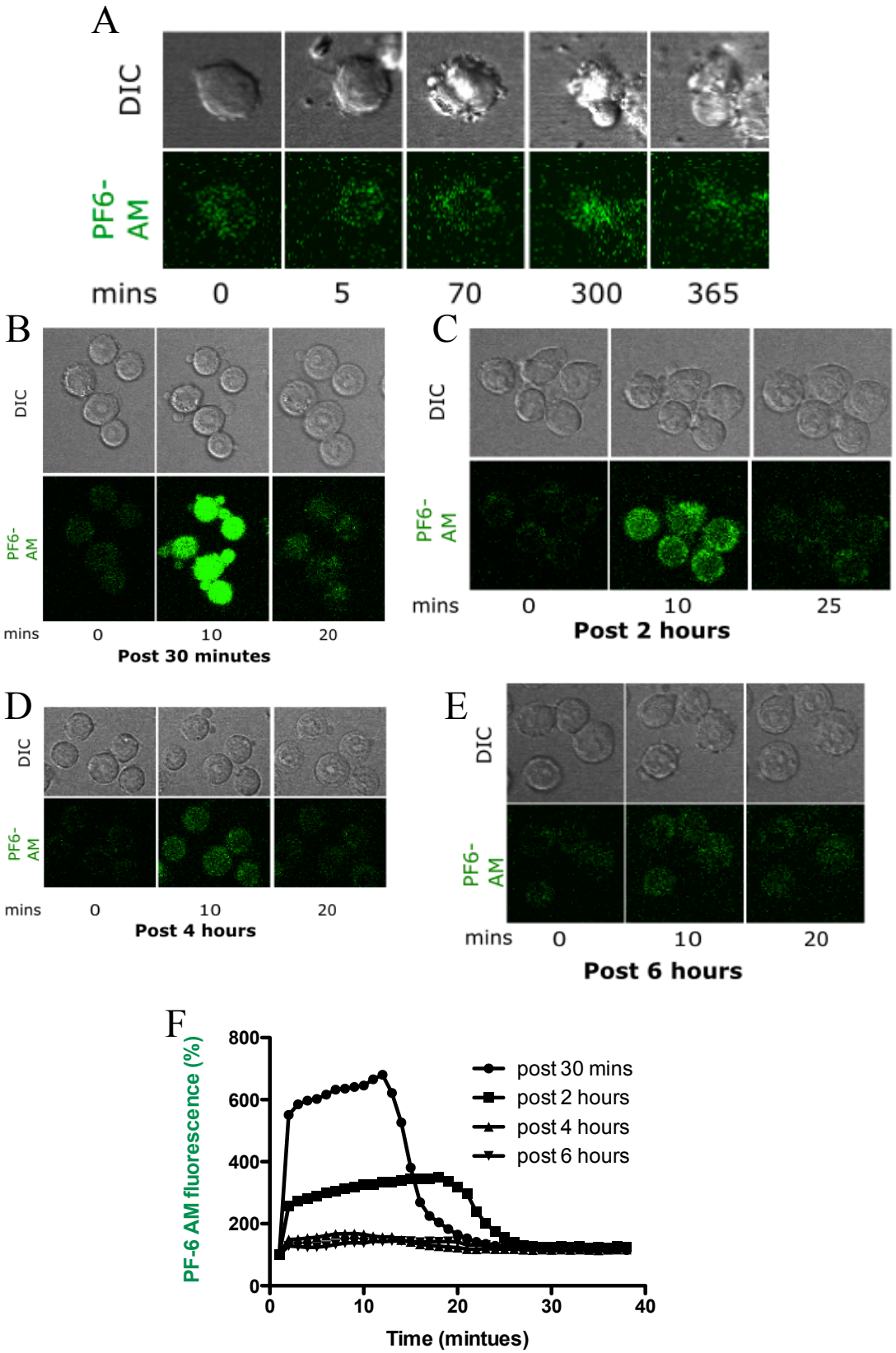

Figure 4.13: PF6-AM is retained poorly by cells

(A) Macrophages loaded with PF6-AM were exposed to crystalline silica and imaged over time. For the entire duration of the experi4ment an increase in PF6-AM fluorescence was not observed. Data is representative of time points following particle uptake (5 and 70 minutes) and during cell death (300 minutes onwards). To test for the retention of the dye, H_2O_2 was added to cells after 30 minutes (B), 2 hours (C), 4 hours (D) or 6 hours (E) following a washout of the dye. (F) A quantification of a region of interest containing at least 25 cells shows a maximum increase in fluorescence when H_2O_2 is added to cells after 30 minutes of washing out PF6-AM. Addition of H_2O_2 after waiting for a longer time following a washout of the dye after waiting for different time points show a decrease in PF6-AM fluorescence. By four hours barely any signal could be detected.

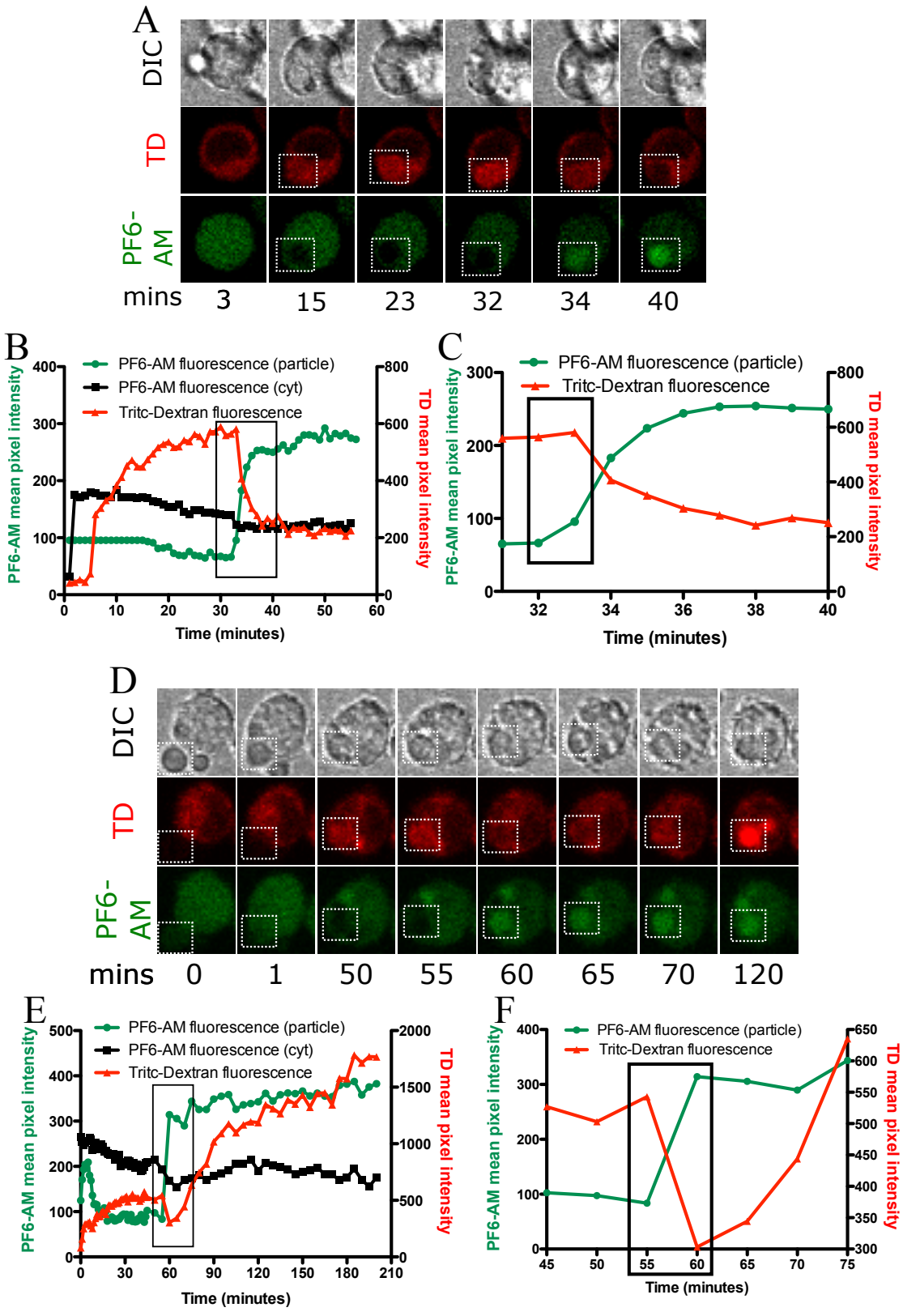

Figure 4.14: H_2O_2 is detected during phagolysosome leakage using PF6-AM

To investigate generation of phagosomal H_2O_2 and phagolysosomal leakage, cells were allowed to endocytose 4 kD TRITC-dextran (TD) following which they were incubated with 10 μM PF6-AM for 30 minutes. The dye was left in the medium and 20 $\mu g/cm^2$ opsonized amorphous spherical silica particles were added to the cells. Cells were imaged every minute on a confocal microscope. (A-C) and (D-F) represent data from two individual particles in different cells. Time when cell interacted with the particle was set as time 0. (A) Following particle uptake and maturation an increase in TRITC-dextran fluorescence and a black hole is observed in PF6-AM channel (15- 32 minutes). Upon phagolysosomal leakage (34-40 minutes) a decrease in TRITC-dextran and an increase in PF6-AM fluorescence is observed in the particle. (B) A quantification of the data in panel A) represent these changes. (C) A further analysis of phagolysosomal dynamics between 30-40 minutes show that an increase in PF6-AM fluorescence in the phagolysosome between 32-33 minutes precedes the release of TRITC-dextran from phagolysosome that occur between 33-34 minutes. (D) Similar data was observed for another particle. Cell-particle interaction occur at 0 minutes following which the particle is internalized. Images were acquired one minute apart for 50 minutes, following which the image acquisition was done 5 minutes apart. An increase in TRITC-dextran fluorescence is observed up to 55 minutes. At 60 minutes a simultaneous decrease in TRITC-dextran fluorescence and in increase in PF6-AM fluorescence is observed in the phagolysosome. A gradual increase in TRITC-dextran fluorescence was observed from 65 minutes onwards that continued progressively. (E) A quantification of data in panel D) represent these changes. (F) A further analysis of phagolysosomal dynamics between 45-75 minutes show that phagolysosomal leakage and an increase in PF6-AM fluorescence occur in a 5 minute window of 55-60 minutes.

4.9: Inhibitors of NADPH oxidase or vATPase delay phagolysosomal leakage caused by silica particles

Our data shows generation of phagosomal ROS prior to phagolysosomal leakage. Whether phagolysosomal leakage is associated with ROS generation could not be determined from this data. In order to understand the relationship between NOX generated ROS and phagolysosomal leakage, macrophages were pretreated with NOX inhibitor, DPI (Savina *et al.*, 2006; Rybicka *et al.*, 2010) and the vATPase inhibitor bafilomycin A1(Yoshimori *et al.*, 1991). NOX is required for electron transport into phagosomes and reduction of oxygen to superoxide is the first known step in ROS generation. Protons pumped in by vATPase to maintain low pH are consumed during conversion of superoxide to H_2O_2 (Fisher, 2009; Winterbourn and Kettle, 2013). We therefore hypothesized that inhibiting either of these processes will prevent phagolysosome leakage. A schematic for the relevant reactions within a phagosome is shown in Figure 4.15 A.

To validate the role of an inhibitory effect of NOX generated ROS on phagolysosomal leakage, macrophages were pre-loaded with 4 kD FITC-dextran and treated with diphenyleneiodonium (DPI) before exposure to silica particles. DPI binds to FAD inhibiting electron transfer via $gp91^{phox}$ into the phagosomal lumen to prevent superoxide formation. Contrary to expectation, DPI did not inhibit phagolysosomal leakage but only delayed it. The time it took for an individual phagosome to leak after particle uptake was tracked in cells that were treated with DPI. In untreated cells, the average time for phagolysosomal leakage was 25 minutes, which increased to 55 minutes upon pre-treatment with 5 μM DPI (Figure 4.15 B). Increasing the concentration of DPI to 10 μM did not prolong the time of phagolysosomal leakage any further. Thus NOX inhibition did not prevent leakage but rather delayed it.

To test if inhibiting H_2O_2 generation will prevent phagolysosomal leakage, cells were exposed to bafilomycin A1, a vATPase inhibitor. vATPase is required for the proton flux to an endosome and lysosome to maintain the acidic pH in these organelles. Endosomes and lysosomes fuse with phagosomes, and the delivery of the vATPase to the phagosomal membrane makes the phagosomal lumen acidic as well. Cells preloaded with FITC-dextran were incubated with bafilomycin A1 and then exposed to silica particles. FITC fluorescence is quenched under acidic conditions but upon incubating cells with bafilomycin-A1 for 30 minutes, an increase in FITC fluorescence was observed indicative of an increase in pH in these organelles (Figure 4.15 D). Following particle uptake, a continuous increase in phagosomal FITC-dextran fluorescence was observed (Figure 4.15 C and D). This is similar to that of an increase in phagosomal fluorescence by pH insensitive TRITC-dextran. Similar to DPI treatment, bafilomycin A1 did not prevent phagolysosomal leakage but only delayed it. It took an average of 100 minutes after uptake for phagolysosomal leakage in bafilomycin A1 treated cells whereas untreated cells leaked by 30 minutes (Figure 4.15).

Surprisingly, the effect of bafilomycin A1 in delaying phagolysosomal leakage was more potent than that of DPI. Considering that neither of these inhibitors prevents phagolysosomal leakage it is possible that either the chemical inhibitors were not completely effective allowing ROS to form more slowly. Alternatively, if the compounds were completely effective, silica induced phagolysosomal leakage occurs independent of NOX activity and NOX only accelerates the process.

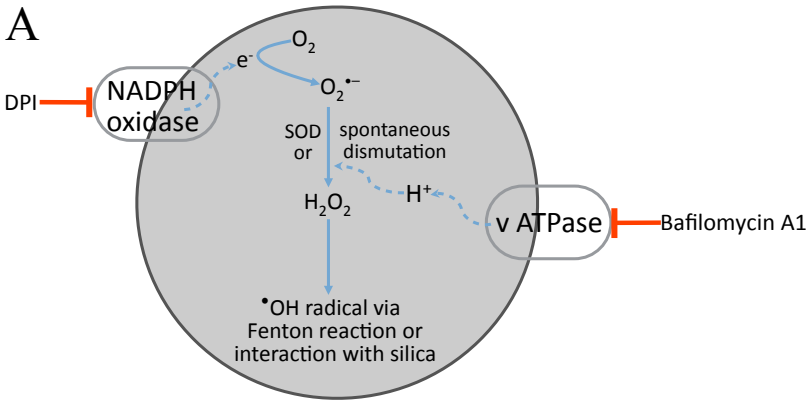
A
DPI
NADPH oxidase
e-
O2
O2•−
SOD or
spontaneous dismutation
H2O2
H+
v ATPase
Bafilomycin A1
•OH radical via Fenton reaction or interaction with silica

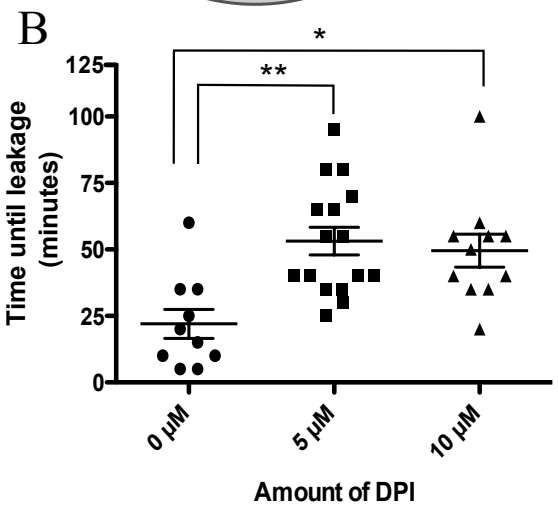
B
Time until leakage (minutes)
125
100
75
50
25
0
*
**
0 µM
5 µM
10 µM
Amount of DPI

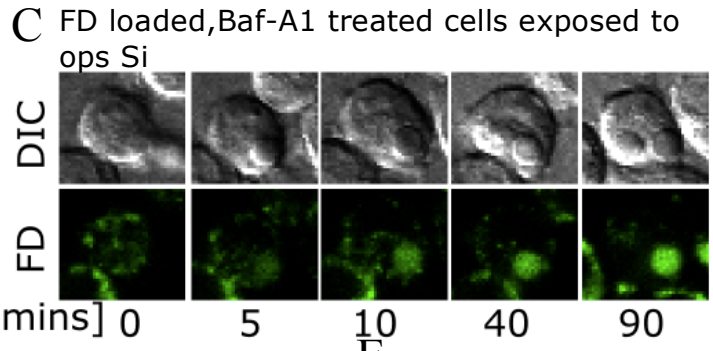
C FD loaded,Baf-A1 treated cells exposed to ops Si
DIC
FD
[mins] 0
5
10
40
90

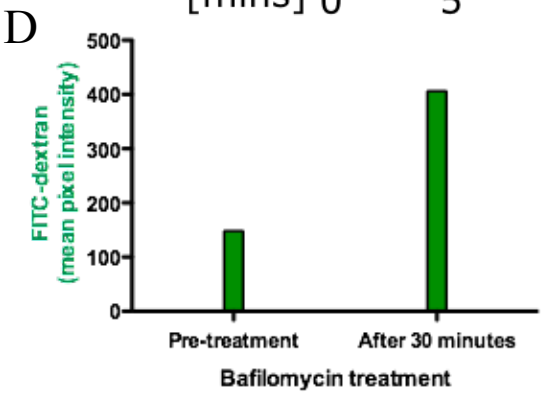
D
FITC-dextran (mean pixel intensity)
500
400
300
200
100
0
Pre-treatment
After 30 minutes
Bafilomycin treatment

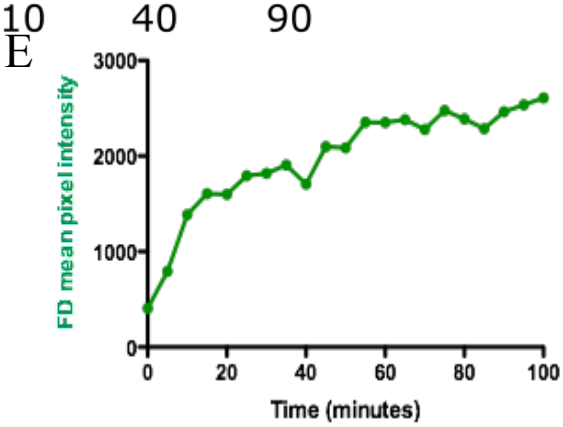
E
FD mean pixel intensity
3000
2000
1000
0
0
20
40
60
80
100
Time (minutes)

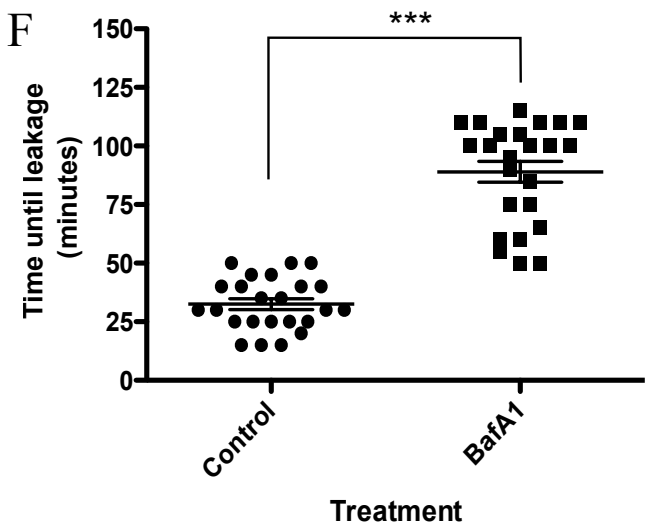

Figure 4.15: Effect of pharmacological inhibition on phagolysosomal leakage in macrophages

(A) A pictorial representation for the inhibitors diphenylene iodonium (DPI) and Bafilomycin-A1 show their targets resulting in inhibition of ROS generation. DPI is an inhibitor of NADPH oxidase preventing generation of superoxide. Bafilomycin-A1 is an inhibitor of vATPase that prevents the flux of protons required to convert superoxide to hydrogen peroxide. Cells were loaded with 4 kD FITC-dextran for 2.5 hours and post-wash of dextran cells were incubated with inhibitors for 30 minutes following which they were exposed to opsonized silica particles. The time it took for an individual phagolysosome to leak FITC-dextran after particle uptake was measured. (B) After treatment with the NADPH oxidase inhibitor DPI (0μM, 5 μM and 10 μM) an average time for phagolysosomal leakage increased from 25 minutes to 60 minutes. **P< 0.001 and * P< 0.01 (C) Following pre-treatment of cells that were loaded with 4kD FITC-dextran to Bafilomycin-A1 and exposure to opsonized silica particles silica particles there is a gradual increase in FITC-dextran fluorescence in a phagosome due to fusion of vesicles containing FITC-dextran with the phagosome. (D) Upon addition of Bafilomycin-A1 there was an increase in FITC-dextran fluorescence confirming the activity of the inhibitor. (E) A

quantification of the phagosome containing opsonized silica particle in panel C) shows an increase in FITC-dextran fluorescence following vesicle fusion. (F) After treatment with 150 nM Bafilomycin-A1 (a vATPase inhibitor) an average time for phagolysosomal leakage increased from 30 minutes to 90 minutes. ***P<0.0001. The bar in the dot plot represents the mean ± SEM of multiple phagolysosomal leakage events for each treatment type.

4.10: Phagolysosomal leakage is detected in Cos7 cells that lack NADPH oxidase upon exposure to silica particles

It has been presumed that ROS is a key player in silica dependent membrane damage. NOX is the major source of ROS in macrophages. In order to investigate the role of NOX generated ROS in membrane damage and leakage, we sought to use cells that do not express NOX and thus should not generate ROS in phagosomes. Thus, Cos7 cells lacking NOX (Price *et al.*, 2002) were used to investigate whether silica particles could cause phagolysosomal leakage in a NOX independent manner. Cos7 cells not only lack NOX subunits but also lack Fc-receptor (FcR), which is required for recognition of opsonized particles and FcR mediated uptake of opsonized particles. Non-opsonized (BSA coated) or opsonized (anti-BSA antibody coated) particle uptake was therefore quantified using the particle uptake assay in Cos7 cells. The FcγRIIA receptor was also transfected into Cos7 cells (FcR-Cos7) to differentiate between specific (FcR-dependent) and non-specific (FcR-independent) uptake. Particle uptake in Cos7 cells was compared with MH-S cells as particle uptake is well characterized for macrophages (Gilberti *et al.*, 2008; Costantini *et al.*, 2011). It is expected that the FcR-Cos7 cells will show greater opsonized particle uptake compared to Cos7 cells while the uptake of non-opsonized particles should be independent of FcR. Upon exposure to non-opsonized silica particles, MH-S macrophages showed higher particle uptake than Cos7 or FcR-Cos7 cells. Both Cos7 and FcR-Cos7 show a similar rate of particle uptake over the first 60 minutes as expected since non-opsonized particle uptake is independent of the Fc receptor (Figure 4.16A). When MH-S macrophages were exposed to opsonized silica particles, they phagocytosed 100% of the particles within 30 minutes. There was no uptake of opsonized silica particles by 30 minutes in Cos7 cells but Fc-Cos7 rapidly phagocytosed opsonized particles, (Figure 4.16 B). In order to determine whether particle uptake continued in Cos7 cells but on a slower time scale than in

macrophages, the uptake kinetics for opsonized and non-opsonized silica particles in Cos7 cells was done over a period of 32 hours. Cos7 cells took up particles over time, but at a much slower rate than macrophages. By 30 hours, 60% non-opsonized and 20% opsonized particles were taken up by these cells (Figure 4.16 C).

To understand whether silica particles can result in NOX independent leakage, Cos7 cells were preloaded with 4 kD TRITC-dextran and exposed to non-opsonized silica particles. A slow rate of particle uptake was confirmed in time-lapse imaging as only few particles were found in TRITC-dextran labeled phagosomes at early time points. Imaging of a phagocytosed particle showed an increase in phagosomal TRITC-dextran fluorescence (up to 85 minutes) followed by a decrease in fluorescence indicative of phagolysosomal leakage (85-90 minutes) and another increase in TRITC-dextran fluorescence indicative of vesicle refusion (95 minutes onward) (Figure 4.17 A). Quantification of the particle in Figure 4.17 A is represented by a red trace in Figure 4.17 B while quantification of other phagocytosed particles is represented by different colored traces in Figure 4.17 C. Time 0 for each particle is adjusted to the time of particle uptake for each particle. Although there is temporal heterogeneity between phagosomes with respect to the time of leakage, all phagosomes examined showed a similar trend of leakage when they contained silica particles.

Phagolysosomal leakage in Cos7 cells was also confirmed by the FITC-dextran leakage assay. Cos7 cells that were allowed to endocytose FITC-dextran and exposed to non-opsonized silica particles showed gradual uptake of particles at different times followed by phagolysosomal leakage (Figure 4.17 D). Quantification of an increase in cytoplasmic and nuclear FITC-dextran fluorescence indicative of leakage is presented in Figure 4.17 E. As individual phagolysosomes leak there is an increase in cytoplasmic and nuclear fluorescence. Due to a leakage of multiple

phagolysosomes in the same cell, a stepwise pattern is observed, consistent with the data from macrophage cells (Figure 4.17 E).

Since opsonized particles were also used to study the dynamics of phagolysosomal leakage in macrophages, we wanted rule out the possibility that leakage was not specific to the non-opsonized particle used in Cos7 cells. To test this, Fc-Cos7 cells were loaded with 4 kD TRITC-dextran and exposed to opsonized silica particles. A red (TRITC-dextran) and green (Fc-GFP) merge show that upon particle uptake there is strong localization of Fc-GFP around the phagosome indicative of an Fc-mediated uptake process (Figure 4.18 A). As time progresses, a decrease in Fc-GFP around the phagosome was observed which could be due to receptor recycling. As a control, FcR-Cos7 cells were exposed to non-opsonized silica particles and upon uptake, no increase in Fc-GFP fluorescence around a particle was observed. During uptake of opsonized particles, there was an increase in TRITC fluorescence followed by a decrease at 135 minutes indicative of leakage. There was an increase in fluorescence from 150 minutes and onwards indicative of membrane sealing and continued endolysosomal vesicle fusion. Interestingly, the rate of increase in phagosomal fluorescence is much greater than it was before leakage. Non-opsonized silica particles also cause phagolysosomal leakage in Cos7 (Figure 4.17) and FcR-Cos7 cells (Figure 4.18). Thus silica can induce phagolysosomal leakage in both MH-S macrophages and Cos7 cells and subsequently the leaky phagosome gets repaired and shows continued endolysosomal fusion. Therefore in Cos7 cells that lack NADPH oxidase, phagolysosomal leakage is NADPH oxidase independent.

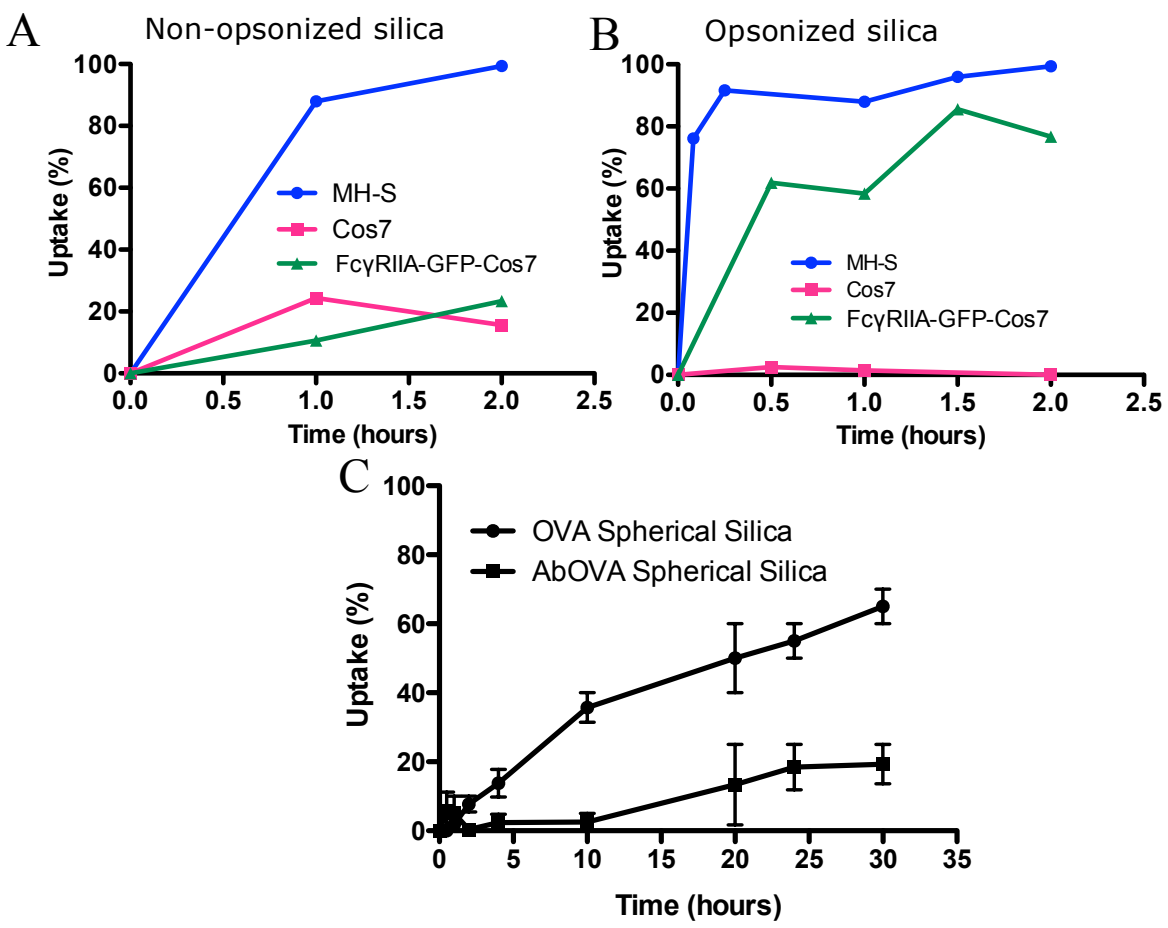

Figure 4.16: Cos7 cells show a delayed uptake of non-opsonized silica particles when compared with macrophages

In order to determine particle uptake MH-S macrophages, Cos7 cells or Cos7 cells expressing FcγRIIA-GFP (Fc-Cos7) were exposed to non-opsonized (A) or opsonized (B) silica particles for different time points following which the cells were fixed and labeled with corresponding antibody. (A) MH-S cells show a rapid uptake of non-opsonized silica particles whereas Cos7 and Fc-Cos7 show little uptake of these particles in first two hours. (B) MH-S cells show a rapid uptake of opsonized silica particles whereas the Cos7 cells known to lack Fc receptors do not show particle uptake. Fc-Cos7 shows an increase in particle uptake although not similar to that of MH-S cells. Data represented is from a single trial. Since a significant amount of particle uptake was not observed for first two hours in Cos7 cells, experiments were performed to determine

particle uptake for extended time period. (C) An increase in uptake of non-opsonized silica particles is observed over the duration of many hours. In comparison to 55 % uptake for non-opsonized silica particles, less than 20% of opsonized silica particles were 4found to be taken up by Cos7 cells by 20 hours. As time progressed there was an increase in uptake of particles (75% for non-opsonized and 17% for opsonized particles). Data is representative of 3 individual experiments.

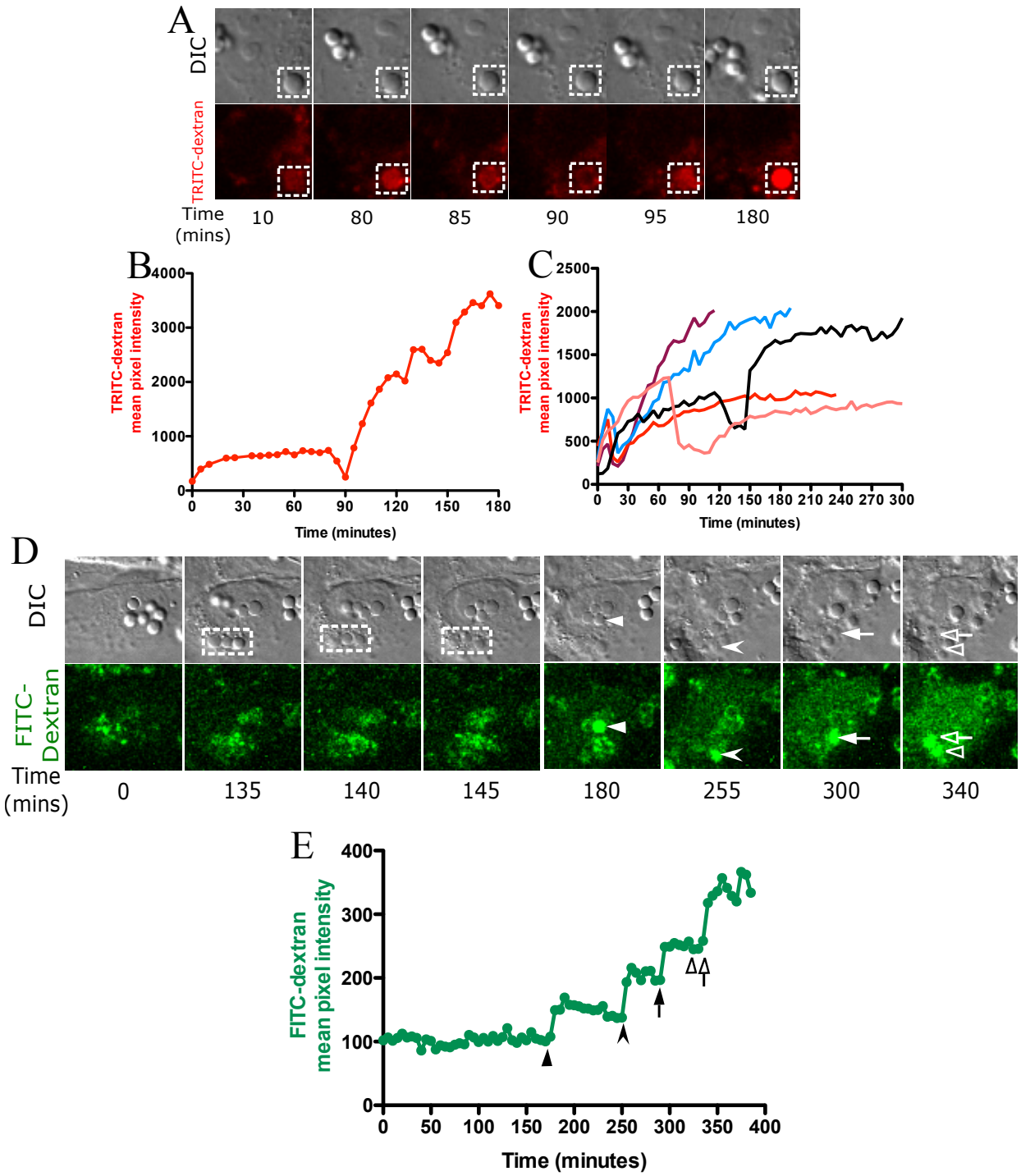

Figure 4.17: NADPH oxidase deficient Cos7 cells can phagocytose silica particles and undergo phagolysosomal leakage

(A) Cos7 cells loaded with 4 kD TRITC-dextran were exposed to 20 µg/cm^2 non-opsonized silica particles and imaged 5 minutes apart. Because Cos7 cells take a long

time to initiate the process of phagocytosis after exposure to particles images were acquired at 5 minutes intervals to prevent any inhibition of particle uptake due to excessive photo-exposure. The phagolysosomal leakage data for Cos7 cells therefore lacks a comparable temporal resolution to that of MH-S cells where particle uptake is rapid and images were acquired 20 seconds apart. A gradual increase in TRITC-dextran fluorescence was observed upon particle phagocytosis (10 and 80 minutes), followed by a decrease in fluorescence starting at 85 minutes with a maximum loss of signal observed at 90 minutes. Vesicle refusion starts at 95 minutes leading to a subsequent gradual increase in TRITC fluorescence. (B) Quantification of the phagosome in Panel A (C) Phagolysosomal leakage of individual phagosomes from different cells. To confirm that a decrease in TRITC-dextran fluorescence is due to phagolysosomal leakage, experiment was performed by allowing cells to endocytose FITC-dextran. Cells were imaged 5 minutes apart upon exposure to non-opsonized silica particles using confocal microscopy. (D) The time-point preceding the uptake of first particle is set at 0. In a flat cell like Cos7 particle uptake can be determined by a change in the refraction property of the particle. In a DIC image, a particle that is not internalized has a strong shadow on one side (particles in dotted rectangular area at 135 minutes). Upon particle uptake the intensity of the shadow decreases (particles in dotted rectangular area at 145 minutes). A quantal release of FITC-dextran from individual phagolysosomes due to leakage results in an increase in nuclear and cytoplasmic FITC-dextran fluorescence. A transient increase in FITC-dextran fluorescence was observed in each of these phagolysosomes (indicated by solid triangle at 180 minutes, arrowhead at 255 minutes, arrow at 300 minutes and an open triangle and open arrow at 340 minutes). This is suggestive of an increase in pH due to permeability

of the phagolysosomal membrane. An increase in cytoplasmic and nuclear fluorescence is observed along with this transient increase in phagolysosomal FITC-dextran fluorescence. (E) Quantification of cytoplasmic and nuclear area show a stepwise increase in FITC-dextran fluorescence during leakage events as indicated by a solid triangle, arrowhead, arrow and an open triangle and an open arrow that correspond to panel D.

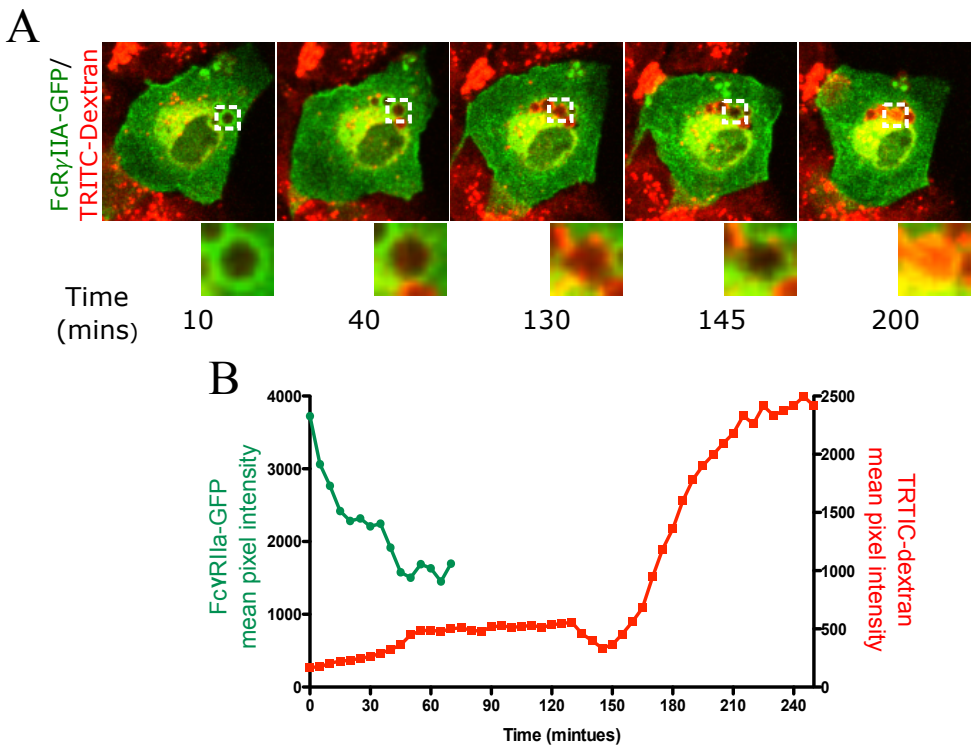

Figure 4.18: Cos7 cells expressing Fc receptor phagocytose opsonized silica particles and undergo phagolysosomal leakage

To confirm that phagolysosomal leakage is not restricted to non-opsonized silica particles in Cos7 cells these were transfected with FcγRIIa-GFP (Fc-Cos7). Fc-Cos7 cells were allowed to endocytose TRITC-dextran to track phagolysosomal leakage following which they were exposed to 20 μg/cm^2 opsonized silica particles. Cells were imaged 2 μm apart in z-direction and 5 minutes apart for the duration of the experiment. (A) A merged image data of Fc-GFP and TRITC-dextran shows an increase in Fc-GFP fluorescence around the phagosome (10 minutes). By 40 minutes the Fc-GFP fluorescence on the phagosome is similar to that of the cytoplasmic GFP. Delivery of TRITC-dextran due to endolysosomal vesicle fusion with the phagosome result in an increase in TRITC-dextran fluorescence at 40 minutes (faintly visible) and continues to increase up to 130 minutes. There is a decrease in TRITC-dextran fluorescence at 145 minutes followed by an

increase at 200 minutes. (B) Quantification of Fc-GFP on periphery of phagosome and TRITC-dextran on the phagosome represent the changes in panel A. While an initial increase in the phagolysosomal TRITC-dextran is not visible in the merged image at 40 minutes a quantification of data represents this early increase in fluorescence. A decrease in TRITC-dextran fluorescence began at 135 minutes and from 150 minutes onwards an increase in TRTIC-dextran fluorescence was observed.

4.11: Phagosomal ROS is detected in a silica phagosome but not in a latex phagosome in Cos7 phagosome

The silica particle surface has been proposed to generate ROS (Fubini and Hubbard, 2003). Silica particles coated with H_2HFF-BSA does not show an increase in fluorescence of the dye comparable to when these are phagocytosed by a macrophage. Thus there may not be sufficient surface generated ROS to result in oxidation of H_2HFF. Further the inhibition of particle uptake using actin inhibitors does not result in cell membrane damage suggesting that the surface generated ROS do not result in damage (Haberzettl *et al.*, 2008; Gilberti and Knecht, 2015). Alternately an inability of ROS generated from the silica surface could be due to its diffusion in the media. Within the confines of a phagosomal membrane this surface generated ROS could be damaging. In order to test the hypothesis that silica particles can generate ROS independent of NOX in a phagolysosome, Cos7 cells loaded with 4 kD TRITC-dextran were exposed to H_2HFF-BSA labeled silica particles. Upon particle uptake, a general trend was observed where there was an increase in TRITC-dextran and H_2HFF fluorescence suggestive of endolysosome-phagosome fusion and ROS generation respectively. For the particle marked by an arrowhead (Figure 4.19 A) there is an increase in H_2HFF fluorescence from 5 minutes onwards while TRITC-dextran fluorescence does not change after uptake for up to 445 minutes. At 440 minutes, there was a transient increase in H_2HFF fluorescence indicative of ROS generation, following which at 445 minutes a simultaneous decrease in TRITC-dextran and H_2HFF fluorescence was observed, indicative of leakage. Post leakage due to vesicle fusion a huge increase in TRITC fluorescence was observed (Figure 4.19 A and B). For the particle labeled with a solid triangle, a similar trend was observed although leakage happened at 85 minutes (Figure 4.19 A and C). Particles that

were not phagocytosed do not show an increase in H_2HFF fluorescence indicating that long time-lapse did not result in photo-oxidation of the dye and that silica by itself does not result in oxidation of H_2HFF (Figure 4.19 D). It is likely that an interaction of silica with phagolysosomal contents causes a chemical reaction that results in ROS generation in the absence of NOX activity.

To validate if the observed ROS generation was specific to silica particles, Cos7 cells loaded with 4 kD TRITC-dextran were exposed to H_2HFF-BSA labeled latex particles. TRITC-dextran fluorescence increased as a ring around the non-porous latex particles (Figure 4.20 A), similar to what occurs in MH-S cells (Figure 4.6). While TRITC-dextran fluorescence continued to increase during phagosome maturation, an increase in H_2HFF fluorescence was not measured (Figure 4.20 B). This is in contrast to MH-S macrophages where phagosomes containing both opsonized and non-opsonized latex particles show ROS generation due to NOX activity (Figures 4.10 D, E and 4.11 C, D). This result further confirms the inability of Cos7 cells to generate ROS upon phagocytosis of latex particles due to absence of NOX whereas silica particle generate ROS in the absence of NOX activity. Latex particles that were not phagocytosed do not show an increase in H_2HFF fluorescence indicating that long time-lapse did not result in photo-oxidation of the dye (Figure 4.20 C). This result indicates that silica surface chemistry is the likely source of ROS molecules that damage phagosomal membranes and cause leakage.

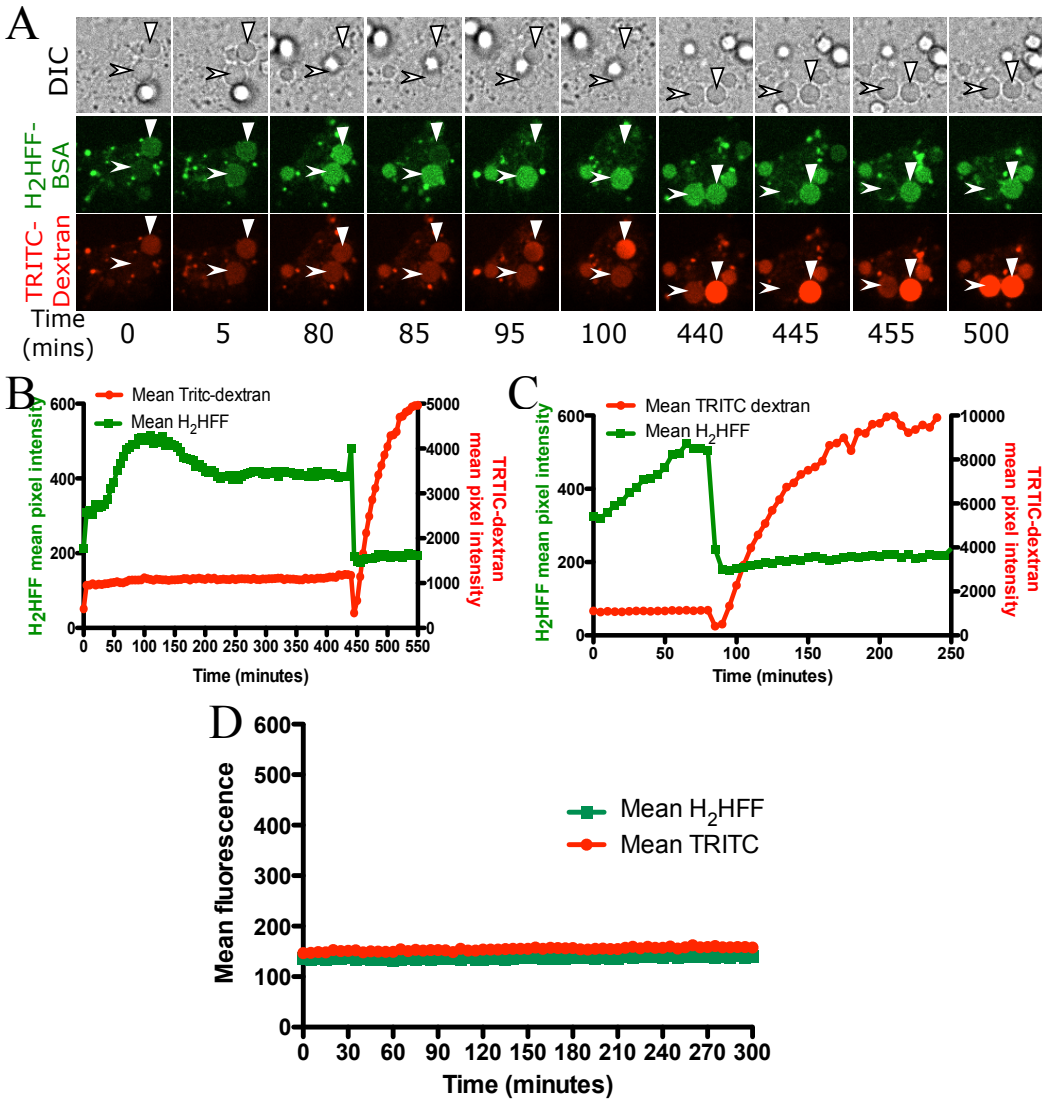

Figure 4.19: ROS is detected in a phagosome containing silica particle in Cos7 cells

(A) Cos7 cells loaded with 4 kD TRITC-dextran were exposed to 20 µg/cm^2 H_2HFF labeled non-opsonized silica particles and imaged at 5 minutes intervals. Upon uptake, an increase in TRITC-dextran fluorescence as well as H_2HFF fluorescence was observed for both phagosomes marked by arrowhead and solid triangle. For a phagolysosome marked by arrowhead, at 445 minutes a decrease in H_2HFF and TRITC-dextran fluorescence due to phagolysosomal leakage was observed. Following leakage, a gradual increase in

TRITC-dextran fluorescence was observed, consistent with continued endosome fusion. However, H_2HFF fluorescence remained low as expected since the dye has leaked out of the phagosome. The particle labeled by a solid triangle was already phagocytosed when imaging began and hence an increase in TRITC-dextran fluorescence at 5 minutes whereas, a gradual increase in H_2HFF fluorescence is observed. At 85 minutes a decrease in both H_2HFF and TRITC-dextran fluorescence was observed indicative of phagolysosomal leakage. 95 minutes onwards a gradual increase in TRITC-dextran fluorescence was observed indicative of endosome fusion. (B) Quantification of fluorescence of the particle indicated by an arrowhead. (C) Quantification of fluorescence of the particle indicated by the solid triangle. (D) Since the images are acquired for a long duration the quantification of fluorescence of the particle in an area outside of the cell show that particles do not undergo either auto-oxidation or photo-oxidation (Mean H_2HFF). Background TRITC fluorescence on the particle remains constant throughout this period (Mean TRITC). Quantification in panel D represents mean $\pm$ SEM of 10 individual particles.

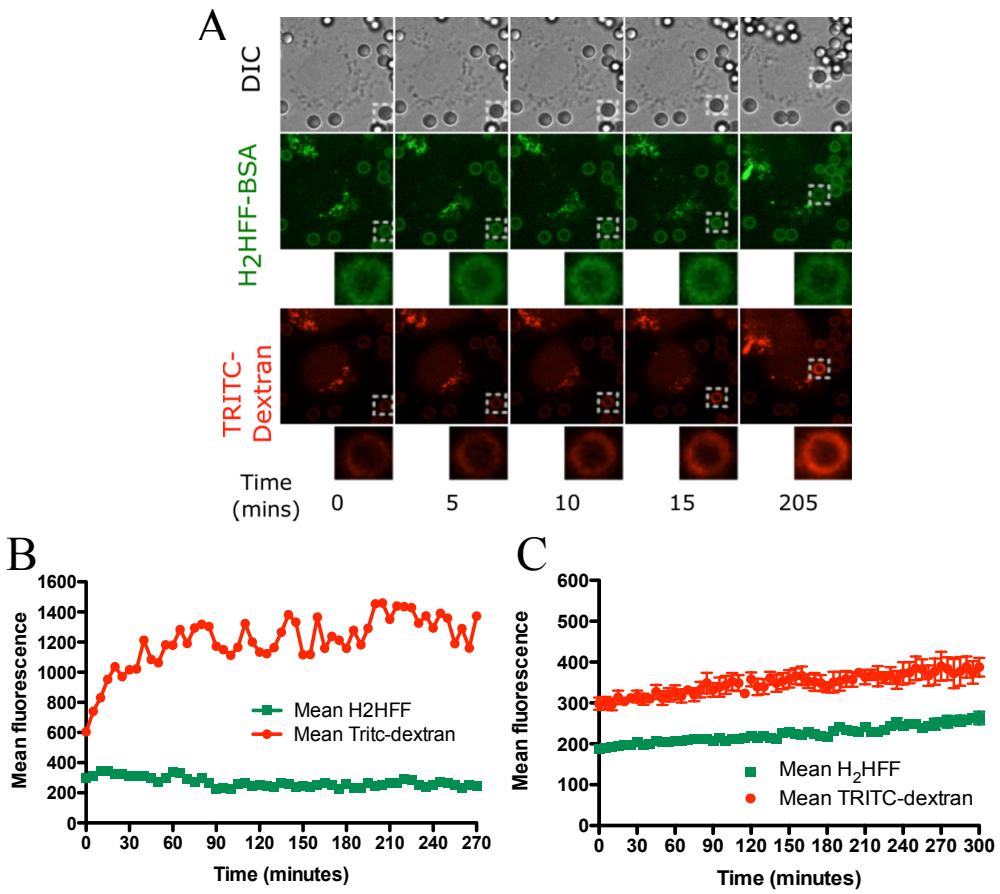

Figure 4.20: ROS is not detected in a phagosome containing latex particle in Cos7 cells

(A) Cos7 cells allowed to endocytose 4 kD TRITC-dextran were exposed to 20 µg/cm^2 H_2HFF labeled non-opsonized latex particles and imaged at 5 minutes intervals. While an increase in TRITC-dextran fluorescence around the latex phagosomes was observed over time, no increase in H_2HFF fluorescence was measured. (B) Quantification of the fluorescence of the particle in Panel D. Representative of 20 individual phagosomes. (C) Since the images are acquired for a long duration the quantification of fluorescence of the particle in an area outside of the cell show that particles do not undergo either auto-oxidation or photo-oxidation (Mean H_2HFF). Background TRITC fluorescence on the particle remains constant throughout this period (Mean TRITC). Quantification in panel D represents mean $\pm$ SEM of 10 individual particles.

4.12: Investigation of ROS in the cytoplasm upon exposure of MH-S macrophages to silica and latex particles

Silica induced ROS generation has been shown to result in upregulation of NF-κB and AP-1 resulting in activation of pro-inflammatory cytokines (Rojanasakul *et al.*, 1999; Kang *et al.*, 2000). These cytokines play a role in progression of disease pathology and development of fibrosis. Various studies have also proposed that silica induced ROS is responsible for cell death (Shen *et al.*, 2001; Deshpande *et al.*, 2002; Hu *et al.*, 2006; 2007). Relating cell death to a real-time measurement of ROS has been impeded by the lack of reliable probes and advanced microscopy procedures. An increase in cytoplasmic ROS has been attributed to NOX activation (Zeidler *et al.*, 2003). However, it is unclear whether phagosomal ROS can make its way to the cytoplasm. Because phagosomal ROS was also detected in phagosomes containing latex particles we decided to compare cytoplasmic ROS in cells exposed to silica and latex particles. This would give an indication whether any cytoplasmic ROS is due to NOX activation or some other source.

Alveolar macrophages were loaded with a non-specific ROS sensor CM-H_2DCFDA that is well retained in the cytoplasm. When ROS is generated, H_2DCFDA oxidizes to the fluorescent product DCF. To confirm the sensitivity of CM-H_2DCFDA to ROS, cells loaded with the probe were exposed to H_2O_2. Using a motorized stage, cells plated in different wells of an 8-well chamber slide were imaged without any particle exposure or upon exposure to silica or latex particles. Cells exposed to no particles or latex particles do not show any increase in CM-H_2DFCDA fluorescence over time whereas cells exposed to silica particles showed an increase in fluorescence (Figure 4.21 B) indicating the presence of ROS in the cytoplasm to be specific to cells exposed to silica particles. Time course evaluation of cells exposed to silica particles show an

increase in ROS upon cell shrinkage (cell 1, 170 minutes) or upon cell blebbing and transition to secondary necrosis, marked by cell swelling (cell 1, 250 minutes onwards). For cell 2, an increase in ROS was observed during blebbing and the transition to secondary necrosis (600 minutes onwards) (Figure 4.21 A). A quantification of these two cells is represented in Figure 4.21C. Other cells show a similar increase in fluorescence upon cell blebbing. In spite of the presence of NOX generated ROS in both the latex and silica phagosomes, cytoplasmic ROS was only detected in cells treated with silica particles

CM-H_2DCFDA is a non-specific sensor and one of the ROS it has been shown to detect is H_2O_2 (Morgan *et al.*, 2011; Kalyanaraman *et al.*, 2012). To specifically detect H_2O_2 and confirm the CM-H_2DCFDA data, MH-S cells were transfected with a plasmid driving expression of the genetically encoded H_2O_2 specific sensor, roGFP2-Orp1. Fusion of redox active GFP (roGFP2) with Orp1, a thiol peroxidase, makes the probe highly sensitive for H_2O_2 (Morgan *et al.*, 2011). Generation of H_2O_2 results in formation of an intermolecular disulfide group on Orp1 that is transferred to roGFP2 by thiol-disulfide exchange, resulting in oxidation of a thiol on roGFP2. This redox change in roGFP2 can be imaged using dual excitation and single emission microscopy and ratiometric quantification. Cells exposed to silica particles show a small increase in the cytoplasmic fluorescence ratio within the first two hours after particle uptake. The increase is statistically significantly higher than observed after uptake of latex particles and control (Figure 4.22 B). The change in the ratio for latex particles is similar to that of control. Upon exposure to silica particle and tracking an individual macrophage over a longer time period, a significant increase in ratio was only observed much later, at the time of

cell blebbing and during secondary necrosis (cell 1, 270 minutes and onwards, Figure A). Quantification for cell 1 and cells 2-5 reveal a similar outcome where a significant change in ratio and thus H_2O_2 generation is observed during the final stages of apoptotic cell death (Figure 4.22 C).

A consistent pattern emerges from the CM-H_2DCFDA and roGFP2-Orp1 probes in which cells exposed to silica particles show a small early increase in cytoplasmic ROS at the same time as we measure an increase in phagosomal ROS. However, a more dramatic increase in cytoplasmic ROS was detected during cell death. In cells exposed to latex particles, ROS was not detected in the cytoplasm at any time and the cells did not die. This suggests one or both of the following where 1) an increase in cytoplasmic ROS is dependent on the type of a particle and it could be independent of phagosomal ROS and 2) The phagosomal ROS generated by NOX in the presence of latex particle can be quenched by intraphagosomal and intracellular antioxidants whereas the ROS produced by silica particles that cannot be quenched and can enter the cytoplasm.

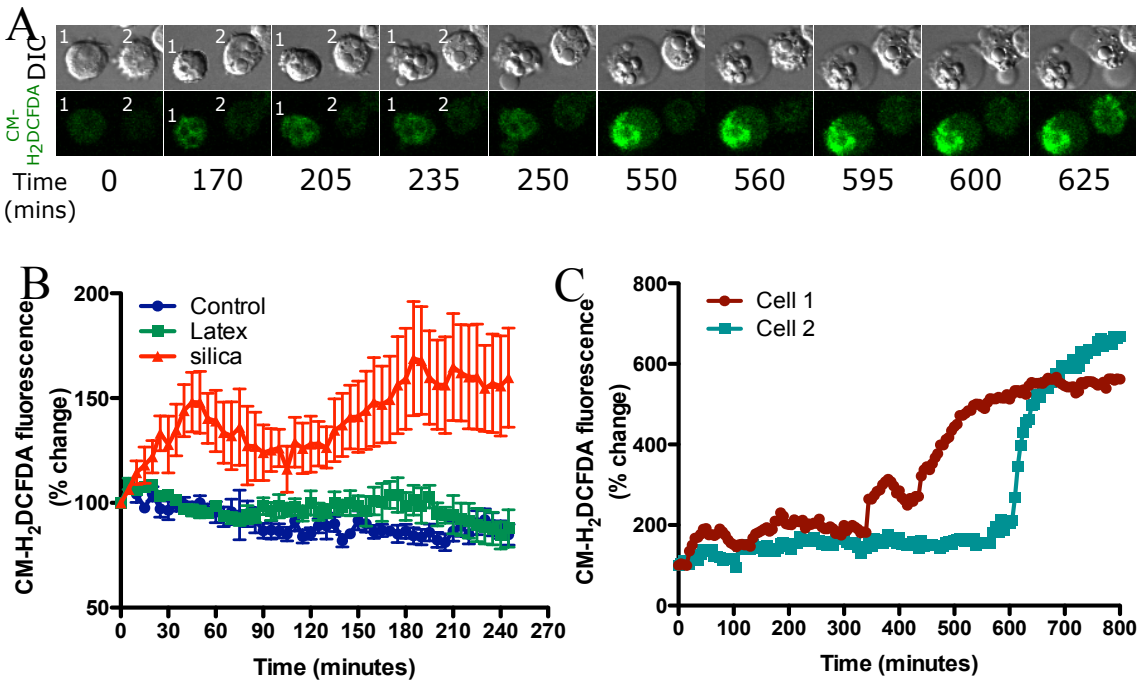

Figure 4.21: A distinct biphasic cytoplasmic ROS is detected upon exposure of MH-S cells to silica particles

MH-S cells were plated in an 8-well chambered slide, labeled with 10µM CM-H_2DCFDA and 4 fields per well were imaged 5 minutes apart after exposure to either opsonized silica particles or latex particles (A-C). (A) A small increase in fluorescence is observed over time in cells 1 and 2 upon particle addition that remain constant up to 250 minutes for cell 1 and 600 minutes for cell 2 (Quantified in Panel C). A further increase in fluorescence is observed following cell blebbing during secondary necrosis (cell swelling) at 550 minutes for cell 1 and 625 minutes for cell 2. (B) Comparison of the change in CM-H_2DCFDA fluorescence in control cells and upon exposure to latex or silica particles show that only silica results in the generation of measurable cytoplasmic ROS. Data represents the mean ± SEM of at least 10 individual cells for each treatment type. (C) Quantification for cells 1 and 2 in Panel A shows a small increase in fluorescence after particle addition as opposed to the huge increase in ROS generation during cell death.

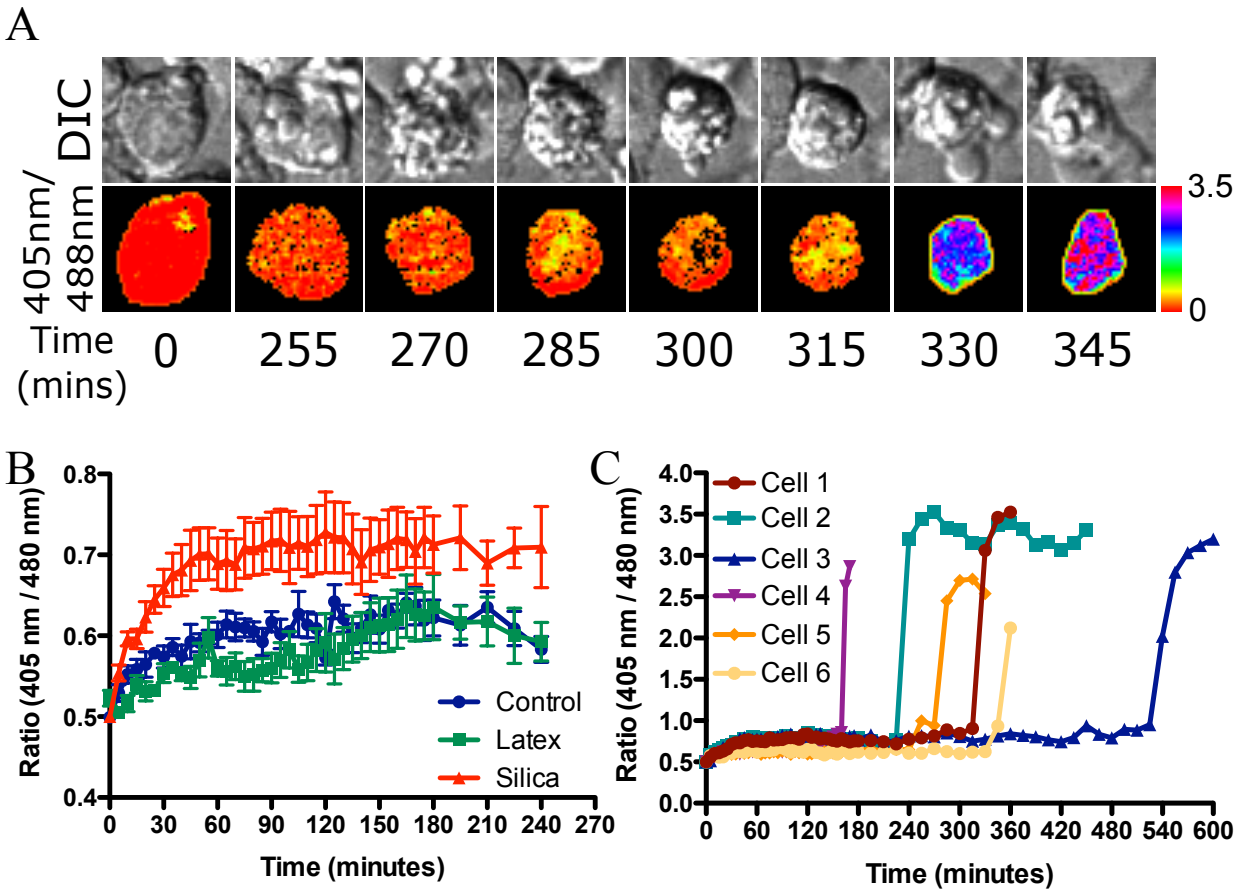

Figure 4.22: roGFP2-Orp1, a novel H_2O_2 sensor confirms the biphasic generation of cytoplasmic ROS in MH-S cells exposed to silica particles

To detect specifically H_2O_2 in cells, MH-S cells expressing roGFP2-Orp1 were exposed to either opsonized silica or latex particles and imaged at 5 minutes intervals. (A) A small increase in roGFP2 ratio is observed in first hour, however this cannot be represented in the ratiometric images. Following cell blebbing a huge change in roGFP2 ratio is observed at 330 minutes. (B) Comparison of the change in roGFP2-Orp1 ratio in control cells and upon exposure to latex or silica particles show that only silica results in the generation of measurable cytoplasmic H_2O_2. Data represents mean ± SEM of at least 10 individual cells for each treatment type. (C) Quantification for cell in D) is represented by

cell 1 and other cells are represented as 2-6. All of these cells show a huge increase in ratio at different time points that relates to cell death.

4.13: Investigation of mitochondrial ROS in MH-S macrophages exposed to silica particles

We have observed mitochondrial hyperpolarization, caspase activation and cell blebbing to occur within a 5-minute time period. Studies have shown mitochondrial dysfunction resulting in cell death cell death (Hu *et al.*, 2007; Park *et al.*, 2009; Arap *et al.*, 2013). We therefore hypothesized that the robust increase in cytoplasmic ROS observed during cell death is associated with ROS generated from mitochondria. To confirm this hypothesis, cells were transfected with mito-roGFP2-Orp1 that can specifically detect H_2O_2 in mitochondria. In ratiometric images, mitochondria are pseudo colored red and orange to indicate basal H_2O_2 levels. The ratio only increases after the cell had started to bleb (390 minutes onwards) represented by shades of blue and pink (Figure 4.23 A). Cell 1 in Figure 4.23 B represents quantification for the cell in Figure 4.23 A and other cells 2-5 show a similar trend where an increase in ratio is only observed upon the initiation of cell blebbing (Figure 4.23 B). Thus it is likely that the ROS detected in the cytoplasm during cell blebbing is mitochondrial in origin.

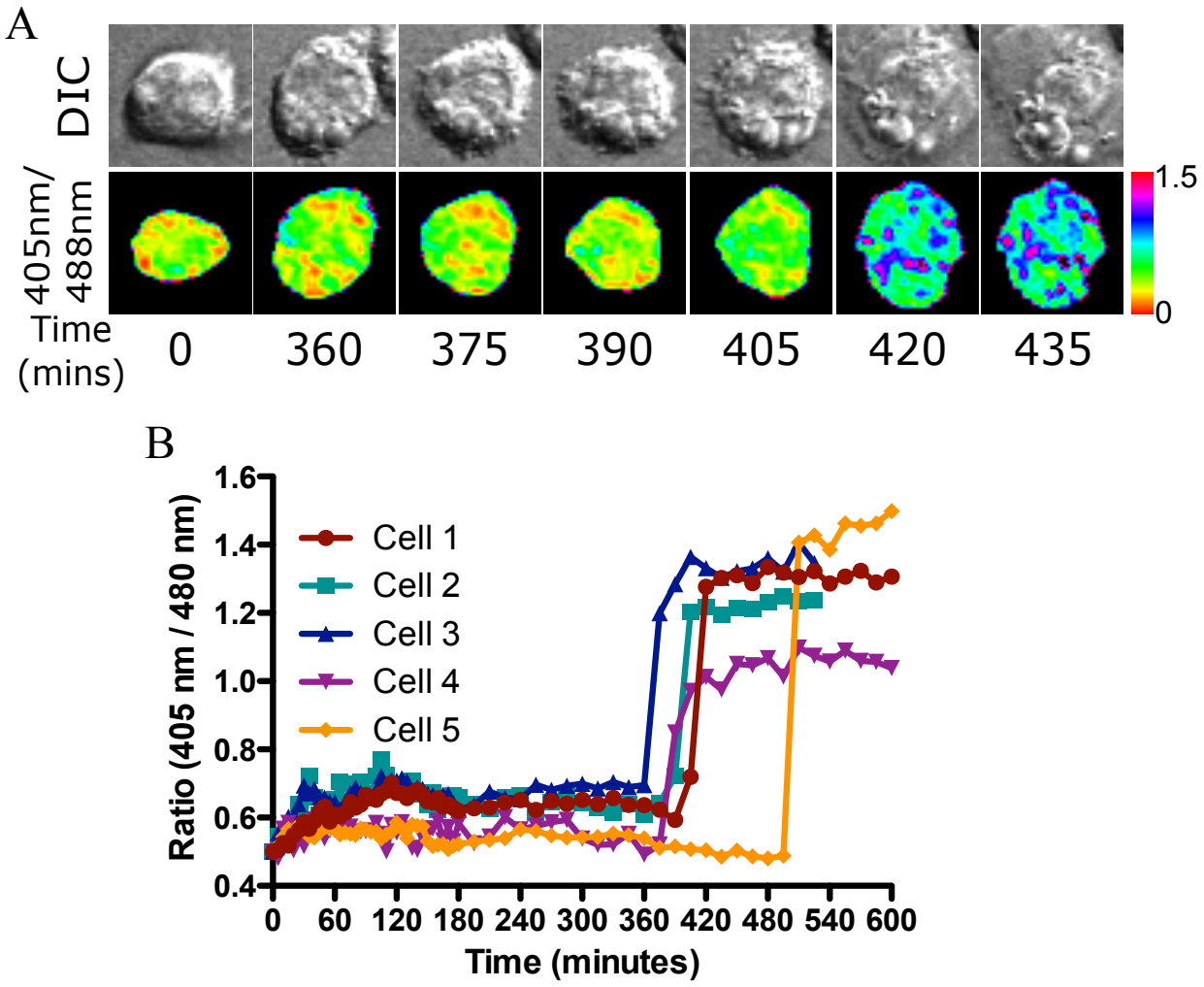

Figure 4.23: roGFP2-Orp1 localized to mitochondria shows a robust H_2O_2 generation upon cell blebbing

To detect mitochondrial H_2O_2, MH-S cells expressing mito-roGFP2-Orp1 were exposed to opsonized silica particles. In pseudocolored ratiometric images, mitochondria appear in red to yellow color indicative of basal H_2O_2 whereas upon secondary necrosis there is an increase in H_2O_2 during (420 minutes onwards), mitochondria appear blue to pink in color. (A) Quantification of cell represented in B) is shown by cell 1. Other cells show a similar trend where a huge increase in ratio is observed during secondary necrosis after 350 minutes.

4.14: A micron sized aggregate of synthesized silica nanoparticles result in phagolysosomal leakage whereas nanoparticles do not result in leakage

The finding that 3 μm silica particles result in ROS generation within a phagosome independent of NOX is novel. The data so far shows that the chemistry of silica is important in this process and uptake of silica particle should be toxic. However, silica nanoparticles are getting used in various applications of biomedical imaging and as vehicles for drug delivery (Brigger *et al.*, 2002). These are likely to stay in circulation for a long period increasing their bioavailability. Both micron and nano sized silica particles have been shown to possess hemolytic activity related to particle chemistry (Pavan *et al.*, 2014). We therefore hypothesized that if silica chemistry was sufficient to cause leakage, then the uptake of nano-sized particle that localize in the endolysosomal vesicle could result in damage to these vesicles.

To further investigate this question, the ability of 200 nm (submicron) and 50 nm (nano) silica particles to damage endolysosomal vesicles was studied. 200 nm silica particles were synthesized using Stöber synthesis (Napierska *et al.*, 2010) by Dr. Puxian Gao laboratory in IMS at UConn. 50 nm silica particles that were synthesized using sol-gel method were purchased from Kisker Corporation. Unlike particles larger than 500 nm that are internalized by phagocytosis, nano and submicron sized particles are presumed to be taken up by endocytosis into endosomal vesicles. Upon vesicle maturation, the endosomes fuse with lysosomes forming an endolysosome.

In order to investigate leakage of endolysosomes, macrophages were loaded with 4 kD FITC-dextran and exposed to 200 nm or 50 nm opsonized silica particles. An artifact of the Stöber synthesis process of 200 nm particles was generation of both individual particles and particle aggregates. It was not possible to completely

disaggregate the particles into a uniform suspension of single particles, unlike the spherical 3 μm particles used in the previous experiments. When 200 nm silica particles were not separated from aggregates, the phagocytosis/frustrated phagocytosis (only a part of the aggregate is inside cell) of aggregates resulted in phagolysosomal leakage (solid triangles in Figure 4.24 A). In macrophages that were decorated with individual silica particles, that were possibly taken up, dextran leakage was not observed. Instead cells formed vacuoles and underwent blebbing and died after 12 hours (Figure 4.24 B). From this data it was not clear if the particles were being internalized by cells. To confirm whether the particles were internalized, cells were exposed to commercially available fluorescent 200 nm silica particles that were opsonized and cells were fixed after an hour of particle exposure. To label the particles that were not internalized, cells were incubated with a secondary antibody tagged with a fluorophore. Because the secondary antibody cannot label particles inside the cells, the ones on the outside are dual colored whereas the internalized ones are single colored (Figure 4.24 C). By one hour, particles were found to be internalized. This finding was also confirmed in cells that were exposed to 200 nm latex particles (Figure 4.24 D). Thus 200 nm opsonized silica or latex particles are taken up by the cells within one hour period. The silica particles that are presumably endocytosed do not cause endolysosomal leakage but result in cell death after a period of 12 hours independent of endolysosomal leakage. An aggregate of the same particles causes phagolysosomal leakage and cell death.

In cells that are were exposed to 50 nm fluorescent silica particles (red), phagolysosomal leakage was observed when cells took up particles that were aggregated (Figure 4.24 E). In cells that took up only individual small particles, these were found to

co-localize with the FITC-dextran containing vesicles (Figure 4.24 F). This indicates that upon internalization, the particles are part of the endolysosomal compartment. There was no increase in the cytoplasmic FITC-dextran fluorescence for up to 500 minutes. This suggests that individual silica particles do not result in vesicle leakage. It is possible that if few endolysosomal vesicles were to leak there may not be enough cytoplasmic and nuclear FITC signal to confirm leakage.

There is an extensive literature proposing silica induced membrane damage to be linked to the chemical properties of surface silanol groups. Our data shows that along with the surface chemistry of silica particles, the mode of particle uptake and the vesicle environment may also contribute towards causing vesicle damage upon particle uptake.

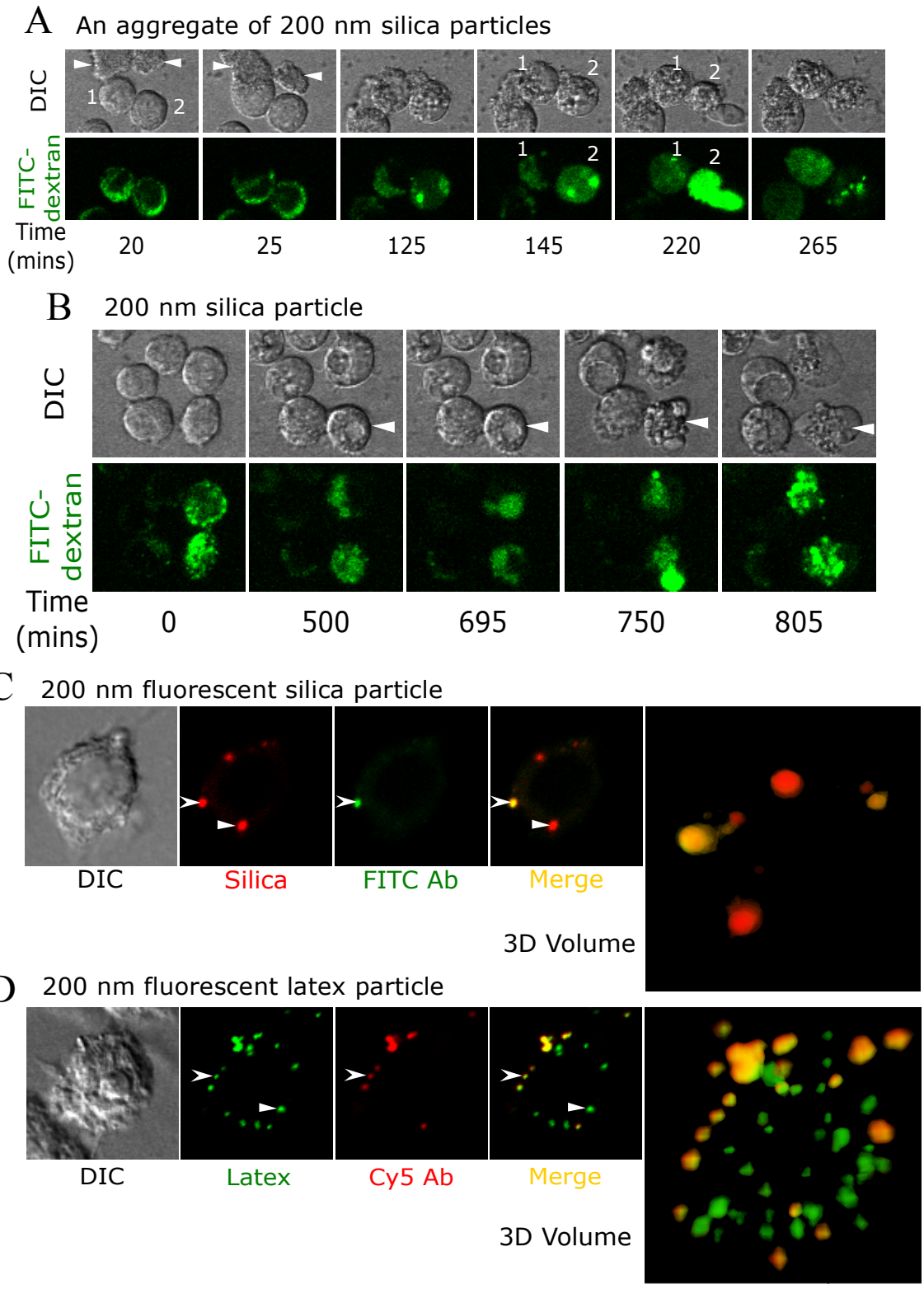
A
An aggregate of 200 nm silica particles
DIC
FITC-dextran
1
2
Time (mins)
20
25
125
145
220
265
B
200 nm silica particle
DIC
FITC-dextran
Time (mins)
0
500
695
750
805
C
200 nm fluorescent silica particle
DIC
Silica
FITC Ab
Merge
3D Volume
D
200 nm fluorescent latex particle
DIC
Latex
Cy5 Ab
Merge
3D Volume

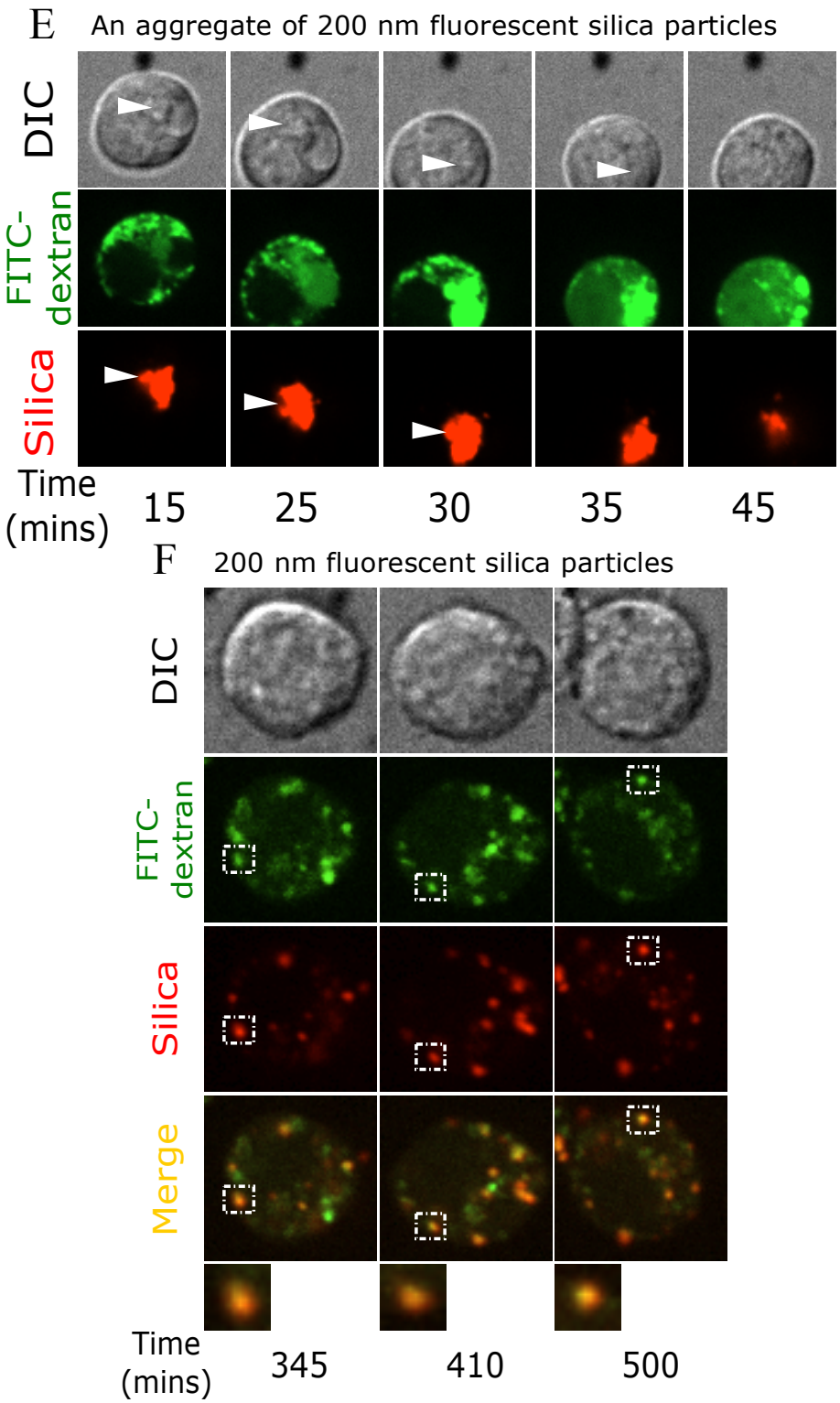

Figure 4.24: Sub-micron and nano-sized silica particles do not cause endolysosome leakage whereas the micron-sized aggregates of the same result in phagolysosome leakage

Alveolar macrophages allowed to endocytose 4 kD FITC-dextran were exposed to 200 nm silica particles and imaged 5 minutes apart. (A) The aggregate of the particles (solid triangle) interacts with the cells, following which the cells phagocytose the aggregate leading to phagolysosomal leakage beginning at 145 minutes for cell 2 and 220 minutes for cell 1. (B) Exposure of cells to individual 200 nm silica particles does not result in release of FITC-dextran from vesicles but cells undergo vacuolization (solid triangle, 500 minutes) and eventually die. (C) Cells were exposed to opsonized 200 nm red fluorescent silica particles. After 60 minutes cells were fixed and labeled with a FITC conjugated secondary antibody. Particles inside the cells appear red where as on the outside are both green and red. Particle internalization is not restricted to silica particles. (D) 200 nm opsonized green fluorescent latex particles are also internalized. Post fixation after 60 minutes of particle exposure and labeling with Cy5 conjugated secondary antibody particles on the outside are both green and red whereas inside appear only green. For both C and D, images were acquired at 150 nm in Z plane. 3D volume reconstruction shows every single particle in the cell. (E) An aggregate of fluorescently labeled opsonized red-fluorescent silica particles also result in phagolysosomal leakage as evidenced by release of FITC-dextran at 35 minutes. (F) Cells allowed to endocytose 4 kD FITC-dextran were exposed to 50 nm red-fluorescent silica particles. Particles that are in the endolysosomal vesicle appear both red and green. A zoom in of a vesicle containing the particle of square area is shown in the blow out image. Images acquired up to 500 minutes do not show any leakage of FITC-dextran from the vesicle.

4.15: The pathway of cellular events following uptake of silica particles

Examination of many cells (macrophages) and particles leads to a model of the molecular events that unfold following silica particle phagocytosis (Figure 4.25). The endolysosomes preloaded with 4 kD FITC-dextran and 4 kD TRITC-dextran are represented by yellow vesicles (Stage 1). Opsonized or non-opsonized silica particles bind to the cell and are taken up into phagosomes (Stages 2-3). Endolysosomal vesicles quickly begin to fuse with the phagosome (Stage 3) delivering their contents to the phagosome, now referred to as a phagolysosome. At this point, the phagolysosomes will have both fluorescent dyes. However, the green fluorescence will transiently dominate the phagosome as FITC-dextran moves from acidic vesicles to a phagosome with neutral pH resulting in a greater fluorescence (Stage 4). As the concentration of TRITC-dextran increases the phagolysosome will appear yellow (Stage 5). vATPases present on the endolysosomal vesicles are now present in the phagolysosomal membrane and pump protons into the phagolysosomal lumen resulting in a pH decrease and hence a decrease in the fluorescence of pH sensitive FITC-dextran so that phagosomes are now red. At the same time, the NOX is assembled on the phagolysosomal membrane and its activity results in ROS generation within the lumen (Stage 6). ROS can also be detected in the cytoplasm prior to phagolysosomal leakage. After about 25 minutes, the phagolysosomal membrane becomes permeable leading to an increase in the pH of the phagolysosome as seen by the rapid increase in phagosomal FITC fluorescence (Stage 7). Within 1.5 minutes, the fluorescence of both FITC and TRITC dextran in the phagosome decreases and the cytoplasmic and nuclear fluorescence of both increase indicating leakage of both into the cytoplasm (Stage 8). After about 10 minutes, the leaky phagolysosome is

resealed during which the dextran begins to accumulate in the phagolysosome due to continued endolysosomal fusion. Only the TRITC-dextran fluorescence increase is detected because the phagolysosome is again at a low pH due to vATPase activity (Stage 9). In latex containing phagosomes, the same early events take place except that no leakage occurs and no ROS is detected in the cytoplasm at any time, even though it is being produced in the phagosome. In Cos7 cells, the same events (stages 1-9) take place, but without NOX generated ROS.

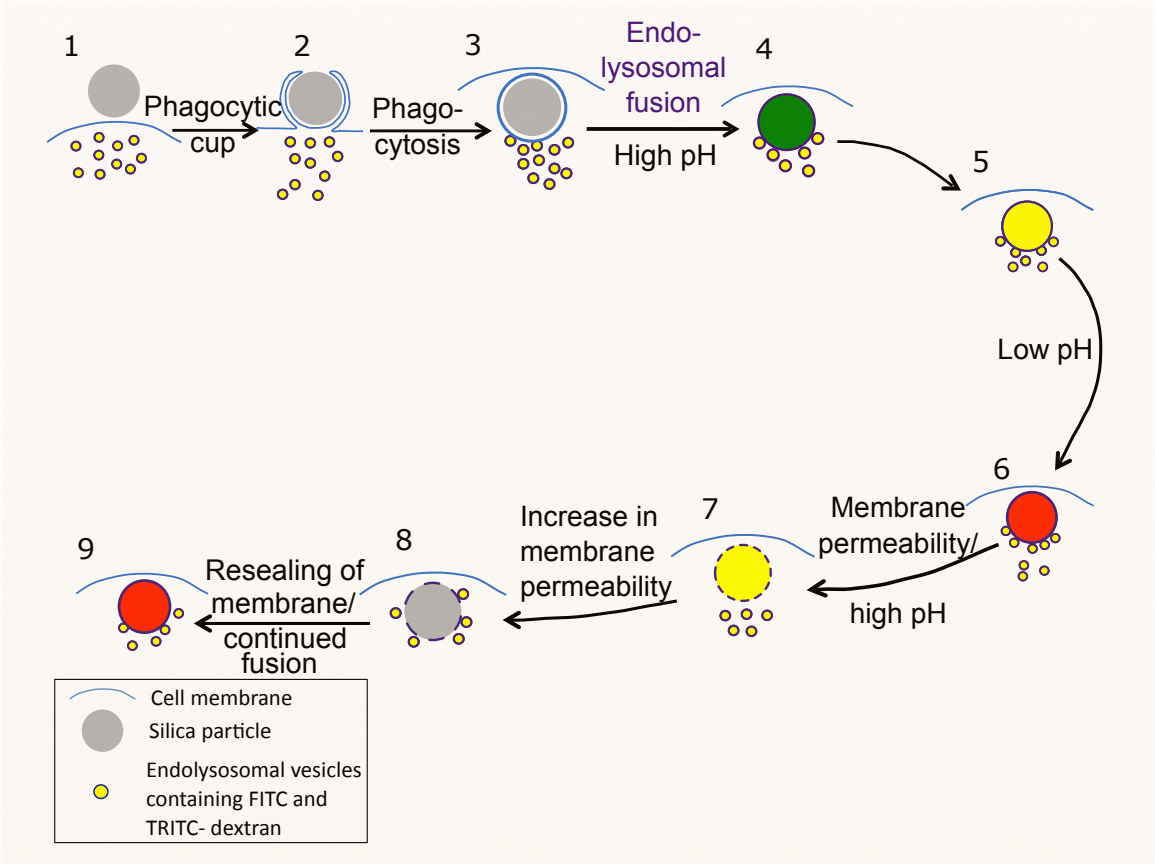

Figure 4.25: The pathway of cellular events upon uptake of silica particles

4.16: Discussion

Phagocytosis of foreign material and generation of phagosomal ROS to kill pathogens is an essential function of the innate immune system. There is no evidence that phagosomal ROS generated in this process results in phagolysosomal membrane damage and or that there is any leakage of phagosomal contents into the cytoplasm. However, it is clear that phagocytosis of silica particles results in phagolysosomal leakage. ROS generation has previously been measured in cells exposed to silica particles but these studies have not provided information regarding the source or intracellular distribution of ROS. This is especially important because ROS generation by NOX in phagosomes is an important normal step in phagosome processing that is expected to occur following any phagocytic uptake event. Thus it is not simply the generation of ROS in macrophage phagosomes that causes cells to die, but rather something about silica particles specifically and the type or amount of ROS that is likely relevant. We therefore investigated if ROS generated by NOX in a phagosome was responsible for phagolysosomal leakage. In this study we show that the NOX dependent oxidative burst associated with phagocytosis in macrophages accelerates the process of silica induced phagolysosomal leakage but leakage can also occur independently of NOX. In macrophage cells, both toxic silica and non-toxic latex particles cause the activation of NOX on phagosomal membranes resulting in the production of phagosomal ROS. Only silica particles cause a measurable increase in cytoplasmic ROS and this occurs at roughly the same time as ROS is detected in the phagosome, but before leakage is detected. This implies that this particular ROS, unlike NOX generated ROS, is able to escape from the phagosome. Unfortunately, there are not sufficiently specific ROS

probes to determine the molecular nature of this ROS. This is the first study to show ROS generation in a phagosome containing silica to be NOX independent. Our data is in agreement with a recently published study showing leakage of phagolysosomes containing silica particles to be NOX independent (Davis *et al.*, 2012).

Our study using dual dextran fluorescent tracers reveals for the first time the kinetics of phagolysosomal leakage. The increase in pH of the phagosome occurs several minutes before we can detect any leakage of dextran into the cytoplasm. There are two possible explanations for this result. The size of the pore might initially be large enough to allow protons to cross the membrane, but not large enough to allow dextran through. Over time, the pore might enlarge in size and begin allowing dextran and other larger molecules to pass. Alternatively, the difference in diffusion rate of protons vs. larger molecules through a fixed size pore might be sufficient to account for the different kinetics. We favor an increase in the size of pores over time as there is a span of several minutes where the FITC-dextran fluorescence is increasing while there is no detectable decrease in the TRITC-dextran fluorescence (Figure 4.3). The parallel timing seen between the decrease in TRITC-dextran and FITC-dextran fluorescence in the phagolysosome and a simultaneous increase in its nuclear fluorescence supports the idea that we are accurately measuring the timing of leakage with this assay. It should be noted that our earlier studies have shown that dextran as large as 70 kD can leak out of phagolysosomes (Joshi and Knecht, 2013b). A pore of this size is consistent with the size of proteins like cathepsins that are suspected to induce the apoptotic cascade once released into the cytoplasm. It should be noted that the path by which molecules are crossing the phagolysosomal membrane is unknown. Whether the pore is purely a lipid

bilayer phenomenon or involves membrane proteins is unknown as well as whether lipid peroxidation by ROS plays a direct role in its formation. There is very little biophysical data or modeling to explain the molecular details of the formation of transient membrane pores (Wong-Ekkabut *et al.*, 2007). Although we have referred to it as a "pore", we do not have any evidence as to the number, size or nature of the permeable region of the membrane.

Surprisingly, we have found that phagolysosomal leakage is a transient event. The leakage of 4 kD dextran takes place for an average of 9 minutes and then stops. After this time, TRITC-dextran fluorescence begins to increase in the phagosome indicating that leakage has stopped and the fusion of endolysosomes with the phagosome has continued throughout the period of leakage or has begun again. We have never seen a phagosome in a macrophage leak once, and then subsequently leak again, nor ever seen one to leak its contents and not recover. This resealing of leaky phagolysosomal membranes was observed with both opsonized and non-opsonized silica particles. After a period of increase, TRITC-dextran fluorescence was seen to level off for latex phagosomes and sometimes for silica containing phagosomes prior to leakage (Figures 4.6 and 4.17). Thus fusion with endolysosomes often ceases after some period of time. However, upon leakage of phagosomes containing silica, a further increase in TRITC-dextran fluorescence was always observed implying renewed fusion events. Thus we hypothesize that release of phagolysosomal contents or membrane damage may trigger recruitment of endolysosomal vesicles and this new membrane may help repair the damaged phagolysosomal membrane. Recently, autophagic machinery was found to be localized to damaged lysosomes suggesting sequestration of damaged phagolysosomes by

autophagosomes (Maejima *et al.*, 2013), so this may be a related process. We cannot ascertain if TRITC-dextran that was endocytosed by cells during loading also got mixed with autophagosomes that are generated *de novo*. A leaky phagolysosome could therefore be sealed by an autophagosome or possibly by other endolysosomal vesicles.

Although ROS was detected in phagosomes containing either silica or latex particles, only silica containing phagosomes become damaged and leak leading eventually to cell death (Thibodeau *et al.*, 2003; Joshi and Knecht, 2013b). One hypothesis to explain more toxic ROS in the presence of silica relates to iron contamination of the silica surface. Crystalline silica particles that cause silicosis have been shown to have traces of iron (Vallyathan *et al.*, 1988; Ghio *et al.*, 1992; Castranova *et al.*, 1997). A micro X-ray fluorescence (micro-XRF) analysis of amorphous silica particles used in this study confirmed traces of iron on these particles (data not shown). Phagosomal H_2O_2 generated by reduction of superoxide could be converted to $^{\bullet}OH$ radicals via oxidation of ferrous (Fe^{2+}) iron in a process known as the Fenton reaction (Kurz *et al.*, 2011). This reaction has been demonstrated with silica using EPR spectroscopy where free radical trap (DMPO) forms a stable adduct with the $^{\bullet}OH$ radical (DMPO-OH) allowing the detection of short lived and highly reactive $^{\bullet}OH$ radicals (Hampton *et al.*, 1998). A suitable fluorescence probe to detect $^{\bullet}OH$ radicals is not available making it difficult to detect this ROS in a phagosome using fluorescence microscopy. Within the phospholipid bilayer of a phagosome, $^{\bullet}OH$ radicals can react with polyunsaturated fatty acids (PUFA) resulting in the formation of lipid hydroperoxide, causing a reduction in membrane fluidity and increasing the permeability of the lipid bilayer (Wong-Ekkabut *et al.*, 2007). However whether this would lead to transient pores

large enough to allow dextran or proteins to diffuse through and how those pores are subsequently closed is unknown.

An argument against toxicity due to iron is from the fact that iron is present in lysosomes (Kon *et al.*, 2010) and so it is hard to imagine why the Fenton chemistry would not also take place in phagolysosomes containing latex particles. Much of this iron is in a redox active form, but sequestered by the protein ferritin. However, some of the free iron in lysosomes can participate in redox reactions (Kurz *et al.*, 2011). Due to the high reducing equivalence of proteins and the acidic nature of lysosomes, most of the free iron has been proposed to be present in the Fe^{2+} form. However, ferrous (Fe^{2+}) and ferric (Fe^{3+}) iron can interconvert and superoxide can reduce ferric iron to ferrous (Kurz *et al.*, 2011; Dixon and Stockwell, 2013). Thus if Fenton chemistry were important, one would hypothesize that phagocytosis of latex particles would also result in generation of $^{\bullet}OH$ radicals and cause phagolysosomal membrane leakage. Our data strongly suggests that even if these reactions were occurring in a latex phagolysosome, the resulting ROS is not sufficient to cause damage to phospholipid bilayer. It is only in the presence of silica that something abnormal happens. We hypothesize this event to be the *de novo* generation of a form of ROS that is particularly damaging to nearby membrane bilayers.

One way of knowing whether phagolysosomal leakage was due to ROS generation was by blocking it at its source (NADPH oxidase) or before H_2O_2 generation, a step that requires protons pumped into the phagosome by vATPase (Winterbourn *et al.*, 2006; Musset *et al.*, 2009). DPI and bafilomycin A1, inhibitors of NOX or vATPase respectively present an opportunity to investigate the role of ROS in leakage (Savina *et al.*, 2006; Hornung *et al.*, 2008; Sandberg *et al.*, 2012). In one study, DPI treated

macrophages exposed to silica were reported to prevent phagolysosomal leakage (Persson, 2005). This was of significance as it suggests a necessary role of NOX generated ROS in silica induced phagolysosomal leakage. In another study where DPI treated macrophages were exposed to silica particles, a partial release of FITC-dextran was observed after one hour (Davis *et al.*, 2012). Our data where DPI pre-treated macrophages were exposed to silica particles show a temporal delay in release of FITC-dextran from individual phagolysosomes. This supports the observation from Davis et. al (Davis *et al.*, 2012) and further shows that the reason for partial release is a delay in phagolysosomal leakage. Treatment of bone marrow derived macrophages with bafilomycin A1 has been shown to result in reduced generation of IL-1β upon silica treatment (Hornung *et al.*, 2008). Our data with bafilomycin A1 treated macrophages exposed to silica show a delay in phagolysosomal leakage. A reduced generation of IL-1β could therefore be due to a delay in phagolysosomal leakage that is required for inflammasome activation, and subsequent IL-1β release. Neither of these inhibitors could be tested for their ability to prevent cell death following leakage as they cause cell death on a shorter time scale than silica.

The role of ROS and NOX in the actual etiology of silicosis is unclear. The effect of silica exposure in mice deficient in NOX has shown conflicting results. $p47^{phox-/-}$ mice show an increase in lung fibrosis and an increase in mRNA transcript levels of inflammatory cytokines compared to wild type mice treated with silica (Fazzi *et al.*, 2014). When $p47^{phox-/-}$ mice were challenged with either LPS or zymosan, an increase in lung fibrosis and an increase in mRNA transcript levels of inflammatory cytokines were observed (Segal *et al.*, 2010). This suggests that although NOX generates ROS, it is also

required for regulating inflammation and inhibiting NOX may not be a good therapeutic intervention. In contrast, mice treated with oligodexoynucleotides (ODN) to suppress $p47^{phox}$ and exposed to silica show an increased life span and a reduction in inflammatory cytokines compared to wild type mice treated with silica alone (Sato *et al.*, 2008). This is further complicated by data that show reduced but measurable ROS generation in cells exposed to silica in which $p47^{phox}$ was knocked down (Sato *et al.*, 2008; van Berlo *et al.*, 2010). Although $p47^{phox}$ is required for stability of the NOX complex, $gp91^{phox}$ is the catalytic unit responsible for electron transport and reduction of oxygen to superoxide (Leto *et al.*, 2009). Inhibition of subunits other than $gp91^{phox}$ can still allow generation of ROS (Kuhns *et al.*, 2010; Li *et al.*, 2010). Thus using $p47^{phox}$ knockout may not be the best strategy to address the effect of NOX on silica toxicity. Cos7 cells therefore provide a good *in vitro* model to study an effect of NOX in silica induced phagolysosomal damage, as they do not express any subunits of NOX.

Because Cos7 cells also lack Fc-receptors they cannot utilize the opsonized phagocytosis pathway of phagocytes for uptake of antibody-coated particles. However, we have shown that non-phagocyte cell types can also take up non-opsonized particles (Costantini *et al.*, 2011). In Cos7 cells, uptake of non-opsonized particles is much slower than in macrophages, but particles are eventually taken up and silica particles caused phagolysosomal leakage. Our data supports the observation from a previous study that showed silica particles to cause phagolysosomal leakage independent of NOX (Davis *et al.*, 2012). Cos7 cells contain other isoforms of NOX that could theoretically contribute to phagosomal ROS. However, the fact that ROS is detected in a silica containing phagosome but not in a latex containing phagosome in Cos7 cells demonstrates that other

NOX isoforms do not result in measurable phagosomal ROS and a complex chemistry involving silica particles and phagolysosomal contents results in leakage. This result that phagolysosomal leakage could occur independent of NOX could explain why exposing bone marrow derived macrophages from gp91^{phox} KO mice to silica resulted in inflammasome activation and release of IL-1β (Hornung *et al.*, 2008). Thus the Cos7 cell model demonstrates that silica induced ROS generation and phagolysosomal leakage are both NOX independent.

It is not well understood whether NOX generated phagosomal ROS translates into an increase in cytoplasmic or mitochondrial ROS. Studies have measured an increase in cytoplasmic ROS upon silica treatment and attributed this to NADPH oxidase activation. The interpretation of this measurement is difficult since cells were pre-activated by either PMA or LPS before exposure to silica and that results in generalized and non-phagosomal NOX activation and an increase in cellular ROS even before exposure to silica (Kahlenberg *et al.*, 2005; Li *et al.*, 2009; Bauernfeind *et al.*, 2011; Brass *et al.*, 2012). Our experiments were therefore performed without pre-activating macrophages. Using ROS sensors we measured an initial small increase in cytoplasmic ROS upon silica exposure and another larger increase during blebbing associated with apoptosis. No cytoplasmic ROS increase was detected in macrophages exposed to latex particles. Since both latex and silica particles activate NOX and result in phagosomal ROS production in macrophages, it was surprising to see an increase in cytoplasmic ROS only with silica particles. This suggests that silica is generating ROS through an alternate mechanism and this ROS can escape through the phagosomal membrane. Mitochondrial specific ROS

probes show that the large increase in mitochondrial ROS production during apoptosis appears to be the source of the late increase in cytoplasmic ROS.

In summary, our study provides a comprehensive data on spatio-temporal generation of ROS upon exposure of cells to silica and latex particles. Most importantly it shows an ability of silica to generate phagosomal ROS and cause phagolysosomal leakage in a NOX independent manner. Our data questions a direct role of ROS in inducing cell death as suggested by some studies (Shen *et al.*, 2001; Hu *et al.*, 2006). We have earlier shown a temporal gap of many hours between phagolysosomal leakage and apoptosis (Joshi and Knecht, 2013b). An intrinsic model of cell death downstream of phagolysosomal leakage has been proposed, the mechanism underlying which is still not well understood (Repnik *et al.*, 2012). It is therefore important to investigate the pathway downstream of phagolysosomal leakage to understand how apoptosis is triggered.

Chapter 5: Conclusions

The goal of this project was to understand the mechanism of oxidative stress and cell death in an alveolar macrophage following silica exposure. Using multidimensional live cell imaging we show that phagolysosomal leakage occurs within 15 minutes of the uptake of crystalline or amorphous silica particles. Upon phagocytosis of amorphous silica particles, NADPH oxidase generated respiratory burst was not an absolute requirement for generation of phagosomal ROS and silica particles alone could generate of phagosomal ROS. Activation of pro-apoptotic proteins such as Bax and Bid did not occur immediately after phagolysosomal leakage. Bax activation preceded Bid activation. A transient increase in mitochondrial membrane potential prior to depolarization was also observed and this could not be temporally distinguished from caspase activation as well as cellular blebbing. Bid activation occur in a temporal window of 5 minutes in which mitochondrial hyperpolarization, caspase activation and cell blebbing were also observed. A few cells were also found to die by necrosis. In macrophages exposed to silica, cytoplasmic ROS generation was observed at two different stages, a small increase following uptake of silica and a massive burst following cell blebbing. A comprehensive sequence of events resulting from our study is presented in Figure 5.

There is an extensive literature in the field of silicosis, which proposes surface chemistry of the silica or iron contaminating the surface of silica or iron in the lysosome to be responsible for the toxicity. Micro-XRF elemental analysis showed some traces of iron on crystalline and amorphous silica particles and hence these particles could possibly generate phagosomal membrane damaging ROS (hydroxyl radicals) through Fenton chemistry. An aggregate of silica nanoparticles lacking iron on its surface behaved

similar to the crystalline and amorphous silica particle. Thus iron on the surface of silica particle is not a determining factor in phagolysosomal leakage. While surface chemistry of the silica cannot be ignored, our data shows that the biological processing of the silica particle could also play an important role in toxicity. The fact that silica nanoparticles did not cause membrane leakage while an aggregate of silica nanoparticle that was microns in size result in leakage shows that the surface of silica is not sufficient to result in membrane damage. Thus there has to be a difference in the processing of an endosome containing a silica particle and a phagolysosome containing a larger silica particle to account for this difference. Our study also demonstrates an ability of silica to generate ROS in a phagosome in the absence of NOX. We cannot identify the type of ROS being produced and if hydroxyl radical mediated lipid peroxidation of the phospholipid bilayer is responsible for phagolysosomal membrane damage and leakage. This needs further investigation. Ours is the only study so far that has used non-toxic latex particle as a control for silica treated cells revealing that *de novo* ROS generated by NOX and any lysosomal iron, if present, does not result in phagolysosomal damage.

Our data demonstrates two important changes that occur in the cell following particle uptake, cytoplasmic ROS generation and phagolysosomal leakage. Cytoplasmic ROS can activate NF-κB responsible for generation of various pro-inflammatory cytokines and chemokines. Phagolysosomal leakage results in inflammasome activation leading to activation and secretion of pro-inflammatory cytokine IL-1β. Thus cellular uptake of silica creates an environment favorable for the pathophysiological alteration of alveolar space contributing to the pathogenesis of silicosis. Also due to a continuous cycle of cell death that causes release of particles into the extracellular space and more

particles getting in the alveolar space due to chronic inhalation and virtually little clearance of these particles, the particle burden persists for a toxic outcome.

There is no effective treatment for silicosis. Currently patients are put on bronchodilators to keep the airways open and the lungs are lavaged to remove the fluid. In a worst-case scenario lung transplant is recommended. Many years of research have identified various mediators of silicosis, whose inhibition has been shown to either reduce or prevent inflammation and fibrosis in animal studies. The list of these mediators include TNF-α (Rojanasakul *et al.*, 1999; Di Giuseppe *et al.*, 2009; Fazzi *et al.*, 2014), IL-17A (Mi *et al.*, 2011), Fas (Borges *et al.*, 2001), TGF- β (Postlethwaite and Seyer, 1990; Sullivan *et al.*, 2005; Wang *et al.*, 2010), ROS (Kang *et al.*, 2000; Shen *et al.*, 2001), iNOS (Srivastava *et al.*, 2002; Zeidler *et al.*, 2003), NALP3 (Peeters *et al.*, 2014), P2X7 receptor (Monção-Ribeiro *et al.*, 2014), cell death (Shen *et al.*, 2001; Borges *et al.*, 2002; Wang *et al.*, 2003), IL-1β (Srivastava *et al.*, 2002; Cassel *et al.*, 2008; Hornung *et al.*, 2008), NF-κB (Hubbard *et al.*, 2002; Brass *et al.*, 2012). While there are biologics available to inhibit the activity of many of these pro-inflammatory mediators (Jalloul and Banks, 2010), targeting IL-1β has yielded positive results in silicosis patients (Cavalli *et al.*, 2015).

In spite of decades of research in the field of silicosis it is difficult to correlate the *in vivo* findings in mice with the chronic progression of silicosis in humans. This is because mice are administered with a dose of silica that an occupational worker is expected to inhale over his lifetime. *In vitro,* in order to understand the release of various cytokines from macrophages, these cells were pre-stimulated with TLR-4 agonist, LPS which is found on bacterial cell wall. A resulting NF-κB activation leads to upregulation

of many pro-inflammatory cytokines. In a healthy occupational worker who gets exposed to silica, this initial critical signal shown in various studies to initiate a pro-inflammatory process is likely to be absent. It is possible that a diseased state due to either a bacterial infection or viral flu can result in generation of various pro-inflammatory cytokines that can now facilitate the process towards development of fibrosis. Our general understanding of the macrophage function has increased in past few years. Resting macrophages can be transformed into either inflammatory (M1) or anti-inflammatory (M2) phenotype (Murray *et al.*, 2014). In a study done to characterize the presence of these phenotypes, it was found that M1/M2 polarization occurred early following silica exposure and it was not related to the fibrotic process (Misson *et al.*, 2004).

IL-1β release from a macrophage has been shown to occur early following silica exposure. Cathepsin B release upon phagolysosomal leakage has been demonstrated to be involved in inflammasome activation leading to IL-1β release. Thus IL-1R antagonists that are used to manage arthritis and gout where production of IL-1β is also observed presents an excellent potential opportunity to manage silicosis. Preliminary data from a recent off-label use of IL-1R antagonist Anakinra has shown positive results in a patient with a progressive decline in lung function due to silicosis. Following 6 months of therapy, there was an improvement in his lung function with no dyspnea and a normal inflammation profile (Cavalli *et al.*, 2015). Thus the understanding of silicosis at the cellular level has led to identification of a key mediator that has great potential for therapeutic management of silicosis.

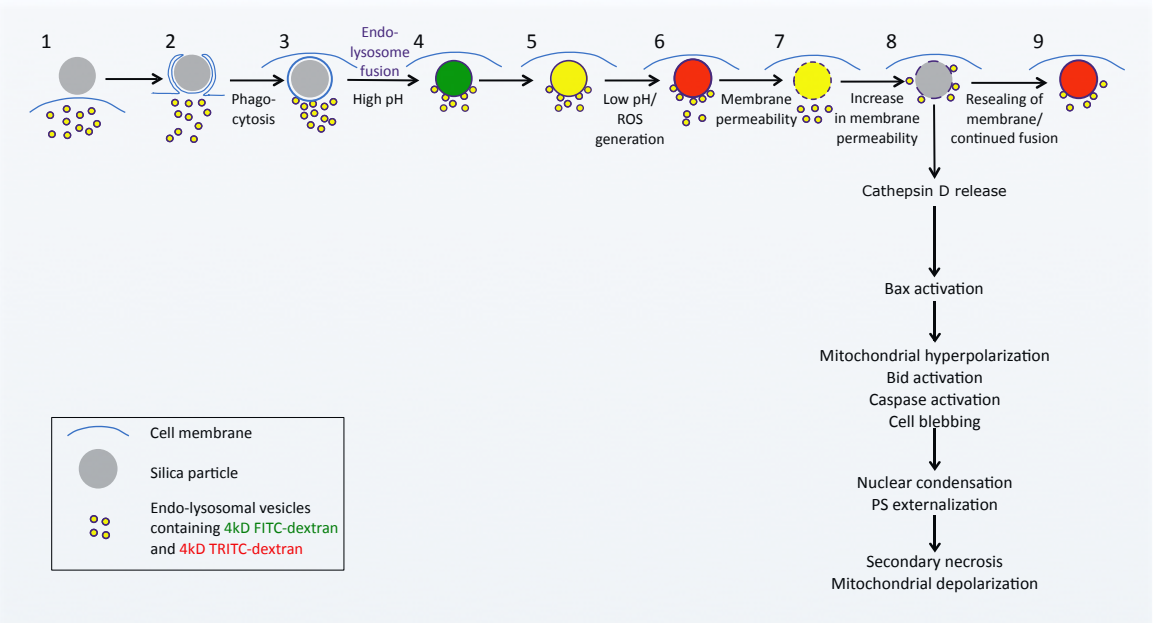

Figure 5: Events in a cell following uptake of silica particle to cell death

Chapter 6: Future directions

6: The pathway to lipid peroxidation

While our data in Chapter 5 conclusively shows that silica generates phagosomal ROS and causes leakage in an NADPH oxidase independent manner, it is not able to validate various prevalent hypotheses in the literature. Generation of hydroxyl radicals in a lysosomal compartment by the Fenton reaction mediated by iron or iron on a silica particle is an extremely attractive hypothesis. Over the years, many of the review articles have even proposed scenarios and cartoons where cytoplasmic ROS can cause lysosomal leakage by generating hydroxyl radicals due to intra-lysosomal iron (Boya and Kroemer, 2008; Kirkegaard and Jäättelä, 2009; Kurz *et al.*, 2011; Terman and Kurz, 2012; Aits and Jäättelä, 2013; Repnik *et al.*, 2014; Galluzzi *et al.*, 2014b). The hydroxyl radicals are proposed to result in lipid peroxidation and damage to the lipid bilayer. While the contamination of iron on silica is well documented, present studies have not directly shown the presence of free iron, generation of hydroxyl radicals or lipid peroxidation of the phagosomal membrane. Each of these issues can be readily addressed by various methods.

6.1: Is ferrous iron (Fe^{2+}) present in the lysosomes?

Our data shows that although ROS is produced in a phagolysosome containing latex particle it does not leak. This shows that free iron, if present, is not sufficient to drive the reaction to produce leakage. In order to detect the redox active pool of labile ferrous (Fe^{2+}) iron, cells could be incubated with Iron Probe-1 (IP-1) that has been developed to specifically detect Fe^{2+} (Au-Yeung *et al.*, 2013). This study was planned

and the probe was requested from Christopher Chang laboratory, but they were unable to provide it to us. Localization of IP-1 to lysosomes could be done using a spectrally distinct probe such as Lysotracker red.

6.2: Is hydroxyl radical generated?

Throughout our study we have hypothesized $^{\bullet}$OH radical generation to be one of the ROS generated in the silica phagosome to be responsible for phagolysosomal leakage. However, we have not shown $^{\bullet}$OH radical generation in our system. Even with the best of the current methods, we would be restricted in detecting hydroxyl radicals at a cellular level, rather than intracellular localization. Because hydroxyl radicals are short lived they become difficult to detect. We could detect hydroxyl radicals using DMPO, a spin trap. In order to accomplish this, MH-S macrophages would be incubated with DMPO that reacts with hydroxyl radicals forming a long-lived DMPO-OH adduct which has a characteristic spectrum when measured by electron paramagnetic spectrum (EPR) spectroscopy. Cells would be exposed to silica particle along with appropriate controls, collected at various time points and analyzed for presence of DMPO-OH adduct.

6.3: Could lipid hydroperoxides be detected?

Malondialdehyde (MDA) and 4-hydroxynonenal (4-HNE) are produced as a byproduct of lipid peroxidation. Reagents that allow colorimetric detection of either MDA or 4-HNE are available that can help with detection of lipid peroxidation (Spickett *et al.*, 2010; Duan *et al.*, 2013; Kalyanaraman, 2013). The silica literature has shown the presence of MDA but the time-points chosen were close to when cells die. It would not

be surprising that upon cell death, cell membranes would undergo lipid peroxidation due to ROS generation. The lipid peroxidation byproducts get converted to other substances by the antioxidant system in the cell. The colorimetric method to detect MDA or 4-HNE could be attempted at time-points when phagosomes leak to detect lipid peroxidation. An alternate and a direct way of detecting lipid peroxidation would be isolation of phagosomes, followed by membrane extraction and running lipids through HPLC. As a control for silica, latex particles would be used.

Appendix: Investigation of the temporal delay in cell death following lysosomal leakage by various inducers

A.1: Introduction

Temporal analysis of silica induced apoptosis shows a delay between phagolysosomal leakage and the initiation of apoptotic events such as mitochondrial hyperpolarization, caspase activation and cell blebbing. Lysosomal damage has been proposed to trigger intrinsic cell death (Boya and Kroemer, 2008; Repnik and Turk, 2010; Aits and Jäättelä, 2013). There is evidence that inhibition of cathepsin D activity reduces silica induced cell death, consistent with the hypothesis that this enzyme could leak out of damaged phagolysosomes into the cytoplasm (Thibodeau *et al.*, 2004). Beyond this, the role of various effectors such as the pro-apoptotic protein Bid and Bax involved in the process of intrinsic cell death during silica induced cell death is not known. The goal of the study presented in this chapter is to investigate the temporal delay between lysosomal leakage and terminal apoptotic events with a focus on the role of the effectors proposed in the intrinsic cell death pathway (Figure A.1).

Lysosomes were discovered by Christian de Duve and aptly termed "suicidal bags" as a release of lysosomal contents into the cytoplasm results in cell death (Duve, 1975). Lysosomes contain various hydrolases and proteases, including cathepsins. The release of cathepsin D has been shown to be involved in the activation of Bid, a Bcl-2 homology 3 (BH-3) domain only Bcl-2 family pro-apoptotic protein, resulting in the formation of its active form, truncated-Bid (t-Bid) (Cirman *et al.*, 2004; Appelqvist *et al.*, 2011). Bid can also be activated following TNF-TNF receptor or FasL-Fas receptor interaction as part of the extrinsic cell death pathway. Ligand binding results in clustering of various cytoplasmic adaptor proteins leading to formation of the TNF receptor activated death

domain (TRADD) or Fas activated death domain (FADD). TRADD or FADD activate caspase-8 that results in Bid activation (Li *et al.*, 1998). Thus both the extrinsic cell death pathway and the intrinsic cell death pathway following lysosomal leakage merge at the Bid activation stage.

Activated Bid (t-Bid) can change the conformation of the pro-apoptotic protein Bax by interacting with the alpha-1 helix of Bax to expose the mitochondrial trans-membrane alpha-9 helix resulting in Bax insertion into the outer mitochondrial membrane (OMM). Here Bax oligomerizes with itself or with another pro-apoptotic protein Bak already present in the OMM to form pores resulting in mitochondrial outer membrane permeabilization (MOMP). Alternatively, t-Bid can interact with alpha-1 helix of Bak resulting in Bak oligomerization and MOMP (Kim *et al.*, 2009). MOMP causes release of mitochondrial inter-membrane space (IMS) proteins such as cytochrome c and second mitochondria derived activator of caspase (Smac) into the cytoplasm (Green and Kroemer, 2005). Cytochrome c is necessary for caspase activation whereas Smac inhibits anti-apoptotic proteins like X-linked inhibitor of apoptosis protein (XIAP) to strengthen the apoptotic response. Cytochrome c is of a particular significance as it participates in the formation of the apoptosome complex resulting in the activation of caspase-9 (initiator caspase). Caspase-9 in turn activates caspase -3 (effector caspase) that signals a "point of no return" in this pathway. A feedback loop mechanism where caspase-3 can promote Bid activation has also been reported which would suggest that caspase activation results in commitment to cell death by further amplifying the pro-apoptotic cell death pathway (Slee *et al.*, 2000). Effector caspase activation also leads to cell membrane blebbing, nuclear condensation and DNA fragmentation (Tyas *et al.*, 2000; Goldstein *et*

al., 2005). The schematic of the pathway under investigation in this study is shown in Figure A.1

Rather than using silica by itself to study the intrinsic cell death pathway upon phagolysosomal leakage, two known inducers of lysosomal leakage, staurosporine, and Leucyl-Leucyl-O-Methyl Ester (LLOMe) were included in this study. This would allow us to compare events that follow silica induced phagolysosomal leakage to that of staurosporine or LLOMe induced lysosomal leakage. This will help to a) confirm the intrinsic cell death pathway reported in the literature and b) determine if the intrinsic cell death pathway following leakage of lysosomal contents is conserved across different inducers. Staurosporine is a general protein kinase inhibitor whose mechanism for causing lysosomal leakage is not well understood (Bidère *et al.*, 2003) but is used to an agent to induce cell death. However, cells exposed to staurosporine are resistant to cell death when treated with a cathepsin-D inhibitor or when cell lines deficient in cathepsin-D are used (Bidère *et al.*, 2003; Michallet *et al.*, 2004; Emert-Sedlak *et al.*, 2005) suggesting a role of cathepsin-D in the cell death process. Being a general protein kinase inhibitor, unexpected effects of staurosporine are expected. This can potentially interfere with the signaling processes in the intrinsic cell death pathway. Hence, LLOMe, a lysosomotropic agent that is reported to selectively permeabilize endolysosomes was also used (Thiele and Lipsky, 1990; Uchimoto *et al.*, 1999). Unlike staurosporine LLOMe has not been reported to affect cell signaling other than causing endolysosomal leakage.

In this study lysosomal leakage in macrophages was confirmed by the FITC-dextran leakage assay following exposure of macrophages to staurosporine or LLOMe. Activation of Bax was studied by expressing GFP-Bax in macrophages. This probe is

localized to the cytoplasm, but upon activation gets redistributed to mitochondria. Bid activation was determined by expressing a Bid based FRET probe in cells where the activated portion of Bid (t-Bid) translocate to mitochondria. MOMP was determined by expressing Smac-RFP in cells that under normal condition resides in the mitochondrial inter-membrane space (IMS). Upon MOMP, Smac-RFP gets redistributed to the cytoplasm. A change in mitochondrial physiology was determined by analyzing alterations in mitochondrial membrane potential using TMRE. Apoptosis was also determined using Annexin V as a marker and a change in cellular morphology. Our preliminary data reveals that the generalized intrinsic apoptotic pathway varies depending on the inducer. Silica resulted in phagolysosomal leakage followed by Bax activation. The activation of Bid, caspase, mitochondrial hyperpolarization and cell blebbing indicative of death occurred on a similar temporal scale. Staurosporine resulted in endolysosomal leakage following which Bid and Bax activation occurred in a close temporal manner that was followed by mitochondrial membrane depolarization and cell blebbing. LLOMe resulted in endolysosomal leakage followed by mitochondrial membrane depolarization. Bax activation and cell blebbing occurred late together. Altogether, there is a variation in the occurrence of events that result in cell death following release of lysosomal contents when macrophages were treated with various inducers.

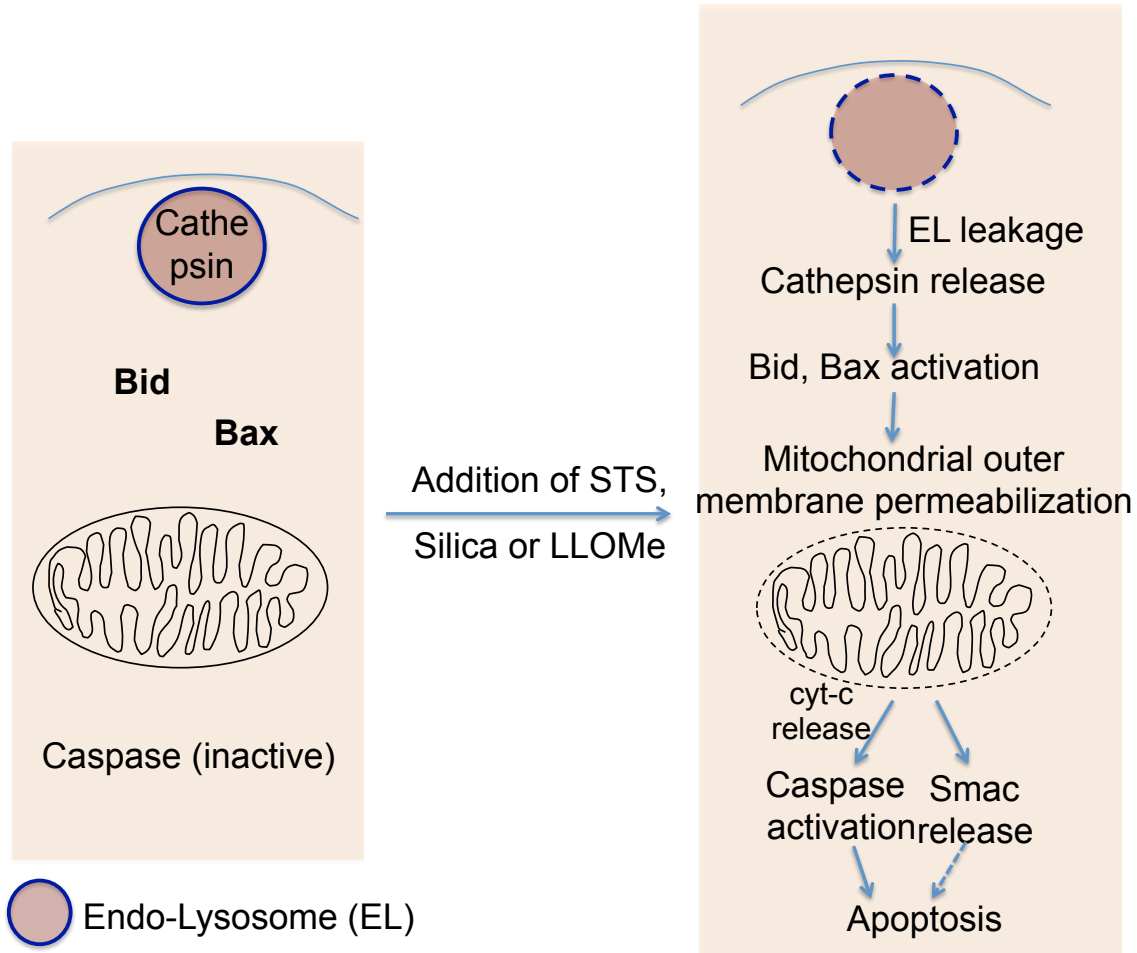

Figure A.1: Pathway under investigation.

Under normal cellular conditions the cathepsin protease is localized in the lysosomal vesicle whereas the inactive Bid, Bax and caspase is localized to the cytoplasm. Certain inducers can cause lysosomal leakage causing release of Cathepsin in to the cytoplasm initiating a cascade where by Bid and Bax get activated resulting in MOMP. A release of cytochrome-c from mitochondria will activate caspases where as the smac activation will inactivate the inhibitor of apoptosis proteins (IAP's).

A.2: Staurosporine, LLOMe and silica result in endolysosomal leakage

To investigate lysosomal leakage following exposure of MH-S macrophages to staurosporine, silica or LLOMe, cells were pre-loaded with 4 kD FITC-dextran and then exposed to these compounds. Exposure of cells to 1μM staurosporine resulted in an increase in both the cytoplasmic and nuclear FITC-dextran fluorescence as early as 40 minutes after exposure. Leakage occurred nearly at the same time in all cells as shown for the two cells in the image (Figure A.2 A and B). It took about 160 minutes for the cytoplasmic FITC-dextran fluorescence to reach a plateau suggestive of a continuous release of dextran from the vesicles over this time.

Being a kinase inhibitor, staurosporine has also been reported to have unintended effects. One such effect is extended filopodial protrusions (Figure A.3). To investigate if the protrusions observed in our data are filopodia, cells expressing GFP-actin were exposed to staurosporine. Filopodia are rich in actin and hence these structures are expected to be fluorescent. Upon addition of staurosporine, small protrusions appear on the cell membrane within 5 minutes that continue to grow as indicated by arrows (Figure A.3 A, DIC and GFP-actin). By 130 minutes these extended protrusions appear tightly attached to the glass substrate as indicated by the arrows. A confirmation that these protrusions are actin rich structures was made by labeling cells with Rhodamine-phalloidin, a probe that binds F-actin (Figure A.3 B). As cell die, these protrusions break giving a punctate appearance (320 minutes). Cell death was determined based on a change in cell morphology that occurs during cell death. While we observed filopodial protrusions, another study where A431 cancer and NRK fibroblast cells were exposed to

staurosporine found lamellipodial protrusions, indicative of a cell type specific effect of staurosporine (Mannherz *et al.*, 2006).

The result from cells exposed to silica particles was consistent with our earlier data in chapter 4 that showed silica induced phagolysosomal leakage. There was heterogeneity in the timing of phagolysosomal leakage between phagosomes following particle uptake (Figure A.2 C and D). On an average it took 30 minutes for phagolysosomal leakage to occur after particle uptake.

Endolysosomal leakage was also investigated upon exposure of cells to LLOMe. LLOMe is a lysosomotropic agent that is taken up by receptor-mediated endocytosis (Uchimoto *et al.*, 1999). When the dipeptide ester like LLOMe accumulates at sufficient concentration, it can increase the endolysosomal pH (Thiele and Lipsky, 1990). The acyl transferase activity of dipeptidyl peptidase I (DPPI, also known as cathepsin-C) results in polymerization of LLOMe and formation of the $(LL)_n$-OMe ($n>3$) which has detergent-like properties causing endolysosomal membrane permeabilization (Thiele and Lipsky, 1990; Uchimoto *et al.*, 1999; Turk and Turk, 2009). The effect of LLOMe is concentration dependent and it varies between cell lines. Different concentrations of LLOMe were tested for their effect on endolysosomal leakage and cell death. Exposure of cells loaded with 4 kD FITC-dextran to 3 mM LLOMe, led to an increase in FITC-dextran fluorescence associated with endolysosomes within 5 minutes (Figure A.2 F, 5 minutes), indicative of an increase in vesicular pH. Cells did not show an increase in nuclear fluorescence for up to 30 minutes indicating a temporal gap between alteration of the endolysosomal pH and actual leakage of 4 kD FITC-dextran out of the vesicles. LLOMe treated cells also show formation of small blebs on the surface but cells are

active and appear to be viable. Cell blebbing, a characteristic of apoptosis was observed at 215 minutes for the cell labeled with an arrow. A similar increase in FITC-dextran fluorescence for 5 cells confirms that the trend is consistent (Figure A.2 E). It should be noted that this quantification is of an entire cell and not of the nuclear area. This shows that LLOMe results in an increase in endolysosomal pH, endolysosomal permeability and cell death.

When cells were exposed to 0.5 mM or 1.5 mM LLOMe, cell death was not observed. This was further investigated using time-lapse imaging of cells loaded with 4 kD FITC-dextran. Macrophages exposed to 1.5 mM LLOMe (Figure A.2 G) and 0.5 mM LLOMe (Figure A.2 H) also show an increase in FITC-dextran fluorescence within 5 minutes, indicative of an increase in vesicular pH. These cells also developed blebs on the cell surface within 5 minutes. However, they show extensive vacuolization in the cytoplasm by 45 minutes by DIC imaging. Cells exposed to 3 mM LLOMe do not show a decrease in FITC-dextran fluorescence after 5 minutes (Figure A.2 F). However, in cells treated with 1.5 mM or 0.5 mM LLOMe, there is a decrease in FITC-dextran fluorescence after the initial increase at 5 minutes (Figure A.2 G, 45 minutes onwards and Figure A.2 H, 65 minutes onwards). It is therefore likely that the FITC-dextran fluorescence we observed is in the vacuoles that are present throughout the cellular area and not in the cytoplasm or nuclear area. The decrease in the fluorescence could be due to mixing of FITC-dextran with the vacuolar contents that have a low pH. Chloroquine is a weak base that raises the pH of endolysosomal compartments. When cells are treated with chloroquine, they also undergo lysosomal membrane permeabilization and cell death. These cells also show the presence of large vesicles that have been identified as

autophagic vacuoles (Boya *et al.*, 2003; 2005), so the same phenomenon may be occurring with LLOMe treated cells. As time progresses, these small vacuoles appear to merge, becoming a larger vacuole that fused with the cell membrane to release its contents extracellularly. The FITC-dextran fluorescence in the large vacuole in the zoomed image at 205 minutes (Figure A.2 H) has low fluorescence that increases by 270 minutes indicative of pH neutralization/increase before the vesicle fused with the cell membrane. An increase in vesicle pH has been reported during exocytosis, a process in which the vesicular contents are released outside the cell (Sundler, 1997). The cells with these vacuoles recover to a normal morphology after approximately 6 hours in the presence of LLOMe. Because we have not done experiments using probes that label autophagosomes, (for example, LC3) we could not confirm that these vacuoles were autophagosomes. In cells treated with 5 mM LLOMe, cells showed a rapid increase in FITC-dextran fluorescence (Figure A.2 I) following which they swell and die by 1.5 hours, indicative of necrosis. Thus a gradient of responses were observed depending on the concentration of LLOMe. At concentrations of 0.5 mM and 1.5 mM, cells recover from the damage, at 3 mM cells show endolysosomal leakage and undergo apoptosis and at 5 mM cells show endolysosomal leakage and die by necrosis.

Irrespective of the concentration, LLOMe resulted in a neutralization of endolysosomal pH within 5 minutes. Although LLOMe has been proposed to be taken up by endocytosis (Thiele and Lipsky, 1990), our data showing LLOMe to neutralize vesicular pH within 5 minutes suggests that LLOMe could pass through cell membrane to get trapped in the acidic compartments. There are three ways that an increase in endolysosomal pH would take place, one by inhibition of vATPase, second by

endolysosomal permeabilization and third by a weak base. LLOMe has not been reported to inhibit vATPase or to be a weak base. It could be assumed from the 3 mM LLOMe data that it might be causing membrane permeabilization with pores small enough for molecules less than 4 kD diffuse in to the endolysosomal vesicles causing an increase in pH. This creates an osmotic difference that could result in further permeability. If permeabilization due to osmotic flux were true, a temporal gap of 25 minutes between pH neutralization and release of 4 kD FITC-dextran in to the cytoplasm would be less likely (Figure A F). Further, at lower concentrations of LLOMe there is neutralization but no leakage (Figures 5 G and H). Altogether this suggests that pH neutralization observed by 5 minutes is not due to endolysosomal permeabilization but due to some effect of the LLOMe in the vesicular compartment causing pH neutralization.

This is the first study showing a detailed comparison between different agents that have been reported to cause endolysosomal leakage. Cells exposed to chemical inducers such as staurosporine and LLOMe show a homogenous response in terms of leakage, the timing of leakage varied between phagosomes containing silica. Endolysosomal leakage in LLOMe cells was concentration dependent such that cells exposed to lower concentrations of LLOMe did not die and showed a characteristic autophagic vacuole like structures at a high concentration cells underwent necrosis. There was an optimal concentration at which cells showed endolysosomal leakage and underwent apoptosis. The same was not observed with staurosporine.

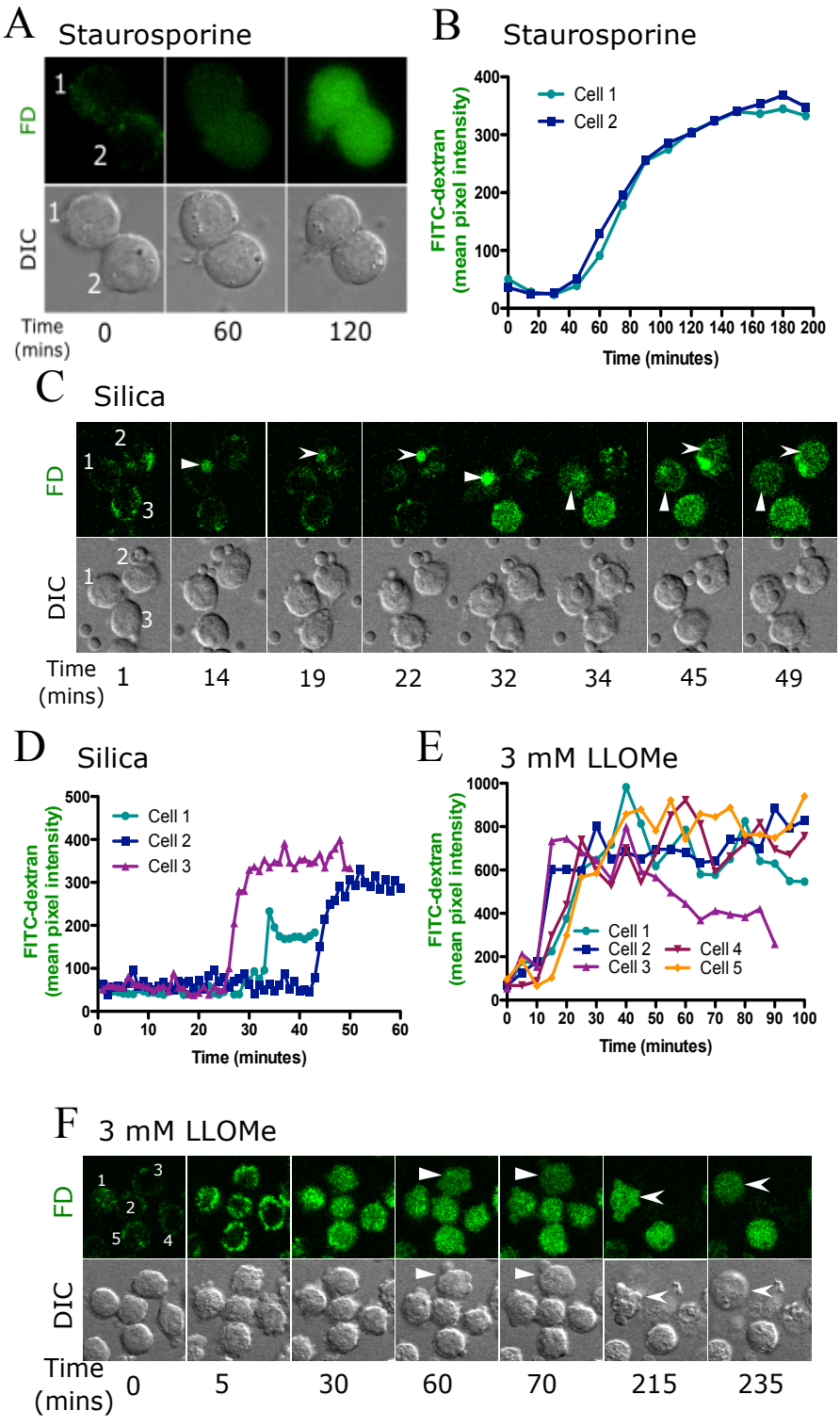
A
Staurosporine
FD
DIC
1
2
Time (mins)
0
60
120
B
Staurosporine
FITC-dextran (mean pixel intensity)
Cell 1
Cell 2
Time (minutes)
C
Silica
FD
DIC
Time (mins)
1
14
19
22
32
34
45
49
D
Silica
FITC-dextran (mean pixel intensity)
Cell 1
Cell 2
Cell 3
Time (minutes)
E
3 mM LLOMe
FITC-dextran (mean pixel intensity)
Cell 1
Cell 2
Cell 3
Cell 4
Cell 5
Time (minutes)
F
3 mM LLOMe
FD
DIC
Time (mins)
0
5
30
60
70
215
235

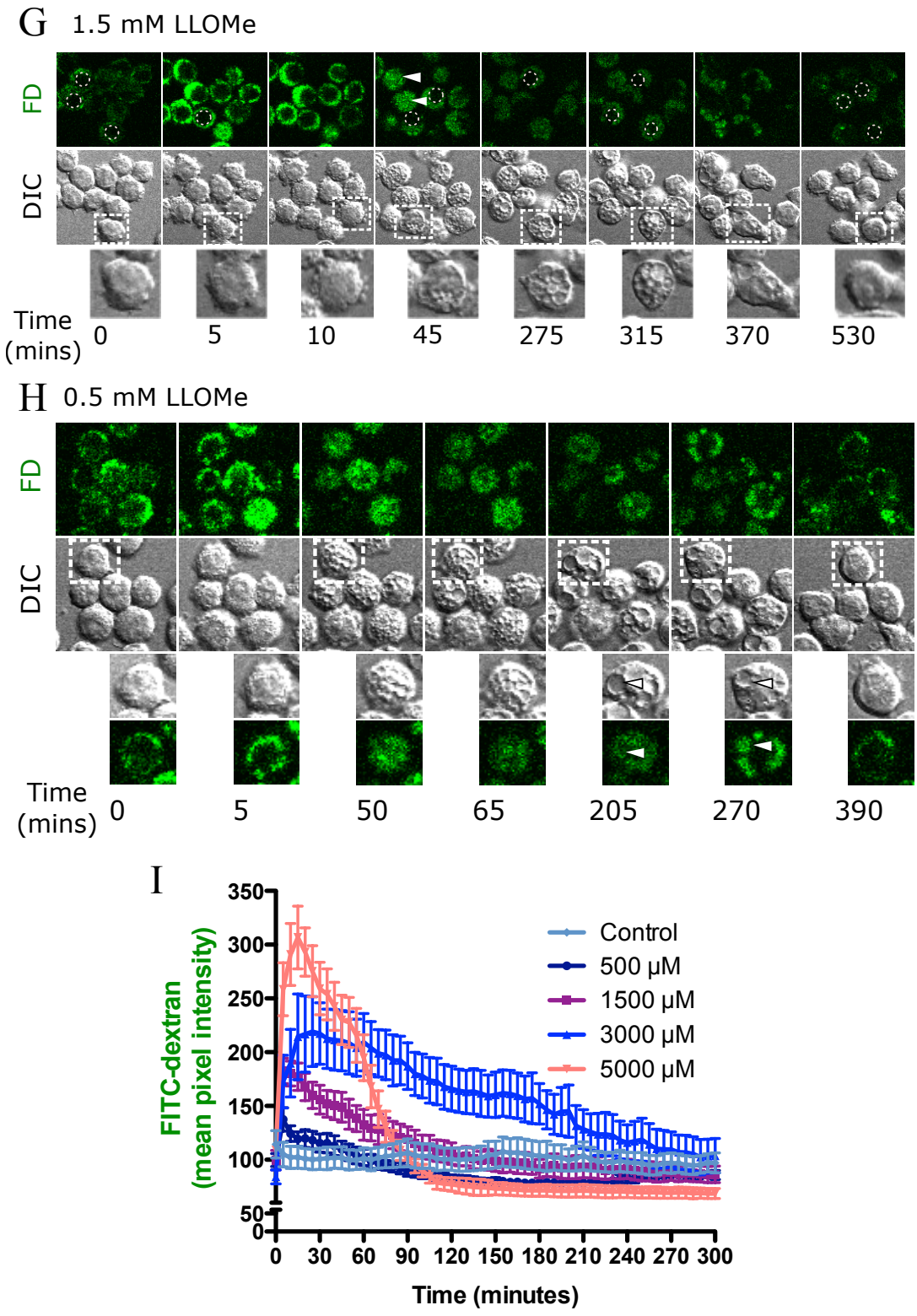

Figure A.2: Treatment of macrophages with staurosporine, silica or LLOMe result in lysosomal leakage

To investigate lysosomal leakage, macrophages were allowed to endocytose 4 kD FITC-dextran following which they were exposed to 1μM STS, 20μg/cm^2 silica or LLOMe. (A) Upon exposure to staurosporine there was an increase in FITC-dextran nuclear fluorescence as seen at 60 minutes that continued to increase. (B) Quantification of this data shows a homogenous response between cells to staurosporine exposure as leakage start at 40 minutes and plateaus by 160 minutes. (C) Cells were exposed to silica particles and imaged 5 minutes apart. Exposure to silica particles resulted in phagolysosomal leakage. Particle labeled by a solid triangle for cell 1 is inside the cell by 14 minutes and begins to leak at 34 minutes. Particle labeled by arrow for cell 2 is inside the cell by 19 minutes and leakage occurs at 49 minutes. (D) Quantification of cells exposed to silica shows heterogeneity between the timing of leakage for each cell. (E and F) Cells were exposed to 3 mM LLOMe following which they were imaged 5 minutes apart. (E) Each trace corresponds to the quantification of FITC-dextran fluorescence of an entire cell in panel F). Although there was a temporal proximity in FITC-dextran increase in the endolysosomes and leakage the same is not true about cell death as determined by cell blebbing. (F) Quantified data for cell in panel E treated with 3 mM LLOMe. Within 5 minutes there was an increase in cellular FITC-dextran fluorescence but it did not leak from endolysosomes, as there is no increase in nuclear fluorescence. Small blebs are observed on the cell surface at the same time (DIC). By 30 minutes there was increase in nuclear FITC-dextran fluorescence in every cell. A persistent blebbing is observed for cell 3 as indicated by a solid triangle (DIC) followed by a loss of FITC-dextran fluorescence upon cell death after 70 minutes. Similarly blebbing is observed for cell 1 at 70 minutes which persists and is extensive at 215 minutes as labeled by an arrow. At 235

minutes the FITC-dextran fluorescence decreases as the cell swells. (G) Macrophages exposed to 1.5 mM LLOMe also result in an increase in the endolysosomal FITC-dextran fluorescence within 5 minutes. At 10 minutes, small blebs are observed on the cells (DIC). By 45 minutes there is an increase in the nuclear fluorescence of cells labeled by triangles whereas the nucleus of cells that did not leak is represented by a dotted circle. Irrespective of the leakage status all cells show massive vacuolization (DIC). As time progressed the FITC-dextran fluorescence decreased, the cells were able to recover from extensive vacuolization and revert to normal morphology (530 minutes, DIC). (H) Macrophages exposed to 0.5 mM LLOMe results in an increase in the endolysosomal FITC-dextran fluorescence within 5 minutes. Over time there is a reduction in the fluorescence (5-65 minutes and onwards). There was extensive vacuolization (50 minutes, DIC) that as the time progressed got consolidated in to fewer but larger vacuoles. These vacuoles (205 minutes, zoomed cell) had low FITC-dextran fluorescence that increased over time (270 mintues, zoomed cell). In the time-lapse data content of these vacuoles appear to get release in the extracellular area following which the cells appear to revert to a normal morphology. (I) Quantification of an area containing at least 25 cells treated with different concentrations of LLOMe show a rapid change in FITC-dextran fluorescence indicative of the extent of FITC-dextran neutralization in endolysosomes.

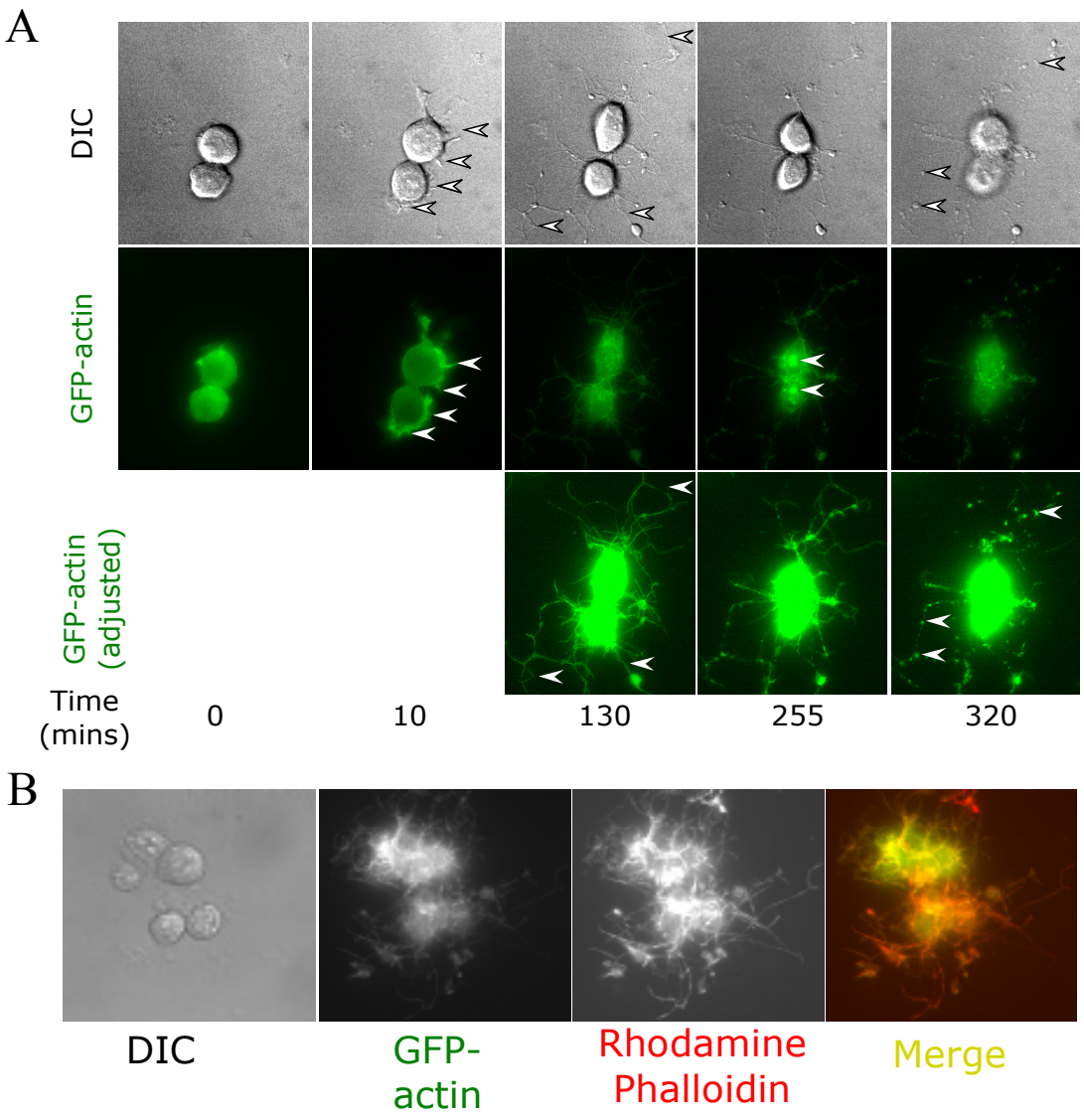

Figure A.3: Exposure to staurosporine result in filopod protrusion

Alveolar macrophages expressing GFP-actin were exposed to 1 mM of STS and imaged 5 minutes apart on an epifluorescence microscope. Upon addition of STS, an increase in filopodial protrusions were observed beginning from 5 minutes and as shown in A) at 10 minutes by arrows. Also a decrease in fluorescence in cytoplasmic actin was observed during the filopodial protrusions compared to 0 minutes. As time progressed the filopodial protrusions continued to grow (130 minutes). These protrusions are visible in both DIC and GFP channel (adjusted) where the contrast is enhanced so that the

fluorescence can be seen in the protrusions. From 255 minutes and onwards the cell protrusions start to break and at 320 minutes they appear as punctae (arrows) during which the cell is dead (DIC). To confirm presence of F-actin in these protrusions cells expressing GFP-actin exposed to STS were fixed, permeabilized and stained with Rhodamine Phalloidin. For most part there is colocalization between GFP and Phalloidin labeled actin.

A.3: Bid activation does not take place immediately after lysosomal leakage in cells exposed to silica and staurosporine

Having shown phagolysosomal and endolysosomal leakage with various inducers, we were interested in understanding whether temporal activation of Bid would follow lysosomal leakage. Biochemical data has shown cathepsin-D can cleave Bid into its active form, t-Bid (Billen *et al.*, 2008b). *In vitro* studies in which cells were exposed to staurosporine or silica have shown a reduction in cell death upon treatment of cells with cathepsin-D inhibitors (Bidère *et al.*, 2003; Thibodeau *et al.*, 2004). However, one would expect that cleavage of Bid would take place soon after the release of cathepsin-D from vesicles into the cytoplasm. However, our data with silica treated cells indicates that caspase activation happens many hours after phagolysosomal leakage. It is unclear why there would be such a long delay in cathepsin-D action. To study Bid activation in real time, cells were transfected with a Bid-FRET probe (YFP-Bid-CFP) in which YFP is fused to N-terminus and CFP to the C-terminus of Bid. When Bid is intact, a FRET signal is observed as energy from CFP can be transferred to YFP. Also, the probe is localized in cytoplasm. Following Bid cleavage, truncated-Bid (t-Bid) attached to CFP will no longer produce a FRET signal and will translocate to mitochondria (Onuki *et al.*, 2002)(Figure A.4 A). Thus Bid activation can be tracked in two different ways, one by quantifying a change in FRET ratio and second by an increase in t-Bid-CFP fluorescence in the mitochondria.

Stable clones of MH-S cells expressing Bid-FRET probe were selected by drug selection and repeated rounds of enrichment. Before exposing cells to either crystalline silica particles or staurosporine, cells were loaded with TMRE to also visualize any changes in mitochondrial membrane potential. In a cell exposed to silica, translocation of

t-Bid to mitochondria, mitochondrial hyperpolarization, cell retraction and blebbing were observed starting at at 720 minutes (Figure A.4 B). All these events occured in a 5 minutes time span. In our earlier data we observed caspase activation to also occur in the same temporal window. Although not shown here, an increase in FRET ratio also occurs at the same time indicating that the spatial separation of the fluorescent proteins in the FRET probe and insertion of t-Bid on OMM also occur in close temporal proximity (Figure A.4 C). Ten cells were quantified and each shows a close temporal correlation between Bid activation and mitochondrial hyperpolarization and a long delay after silica uptake and leakage.

Before exposure to staurosporine, the t-Bid (CFP) fluorescence is cytoplasmic and TMRE fluorescence at base line levels. In the t-Bid (CFP) fluorescence data at time 0, the cytoplasmic fluorescence appears vesicular rather than an evenly distributed cytoplasmic signal as observed with Figure A.4 A. This is due to confocal imaging of cells at low resolution and cropping of a single cell from the large data set. The experiments that were done with silica were performed using epifluorescence microscopy. Upon exposure to staurosporine, an immediate increase in TMRE fluorescence was observed which reached its peak within 20 minutes and remained steady for another 90 minutes until the start of mitochondrial depolarization (Figure A.4 E). Translocation of t-Bid to mitochondria was observed after 104 minutes during which the individual punctae appear (as indicated by arrows). These punctae localize with the mitochondria and over time become stronger in their fluorescence. This localization can be confirmed by comparing t-Bid fluorescence with TMRE fluorescence (Figure A.4 D). The t-Bid-CFP fluorescence is likely increasing as the cytoplasmic probe is getting recruited to mitochondria that are in the imaging plane

upon Bid activation. Since imaging was not done at varying height in a cell, this cannot be confirmed. Although Bid insertion took place on the OMM, mitochondrial membrane potential was sustained for the next 10 minutes following which there was a gradual depolarization (Figure A.4 F). Cell blebbing was observed only after the loss of mitochondrial membrane potential after 231 minutes.

Upon exposure to either silica or staurosporine, lysosomal leakage has been observed to occur within 30 minutes or 45 minutes respectively. Cathepsin D is therefore released from the lysosomes into the cytoplasm and hence Bid activation was expected to occur shortly after this. Our data shows that Bid activation takes place after a long delay and much closer to cell death and therefore we suggest that leaked cathepsin-D is not the activator of Bid or something prevents it from acting on Bid for a substantial period of time. Thus a direct activation of Bid by cathepsin D inside a cell could be more complex than suggested by the biochemistry data.

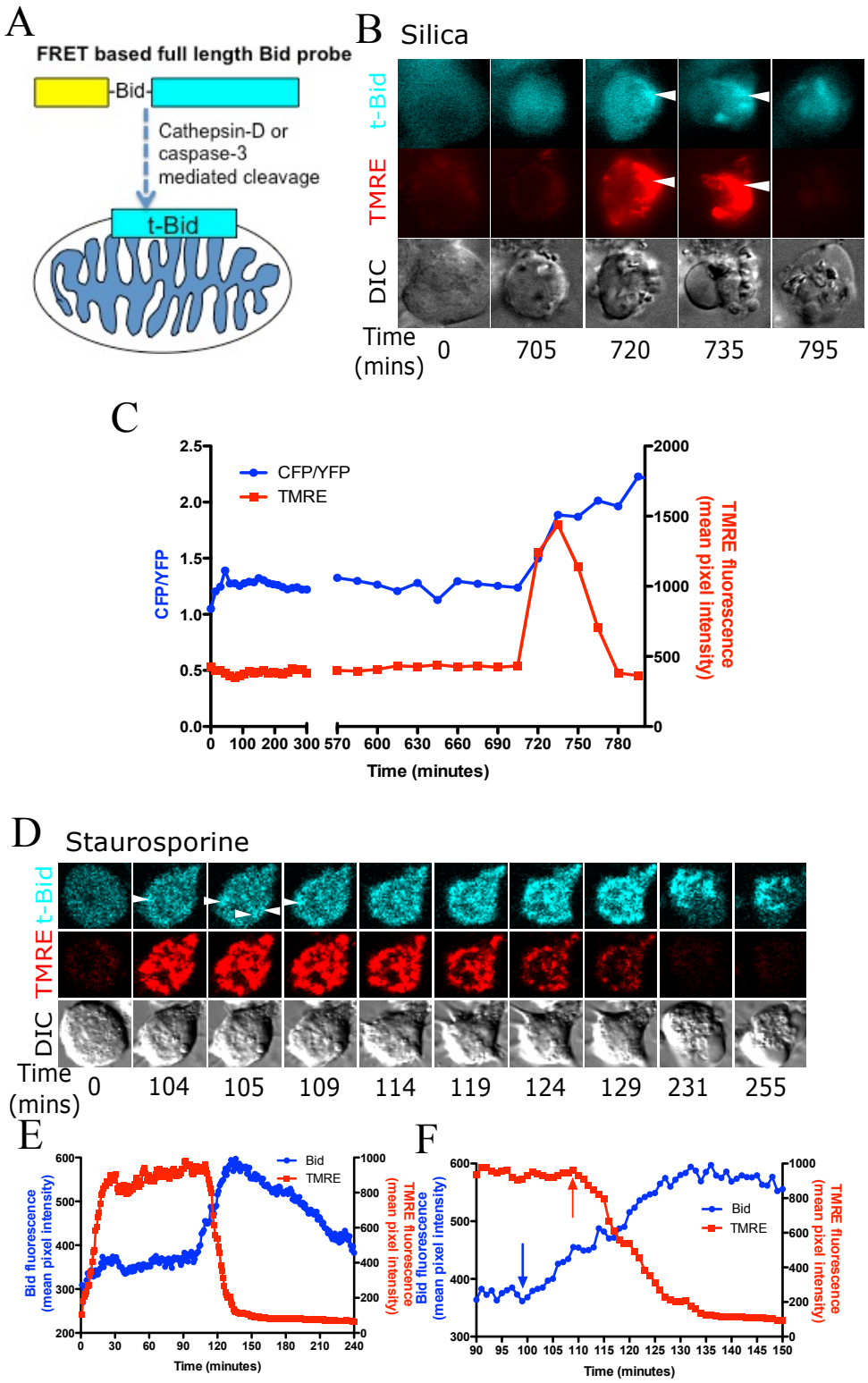

Figure A.4: Bid activation occur late during cell death

(A) The FRET based Bid sensor allows detection of an active Bid (t-Bid) that migrates to mitochondria. Macrophages expressing Bid-FRET sensor were loaded with the potentiometric dye TMRE (50 nM) to detect any changes in mitochondrial membrane potential. (B) Time-lapse was acquired using epifluorescence microscope with 5 minutes time interval for first 500 minutes followed by 15 minutes interval. Upon exposure of silica particles, an increase in t-Bid-CFP signal, mitochondrial hyperpolarization and cell blebbing occur together in a 15-minute time window (720 minutes). With time the localization of t-Bid signal in the mitochondria get stronger. (C) The FRET ratio also shows an increase in signal at 720 minutes along with mitochondrial hyperpolarization. (D) Time-lapse was acquired every minute using a confocal microscope to eliminate out of focus light for better visualization of t-Bid translocation in to the mitochondria. Upon exposure to 1 μM STS a rapid increase in mitochondrial fluorescence was observed that stayed constant. At 104 minutes there was an increase in Bid-CFP fluorescence that continued to increase over time that colocalized to the TMRE fluorescence in the mitochondria. From 119 minutes the TMRE fluorescence begin to decrease indicative of mitochondrial hyperpolarization. The cell blebbing did not begin until 231 minutes. (E) A quantification of the data show the changes observed in D) where as F) shows a zoom in version of time line between 90 and 150 minutes. Bid activation occur from 100 minutes as seen by an increase in CFP fluorescence and its localization in to the mitochondria from 104 minutes. Mitochondrial depolarization begins from 110 minutes onwards.

A.4: Staurosporine and silica, but not LLOMe show a prominent mitochondrial Bax localization during cell death

Bid activation has been proposed to activate Bax following which Bax localizes to mitochondria. We therefore hypothesized that the temporal dynamics of Bax activation will follow that of Bid activation. Cells transiently expressing GFP-Bax were exposed to staurosporine, silica or LLOMe. To understand the relationship between mitochondrial localization of Bax and a change in mitochondrial membrane potential, cells were also loaded with TMRE. Before exposure to any agents, GFP-Bax is localized throughout the cytoplasm in an inactive state.

In the GFP-Bax fluorescence data, at time 0, the cytoplasmic fluorescence in the image appear to be vesicular as the cell presented here is cropped from a large data set that was imaged at low resolution using a confocal microscope. Following addition of staurosporine, GFP-Bax is cytoplasmic until 166 minutes. At 167 minutes GFP-Bax fluorescence appears to localize with TMRE (indicated by the arrow in Figure A.5A). The mitochondrial GFP-Bax fluorescence progressively increases indicative of a gradual distribution of Bax to mitochondria. While Bax continues to localize with mitochondria, the mitochondrial membrane potential does not change. Bax redistribution to mitochondria has been shown to result in MOMP (Kuwana *et al.*, 2005). In spite of MOMP, mitochondria are able to sustain the membrane potential for some time before undergoing complete depolarization. A progressive decrease in mitochondrial membrane potential begins after 171 minutes and a complete depolarization is observed at 210 minutes. A change in mitochondrial TMRE fluorescence is represented in Figure A.5 B. Similar events were observed for other cells. When macrophages expressing GFP-Bax were exposed to staurosporine, the kinetics of the change in TMRE fluorescence was

different compared to macrophages that do not express GFP-Bax. In a macrophage that does not express GFP-Bax, a gradual increase in TMRE fluorescence was observed when the cell was exposed to staurosporine. After reaching a peak, the TMRE fluorescence leveled off and stayed constant until the time of mitochondrial depolarization (Figure A.5 C). Thus expression of GFP-Bax likely results in some alteration such that this increase in TMRE fluorescence is not observed.

We did not have a correct combination of fluorescent probes to simultaneously detect Bid and Bax activation. Therefore, the time to complete mitochondrial depolarization following Bid and Bax activation was compared (Figure A.5 D). Although there is heterogeneity in the time it takes each cell to depolarize, the mean time between Bid or Bax activation and mitochondrial depolarization was about 40 minutes for each probe. Bid and Bax activation was defined by appearance of these probes on mitochondria. This suggests that Bid and Bax activation are likely to occur in a close temporal proximity to each other.

When cells were exposed to silica particles, there was no change in Bax localization or TMRE fluorescence for up to 160 minutes (Figure A.5 E). Surprisingly, GFP-Bax localized to the phagosome containing silica particle as indicated by the solid triangle. Based on the timing, the appearance of GFP-Bax on the phagolysosome is likely to occur once the leaked phagosome was resealed. At 165 minutes GFP-Bax got redistributed to the mitochondria (indicated by an arrow in Figure A.5 E) and an overlap colocalized with TMRE fluorescence. Mitochondrial depolarization occured soon after Bax insertion (Figure A.5 F) but cell death was not observed until 380 minutes, suggestive of a significant delay in the progression towards cell death. However, this was

not the case with every cell that was analyzed. A huge variation in timing was observed between mitochondrial Bax insertion and cell blebbing (Figure A.5 G). Cell blebbing was selected as an indicator since our data has shown caspase activation to occur at the same time as cell blebbing (Joshi, 2013). This points towards a scenario where either Bax is not causing MOMP or that there is insufficient MOMP to relieve the inhibitory effects of anti-apoptotic protein XIAP on caspases.

In cells exposed to 3 mM LLOMe a sudden drop in TMRE fluorescence was observed after 20 minutes of treatment. The FITC-dextran leakage data show that by this time a partial endolysosomal leakage had occurred. After 50 minutes, TMRE fluorescence reached a new baseline level and stayed that way until a further mitochondrial depolarization. Mitochondrial redistribution of Bax did not take place until the cells started to bleb (147 minutes and onwards). Bax was not distributed throughout the mitochondria but only to a small area and its distribution throughout the mitochondria took place only upon further blebbing of cells (152 minutes and onwards). Cells are already enroute to death during blebbing as caspases that are considered to be a point of no return in the cell death process were found be active during silica induced apoptosis at blebbing stage. However, this needs to be confirmed with LLOMe. Contrary to the literature where LLOMe is selectively used to induce lysosomal leakage, it also appears to have a side effect that occurs directly by depolarizing the mitochondria. However this shows that even after losing membrane potential cells are able to survive for many minutes to hours before dying (Figures A.5 H and I).

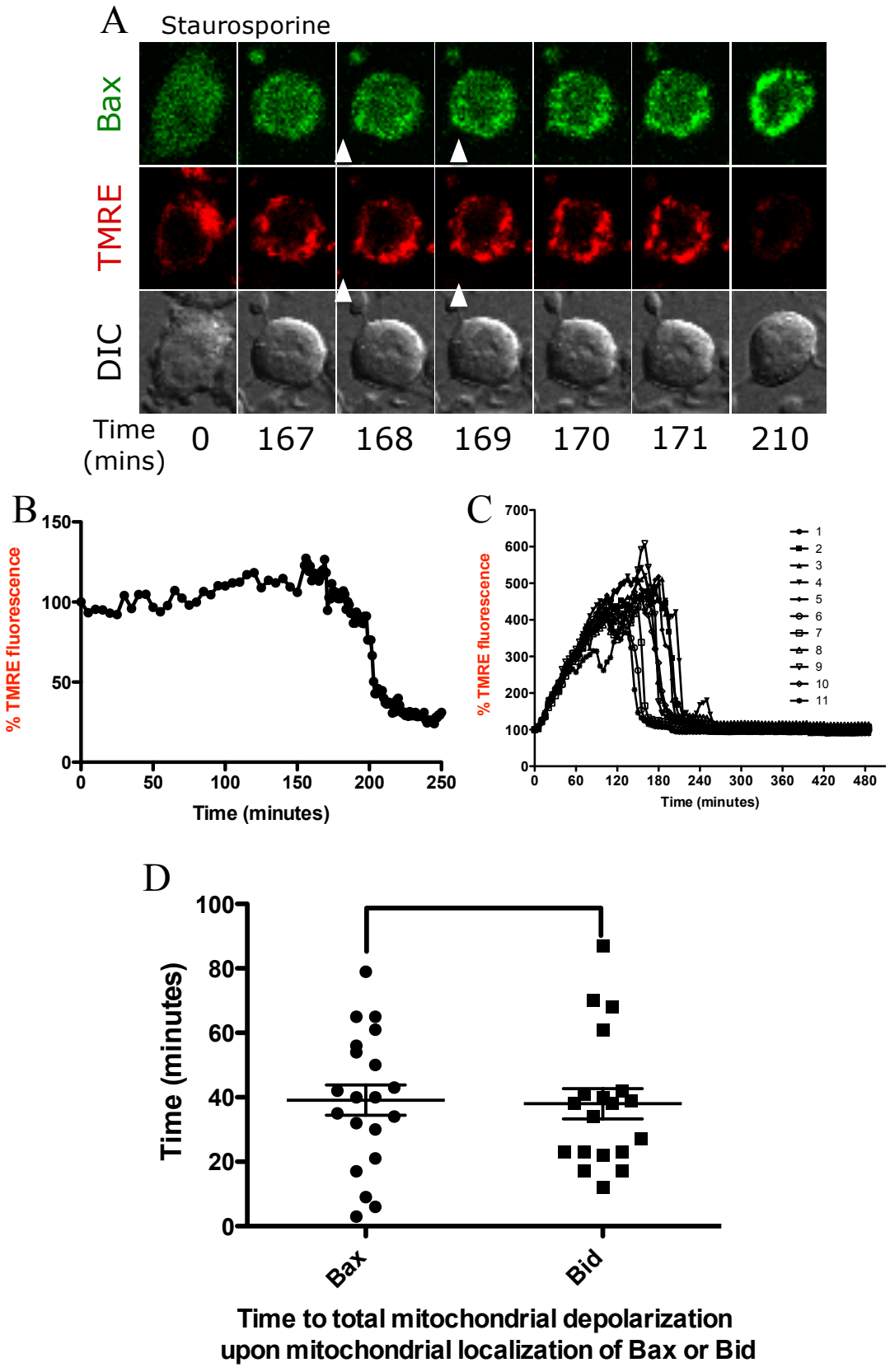

Time to total mitochondrial depolarization upon mitochondrial localization of Bax or Bid

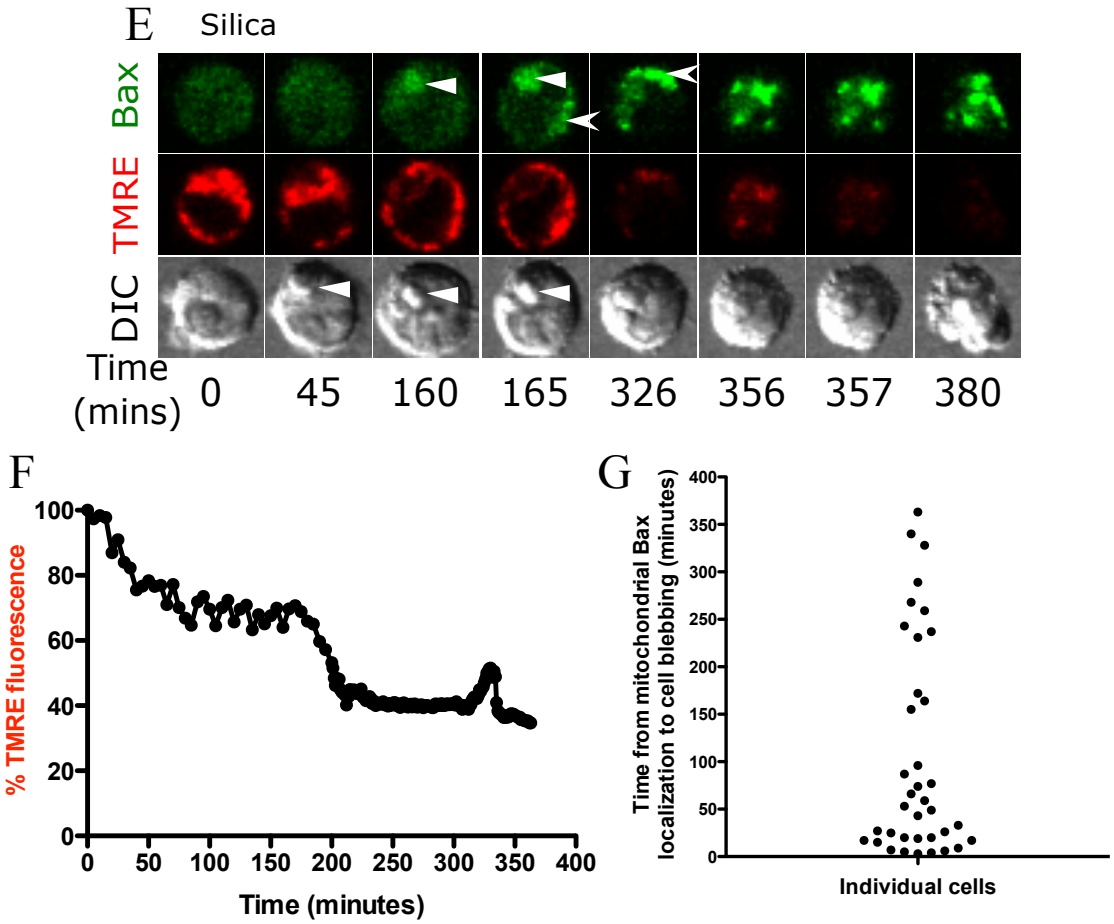
E
Silica
Bax
TMRE
DIC
Time (mins)
0
45
160
165
326
356
357
380
F
% TMRE fluorescence
Time (minutes)
G
Time from mitochondrial Bax localization to cell blebbing (minutes)
Individual cells
H
3 mM LLOMe
Bax
TMRE
DIC
Time (mins)
0
5
50
147
149
152
171
173

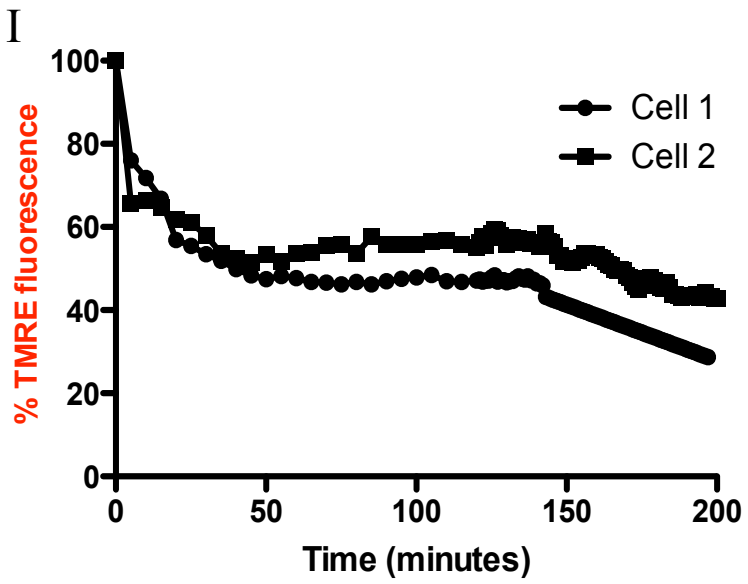

Figure A.5: Bax dynamics and alterations in mitochondrial physiology upon treatment of cells with staurosporine, silica and LLOMe

To visualize Bax activation and its translocation to mitochondria, cells were allowed to express GFP fused with Bax. In order to investigate a relationship between Bax activation and mitochondrial depolarization cells were loaded with 50 nM TMRE and exposed to either staurosporine, silica or LLOMe. (A) Upon exposure to 1 μM staurosporine, GFP-Bax localized to mitochondria at 167 minutes and the intensity of GFP increased over time. Mitochondrial fluorescence stayed constant in these cells and decreased after 171 minutes. (B) Quantification of a change in TMRE fluorescence in panel A). Upon exposure to staurosporine in t-Bid expressing cells loaded with TMRE, an increase in TMRE fluorescence was observed. However, the same was not observed in cells expressing GFP-Bax. To confirm that either Bid or Bax overexpression was not altering mitochondrial membrane potential cells that did not express any fusion protein were loaded with TMRE and exposed to STS. (C) There was an increase in TMRE fluorescence for 11 different cells upon addition of STS. This is similar to that of cells

expressing t-Bid. (D) A total loss of mitochondrial membrane potential following localization of either t-Bid or Bax into mitochondria was approximately 40 minutes upon STS exposure. Data representative of 20 individual cells, Mean $\pm$ SEM, $p < 0.01$. (E) In a cell exposed to silica, Bax was found to localize around a particle labeled with solid triangle after a prolong period (160 minutes). The same particle is inside the cell by 45 minutes (solid triangle). The particle labeled with solid triangle does not show any GFP-Bax fluorescence at 45 minutes but at 160 minutes it was fluorescent. Other than the phagosome, GFP-Bax did not co-localize with the mitochondria. At 165 minutes, GFP-Bax co-localized with mitochondria as indicated by the arrow but the membrane potential did not change. GFP-Bax continues to redistribute itself into the mitochondria and by 326 minutes mitochondria are depolarize whereas the cell blebbing occur at 380 minutes. (F) The trend from the quantification of data for a change in mitochondrial membrane potential from panel E) is shown here. (G) A quantification for the time it took for a cell to undergo blebbing following Bax localization to mitochondria shows a huge temporal variation between cells. Each dot represents an individual cells. (H) Upon exposure of macrophages to 3 mM LLOMe a rapid decrease in TMRE fluorescence is observed beginning as early as 5 minutes. GFP-Bax localization was seen in some spots at 149 minutes as indicated by solid arrow. (I) A quantification of TMRE fluorescence for cells 1 and 2 show a rapid loss of mitochondrial membrane potential for cells 1 and 2 in panel H).

A.5: Mitochondrial inter-membrane space proteins are released upon Bax association with mitochondria

The delay in death following Bax insertion observed for both the staurosporine and silica suggested that there could be a delay in MOMP and/or the release of IMS proteins following Bax insertion into the OMM. To validate MOMP upon Bax translocation to mitochondria, MH-S cells were co-transfected with GFP-Bax and Smac-RFP. Smac is a mitochondrial inter-membrane space protein that re-distributes to the cytoplasm upon MOMP. These cells were then exposed to staurosporine.

Depending on the microscopy technique used, two different scenarios were observed. On a widefield epifluorescence microscope, Smac release preceded Bax insertion whereas with a spinning disk confocal microscope Bax insertion and Smac release occured within one minute of each other.. Before exposure to staurosporine, Smac was found localized to the mitochondria whereas Bax was localized to the cytoplasm. After exposure to staurosporine, when cells were imaged using epifluorescence microscopy, Smac that was localized to mitochondria at 300 minutes got redistributed in to the cytoplasm at 301 minutes (Figure A.6 A). Puncta of Bax appeared at 303 minutes as indicated by the triangles. It is possible that the redistribution of Bax to mitochondria was not observed at at earlier times due to the high cytoplasmic background of Bax. A resulting low signal to noise could make it difficult to detect a low level of mitochondrial Bax fluorescence. A similar observation has been commented upon by Albeck et al. (Albeck *et al.*, 2008b). To circumvent this issue, the same experiment was done using a confocal microscope. The redistribution of Bax into mitochondria and that of Smac into the cytoplasm was found to occur simultaneously at 30 minutes in this cell (Figure A.6 B). The timing of MOMP as well as the aggregated appearance of the mitochondria was

unusual for this cell when compared to other cells from an earlier experiment on epifluorescence microscope. It was difficult to get data from many cells as only a few cells in the population co-express Smac-RFP and GFP-Bax.

Temporal analysis of IMS protein release was only performed with staurosporine and our data is consistent with literature where a simultaneous release of inter-membrane space reporter protein was observed along with Bax translocation (Muñoz-Pinedo, 2006).. However, more single cell data needs to be collected to better understand the relationship between Bax activation, MOMP, release of IMS proteins and death upon exposure to staurosporine and silica. It is however surprising that many cells show a significant temporal delay in death following Bax induced MOMP. This is suggestive of a complex process that may regulate cell death.

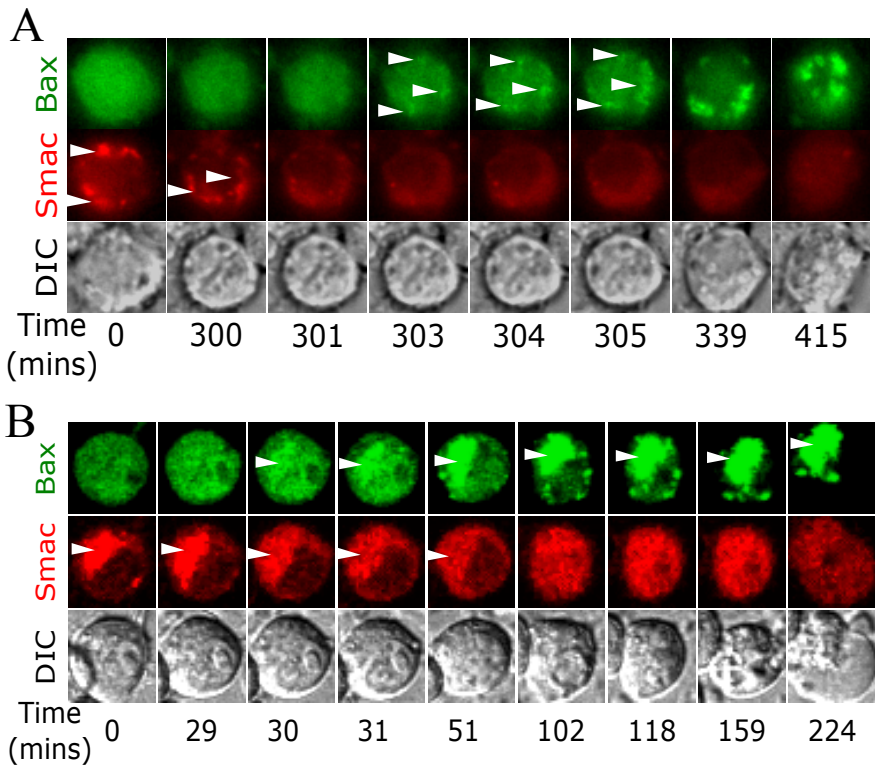

Figure A.6: Investigation of MOMP in macrophages exposed to staurosporine

In order to investigate MOMP in cells exposed to staurosporine, cells were allowed to co-express GFP-Bax and Smac-RFP. (A) In cells imaged using epi-fluroescence microscopy Bax is distributed in the cytoplasm and Smac in the mitochondria (0 minutes). At 300 minutes, Smac is still present in the mitochondria as observed by the punctate appearance (triangles). At 301 minutes this punctate appearance is lost and Smac is redistributed in to the cytoplasm. Mitochondrial Bax fluorescence appears only at 303 minutes as indicated by triangles. (B) In cells imaged using confocal microscopy the Bax fluorescence is appear cytoplasmic and Smac in the mitochondria at 0 minutes. Upon addition of staurosporine, Bax redistribute to mitochondria at 30 minutes as seen by an increase in fluorescence and indicated by triangle. Smac fluorescence also decreases at the same time

and continues to redistribute itself throughout the cytoplasm as time progresses. As time progresses the Bax fluorescence increases over time in the mitochondria.

A.6: A variation in the timing of phosphatidylserine exposure relative to other events is observed between silica and staurosporine exposure

The phospholipid phosphatidylserine (PS) is restricted to the inner leaflet of the plasma membrane under normal circumstances. During apoptosis, phosphatidylserine is externalized to the outer leaflet of the plasma membrane. This change in membrane asymmetry is a gold standard in the field of apoptosis detection. Annexin V has an affinity for PS and hence Annexin V conjugated to a fluorophore (example, Annexin V-FITC) is commonly used to detect PS externalization. Recently, it has been shown that the flipping of PS to the outer leaflet is mediated by caspase cleavage of the phospholipid flippase (Segawa *et al.*, 2014) that normally helps to maintain the phospholipid bilayer asymmetry (Daleke, 2007).

Cells were incubated in medium containing Annexin V-FITC and exposed to staurosporine (Figure A.7 A and C). Cell 1 became Annexin V-FITC positive at 205 minutes following which it blebbed. The cell undergoing apoptosis later undergoes swelling indicative of secondary necrosis. Similar data was observed for cell 2 which becomes Annexin V positive at 285 minutes and later blebs (Figure A.7 A). A quantitative analysis of individual cells shows that on an average cells exhibit normal morphology for an average of 300 minutes following which they are Annexin V positive for 60 minutes after which they bleb and undergo secondary necrosis (Figure A.7 C). Although there was heterogeneity in the timing of these events, every cell exhibited a same pattern. This is consistent with earlier studies where Annexin V is used an early marker of apoptosis.

In cells that were incubated in a medium containing Annexin V-FITC and exposed to silica particles, cell 1 retracts and blebs at 270 minutes (Figure A.7 B). At 420

minutes the cell becomes AnnexinV positive. During secondary necrosis this fluorescence is lost. Cell 2 begins to bleb at 300 minutes whereas it becomes AnnexinV positive at 360 minutes. A quantitative analysis of individual cells shows that on average, cells retain their normal morphology for 330 minutes following which they retract and bleb for 70 minutes. Cells become Annexin V positive and stay in that phase for another hour following which they undergo secondary necrosis.

A temporal variation in the execution of events between cells for the same treatment and a difference in sequence of events for cells exposed to staurosporine and silica was observed. From our earlier data in chapter 3, it can be concluded that upon silica exposure, PS flipping occurs following caspase activation that was found to occur during cell blebbing. This is in agreement with a recent study where caspase mediated cleavage of flippase was shown to disturb the phospholipid arrangement exposing PS on the outer leaflet (Segawa *et al.*, 2014). In a cell exposed to staurosporine, Annexin V binding precedes cell blebbing that is contrary to our observation for cells exposed to silica. Because a relationship between caspase activation and a morphological change (cell blebbing) is not known it could not be ascertained when PS flipping takes place in a cell exposed to staurosporine. If a disturbance of phospholipid asymmetry is due to caspase activation then timing of PS exposure on outer leaflet of the cell shows that caspase activation precedes cell blebbing in macrophages exposed to staurosporine.

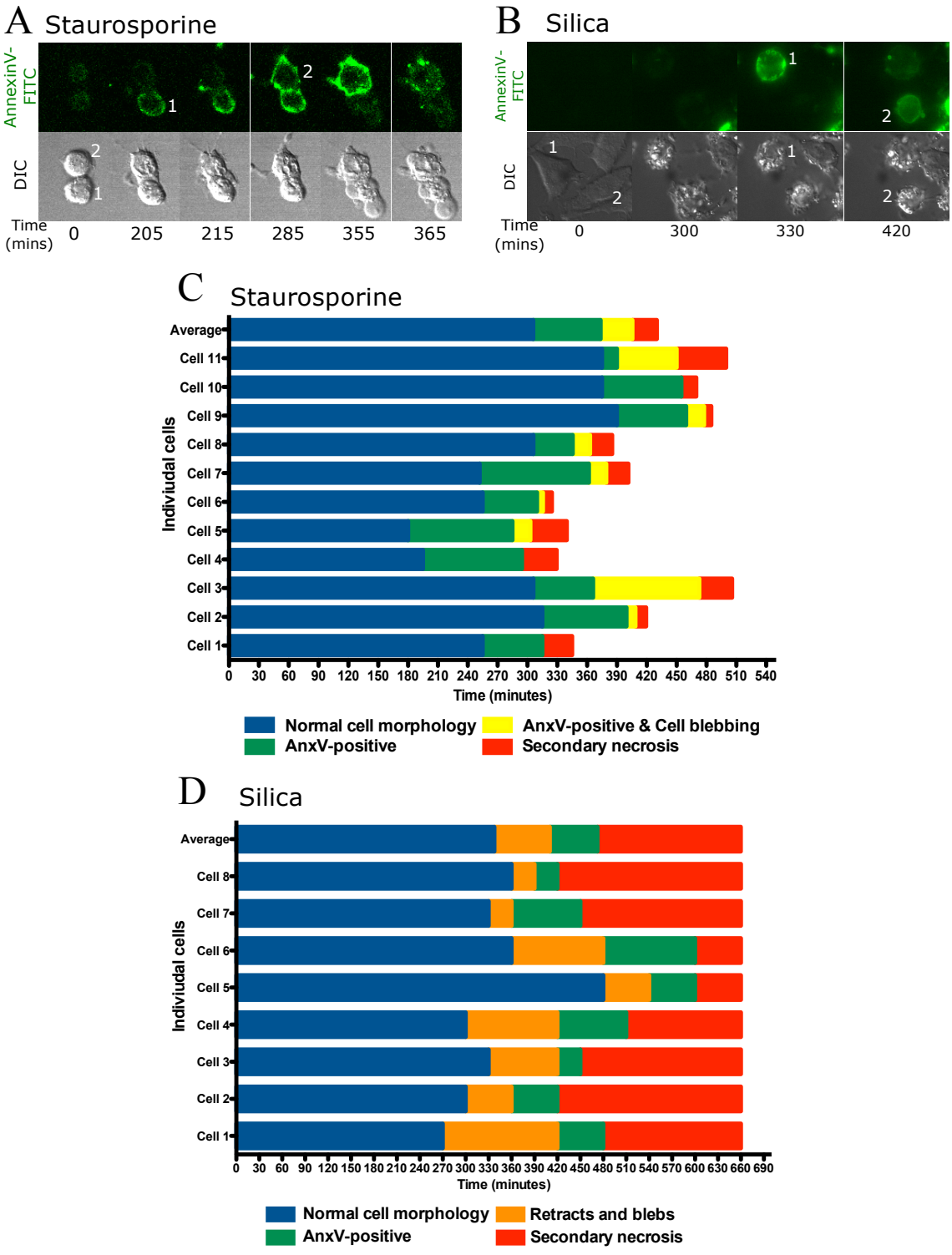

Figure A.7: Temporal analysis of apoptotic maker, AnnexinV-FITC in cells exposed to staurosporine or silica

(A and C) Macrophages labeled with AnnexinV-FITC and exposed to silica particles become AnnexinV-FITC positive only after cells have started to bleb. A quantitative temporal analysis of different cells confirms this observation. (B and D) Macrophages labeled with AnnexinV-FITC and exposed to Staurosporine become AnnexinV-FITC positive before cell blebbing. A quantitative temporal analysis of different cells confirms this observation.

A.7: Discussion

This is the first study to investigate if the cell death pathway is conserved following the induction of endolysosomal leakage by different compounds. If the proximal critical event in the apoptosis pathway is the leakage of enzymes like cathepsin-D out of phagolysosomes or endolysosomes, then one would expect the same events to follow regardless of how the leakage was initiated. We found a difference in the timing of endolysosomal leakage between silica, staurosporine and LLOMe. Silica induced phagolysosomal leakage ranged anywhere from 10-50 minutes following particle uptake. Staurosporine treated cells showed evidence of endolysosomal leakage on an average after 45 minutes of compound treatment and leveled out at 145 minutes. Following addition of LLOMe, endolysosomal leakage started at 10 minutes and leveled out at 30 minutes. Unlike silica, where the timing of phagolysosomal leakage varied for each phagosome following particle uptake, there was a lesser variability in the initiation of the timing of endolysosomal leakage in cells treated with chemical compounds such as staurosporine or LLOMe.

While all these agents cause endolysosomal leakage, the mechanism by which they cause leakage varies. Silica induced leakage is proposed to occur by lipid peroxidation of the phagolysosomal membrane. LLOMe is proposed to have a detergent like property resulting in leakage (Thiele and Lipsky, 1990) whereas the mechanism of leakage for staurosporine is not known. Under certain conditions where there is an increased accumulation of cholesterol and sphingolipids in the lysosomes of cells in individuals with Niemann-Pick C (NPC) disease lysosomes were found to become resistant to staurosporine or another detergent-like compound O-methyl serine

dodecylamide hydrochloride (O-MSDH). In these cells or cells treated with the drug U18666A that inhibits cholesterol recycling there was reduced vesicle leakage and cell death (Appelqvist *et al.*, 2011). When U18666A treated cells were exposed to crystalline silica, a decrease in IL-1β release and an increase in cell viability was observed. Although the study did not look at leakage, the data is suggestive of a possible delay in leakage (Biswas *et al.*, 2014). Thus the composition of the phospholipid bilayer can influence leakage.

We also found differences in the timing and in the order of activation of the pro-apoptotic proteins Bid and Bax following endolysosomal leakage. Figure A.8 summarizes the order of events observed upon exposure of cells to different inducers. Following phagolysosomal leakage upon exposure of cells to silica, Bax was found to localize to mitochondria and the phagolysosome. While the significance of Bax localizing to a phagolysosome is not known, localization of Bax to mitochondria is suggestive of MOMP. Because a phagolysosome did not leak again, Bax present in the phagolysosome does not appear to be causing membrane damage. Following mitochondrial insertion of Bax, cells were found to either rapidly undergo apoptosis or stay in this state for many hours (up to 5 hours). Bid activation, mitochondrial hyperpolarization, caspase activation and cell blebbing were all observed in a temporal window of 5 minutes. Following MOMP, a quick and rapid apoptotic response is expected but a delay could possibly be due to incomplete MOMP (iMOMP). A partial release of IMS content due to iMOMP has been shown to result in cell survival (Biswas *et al.*, 2014). Activation of Bid following Bax activation and MOMP is not a usual process. At least one study has shown Bid

cleavage by caspase-3 to provide a feedback loop amplification in cell death upon caspase-3 activation (Slee *et al.*, 2000).

In staurosporine treated cells, endolysosomal leakage was found to start at 45 minutes and level off at 145 minutes. Bid activation and Bax activation appeared to occur close to each other when complete mitochondrial depolarization was kept as a common denominator. Both pro-apoptotic proteins were activated after 100 minutes of endolysosomal leakage. It is possible that a certain concentration of cathepsin D is required in the cytoplasm to activate Bid. Therefore, even when endolysosomal leakage started at 45 minutes it took time before Bid activation could be observed. We also observed a delay in mitochondrial membrane depolarization upon mitochondrial localization of Bid and Bax. Two different scenarios with regards to MOMP and mitochondrial membrane depolarization has been shown in the literature, one where MOMP and depolarization takes place simultaneously (Düssmann *et al.*, 2003) and another where depolarization follows MOMP and the timing of depolarization is variable (Muñoz-Pinedo, 2006). Our data is consistent with the latter scenario where a temporal delay of a few minutes to 60 minutes is observed following Bax or Bid localization to mitochondria. This gradual loss of membrane potential following MOMP has been showed to be dependent on caspase activation (Waterhouse *et al.*, 2001; Ricci *et al.*, 2003). Since we do not have data on caspase activation in macrophages treated with staurosporine, a relationship between mitochondrial membrane depolarization, caspase activation and cell blebbing could not be established. Associating physiological changes detected by various markers to cell death between silica and staurosporine treatment is further complicated by Annexin V data. Staurosporine treated cells become Annexin V

positive before cell blebbing where as silica treated cells become Annexin V positive after cell blebbing.

LLOMe is frequently used as a control for lysosomal leakage to understand inflammasome activation. The ability of LLOMe to induce lysosomal leakage and toxicity is dependent on the processing of LLOMe by cathepsin-C, as macrophages deficient in cathepsin-C did not result in lysosomal leakage and cell death (Lima *et al.*, 2013). Recently, chemical inhibitors of cathepsin B and D (CA-074-Me and Pepstatin A) as well as prevention of endolysosomal acidification by either bafilomycin A or NH_4Cl treatment were found to prevent cell death (Brojatsch *et al.*, 2015). Thus low endolysosomal pH and various cathepsins seem to regulate either LLOMe activation or LLOMe induced cell death. Our study found an unusual effect of LLOMe; a rapid mitochondrial depolarization that occurred within 5 minutes of LLOMe addition. The cells reached a new baseline mitochondrial membrane potential by 50 minutes that persisted until the cells died during which further depolarization was observed. Effect of various concentrations of LLOMe on mitochondrial depolarization was not tested in this study. Since LLOMe has been reported to be endocytosed by cells it was surprising to see it causing vesicle neutralization and depolarizing mitochondria within 5 minutes. It is yet to be shown with any of the inhibitors of endocytosis that any of the effects of LLOMe could be prevented. Unlike silica and staurosporine, where there was a temporal delay between Bax translocation to mitochondria and cell blebbing, in LLOMe treated cells, blebbing and Bax translocation was observed simultaneously. As cells continued to bleb, the Bax signal localized to mitochondria became stronger, suggestive of a feedback effect of cell death on the activation of pro-apoptotic proteins. While concentration dependent

cell death with LLOMe is not new, the imaging approach has allowed us to show that at lower concentrations of LLOMe, cells are able to recover from vesicle injury while at higher concentrations, cells undergo necrosis. Thus there is an optimal concentration at which cells die by apoptosis.

The temporal events following activation of the extrinsic cell death pathway are well characterized. Comparisons between the initial sets of events following activation of the extrinsic and intrinsic cell death pathway upon lysosomal leakage are therefore warranted. For the extrinsic cell death pathway, following activation by TNF or TRAIL ligand, activation of caspase-8 results in Bid activation. Similarly, following lysosomal leakage, cathepsin-D in the cytoplasm can also result in Bid activation due to a cathepsin cleavage site in Bid (Billen *et al.*, 2008b). Activated Bid (t-Bid) can act as an as an activator for Bax and Bak as well as an inhibitor for the Bcl-2 family of anti-apoptotic proteins. In studies where post-TNF caspase-8 activity was measured using a FRET probe, a steady increase in FRET ratio was observed over a period of 8 hours prior to MOMP (Albeck *et al.*, 2008b). The fact that there is a prolonged period with active caspase-8 in the extrinsic cell death pathway and presumably that of cathepsin D upon vesicle leakage during intrinsic cell death pathway but no immediate MOMP is a new observation. Our data shows that upon staurosporine induced endolysosomal leakage the sequence of activation of Bid and Bax is similar to the proposed model (Figure A.1), whereas, upon phagolysosomal leakage with silica, Bid activation was observed along with cell death. It is possible that the amount of cathepsin released could be a critical factor, as phagolysosomal leakage would release little vesicle contents as compared to vesicle leakage by staurosporine. An experiment with LLOMe will be able to address this

question as the release of endolysosomal contents between LLOMe and staurosporine should be comparable. There will be a bulk release of endolysosomal contents with either LLOMe or staurosporine compared to cells containing a single silica particle.

Biochemical studies have shown Bax activation to be a quick process upon interaction with BH-3 only protein, t-Bid (Billen *et al.*, 2008a; Kim *et al.*, 2009; Walensky and Gavathiotis, 2011). Along with Bax activation, t-Bid has been shown to insert itself into the mitochondrial outer membrane allowing for homo-oligomerization of Bax. In the absence of t-Bid, Bax failed to oligomerize to cause MOMP (Lovell *et al.*, 2008). In other biochemical studies, Bax was still able to cause MOMP in the absence of t-Bid. However, a high concentration of Bax was required and it took longer to cause permeabilization (Shamas-Din *et al.*, 2014). Bax was also found to permeabilize membranes that were primed by t-Bid (Shamas-Din *et al.*, 2014; Gillies *et al.*, 2015). A separate study has shown inactive Bax to exist in equilibrium between cytoplasm and mitochondria. It is loosely bound to mitochondria and the presence of the anti-apoptotic protein Bcl-xL on the OMM prevents Bax from localizing to the outer mitochondrial membrane (Schellenberg *et al.*, 2013). In spite of this overwhelming biochemical data, we still do not understand how these events occur within a cell and the deciding factors that prevent this sequence of events when cells are exposed to different inducers.

Understanding of the intrinsic cell death pathway following lysosomal leakage can also be important in the process of drug discovery. Many lipophilic and amphiphilic compounds with a positive charge get trapped in lysosomes upon protonation, a property known as lysosomotropism (Nadanaciva *et al.*, 2011). While they accumulate in the lysosomes it is not known if they induce leakage (Boya and Kroemer, 2008; Nadanaciva

et al., 2011; Boya, 2012). A compound can have this undesirable property or such a property of the compound to cause lysosomal leakage can be specifically used to induce cell death in cancer cells. More work is therefore required to further understand and connect the processes that were identified in this preliminary data following lysosomal leakage.

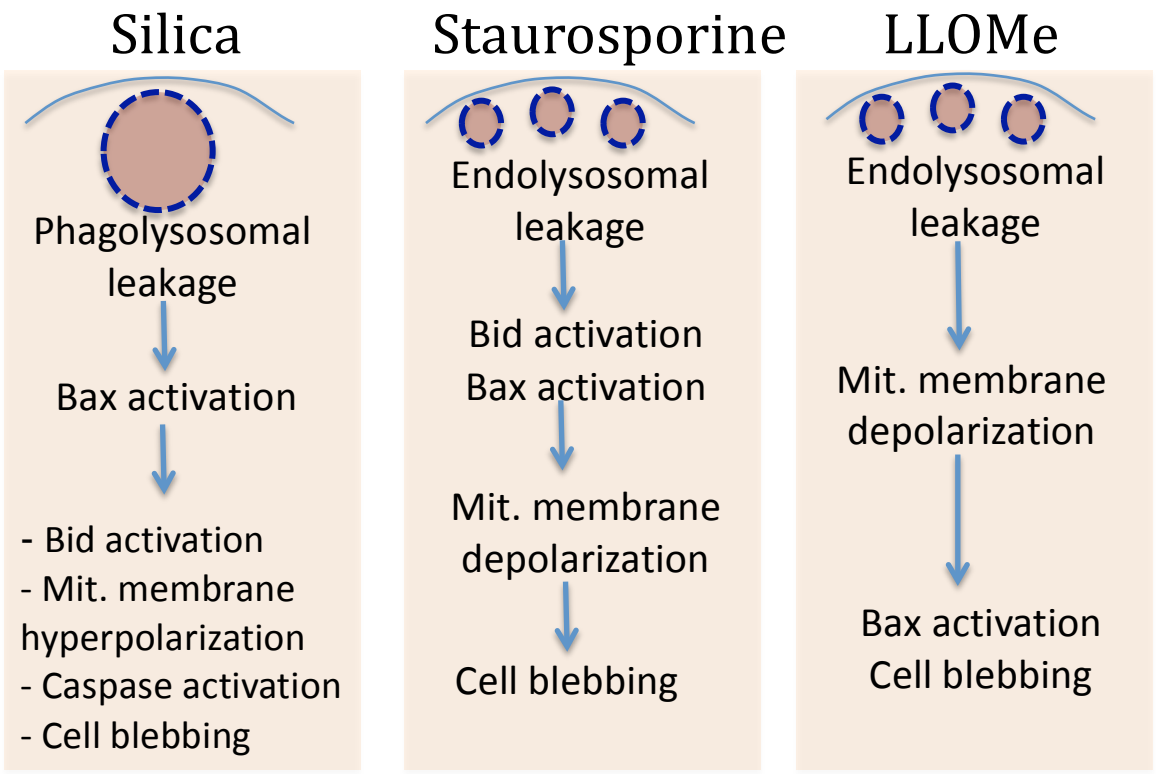

Figure A.8: Variation in the order of activation of various pro-apoptotic proteins and events leading up to cell blebbing in macrophages treated with different inducers

A.8: Future Directions

This section contains questions and investigational approaches to further help understand the sequence of events and processes from phagolysosomal or lysosomal leakage to cell death. The preliminary data in the appendix lacks some supporting information that would help to proceed with the next set of questions. These include, understanding the release of 70 kD FITC-dextran into the cytoplasm with both staurosporine and LLOMe at different concentrations of these compounds. While release of cathepsins has been shown in the literature upon treatment of cells with staurosporine and LLOMe, we would also like to confirm this in our system.

A.8.1: Does phagolysosomal or lysosomal leakage stimulate autophagy and is autophagy responsible for resealing of a leaky vesicle?

Our data in chapter 4 show resealing of a phagolysosome as demonstrated by the reaccumulation of TRITC-dextran phagosomal fluorescence after leakage. Other studies have reported fusion of a leaky phagosome with an autophagosome. Inhibiting autophagy prevented fusion of an autophagosome and a leaky phagosome(Maejima *et al.*, 2013). The presence of autophagosomes on a leaky phagosome could be confirmed by expressing microtubule associated protein 1A/1B-light chain-3 fused to GFP (LC3-GFP) in a cell. LC3-GFP is a marker for autophagy that is expected to localize to a leaking phagolysosome. Inhibitors of autophagy will prevent LC3-GFP localization to the leaky phagolysosome. If the fusion of TRITC-dextran containing vesicles were still observed on a leaking phagolysosome after inhibiting autophagy, it would be indicative of phagolysosomal resealing independent of autophagy. If inhibiting autophagy were to

prevent phagolysosome resealing, then its effect on cell death would be investigated. It is predicted that cells would undergo rapid activation of pro-apoptotic proteins and apoptosis, as there would be continuous release of phagolysosomal contents. Alternately, an increase in release of lysosomal contents can also drive cells to necrosis as suggested by some studies. An autophagic response towards leaky vesicles due to staurosporine treatment of cells has not been demonstrated. While localization of LC3-GFP as punctae on a leaky lysosome that occur upon LLOMe or staurosporine treatment might be difficult to detect, such leakiness can be detected by expressing cells with Galectin-3 fused with a fluorescent probe that gets localized in the cytoplasm. Following lysosomal leakage, Galectin-3 will bind to the N-acetylgalactosamine containing glycans found in lysosomes and appear punctate (Maejima *et al.*, 2013; Aits *et al.*, 2015).

A.8.2: What is the role of various cathepsins and pro-apoptotic proteins in the cell death process?

Before investigating any alterations in the apoptotic cascade in real-time, the role of cathepsins B, C and D, Bid and Bax in cell death upon lysosomal leakage should be investigated by either chemical inhibition, use of a cell-line lacking these proteins or by siRNA knockdown. Cell death would be investigated at different time points using a microplate reader or a flow cytometry based assay. Inhibition of a protein that either prevents or reduces cell death will be further investigated in real time and its relationship to other proteins (Bid, Bax and caspases) and physiological events (mitochondria membrane polarization) during cell death would be investigated. This would allow us to address following questions

- If inhibition of cathepsin reduces cell death then is the intrinsic cell death pathway still followed or is there is an alternate mode to death?
- Since Bid is proposed to activate Bax, will knocking down Bid prevent Bax activation or change the sequence of its activation with respect to other events?
- Bid is also proposed to have an inhibitory effect on the anti-apoptotic Bcl-2 protein that prevents Bax activation. If Bcl-2 is inhibited by a BH-3 mimetic compound like ABT-737 then will Bid activation and Bax induced MOMP occur quickly to induce cell death rapidly? This will be addressed by expressing Bax-RFP in cells expressing the Bid-FRET probe.
- Bax and Bak are the two pro-apoptotic proteins that have been pre-dominantly shown to be involved in MOMP following t-Bid activation and insertion to OMM (Zaltsman *et al.*, 2010; Shamas-Din *et al.*, 2014). In a Bax and Bak double knockout cell line we would like to confirm that t-Bid activation would not result in MOMP.

References:

Aits, S., and Jäättelä, M. (2013). Lysosomal cell death at a glance. J Cell Sci *126*, 1905–1912.

Aits, S., Jäättelä, M., and Nylandsted, J. (2015). Methods for the quantification of lysosomal membrane permeabilization: A hallmark of lysosomal cell death. Methods Cell Biol. *126*, 261–285.

Albeck, J., Burke, J., Aldridge, B., Zhang, M., Lauffenburger, D., and Sorger, P. (2008a). Quantitative analysis of pathways controlling extrinsic apoptosis in single cells. Mol Cell *30*, 11–25.

Albeck, J., Burke, J., Spencer, S., Lauffenburger, D., and Sorger, P. (2008b). Modeling a Snap-Action, Variable-Delay Switch Controlling Extrinsic Cell Death. PLoS Biol *6*, e299.

Appelqvist, H., Nilsson, C., Garner, B., Brown, A. J., Kågedal, K., and Ollinger, K. (2011). Attenuation of the Lysosomal Death Pathway by Lysosomal Cholesterol Accumulation. Am J Pathol *178*, 629–639.

Arap, W., Pasqualini, R., Montalti, M., Petrizza, L., Prodi, L., Rampazzo, E., Zaccheroni, N., and Marchiò, S. (2013). Luminescent silica nanoparticles for cancer diagnosis. Curr. Med. Chem. *20*, 2195–2211.

Au-Yeung, H. Y., Chan, J., Chantarojsiri, T., and Chang, C. J. (2013). Molecular imaging of labile iron(II) pools in living cells with a turn-on fluorescent probe. J. Am. Chem. Soc. *135*, 15165–15173.

Babior, B. M. (2004). NADPH oxidase. Curr Opin Immunol *16*, 42–47.

Banki, K., Hutter, E., Gonchoroff, N., and Perl, A. (1999). Elevation of Mitochondrial Transmembrane Potential and Reactive Oxygen Intermediate Levels Are Early Events and Occur Independently from Activation of Caspases in Fas Signaling. The Journal of Immunology *162*, 1466.

Barrett, E. G., Johnston, C., Oberdörster, G., and Finkelstein, J. N. (1998). Silica-induced chemokine expression in alveolar type II cells is mediated by TNF-alpha. Am J Physiol *275*, L1110–L1119.

Battegay, E. J., Raines, E. W., Colbert, T., and Ross, R. (1995). TNF-alpha stimulation of fibroblast proliferation. Dependence on platelet-derived growth factor (PDGF) secretion and alteration of PDGF receptor expression. The Journal of Immunology *154*, 6040–6047.

Bauernfeind, F. G. *et al.* (2009). Cutting Edge: NF- B Activating Pattern Recognition and Cytokine Receptors License NLRP3 Inflammasome Activation by Regulating NLRP3 Expression. J Immunol *183*, 787–791.

Bauernfeind, F., Bartok, E., Rieger, A., Franchi, L., Nuñez, G., and Hornung, V. (2011).

Cutting Edge: Reactive Oxygen Species Inhibitors Block Priming, but Not Activation, of the NLRP3 Inflammasome. J Immunol *187*, 613–617.

Becher, R., Bucht, A., Øvrevik, J., Hongslo, J. K., Dahlman, H. J., Samuelsen, J. T., and Schwarze, P. E. (2007). Involvement of NADPH oxidase and iNOS in rodent pulmonary cytokine responses to urban air and mineral particles. Inhalation Toxicology *19*, 645–655.

Bedard, K., and Krause, K.-H. (2007). The NOX family of ROS-generating NADPH oxidases: physiology and pathophysiology. Physiol Rev *87*, 245–313.

Berghe, T. V., Vanlangenakker, N., Parthoens, E., Deckers, W., Devos, M., Festjens, N., Guerin, C. J., Brunk, U. T., Declercq, W., and Vandenabeele, P. (2010). Necroptosis, necrosis and secondary necrosis converge on similar cellular disintegration features. *17*, 922–930.

Bergsbaken, T., Fink, S. L., and Cookson, B. T. (2009). Pyroptosis: host cell death and inflammation. Nat. Rev. Microbiol. *7*, 99–109.

Bhola, P. D., Mattheyses, A. L., and Simon, S. M. (2009). Spatial and Temporal Dynamics of Mitochondrial Membrane Permeability Waves during Apoptosis. Biophys J *97*, 2222–2231.

Bidère, N., Lorenzo, H. K., Carmona, S., Laforge, M., Harper, F., Dumont, C., and Senik, A. (2003). Cathepsin D triggers Bax activation, resulting in selective apoptosis-inducing factor (AIF) relocation in T lymphocytes entering the early commitment phase to apoptosis. J Biol Chem *278*, 31401–31411.

Billen, L. P., Kokoski, C. L., Lovell, J. F., Leber, B., and Andrews, D. W. (2008a). Bcl-XL inhibits membrane permeabilization by competing with Bax. PLoS Biol *6*, e147.

Billen, L. P., Shamas-Din, A., and Andrews, D. W. (2008b). Bid: a Bax-like BH3 protein. Oncogene *27 Suppl 1*, S93–S104.

Biswas, R., Hamilton, R. F., and Holian, A. (2014). Role of Lysosomes in Silica-Induced Inflammasome Activation and Inflammation in Absence of MARCO. Journal of Immunology Research *2014*, 1–10.

Bohdanowicz, M., Cosío, G., Backer, J. M., and Grinstein, S. (2010). Class I and class III phosphoinositide 3-kinases are required for actin polymerization that propels phagosomes. *191*, 999–1012.

Borges, V. M. *et al.* (2001). Fas ligand triggers pulmonary silicosis. J Exp Med *194*, 155–164.

Borges, V. M., Lopes, M. F., Falcão, H., Leite-Júnior, J. H., Rocco, P. R. M., Davidson, W. F., Linden, R., Zin, W. A., and DosReis, G. A. (2002). Apoptosis underlies immunopathogenic mechanisms in acute silicosis. Am J Respir Cell Mol Biol *27*, 78–84.

Bossy-Wetzel, E., Newmeyer, D. D., and Green, D. R. (1998). Mitochondrial cytochrome c release in apoptosis occurs upstream of DEVD-specific caspase activation and independently of mitochondrial transmembrane depolarization. Embo J *17*, 37–49.

Boya, P. (2012). Lysosomal function and dysfunction: mechanism and disease. Antioxid Redox Signal *17*, 766–774.

Boya, P. *et al.* (2005). Inhibition of macroautophagy triggers apoptosis. Mol Cell Biol *25*, 1025–1040.

Boya, P., and Kroemer (2008). Lysosomal membrane permeabilization in cell death. Oncogene *27*, 6434–6451.

Boya, P., Gonzalez-Polo, R.-A., Poncet, D., Andreau, K., Vieira, H. L. A., Roumier, T., Perfettini, J.-L., and Kroemer, G. (2003). Mitochondrial membrane permeabilization is a critical step of lysosome-initiated apoptosis induced by hydroxychloroquine. Oncogene *22*, 3927–3936.

Brass, D. M., Spencer, J. C., Li, Z., Potts-Kant, E., Reilly, S. M., Dunkel, M. K., Latoche, J. D., Auten, R. L., Hollingsworth, J. W., and Fattman, C. L. (2012). Innate immune activation by inhaled lipopolysaccharide, independent of oxidative stress, exacerbates silica-induced pulmonary fibrosis in mice. PLoS ONE *7*, e40789.

Brigger, I., Dubernet, C., and Couvreur, P. (2002). Nanoparticles in cancer therapy and diagnosis. Adv Drug Deliv Rev *54*, 631–651.

Brojatsch, J., Lima, H., Palliser, D., Jacobson, L. S., Muehlbauer, S. M., Furtado, R., Goldman, D. L., Lisanti, M. P., and Chandran, K. (2015). Distinct cathepsins control necrotic cell death mediated by pyroptosis inducers and lysosome-destabilizing agents. Cell Cycle *14*, 964–972.

Brumatti, G., Sheridan, C., and Martin, S. J. (2008). Expression and purification of recombinant annexin V for the detection of membrane alterations on apoptotic cells. Methods *44*, 235–240.

Buschow, S. I., Lasonder, E., Szklarczyk, R., Oud, M. M., de Vries, I. J. M., and Figdor, C. G. (2012). Unraveling the human dendritic cell phagosome proteome by organellar enrichment ranking. J Proteomics *75*, 1547–1562.

Cassel, S. L., Eisenbarth, S. C., Iyer, S. S., Sadler, J. J., Colegio, O. R., Tephly, L. A., Carter, A. B., Rothman, P. B., Flavell, R. A., and Sutterwala, F. S. (2008). The Nalp3 inflammasome is essential for the development of silicosis. Proc Natl Acad Sci USA *105*, 9035–9040.

Castranova, V. (2004). Signaling pathways controlling the production of inflammatory mediators in response to crystalline silica exposure: role of reactive oxygen/nitrogen species. Free Radic Biol Med *37*, 916–925.

Castranova, V., Vallyathan, V., Ramsey, D. M., McLaurin, J. L., Pack, D., Leonard, S., Barger, M. W., Ma, J. Y., Dalal, N. S., and Teass, A. (1997). Augmentation of pulmonary reactions to quartz inhalation by trace amounts of iron-containing particles. Environ Health Perspect *105 Suppl 5*, 1319–1324.

Castranova, V., Walker, W. E., and Vallyathan, V. (1995). Silica and Silica-Induced Lung Diseases, CRC Press.

Cavalli, G., Fallanca, F., Dinarello, C. A., and Dagna, L. (2015). Treating pulmonary silicosis by blocking interleukin 1. Am J Respir Crit Care Med *191*, 596–598.

Chao S K et al (2001). Cell Surface Regulation of Silica-Induced Apoptosis by the SR-A Scavenger Receptor in a Murine Lung Macrophage Cell Line (MH-S).

Cherniack, M. (1986). Hawk"s nest incident: America"s worst industrial disaster.

Cho, Y. J., Seo, M. S., Kim, J. K., Lim, Y., Chae, G., Ha, K. S., and Lee, K. H. (1999). Silica-induced generation of reactive oxygen species in Rat2 fibroblast: role in activation of mitogen-activated protein kinase. Biochem Biophys Res Commun *262*, 708–712.

Cirman, T., Oresić, K., Mazovec, G. D., Turk, V., Reed, J. C., Myers, R. M., Salvesen, G. S., and Turk, B. (2004). Selective disruption of lysosomes in HeLa cells triggers apoptosis mediated by cleavage of Bid by multiple papain-like lysosomal cathepsins. J Biol Chem *279*, 3578–3587.

Costantini, L. M., Gilberti, R. M., and Knecht, D. A. (2011). The Phagocytosis and Toxicity of Amorphous Silica. PLoS ONE *6*, e14647.

D Rosner, G. M. (1991). Consumption, silicosis, and the social construction of industrial disease. The Yale Journal of Biology and Medicine *64*, 481–498.

Daëron, M. (2003). Fc RECEPTOR BIOLOGY. Http://Dx.Doi.org/10.1146/Annurev.Immunol.15.1.203 *15*, 203–234.

Daleke, D. L. (2007). Phospholipid flippases. J Biol Chem *282*, 821–825.

Dauber, J. H., Rossman, M. D., Pietra, G. G., Jimenez, S. A., and Daniele, R. P. (1980). Experimental silicosis: morphologic and biochemical abnormalities produced by intratracheal instillation of quartz into guinea pig lungs. Am J Pathol *101*, 595–612.

Davis, M. J., and Swanson, J. A. (2010). Technical advance: caspase-1 activation and IL-1{beta} release correlate with the degree of lysosome damage, as illustrated by a novel imaging method to quantify phagolysosome damage. J Leukoc Biol.

Davis, M. J., Gregorka, B., Gestwicki, J. E., and Swanson, J. A. (2012). Inducible renitence limits Listeria monocytogenes escape from vacuoles in macrophages. J Immunol *189*, 4488–4495.

DeLeo, F. R., Allen, L. A., Apicella, M., and Nauseef, W. M. (1999). NADPH oxidase activation and assembly during phagocytosis. J Immunol *163*, 6732–6740.

Deshpande, A., Narayanan, P. K., and Lehnert, B. E. (2002). Silica-induced generation of extracellular factor(s) increases reactive oxygen species in human bronchial epithelial cells. Toxicol Sci *67*, 275–283.

Di Giuseppe, M. *et al.* (2009). Systemic inhibition of NF-kappaB activation protects from silicosis. PLoS ONE *4*, e5689.

Dickinson, B. C., and Chang, C. J. (2011). Chemistry and biology of reactive oxygen species in signaling or stress responses. Nat. Chem. Biol. *7*, 504–511.

Dickinson, B. C., Huynh, C., and Chang, C. J. (2010). A palette of fluorescent probes with varying emission colors for imaging hydrogen peroxide signaling in living cells. J. Am. Chem. Soc. *132*, 5906–5915.

Dixon, S. J. *et al.* (2012). Ferroptosis: an iron-dependent form of nonapoptotic cell death. Cell *149*, 1060–1072.

Dixon, S. J., and Stockwell, B. R. (2013). The role of iron and reactive oxygen species in cell death. Nat. Chem. Biol. *10*, 9–17.

Donaldson, K., and Borm, P. (2006). Particle Toxicology, CRC Press.

Dostert, C., Petrilli, V., Van Bruggen, R., Steele, C., Mossman, B. T., and Tschopp, J. (2008). Innate Immune Activation Through Nalp3 Inflammasome Sensing of Asbestos and Silica. *320*, 674–677.

Driscoll, K. E. (2000). TNFalpha and MIP-2: role in particle-induced inflammation and regulation by oxidative stress. Toxicol Lett *112-113*, 177–183.

Driscoll, K. E., Hassenbein, D. G., Carter, J., Poynter, J., Asquith, T. N., Grant, R. A., Whitten, J., Purdon, M. P., and Takigiku, R. (1993). Macrophage inflammatory proteins 1 and 2: expression by rat alveolar macrophages, fibroblasts, and epithelial cells and in rat lung after mineral d... - PubMed - NCBI. Am J Respir Cell Mol Biol *8*, 311–318.

Driscoll, K. E., Howard, B. W., Carter, J. M., Asquith, T., Johnston, C., Detilleux, P., Kunkel, S. L., and Isfort, R. J. (1996). Alpha-quartz-induced chemokine expression by rat lung epithelial cells: effects of in vivo and in vitro particle exposure. Am J Pathol *149*, 1627–1637.

Droga-Mazovec, G., Bojic, L., Petelin, A., Ivanova, S., Romih, R., Repnik, U., Salvesen, G. S., Stoka, V., Turk, V., and Turk, B. (2008). Cysteine Cathepsins Trigger Caspase-dependent Cell Death through Cleavage of Bid and Antiapoptotic Bcl-2 Homologues. J Biol Chem *283*, 19140–19150.

Duan, J., Yu, Y., Li, Y., Yu, Y., Li, Y., Zhou, X., Huang, P., and Sun, Z. (2013). Toxic

effect of silica nanoparticles on endothelial cells through DNA damage response via Chk1-dependent G2/M checkpoint. PLoS ONE *8*, e62087.

Duve, C. (1975). Exploring cells with a centrifuge. *189*, 186–194.

Düssmann, H., Rehm, M., Kögel, D., and Prehn, J. H. M. (2003). Outer mitochondrial membrane permeabilization during apoptosis triggers caspase-independent mitochondrial and caspase-dependent plasma membrane potential depolarization: a single-cell analysis. J Cell Sci *116*, 525–536.

Edelstein, A., Amodaj, N., Hoover, K., Vale, R., and Stuurman, N. (2010). Computer control of microscopes using μManager. Curr Protoc Mol Biol *Chapter 14*, Unit14.20–14.20.17.

Ehrenberg, B., Montana, V., Wei, M. D., Wuskell, J. P., and Loew, L. M. (1988). Membrane potential can be determined in individual cells from the nernstian distribution of cationic dyes. Biophys J *53*, 785–794.

Ellson, C., Davidson, K., Anderson, K., Stephens, L. R., and Hawkins, P. T. (2006). PtdIns3P binding to the PX domain of p40phox is a physiological signal in NADPH oxidase activation. Embo J *25*, 4468–4478.

Emert-Sedlak, L., Shangary, S., Rabinovitz, A., Miranda, M. B., Delach, S. M., and Johnson, D. E. (2005). Involvement of cathepsin D in chemotherapy-induced cytochrome c release, caspase activation, and cell death. Mol Cancer Ther *4*, 733–742.

Englen, M. D., Taylor, S. M., Laegreid, W. W., Silflow, R. M., and Leid, R. W. (1990). The effects of different silicas on arachidonic acid metabolism in alveolar macrophages. Exp Lung Res *16*, 691–709.

Esswein, E. J., Breitenstein, M., Snawder, J., Kiefer, M., and Sieber, W. K. (2013). Occupational exposures to respirable crystalline silica during hydraulic fracturing. J Occup Environ Hyg *10*, 347–356.

Fazzi, F. *et al.* (2014). TNFR1/Phox Interaction and TNFR1 Mitochondrial Translocation Thwart Silica-Induced Pulmonary Fibrosis. J Immunol *192*, 3837–3846.

Fenoglio, I., Fonsato, S., and Fubini, B. (2003). Reaction of cysteine and glutathione (GSH) at the freshly fractured quartz surface: a possible role in silica-related diseases? Free Radic Biol Med *35*, 752–762.

Fisher, A. B. (2009). Redox signaling across cell membranes. Antioxid Redox Signal *11*, 1349–1356.

Flannagan, R. S., Cosío, G., and Grinstein, S. (2009). Antimicrobial mechanisms of phagocytes and bacterial evasion strategies. Nat. Rev. Microbiol. *7*, 355–366.

Flannagan, R. S., Jaumouillé, V., and Grinstein, S. (2012). The cell biology of

phagocytosis. Annu Rev Pathol *7*, 61–98.

Franchi, L., Eigenbrod, T., Muñoz-Planillo, R., and Nuñez, G. (2009). The inflammasome: a caspase-1-activation platform that regulates immune responses and disease pathogenesis. Nat Immunol *10*, 241–247.

Fubini, B. (1998). Surface chemistry and quartz hazard. Ann Occup Hyg *42*, 521–530.

Fubini, B., and Hubbard, A. (2003). Reactive oxygen species (ROS) and reactive nitrogen species (RNS) generation by silica in inflammation and fibrosis. Free Radic Biol Med *34*, 1507–1516.

Galluzzi, L. *et al.* (2014a). Essential versus accessory aspects of cell death: recommendations of the NCCD 2015. –.

Galluzzi, L., Bravo-San Pedro, J. M., and Kroemer, G. (2014b). Organelle-specific initiation of cell death. Nat Cell Biol *16*, 728–736.

Galluzzi, Maiuri, Vitale, Zischka, Castedo, Zitvogel, and Kroemer (2007). Cell death modalities: classification and pathophysiological implications.

Gao, H.-S., Rong Xue, Peng Ding, Chen, N.-F., Bing Meng, Zhao, H.-B., Zhen Yang, and Wang, S.-X. (2011). Cross-talk of the related bioactivity mediators in serum after injection of soluble TNF-α receptor on silicosis model of rats. Toxicology and Industrial Health *27*, 607–616.

Gardner, D. E. (1984). Alterations in macrophage functions by environmental chemicals. Environ Health Perspect *55*, 343–358.

Ghio, A. J., Kennedy, T. P., Whorton, A. R., Crumbliss, A. L., Hatch, G. E., and Hoidal, J. R. (1992). Role of surface complexed iron in oxidant generation and lung inflammation induced by silicates. Am J Physiol *263*, L511–L518.

Gilberti, R. M., and Knecht, D. A. (2015). Macrophages phagocytose nonopsonized silica particles using a unique microtubule-dependent pathway. Mol Biol Cell *26*, 518–529.

Gilberti, R. M., Joshi, G. N., and Knecht, D. A. (2008). The phagocytosis of crystalline silica particles by macrophages. Am J Respir Cell Mol Biol *39*, 619–627.

Gillies, L. A., Du, H., Peters, B., Knudson, C. M., Newmeyer, D. D., and Kuwana, T. (2015). Visual and functional demonstration of growing Bax-induced pores in mitochondrial outer membranes. Mol Biol Cell *26*, 339–349.

Giovannini, C., Matarrese, P., Scazzocchio, B., Sanchez, M., Masella, R., and Malorni, W. (2002). Mitochondria hyperpolarization is an early event in oxidized low-density lipoprotein-induced apoptosis in Caco-2 intestinal cells. FEBS Lett *523*, 200–206.

Goldstein, J. C., Muñoz-Pinedo, C., Ricci, J.-E., Adams, S. R., Kelekar, A., Schuler, M.,

Tsien, R. Y., and Green, D. R. (2005). Cytochrome c is released in a single step during apoptosis. *12*, 453–462.

Goldstein, J. C., Waterhouse, N. J., Juin, P., Evan, G. I., and Green, D. R. (2000). The coordinate release of cytochrome c during apoptosis is rapid, complete and kinetically invariant. Nat Cell Biol *2*, 156–162.

Goyette, G. *et al.* (2012). Proteomic characterization of phagosomal membrane microdomains during phagolysosome biogenesis and evolution. Mol. Cell Proteomics *11*, 1365–1377.

Green, D. R., and Kroemer, G. (2005). Pharmacological manipulation of cell death: clinical applications in sight? J Clin Invest *115*, 2610–2617.

Green, D. R., and Reed, J. C. (1998). Mitochondria and apoptosis. *281*, 1309–1312.

Guo, J., Gu, N., Chen, J., Shi, T., Zhou, Y., Rong, Y., Zhou, T., Yang, W., Cui, X., and Chen, W. (2013). Neutralization of interleukin-1 beta attenuates silica-induced lung inflammation and fibrosis in C57BL/6 mice. Arch. Toxicol. *87*, 1963–1973.

Haberzettl, P., Schins, R. P. F., Höhr, D., Wilhelmi, V., Borm, P. J. A., and Albrecht, C. (2008). Impact of the FcgammaII-receptor on quartz uptake and inflammatory response by alveolar macrophages. Am J Physiol Lung Cell Mol Physiol *294*, L1137–L1148.

Halliwell, B. (2006). Phagocyte-derived reactive species: salvation or suicide? Trends Biochem Sci *31*, 509–515.

Hamilton, R. F., de Villiers, W. J., and Holian, A. (2000). Class A type II scavenger receptor mediates silica-induced apoptosis in Chinese hamster ovary cell line. Toxicol Appl Pharmacol *162*, 100–106.

Hamilton, R. F., Thakur, S. A., and Holian, A. (2008). Silica binding and toxicity in alveolar macrophages. Free Radic Biol Med *44*, 1246–1258.

Hampton, M., Kettle, A., and Winterbourn, C. (1998). Inside the Neutrophil Phagosome: Oxidants, Myeloperoxidase, and Bacterial Killing. Blood *92*, 3007.

He, L., Wu, X., Siegel, R., and Lipsky, P. (2006). TRAF6 Regulates Cell Fate Decisions by Inducing Caspase 8-dependent Apoptosis and the Activation of …. Journal of Biological Chemistry.

Hengartner, M. O., Ellis, R. E., and Horvitz, H. R. (1992). Caenorhabditis elegans gene ced-9 protects cells from programmed cell death. Nature *356*, 494–499.

Hoppe, A. D., and Swanson, J. A. (2004). Cdc42, Rac1, and Rac2 display distinct patterns of activation during phagocytosis. Mol Biol Cell *15*, 3509–3519.

Hornung, V., and Latz, E. (2010). Critical functions of priming and lysosomal damage

for NLRP3 activation. Eur J Immunol *40*, 620–623.

Hornung, V., Bauernfeind, F., Halle, A., Samstad, E. O., Kono, H., Rock, K. L., Fitzgerald, K. A., and Latz, E. (2008). Silica crystals and aluminum salts activate the NALP3 inflammasome through phagosomal destabilization. Nat Immunol *9*, 847–856.

Hu, S., Zhao, H., Al-Humadi, N. H., Yin, X. J., and Ma, J. K. H. (2006). Silica-induced apoptosis in alveolar macrophages: evidence of in vivo thiol depletion and the activation of mitochondrial pathway. J Toxicol Environ Health Part A *69*, 1261–1284.

Hu, S., Zhao, H., Yin, X. J., and Ma, J. K. H. (2007). Role of mitochondria in silica-induced apoptosis of alveolar macrophages: inhibition of apoptosis by rhodamine 6G and N-acetyl-L-cysteine. J Toxicol Environ Health Part A *70*, 1403–1415.

Huang, J., Canadien, V., Lam, G. Y., Steinberg, B. E., Dinauer, M. C., Magalhaes, M. A. O., Glogauer, M., Grinstein, S., and Brumell, J. H. (2009). Activation of antibacterial autophagy by NADPH oxidases. Proceedings of the National Academy of Sciences *106*, 6226–6231.

Huang, S. H., Hubbs, A. F., Stanley, C. F., Vallyathan, V., Schnabel, P. C., Rojanasakul, Y., Ma, J. K., Banks, D. E., and Weissman, D. N. (2001). Immunoglobulin responses to experimental silicosis. Toxicol Sci *59*, 108–117.

Huaux, F. (2007). New developments in the understanding of immunology in silicosis. Curr Opin Allergy Clin Immunol *7*, 168–173.

Hubbard, A. K., Timblin, C. R., Shukla, A., Rincón, M., and Mossman, B. T. (2002). Activation of NF-kappaB-dependent gene expression by silica in lungs of luciferase reporter mice. Am J Physiol Lung Cell Mol Physiol *282*, L968–L975.

Humphries, W. H., Szymanski, C. J., and Payne, C. K. (2011). Endo-lysosomal vesicles positive for Rab7 and LAMP1 are terminal vesicles for the transport of dextran. PLoS ONE *6*, e26626.

Iyer, R., Hamilton, R. F., Li, L., and Holian, A. (1996). Silica-induced apoptosis mediated via scavenger receptor in human alveolar macrophages. Toxicol Appl Pharmacol *141*, 84–92.

J F R Kerr, A. H. W. A. R. C. (1972). Apoptosis: A Basic Biological Phenomenon with Wide-ranging Implications in Tissue Kinetics. British Journal of Cancer *26*, 239.

Jalloul, A., and Banks, D. (2010). Can We Translate Our Understanding of the Pathogenic

Mechanisms of Silicosis Into a Therapeutic Plan? Interstitial, Inflammatory, and Occupational Lung Disease *17*, 266–275.

Jindal, S. K. (2013). Silicosis in India. Current Opinion in Pulmonary Medicine *19*, 163–

168.

Joshi, G. N., and Knecht, D. A. (2013a). Multi-parametric analysis of cell death pathways using live-cell microscopy. Curr Protoc Toxicol *58*, Unit4.40.

Joshi, G. N., and Knecht, D. A. (2013b). Silica phagocytosis causes apoptosis and necrosis by different temporal and molecular pathways in alveolar macrophages. Apoptosis *18*, 271–285.

Kahlenberg, J. M., Lundberg, K. C., Kertesy, S. B., Qu, Y., and Dubyak, G. R. (2005). Potentiation of Caspase-1 Activation by the P2X7 Receptor Is Dependent on TLR Signals and Requires NF- B-Driven Protein Synthesis. J Immunol *175*, 7611–7622.

Kalyanaraman, B. (2013). Teaching the basics of redox biology to medical and graduate students: Oxidants, antioxidants and disease mechanisms. Redox Biol *1*, 244–257.

Kalyanaraman, B., Darley-Usmar, V., Davies, K. J. A., Dennery, P. A., Forman, H. J., Grisham, M. B., Mann, G. E., Moore, K., Roberts, L. J., and Ischiropoulos, H. (2012). Measuring reactive oxygen and nitrogen species with fluorescent probes: challenges and limitations. Free Radic Biol Med *52*, 1–6.

Kamen, L. A., Levinsohn, J., Cadwallader, A., Tridandapani, S., and Swanson, J. A. (2008). SHIP-1 increases early oxidative burst and regulates phagosome maturation in macrophages. J Immunol *180*, 7497–7505.

Kanai, F., Liu, H., Field, S. J., Akbary, H., Matsuo, T., Brown, G. E., Cantley, L. C., and Yaffe, M. B. (2001). The PX domains of p47phox and p40phox bind to lipid products of PI(3)K. Nat Cell Biol *3*, 675–678.

Kane, A. B., Stanton, R. P., Raymond, E. G., Dobson, M. E., Knafelc, M. E., and Farber, J. L. (1980). Dissociation of intracellular lysosomal rupture from the cell death caused by silica. *87*, 643–651.

Kang, J. L., Go, Y. H., Hur, K. C., and Castranova, V. (2000). Silica-induced nuclear factor-kappaB activation: involvement of reactive oxygen species and protein tyrosine kinase activation. J Toxicol Environ Health Part A *60*, 27–46.

Kao, Y.-Y., Gianni, D., Bohl, B., Taylor, R. M., and Bokoch, G. M. (2008). Identification of a conserved Rac-binding site on NADPH oxidases supports a direct GTPase regulatory mechanism. J Biol Chem *283*, 12736–12746.

Kawai, H., Suzuki, T., Kobayashi, T., Mizuguchi, H., Hayakawa, T., and Kawanishi, T. (2004). Simultaneous imaging of initiator/effector caspase activity and mitochondrial membrane potential during cell death in living HeLa cells. Biochim Biophys Acta *1693*, 101–110.

Kawasaki, H. (2015). A mechanistic review of silica-induced inhalation toxicity. Inhalation Toxicology *27*, 363–377.

Kim, H., Tu, H.-C., Ren, D., Takeuchi, O., Jeffers, J. R., Zambetti, G. P., Hsieh, J. J.-D., and Cheng, E. H.-Y. (2009). Stepwise Activation of BAX and BAK by tBID, BIM, and PUMA Initiates Mitochondrial Apoptosis. Mol Cell *36*, 487–499.

Kirkegaard, T., and Jäättelä, M. (2009). Lysosomal involvement in cell death and cancer. Biochim Biophys Acta *1793*, 746–754.

Knaapen, A. M. (2002). DNA damage in lung epithelial cells isolated from rats exposed to quartz: role of surface reactivity and neutrophilic inflammation. Carcinogenesis *23*, 1111–1120.

Kon, K., Kim, J.-S., Uchiyama, A., Jaeschke, H., and Lemasters, J. J. (2010). Lysosomal iron mobilization and induction of the mitochondrial permeability transition in acetaminophen-induced toxicity to mouse hepatocytes. Toxicol Sci *117*, 101–108.

Kuhns, D. B. *et al.* (2010). Residual NADPH oxidase and survival in chronic granulomatous disease. N Engl J Med *363*, 2600–2610.

Kuroda, E., Ishii, K. J., Uematsu, S., Ohata, K., Coban, C., Akira, S., Aritake, K., Urade, Y., and Morimoto, Y. (2011). Silica Crystals and Aluminum Salts Regulate the Production of Prostaglandin in Macrophages via NALP3 Inflammasome-Independent Mechanisms. Immunity *34*, 514–526.

Kurz, T., Eaton, J. W., and Brunk, U. T. (2011). The role of lysosomes in iron metabolism and recycling. Int. J. Biochem. Cell Biol. *43*, 1686–1697.

Kuwana, T., Bouchier-Hayes, L., Chipuk, J. E., Bonzon, C., Sullivan, B. A., Green, D. R., and Newmeyer, D. D. (2005). BH3 domains of BH3-only proteins differentially regulate Bax-mediated mitochondrial membrane permeabilization both directly and indirectly. Mol Cell *17*, 525–535.

Labiris, N. R., and Dolovich, M. B. (2003). Pulmonary drug delivery. Part I: physiological factors affecting therapeutic effectiveness of aerosolized medications. Br J Clin Pharmacol *56*, 588–599.

Lambeth, J. D. (2007). Nox enzymes, ROS, and chronic disease: an example of antagonistic pleiotropy. Free Radic Biol Med *43*, 332–347.

Lamkanfi, M., and Dixit, V. M. (2014). Mechanisms and Functions of Inflammasomes. Cell *157*, 1013–1022.

Leto, T. L., Morand, S., Hurt, D., and Ueyama, T. (2009). Targeting and regulation of reactive oxygen species generation by Nox family NADPH oxidases. Antioxid Redox Signal *11*, 2607–2619.

Lettre, G., and Hengartner, M. O. (2006). Developmental apoptosis in C. elegans: a complex CEDnario. Nat Rev Mol Cell Biol *7*, 97–108.

Li, H., Zhu, H., Xu, C.-J., and Yuan, J. (1998). Cleavage of BID by Caspase 8 Mediates the Mitochondrial Damage in the Fas Pathway of Apoptosis. Cell *94*, 491–501.

Li, X. J., Marchal, C. C., Stull, N. D., Stahelin, R. V., and Dinauer, M. C. (2010). p47phox Phox homology domain regulates plasma membrane but not phagosome neutrophil NADPH oxidase activation. J Biol Chem *285*, 35169–35179.

Li, X. J., Tian, W., Stull, N. D., Grinstein, S., Atkinson, S., and Dinauer, M. C. (2009). A fluorescently tagged C-terminal fragment of p47phox detects NADPH oxidase dynamics during phagocytosis. Mol Biol Cell *20*, 1520–1532.

Lim, Y., Kim, S. H., Cho, Y. J., Kim, K. A., Oh, M. W., and Lee, K. H. (1997). Silica-induced oxygen radical generation in alveolar macrophage. Industrial Health *35*, 380–387.

Lima, H., Jacobson, L. S., Goldberg, M. F., Chandran, K., Diaz-Griffero, F., Lisanti, M. P., and Brojatsch, J. (2013). Role of lysosome rupture in controlling Nlrp3 signaling and necrotic cell death. Cell Cycle *12*, 1868–1878.

Lin, V. S., Dickinson, B. C., and Chang, C. J. (2013). Boronate-based fluorescent probes: imaging hydrogen peroxide in living systems. Meth Enzymol *526*, 19–43.

Linkermann, A., Stockwell, B. R., Krautwald, S., and Anders, H.-J. (2014). Regulated cell death and inflammation: an auto-amplification loop causes organ failure. Nat Rev Immunol, –.

Loew, L. M., Tuft, R. A., Carrington, W., and Fay, F. S. (1993). Imaging in five dimensions: time-dependent membrane potentials in individual mitochondria. Biophys J *65*, 2396–2407.

Lovell, J. F., Billen, L. P., Bindner, S., Shamas-Din, A., Fradin, C., Leber, B., and Andrews, D. W. (2008). Membrane Binding by tBid Initiates an Ordered Series of Events Culminating in Membrane Permeabilization by Bax. Cell *135*, 1074–1084.

Luna-Gomes, T., Santana, P. T., and Coutinho-Silva, R. (2015). Silica-induced inflammasome activation in macrophages: role of ATP and P2X7 receptor. Immunobiology *220*, 1101–1106.

Ly, J. D., Grubb, D. R., and Lawen, A. (2003). The mitochondrial membrane potential (deltapsi(m)) in apoptosis; an update. Apoptosis *8*, 115–128.

Madl, A. K., Donovan, E. P., Gaffney, S. H., McKinley, M. A., Moody, E. C., Henshaw, J. L., and Paustenbach, D. J. (2008). State-of-the-science review of the occupational health hazards of crystalline silica in abrasive blasting operations and related requirements for respiratory protection. J Toxicol Environ Health B Crit Rev *11*, 548–608.

Maeda, M., Nishimura, Y., Kumagai, N., Hayashi, H., Hatayama, T., Katoh, M., Miyahara, N., Yamamoto, S., Hirastuka, J., and Otsuki, T. (2010). Dysregulation of the immune system caused by silica and asbestos. J Immunotoxicol *7*, 268–278.

Maejima, I. *et al.* (2013). Autophagy sequesters damaged lysosomes to control lysosomal biogenesis and kidney injury. Embo J *32*, 2336–2347.

Majno, G., and Joris, I. (1995). Apoptosis, oncosis, and necrosis. An overview of cell death. Am J Pathol *146*, 3–15.

Mannherz, H. G., Gonsior, S. M., Wu, X., Polzar, B., Pope, B. J., Wartosch, L., and Weeds, A. G. (2006). Dual effects of staurosporine on A431 and NRK cells: microfilament disassembly and uncoordinated lamellipodial activity followed by cell death. Eur J Cell Biol *85*, 785–802.

Martin, S. J., Reutelingsperger, C. P., McGahon, A. J., Rader, J. A., van Schie, R. C., LaFace, D. M., and Green, D. R. (1995). Early redistribution of plasma membrane phosphatidylserine is a general feature of apoptosis regardless of the initiating stimulus: inhibition by overexpression of Bcl-2 and Abl. J Exp Med *182*, 1545–1556.

Matute, J. D., Arias, A. A., Dinauer, M. C., and Patiño, P. J. (2005). p40phox: the last NADPH oxidase subunit. Blood Cells Mol Dis *35*, 291–302.

Mbawuike, I. N., and Herscowitz, H. B. (1989). MH-S, a murine alveolar macrophage cell line: morphological, cytochemical, and functional characteristics. J Leukoc Biol *46*, 119–127.

McStay, G. P., Salvesen, G. S., and Green, D. R. (2008). Overlapping cleavage motif selectivity of caspases: implications for analysis of apoptotic pathways. *15*, 322–331.

Mi, S., Li, Z., Yang, H.-Z., Liu, H., Wang, J.-P., Ma, Y.-G., Wang, X.-X., Liu, H.-Z., Sun, W., and Hu, Z.-W. (2011). Blocking IL-17A Promotes the Resolution of Pulmonary Inflammation and Fibrosis Via TGF-{beta}1-Dependent and -Independent Mechanisms. J Immunol *187*, 3003–3014.

Michallet, M.-C., Saltel, F., Flacher, M., Revillard, J.-P., and Genestier, L. (2004). Cathepsin-dependent apoptosis triggered by supraoptimal activation of T lymphocytes: a possible mechanism of high dose tolerance. J Immunol *172*, 5405–5414.

Misson, P., van den Brûle, S., Barbarin, V., Lison, D., and Huaux, F. (2004). Markers of macrophage differentiation in experimental silicosis. J Leukoc Biol *76*, 926–932.

Monção-Ribeiro, L. C. *et al.* (2014). P2X7 receptor modulates inflammatory and functional pulmonary changes induced by silica. PLoS ONE *9*, e110185.

Morgan, B., Sobotta, M. C., and Dick, T. P. (2011). Measuring E(GSH) and H(2)O(2) with roGFP2-based redox probes. Free Radic Biol Med *51*, 1943–1951.

Mossman, B. T., and Churg, A. (1998). Mechanisms in the pathogenesis of asbestosis and silicosis. Am J Respir Crit Care Med *157*, 1666–1680.

Muñoz-Pinedo, C. (2006). Different mitochondrial intermembrane space proteins are

released during apoptosis in a manner that is coordinately initiated but can vary in duration. Proceedings of the National Academy of Sciences *103*, 11573–11578.

Murray, P. J. *et al.* (2014). Macrophage activation and polarization: nomenclature and experimental guidelines. Immunity *41*, 14–20.

Musset, B., Cherny, V. V., Morgan, D., and DeCoursey, T. E. (2009). The intimate and mysterious relationship between proton channels and NADPH oxidase. FEBS Lett *583*, 7–12.

Nadanaciva, S., Lu, S., Gebhard, D. F., Jessen, B. A., Pennie, W. D., and Will, Y. (2011). A high content screening assay for identifying lysosomotropic compounds. Toxicology in Vitro *25*, 715–723.

Nadler, S., and Goldfischer, S. (1970). The intracellular release of lysosomal contents in macrophages that have ingested silica. J. Histochem. Cytochem. *18*, 368–371.

Napierska, D., Thomassen, L. C. J., Lison, D., Martens, J. A., and Hoet, P. H. (2010). The nanosilica hazard: another variable entity. Particle and Fibre Toxicology *7*, 39.

Nash, T., Allison, A. C., and Harington, J. S. (1966). Physico-chemical properties of silica in relation to its toxicity. Nature *210*, 259–261.

National Toxicology Program (2002). 10th ROC: Respirable crystalline silica (RCS). Independent Source.

Oberdörster, G., Oberdörster, E., and Oberdörster, J. (2005). Nanotoxicology: an emerging discipline evolving from studies of ultrafine particles. Environ Health Perspect *113*, 823–839.

Onuki, R., Nagasaki, A., Kawasaki, H., Baba, T., Uyeda, T. Q. P., and Taira, K. (2002). Confirmation by FRET in individual living cells of the absence of significant amyloid beta -mediated caspase 8 activation. Proc Natl Acad Sci USA *99*, 14716–14721.

Park, J.-H., Gu, L., Maltzahn, von, G., Ruoslahti, E., Bhatia, S. N., and Sailor, M. J. (2009). Biodegradable luminescent porous silicon nanoparticles for in vivo applications. Nature Materials *8*, 331–336.

Pavan, C., Rabolli, V., Tomatis, M., Fubini, B., and Lison, D. (2014). Why does the hemolytic activity of silica predict its pro-inflammatory activity? Particle and Fibre Toxicology *11*, 76.

Peeters, P. M., Eurlings, I. M. J., Perkins, T. N., Wouters, E. F., Schins, R. P. F., Borm, P. J. A., Drommer, W., Reynaert, N. L., and Albrecht, C. (2014). Silica-induced NLRP3 inflammasome activation in vitro and in rat lungs. Particle and Fibre Toxicology *11*, S279.

Pelucchi, C., Pira, E., Piolatto, G., Coggiola, M., Carta, P., and La Vecchia, C. (2006).

Occupational silica exposure and lung cancer risk: a review of epidemiological studies 1996-2005. Ann Oncol *17*, 1039–1050.

Perl, A., Gergely, P., Nagy, G., Koncz, A., and Banki, K. (2004). Mitochondrial hyperpolarization: a checkpoint of T-cell life, death and autoimmunity. Trends Immunol *25*, 360–367.

Persson, H. L. (2005). Iron-dependent lysosomal destabilization initiates silica-induced apoptosis in murine macrophages. Toxicol Lett *159*, 124–133.

Pfau, J. C., Brown, J. M., and Holian, A. (2004). Silica-exposed mice generate autoantibodies to apoptotic cells. Toxicology *195*, 167–176.

Piguet, P. F., and Vesin, C. (1994). Treatment by human recombinant soluble TNF receptor of pulmonary fibrosis induced by bleomycin or silica in mice. Eur. Respir. J. *7*, 515–518.

Porter, D. W. *et al.* (2004). Progression of lung inflammation and damage in rats after cessation of silica inhalation. Toxicol Sci *79*, 370–380.

Postlethwaite, A. E., and Seyer, J. M. (1990). Stimulation of fibroblast chemotaxis by human recombinant tumor necrosis factor alpha (TNF-alpha) and a synthetic TNF-alpha 31-68 peptide. J Exp Med *172*, 1749–1756.

Price, M. O., McPhail, L. C., Lambeth, J. D., Han, C.-H., Knaus, U. G., and Dinauer, M. C. (2002). Creation of a genetic system for analysis of the phagocyte respiratory burst: high-level reconstitution of the NADPH oxidase in a nonhematopoietic system. Blood *99*, 2653–2661.

Rego, A. C., Vesce, S., and Nicholls, D. G. (2001). The mechanism of mitochondrial membrane potential retention following release of cytochrome c in apoptotic GT1-7 neural cells. *8*, 995–1003.

Rehm, M., Dussmann, H., Janicke, R. U., Tavare, J. M., Kogel, D., and Prehn, J. H. M. (2002). Single-cell fluorescence resonance energy transfer analysis demonstrates that caspase activation during apoptosis is a rapid process. Role of caspase-3. J Biol Chem *277*, 24506–24514.

Rehm, M., Huber, H. J., Hellwig, C. T., Anguissola, S., Dussmann, H., and Prehn, J. H. M. (2009). Dynamics of outer mitochondrial membrane permeabilization during apoptosis. *16*, 613–623.

Repnik, U., and Turk, B. (2010). Lysosomal-mitochondrial cross-talk during cell death. Mitochondrion *10*, 662–669.

Repnik, U., Hafner Česen, M., and Turk, B. (2014). Lysosomal membrane permeabilization in cell death: Concepts and challenges. Mitochondrion *19*, 49–57.

Repnik, U., Stoka, V., Turk, V., and Turk, B. (2012). Lysosomes and lysosomal cathepsins in cell death. Biochim Biophys Acta *1824*, 22–33.

Ricci, J.-E., Gottlieb, R. A., and Green, D. R. (2003). Caspase-mediated loss of mitochondrial function and generation of reactive oxygen species during apoptosis. *160*, 65–75.

Rimal, B., Greenberg, A. K., and Rom, W. N. (2005). Basic pathogenetic mechanisms in silicosis: current understanding. Current Opinion in Pulmonary Medicine *11*, 169–173.

Rojanasakul, Y., Ye, J., Chen, F., Wang, L., Cheng, N., Castranova, V., Vallyathan, V., and Shi, X. (1999). Dependence of NF-kappaB activation and free radical generation on silica-induced TNF-alpha production in macrophages. Mol Cell Biochem *200*, 119–125.

Roos, D. (1979). Oxygen free radicals and tissue damage.

Rosner, D., Markowitz, G., and Markowitz, G. E. (1994). Deadly Dust, Princeton University Press.

Ross, M. H., and Murray, J. (2004). Occupational respiratory disease in mining. Occupational Medicine (Oxford, England) *54*, 304–310.

Roursgaard, M., Poulsen, S. S., Poulsen, L. K., Hammer, M., Jensen, K. A., Utsunomiya, S., Ewing, R. C., Balic-Zunic, T., Nielsen, G. D., and Larsen, S. T. (2010). Time-response relationship of nano and micro particle induced lung inflammation. Quartz as reference compound. Human & Experimental Toxicology.

Russell, D. G., VanderVen, B. C., Glennie, S., Mwandumba, H., and Heyderman, R. S. (2009). The macrophage marches on its phagosome: dynamic assays of phagosome function. Nat Rev Immunol *9*, 594–600.

Rybicka, J. M., Balce, D. R., Khan, M. F., Krohn, R. M., and Yates, R. M. (2010). NADPH oxidase activity controls phagosomal proteolysis in macrophages through modulation of the lumenal redox environment of phagosomes. Proc Natl Acad Sci USA *107*, 10496–10501.

Sandberg, W. J., Låg, M., Holme, J. A., Friede, B., Gualtieri, M., Kruszewski, M., Schwarze, P. E., Skuland, T., and Refsnes, M. (2012). Comparison of non-crystalline silica nanoparticles in IL-1β release from macrophages. Particle and Fibre Toxicology *9*, 32.

Santarelli, L., Recchioni, R., Moroni, F., Marcheselli, F., and Governa, M. (2004). Crystalline silica induces apoptosis in human endothelial cells in vitro. Cell Biol Toxicol *20*, 97–108.

Sato, T., Shimosato, T., Alvord, W. G., and Klinman, D. M. (2008). Suppressive oligodeoxynucleotides inhibit silica-induced pulmonary inflammation. J Immunol *180*, 7648–7654.

Savina, A., Jancic, C., Hugues, S., Guermonprez, P., Vargas, P., Moura, I. C., Lennon-Duménil, A.-M., Seabra, M. C., Raposo, G., and Amigorena, S. (2006). NOX2 Controls Phagosomal pH to Regulate Antigen Processing during Crosspresentation by Dendritic Cells. Cell *126*, 205–218.

Savina, A., Vargas, P., Guermonprez, P., Lennon, A.-M., and Amigorena, S. (2010). Measuring pH, ROS production, maturation, and degradation in dendritic cell phagosomes using cytofluorometry-based assays. Methods Mol Biol *595*, 383–402.

Schellenberg, B. *et al.* (2013). Bax exists in a dynamic equilibrium between the cytosol and mitochondria to control apoptotic priming. Mol Cell *49*, 959–971.

Schins, R. P. F., Duffin, R., Höhr, D., Knaapen, A. M., Shi, T., Weishaupt, C., Stone, V., Donaldson, K., and Borm, P. J. A. (2002). Surface modification of quartz inhibits toxicity, particle uptake, and oxidative DNA damage in human lung epithelial cells. Chem Res Toxicol *15*, 1166–1173.

Schneider, C. A., Rasband, W. S., and Eliceiri, K. W. (2012). NIH Image to ImageJ: 25 years of image analysis. Nat Methods *9*, 671–675.

Schroder, K., Sagulenko, V., Zamoshnikova, A., Richards, A. A., Cridland, J. A., Irvine, K. M., Stacey, K. J., and Sweet, M. J. (2012). Acute lipopolysaccharide priming boosts inflammasome activation independently of inflammasome sensor induction. Immunobiology.

Schwartz, S. (1998). Cell Death and the Caspase Cascade. Circulation *97*, 227.

Segal, B. H. *et al.* (2010). NADPH oxidase limits innate immune responses in the lungs in mice. PLoS ONE *5*, e9631.

Segawa, K., Kurata, S., Yanagihashi, Y., Brummelkamp, T. R., Matsuda, F., and Nagata, S. (2014). Caspase-mediated cleavage of phospholipid flippase for apoptotic phosphatidylserine exposure. *344*, 1164–1168.

Sellamuthu, R., Umbright, C., Li, S., Kashon, M., and Joseph, P. (2011). Mechanisms of crystalline silica-induced pulmonary toxicity revealed by global gene expression profiling. Inhalation Toxicology *23*, 927–937.

Shamas-Din, A., Satsoura, D., Khan, O., Zhu, W., Leber, B., Fradin, C., and Andrews, D. W. (2014). Multiple partners can kiss-and-run: Bax transfers between multiple membranes and permeabilizes those primed by tBid. Cell Death Dis *5*, e1277.

Shen, H. M., Zhang, Z., Zhang, Q. F., and Ong, C. N. (2001). Reactive oxygen species and caspase activation mediate silica-induced apoptosis in alveolar macrophages. Am J Physiol Lung Cell Mol Physiol *280*, L10–L17.

Shui, W., Sheu, L., Liu, J., Smart, B., Petzold, C. J., Hsieh, T.-Y., Pitcher, A., Keasling, J. D., and Bertozzi, C. R. (2008). Membrane proteomics of phagosomes suggests a

connection to autophagy. Proceedings of the National Academy of Sciences *105*, 16952–16957.

Slee, E. A. *et al.* (1999). Ordering the cytochrome c-initiated caspase cascade: hierarchical activation of caspases-2, -3, -6, -7, -8, and -10 in a caspase-9-dependent manner. *144*, 281–292.

Slee, E. A., Keogh, S. A., and Martin, S. J. (2000). Cleavage of BID during cytotoxic drug and UV radiation-induced apoptosis occurs downstream of the point of Bcl-2 action and is catalysed by caspase-3: a potential feedback loop for amplification of apoptosis-associated mitochondrial cytochrome c release. *7*, 556–565.

Sokolovska, A. *et al.* (2013). Activation of caspase-1 by the NLRP3 inflammasome regulates the NADPH oxidase NOX2 to control phagosome function. Nat Immunol *14*, 543–553.

Spencer, S. L., and Sorger, P. K. (2011). Measuring and modeling apoptosis in single cells. Cell *144*, 926–939.

Spencer, S. L., Gaudet, S., Albeck, J. G., Burke, J. M., and Sorger, P. K. (2009). Non-genetic origins of cell-to-cell variability in TRAIL-induced apoptosis. Nature *459*, 428–432.

Spickett, C. M., Wiswedel, I., Siems, W., Zarkovic, K., and Zarkovic, N. (2010). Advances in methods for the determination of biologically relevant lipid peroxidation products. Free Radic. Res. *44*, 1172–1202.

Srivastava, K. D., Rom, W. N., Jagirdar, J., Yie, T.-A., Gordon, T., and Tchou-WOng, K.-M. (2002). Crucial role of interleukin-1beta and nitric oxide synthase in silica-induced inflammation and apoptosis in mice. Am J Respir Crit Care Med *165*, 527–533.

Steenland, K. (2005). One agent, many diseases: exposure-response data and comparative risks of different outcomes following silica exposure. Am J Ind Med *48*, 16–23.

Steinberg, B. E., and Grinstein, S. (2008). Pathogen destruction versus intracellular survival: the role of lipids as phagosomal fate determinants. J Clin Invest *118*, 2002–2011.

Suh, C.-I., Stull, N. D., Li, X. J., Tian, W., Price, M. O., Grinstein, S., Yaffe, M. B., Atkinson, S., and Dinauer, M. C. (2006). The phosphoinositide-binding protein p40phox activates the NADPH oxidase during FcgammaIIA receptor-induced phagocytosis. J Exp Med *203*, 1915–1925.

Sullivan, D. E., Ferris, M., Pociask, D., and Brody, A. R. (2005). Tumor necrosis factor-alpha induces transforming growth factor-beta1 expression in lung fibroblasts through the extracellular signal-regulated kina... - PubMed - NCBI. Am J Respir Cell Mol Biol *32*, 342–349.

Sundler, R. (1997). Lysosomal and cytosolic pH as regulators of exocytosis in mouse

macrophages. Acta Physiologica Scandinavica *161*, 553–556.

Swanson, J. A., and Hoppe, A. D. (2004). The coordination of signaling during Fc receptor-mediated phagocytosis. J Leukoc Biol *76*, 1093–1103.

Tait, S. W. G., and Green, D. R. (2010). Mitochondria and cell death: outer membrane permeabilization and beyond. Nat Rev Mol Cell Biol.

Tait, S. W. G., Parsons, M. J., Llambi, F., Bouchier-Hayes, L., Connell, S., Muñoz-Pinedo, C., and Green, D. R. (2010). Resistance to Caspase-Independent Cell Death Requires Persistence of Intact Mitochondria. Dev Cell *18*, 802–813.

Terman, A., and Kurz, T. (2012). Lysosomal Iron, Iron Chelation, and Cell Death. Antioxid Redox Signal.

Thibodeau, M. S., Giardina, C., Knecht, D. A., Helble, J., and Hubbard, A. K. (2004). Silica-induced apoptosis in mouse alveolar macrophages is initiated by lysosomal enzyme activity. Toxicol Sci *80*, 34–48.

Thibodeau, M., Giardina, C., and Hubbard, A. K. (2003). Silica-induced caspase activation in mouse alveolar macrophages is dependent upon mitochondrial integrity and aspartic proteolysis. Toxicol Sci *76*, 91–101.

Thiele, D. L., and Lipsky, P. E. (1990). Mechanism of L-leucyl-L-leucine methyl ester-mediated killing of cytotoxic lymphocytes: dependence on a lysosomal thiol protease, dipeptidyl peptidase I, that is enriched in these cells. Proc Natl Acad Sci USA *87*, 83–87.

Thomas, C. R., and Kelley, T. R. (2010). A brief review of silicosis in the United States. Environ Health Insights *4*, 21–26.

Tian, W., Li, X. J., Stull, N. D., Ming, W., Suh, C. I., Bissonnette, S. A., Yaffe, M. B., Grinstein, S., Atkinson, S. J., and Dinauer, M. C. (2008). Fc R-stimulated activation of the NADPH oxidase: phosphoinositide-binding protein p40phox regulates NADPH oxidase activity after enzyme assembly on the phagosome. Blood *112*, 3867–3877.

Tlili, A., Dupré-Crochet, S., Erard, M., and Nüße, O. (2010). Kinetic analysis of phagosomal production of reactive oxygen species. Free Radic Biol Med.

Tlili, A., Erard, M., Faure, M.-C., Baudin, X., Piolot, T., Dupré-Crochet, S., and Nüße, O. (2012). Stable accumulation of p67phox at the phagosomal membrane and ROS production within the phagosome. J Leukoc Biol *91*, 83–95.

Tsujino, M., Hirata, Y., Imai, T., Kanno, K., Eguchi, S., Ito, H., and Marumo, F. (1994). Induction of nitric oxide synthase gene by interleukin-1 beta in cultured rat cardiocytes. Circulation *90*, 375–383.

Turk, B., and Turk, V. (2009). Lysosomes as “Suicide Bags” in Cell Death: Myth or Reality? J Biol Chem *284*, 21783–21787.

Tyas, L., Brophy, V. A., Pope, A., Rivett, A. J., and Tavaré, J. M. (2000). Rapid caspase-3 activation during apoptosis revealed using fluorescence-resonance energy transfer. *1*, 266–270.

Uchimoto, T., Nohara, H., Kamehara, R., Iwamura, M., Watanabe, N., and Kobayashi, Y. (1999). Mechanism of apoptosis induced by a lysosomotropic agent, L-Leucyl-L-Leucine methyl ester. Apoptosis *4*, 357–362.

Vallyathan, V., Shi, X. L., Dalal, N. S., Irr, W., and Castranova, V. (1988). Generation of free radicals from freshly fractured silica dust. Potential role in acute silica-induced lung injury. Am. Rev. Respir. Dis. *138*, 1213–1219.

van Berlo, D., Wessels, A., Boots, A. W., Wilhelmi, V., Scherbart, A. M., Gerloff, K., van Schooten, F. J., Albrecht, C., and Schins, R. P. F. (2010). Neutrophil-derived ROS contribute to oxidative DNA damage induction by quartz particles. Free Radic Biol Med *49*, 1685–1693.

vander Heiden, M. G., Chandel, N. S., Williamson, E. K., Schumacker, P. T., and Thompson, C. B. (1997). Bcl-xL regulates the membrane potential and volume homeostasis of mitochondria. Cell *91*, 627–637.

VanderVen, B. C., Yates, R. M., and Russell, D. G. (2009). Intraphagosomal measurement of the magnitude and duration of the oxidative burst. Traffic *10*, 372–378.

Vieira, O. V., Botelho, R. J., and Grinstein, S. (2002). Phagosome maturation: aging gracefully. Biochem J *366*, 689–704.

Walensky, L. D., and Gavathiotis, E. (2011). BAX unleashed: the biochemical transformation of an inactive cytosolic monomer into a toxic mitochondrial pore. Trends Biochem Sci *36*, 642–652.

Wang, L., Antonini, J. M., Rojanasakul, Y., Castranova, V., Scabilloni, J. F., and Mercer, R. R. (2003). Potential role of apoptotic macrophages in pulmonary inflammation and fibrosis. J Cell Physiol *194*, 215–224.

Wang, L., Bowman, L., Lu, Y., Rojanasakul, Y., Mercer, R. R., Castranova, V., and Ding, M. (2005). Essential role of p53 in silica-induced apoptosis. Am J Physiol Lung Cell Mol Physiol *288*, L488–L496.

Wang, X., Lv, L., Chen, Y., and Chen, J. (2010). A CD36 synthetic peptide inhibits silica-induced lung fibrosis in the mice. Toxicology and Industrial Health *26*, 47–53.

Waterhouse, N. J., Goldstein, J. C., Ahsen, von, O., Schuler, M., Newmeyer, D. D., and Green, D. R. (2001). Cytochrome c maintains mitochondrial transmembrane potential and ATP generation after outer mitochondrial membrane permeabilization during the apoptotic process. *153*, 319–328.

Weisz, A., Cicatiello, L., and Esumi, H. (1996). Regulation of the mouse inducible-type

nitric oxide synthase gene promoter by interferon-gamma, bacterial lipopolysaccharide and NG-monomethyl-L-arginine. Biochem J *316 (Pt 1)*, 209–215.

Winterbourn, C. C. (2008). Reconciling the chemistry and biology of reactive oxygen species. Nat. Chem. Biol. *4*, 278–286.

Winterbourn, C. C., and Kettle, A. J. (2013). Redox reactions and microbial killing in the neutrophil phagosome. Antioxid Redox Signal *18*, 642–660.

Winterbourn, C. C., Hampton, M. B., Livesey, J. H., and Kettle, A. J. (2006). Modeling the reactions of superoxide and myeloperoxidase in the neutrophil phagosome: implications for microbial killing. J Biol Chem *281*, 39860–39869.

Wong-Ekkabut, J., Xu, Z., Triampo, W., Tang, I.-M., Tieleman, D. P., and Monticelli, L. (2007). Effect of lipid peroxidation on the properties of lipid bilayers: a molecular dynamics study. Biophys J *93*, 4225–4236.

Yoshimori, T., Yamamoto, A., Moriyama, Y., Futai, M., and Tashiro, Y. (1991). Bafilomycin A1, a specific inhibitor of vacuolar-type H(+)-ATPase, inhibits acidification and protein degradation in lysosomes of cultured cells. J Biol Chem *266*, 17707–17712.

Zaltsman, Y., Shachnai, L., Yivgi-Ohana, N., and Schwarz, M. (2010). MTCH2/MIMP is a major facilitator of tBID recruitment to mitochondria. Nature Cell … *12*, 553–562.

Zeidler, P. C., Roberts, J. R., Castranova, V., Chen, F., Butterworth, L., Andrew, M. E., Robinson, V. A., and Porter, D. W. (2003). Response of alveolar macrophages from inducible nitric oxide synthase knockout or wild-type mice to an in vitro lipopolysaccharide or silica exposure. J Toxicol Environ Health Part A *66*, 995–1013.

Zhang, G., Gurtu, V., Kain, S. R., and Yan, G. (1997). Early detection of apoptosis using a fluorescent conjugate of annexin V. BioTechniques *23*, 525–531.